The University of Sheffield

BIOFOULING STUDIES ON REVERSE OSMOSIS DESALINATION OF HYPERSALINE WATERS

A Thesis Submitted to The University of Sheffield

By

Bashir Ali Ashhuby, BSc. MSc. PhD.

for the degree of

Doctor of Philosophy

Project Supervisors:

Professor Dr. Phillip C. Wright

Chemical and Process Engineering Department

And

Dr Daniel James Gilmour

Molecular Biology and Biotechnology Department

July-2007

ABSTRACT

Biological fouling of reverse osmosis (RO) membranes is affected by many factors, and it is not clearly understood, especially with respect to hypersaline waters. Biofouling minimisation requires understanding of the fundamentals of the biofilm development. It is also necessary to monitor biofilm development at various stages and its relation to concentration polarisation phenomena.

The two main goals were to explore the biological diversity of a hypersaline lake called "Qabar-Onn", located in the Sahara; and to better understand what biotic and abiotic factors govern biofouling of RO membranes treating hypersaline waters.

Three halotolerant bacterial strains (*Euhalothece* species, BAA001 and BAA002, and *Halomonas pantelleriensis* species, BAA003) were isolated from the lake using conventional culturing methods, and were identified based on 16S rRNA sequencing. Two isolated species, *Euhalothece* species BAA001 and *Halomonas pantelleriensis* species BAA003 were used as model microorganisms to evaluate the potential of biofilm development on RO membranes. Salinity and surface roughness, which affect biofilm initiation and growth, were investigated. A novel, *in-situ* monitoring device was used to detect initiation of biofilm formation, and its relation to solutes and concentrations near RO membrane surfaces.

The results showed that Qabar-Onn Lake is inhabited by a wide range of microorganisms, which seem to have a strong potential to adapt to the rapid increase in the lake salinity. In addition to salinity, pH also is limiting factor on biodiversity and microorganisms' dominance. Biofouling was strongly controlled by membrane characteristics and feed salinity. Lower surface roughness and low salinity contributed to less biofilm formation. Furthermore, the absence of monovalent anions (i.e. chloride) in the feed enhanced flux at low salinities; however, its absence severely decreased flux at higher salinities. Similarly, microorganisms present in the feed extremely enhanced the permeate flux at low salinities, however, at high salinities the flux decreased in the presence of microorganisms.

ACKNOWLEDGEMENTS

No task of this magnitude is accomplished alone, and therefore I would like to acknowledge all those who helped me succeed.

I equally would like to thank my two supervisors: Professor Dr Phillip C. Wright at Chemical and Process Engineering Department, and Dr Daniel James Gilmour at Molecular Biology and Biotechnology Department for all their guidance, support and time during different research stages.

My thanks also extends to Mr Stuart Creasy, from Hallam University, Sheffield for his help in providing The Environmental SEM facility, and for his flexibility and advice. Equally, I also would like to thank Professor Dr Mike Williamson, from Molecular Biology and Biotechnology Department, The University of Sheffield for his help in running NMR instrument, and also for his help in results analysis and solutes identifications.

I am deeply grateful to Mrs Dawn Bussey, from Materials Engineering Department, The University of Sheffield for her assistance in AFM picturing of membrane samples. I am also grateful to the Dean and colleagues at the Faculty of Engineering and Technology, University of Sebha, Libya for providing data and information about Qabar-Onn Lake and for their help in transportation, as well as providing the required technical equipment during the lake visits.

I also would like to thank all my co-workers those have helped me directly or indirectly. I mainly want to mention Robert Bachman, Jagroop Pandhal, Mark Scafe, Talia Ortiga, Christopher Alloyds, Victoria Truck, and Ian Gafford. In addition, I would like to thank the people supported me outside the academia, at home: my wife and kids for their patience, support and understanding throughout my PhD life, I will be forever grateful.

Allah bless you all!

TABLE OF CONTENTS

List Of Figures

List Of Tables

Nomenclature

A	membrane surface area
Alk.	carbonate alkalinity (mg l^{-1})
AN	ammonical nitrogen, NH_3-N (mg l^{-1})
Aramid	aromatic polyamide membrane
BOD_5	five-day biochemical oxygen demand (mg l^{-1})
Bp	base pair
CA	cellulose acetate membrane
CAPS	compact accelerated pretreatment softening
CFU	colony forming units
Cf	salt concentration in feed stream
Chl-a	chlorophyll-a
Chl-b	chlorophyll-b
Chl-t	chlorophyll-total
ci	molar concentration of the solute
cm	centimetre
COD	chemical oxygen demand (mg l^{-1})
Cp	salt concentration in product stream
Da	Dalton
DBP	disinfection by-products
DDW	deionised distilled water
DGGE	denaturing gradient gel electrophoresis
DO	dissolved oxygen
ED	electrodialysis
EPS	extra-cellular polysaccharides
ESEM	environmental scanning electron microscope
g l^{-1}	gram per litre
GAC	granular activated carbon
HPROMTS	high-pressure reverse osmosis membranes test system
IC	ion chromatograph
j	flux
j_c	critical flux
j_t	total flux
K_S	membrane permeability coefficient for salt
K_W	membrane permeability coefficient for water
M	molar
MED	multi effect distillation
MF	microfiltration
mg l^{-1}	milligrams per litre
mM	millimole
MPa	mega Pascal

MSF	multi-stage flash distillation
MWCO	molecular weight cut-off
NF	nanofiltration
NTU	n turbidity unit
°C	temperature (degrees Celsius)
OD	optical density
ON	organic nitrogen (mg l^{-1})
ppm	part per million
Q_f	feed stream flow rate
Q_p	product stream flow rate
Q_s	salt flow through the membrane
Q_w	water flow rate through the membrane
R	gas constant
RO	reverse osmosis
SDI	silt density index
SEM	scanning electronic microscopy
SP	% salt passage
SS	suspended solids
T	absolute temperature
TDS	total dissolved solids
TEM	transmission electron microscope
TFC	Thin Film Composite
THM	trihalomethanes
TKN	total kjeildahl nitrogen (mg l^{-1}l)
TN	total nitrogen (mg l^{-1})
TOC	total organic carbon
TS	total solids (mg l^{-1})
TSS	total suspended solids (mg l^{-1})
UF	ultrafiltration
v	cross flow velocity
VC	vapour compression
v_i	number of ions formed if the solute dissociates
VS	volatile solids (mg l^{-1})
VSS	volatile suspended solids (mg l^{-1})
Y	% recovery or conversion
t	membrane thickness
µg	microgram
µm	micrometer
µM	micromole
$\Delta P_{feed/brine}$	pressure drop between feed and brine
$\Delta P_{membrane}$	pressure drop caused by membrane
ΔC	salt concentration differential across membrane
ΔP	hydraulic pressure differential across membrane
$\Delta \pi$	osmotic pressure differential across membrane
π	osmotic pressure

Chapter 1

INTRODUCTION

1.1 Background

All natural waters (except for pure rain water) contain dissolved salts in one concentration or another. Water classification is mainly based on the salt content (salinity), which is expressed as the total dissolved solids (TDS) content of particular water. Table 1.1 represents classification of water types based on their salinities (Heitmann, 1990).

Table 1.1: Classification of water types based on salinity.

Water Type	Salinity	
	Range (mg l^{-1})	Typical value (mg l^{-1})
Fresh water	0 – 500	<500
Brackish water	500 – 22,000	17,000
Seawater	28,000 – 37,000	32,500
Hypersaline water	50,000 – 180,000	>50,000

Source: Heitmann (1990)

For most countries in the Middle East and North Africa, the availability of fresh water has become problematic (Al-Ahmad *et al*, 2000; Hamrouni and Dhahbi, 2001; Al-Suleimani and Rajendran Nair, 2000). This is due to the fast increase in the population, social and economic living standards and large-scale expansion in industrial and agricultural activities. Existing resources of water, including groundwater, are almost exhausted, and the desalination of both seawater and brackish water has become a desirable option for future unlimited fresh water supply. Today, many countries in the region rely heavily on desalination technologies to meet their needs of fresh water (Al-Suleimani and Rajendran Nair, 2000; Ahmed *et. al*, 2001; Darwish and Al-Najem, 2000). However, the adopted technologies are still

limited due to the high capital and operating costs and lack of professional operators (Darwish and Al-Najem, 2000).

Libya is one of the countries suffering most from the shortage of fresh water resources. In addition, the excessive use of ground water resources in the past few decades has resulted in a serious change in both quantity and quality of these waters (Abufayed, 2000). Desalination is considered an alternative solution to cover the water deficit in both coastal and non-coastal areas. The desalination of seawater has been used to provide a big share of fresh drinking water in the urban coastal areas. In 2001, a published report by Kershman indicates that building a series of desalination plants along the coast can be a solution for securing potable water in urban communities. However, fresh water supply in non-coastal areas is still problematic.

Brackish water in Libya is likely to be a potential water resource in the near future (Kershman, 2001). Utilising reverse osmosis (RO) for desalinating brackish water offers a viable option for Libya to meet the unsatisfied water demand. The geographical distribution of brackish water in the country (Libya) is spread along the seaside strip in the north and throughout many basins in the south such as Fezzan, Morzuk and Al-Kofrah. This feature offers a positive impact in utilising unsatisfied water demand for specific users such as domestic, industrial and wild animal grazing through the establishment of medium size RO systems, in different locations.

Qabar-Onn Lake (Figure 1.1) is a hypersaline lake located 13°30'N and 26°51'E in the heart of the Sahara, south west of Libya, about 115 km south west of the city of Sebha (Figure 1.2). The lake has an area of about 0.055 km^2 and a maximum depth of 8.5 m, and it lies 200 m above sea level. The lake has a high salinity, which varies with sampling location and season. The salinity varies between 90,000 mg l^{-1} and 160,000 mg l^{-1}, with an average of 125,000 mg l^{-1}. This figure is more than 3.7 times higher than that for open seas and oceans (i.e. 33,500 mg l^{-1}). Figure 1.3 shows comparative values for the total dissolved salts (TDS), sodium, magnesium, potassium, chloride, and sulphate contents of seawater, Qabar-Onn Lake, and the Dead Sea. As it can be seen, the salinities are far great than seawater.

Figure 1.1: An aerial view of Qabar-Onn Lake.

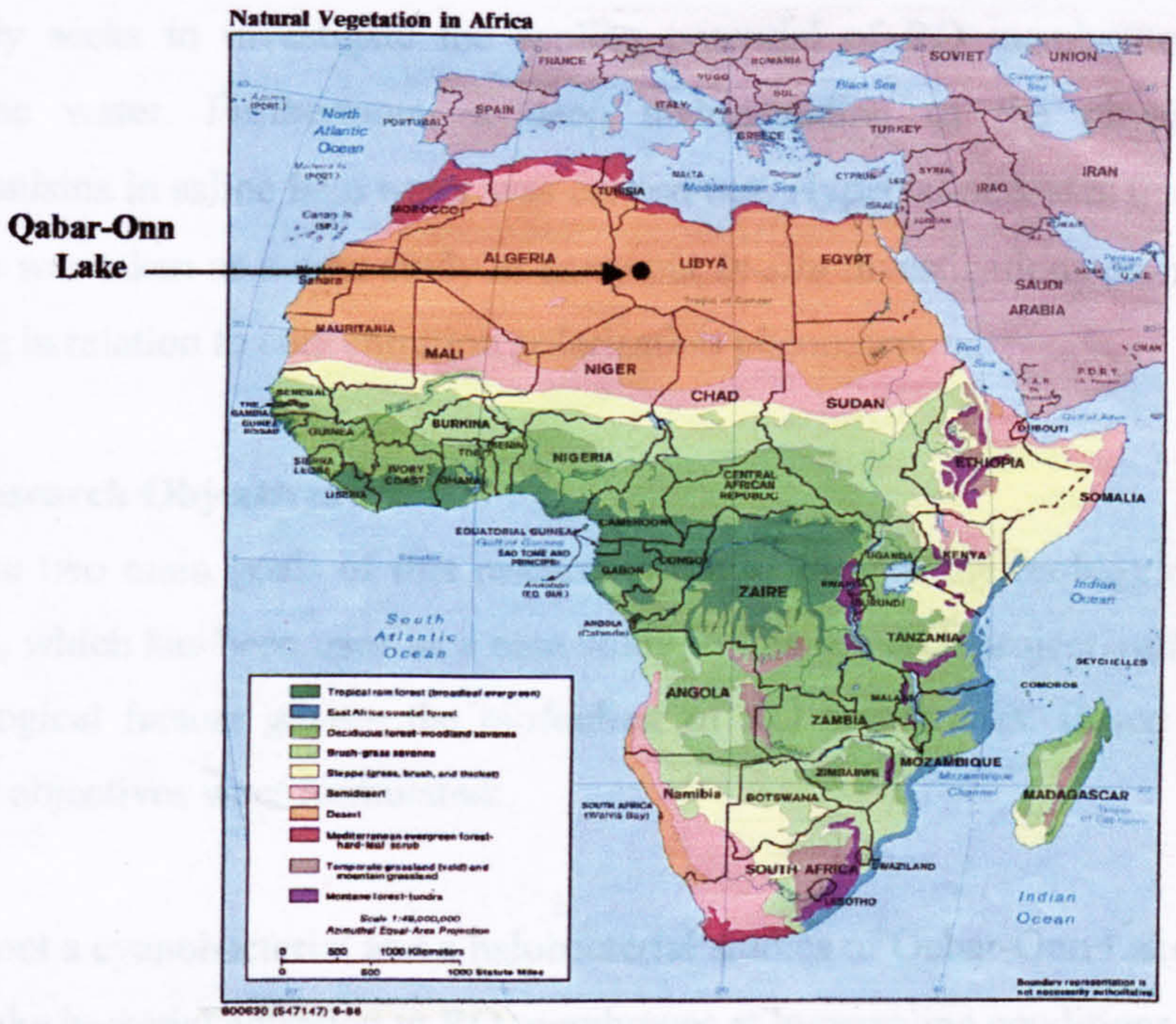

Figure 1.2: Map of Africa: showing location of Qabar-Onn Lake in the south west of Libya.

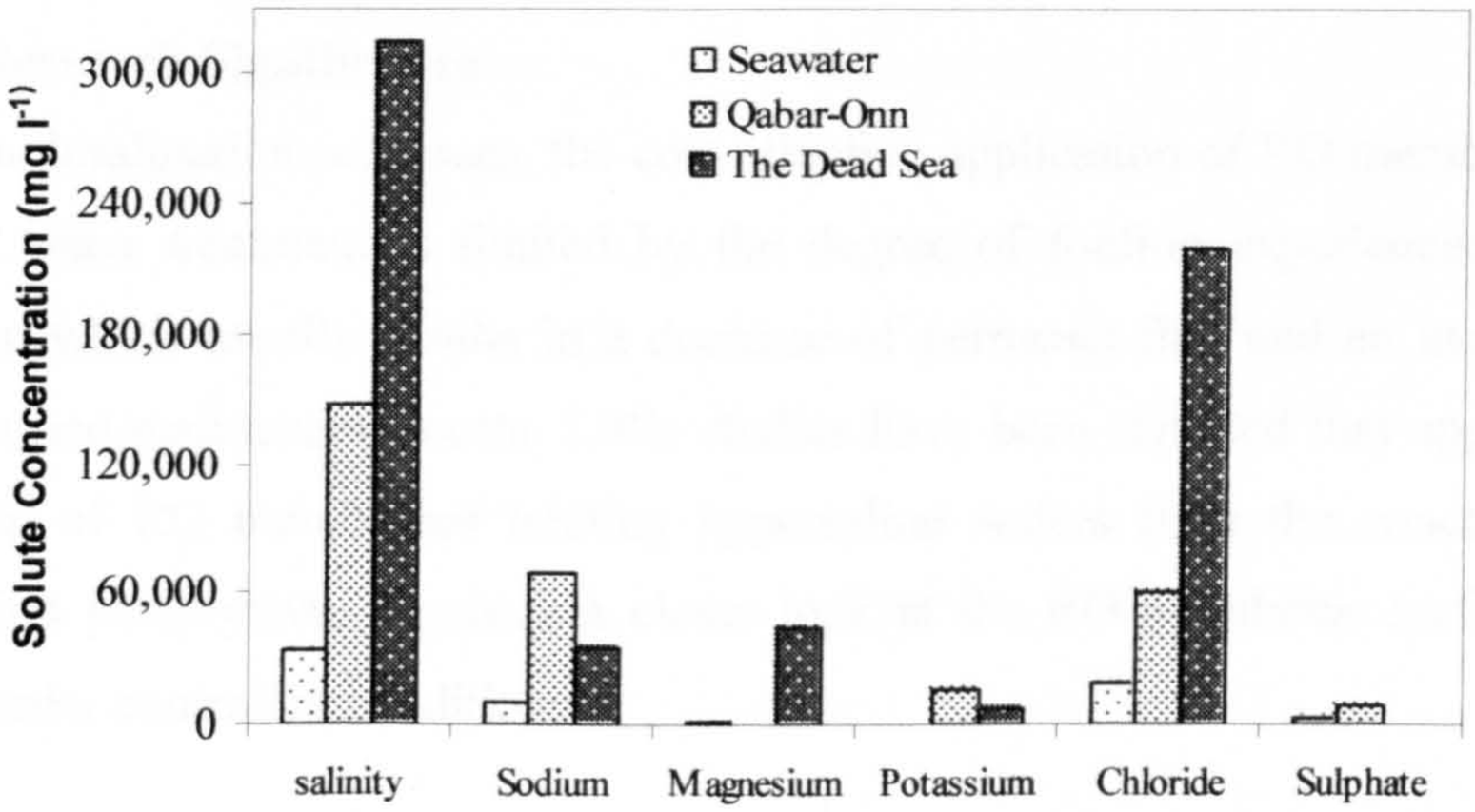

Figure 1.3: Salinity, and major cations and anions concentrations in seawater, Qabar-Onn Lake and the Dead Sea. *(Source: This study; Klein-BenDavid, 2004)*.

This study seeks to investigate the fouling potential of RO membranes treating hypersaline water. Furthermore, a deep understanding of the physiology of microorganisms in saline lake water was carried out. Hypersaline water from Qabar-Onn Lake was taken as a case study to carry out *in-situ* investigations on membrane biofouling in relation to concentration polarisation phenomenon.

1.2 Research Objectives

The two main goals of this research were to explore the biology of Qabar-Onn Lake, which has been used as a case study in this research project, and to study what biological factors govern the biofouling of RO membranes. Based on these goals four objectives were formulated:

1. Carry out a cyanobacterial and a halobacterial studies of Qabar-Onn Lake water,
2. Study the bacterial adhesion to RO membranes at hypersaline conditions,
3. Carry out investigations on the impact of different foulants on certain types of RO membranes, and
4. Study the relationship between concentration polarisation and the biofouling in RO membranes at hypersaline conditions.

1.3 Research Significance

In desalination processes, the cost-effective application of RO membranes in drinking water treatment is limited by the degree of fouling experienced during operation, which usually results in a decrease of permeate flux and an increase in operation and maintenance costs. Little studies have been reported that approaches biofouling of RO membranes treating hypersaline waters from the concentration polarisation perspective, in which a closer look at the RO membrane surface was studied under controlled conditions.

In this research, a microbiological screening study of Qabar-Onn Lake was carried out. Three out of five bacterial species isolated from this lake were identified and characterised, and all of the three identified species were assigned as novel species. These identified species, then, were used to inoculate the hypersaline water samples for bacterial attachment to RO membranes studies.

Another extremely important engineering issue associated with membrane fouling is the feasibility to monitor biofouling progression in parallel with salt crystals initiation in/on membrane channels. Currently, there are no methods reported that directly monitor biofouling (in hypersaline water desalination) and relate it to the presence of salt ions. In this thesis, a unique technique was evaluated that enabled *in-situ* visualisation of salt ions crystallisation before destructively sampling membrane elements. This method greatly helped in monitoring the initiation of fouling of RO membranes and hence the study of biofouling/concentration polarisation relationship was possible.

1.4 Thesis Approach

This thesis is comprised of eight chapters. Chapter 2 includes a general literature review of desalination methods, pre-treatment techniques, membrane processes, membrane fouling, biofouling, and biology of hypersaline waters. Chapter 3 describes the general analytical methodologies and experimental apparatus used. Chapter 4 includes the cyanobacterial investigations of Qabar-Onn Lake water which

include sampling, isolation, growth optimisation, study of parameters influencing growth, phylogenetic identification, and determination of compatible solutes (objective 1 "part 1" is addressed in this chapter). Chapter 5 includes halobacterial studies of this lake water, which also includes sampling, isolation, growth profile studies, identification and characterisation, chemotaxonomic studies and compatible solutes determinations (objective 1 "part 2" is addressed in this chapter). In Chapter 6, the isolated halobacterial and cyanobacterial species were used as model microorganisms to assess the potential of the effect of the biological constituents on biofilm formation and growth on RO membranes (objective 2 is addressed in this chapter). The study of the biofouling of RO membranes and flux behaviour are presented in Chapter 7 (objectives 3 and 4 are addressed in this chapter). Finally, Chapter 8 summarises the most important results of the entire thesis, and conclusions and recommendations are presented.

Chapter 2

LITERATURE REVIEW

2.1 Biology of Hypersaline Waters

The biology of waters, characterised with high salinities, is very unique and represents a case of relatively low water activity. For example, the majority of bacterial groups, which live in soil and fresh water, cannot tolerate seawater salinity. Hypersaline ecosystems are generally inhabited by a limited variety of life forms. The upper limit of salt concentration for vertebrates, such as *Tilapia sp.*, was reported to be not more than 10% (w/v) (Ollivier, *et al*, 1994). Above this level, only invertebrates such as brine shrimps (*Artemia salina*) or brine flies, algae (*Dunaliella salina*), bacteria (members of families *Halobacteriaceae* and *Haloanaerobiaceae*, methanogens, etc), and cyanobacteria (*Oscillatoria spp.*) have been reported (Paerl *et al.*, 2000). Qabar-Onn Lake, which has salinity of 3.7 times higher than seawater salinity (Alajaili *et al*, 1984), is inhabited by only a few organisms. In such habitats, many bacteria, flagellated alga (e.g. *Dunaliella viridis)* and brine shrimp (e.g. *Artemia salina)* can tolerate such high salt concentrations, but only members of the prokaryotes find their optimum growth conditions there (Balows, *et al.*, 1992b).

On the basis of fundamental cytological distinctions of living systems (Figure 2.1), eukaryotes are distinguished from prokaryotes in that the former have cells containing a membrane-bounded nucleus and certain organelles, however, the latter lack these features (Balows, *et al.*,1992a). Though prokaryotes are distinguished from eukaryotic life forms by being structurally simple, they are functionally diverse (Paerl, *et al.*, 2000).

The halophilic bacteria, which are dominant in hypersaline habitats, are divided into three groups. The extremely halophilic bacteria, the moderately halophilic bacteria and slightly halophilic bacteria, which have their optimum growth at 200 to 300 g l^{-1}

salt, 50 to 200 g l^{-1} salt and 20 to 50 g l^{-1} salt, respectively (Table 2.1). The extremely halophilic bacteria such as *Halobacterium cutirubrum, H. salinarium* and *Halococcus morrhuae*, are found in the evaporation ponds for salt production, and occasionally on salted fish and hides. They can be easily recognised by their red colour caused by carotenoids. The moderately halophilic bacteria inhabit similar habitats such as salt brine and mud. This group of bacteria are often found in curing brines for meat, fish, and vegetables. It is also reported that the majority of bacteria inhabiting the sea and other marine ecosystems require 20-50 g l^{-1} sodium chloride (Balows, *et al.*, 1992a).

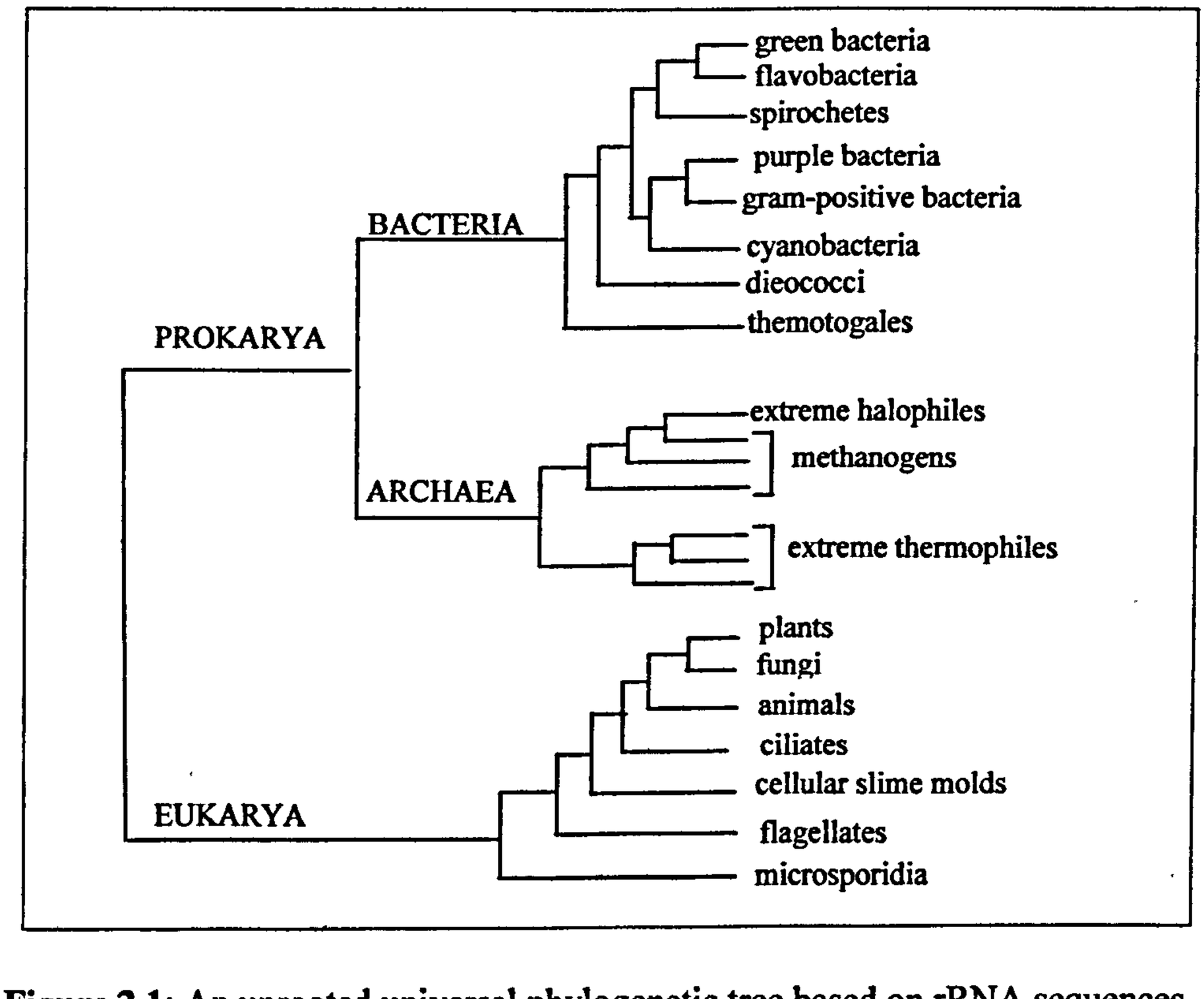

Figure 2.1: An unrooted universal phylogenetic tree based on rRNA sequences.

Table 2.1: Halophilic phototrophic bacteria grouped according to their salt requirement and classification of halophilic organisms. (x) Indicates the optimum salinity for various species.

Type of Halophiles	Species	NaCl concentration (g l^{-1})										
		25	50	75	100	125	150	175	200	225	250	
Slight Halophiles	*Chromatium buderi*											
	Chloroherpeton thalassium											
	Ectothiorhodospira mobilis	x										
	Rhodobacter sulfidophilus	x										
	Pelodictyon phaeum											
	Rhodopseudomonas marina											
	Ectothiorhodospira vacuolata											
	Prostecochloris phaeoasteroidea											
	Thiorhodovibrio winogradskyi		x									
	Chlorobium chlorovibrioides											
	Chromatium purpuratum											
	Rhodobacter adriaticus		x									
	Prostecochloris aestuarii											
	Chromatium vinosum HPC		x									
	Lamprobacter modestohalophilus											
Moderate Halophiles	*Rhodospirillum mediosalinum*			x								
	Rhodospirillum saexigens			x								
	Ectothiorhodospira marismortui			x								
	Thiocapsa halophila				x							
	Chromatium saexigens					x						
	Ectothiorhodospira abdelmalekii						x					
	Rhodospirillum salinarum						x					
Extreme Halophiles	*Ectothiorhodospira halophila*							x				
	Ectothiorhodospira halochloris								x			

Reproduced and updated from Martinez-Canovas et al., 2004.

Sources of organic matter in hypersaline environments originate from dead cells and metabolites of halophilic organisms growing in such ecosystems, algae and plants growing nearby may also input organic matter into the hypersaline system (Ollivier, *et al*, 1994). However, invertebrates, algae, and prokaryotes are the major sources of oxidisable compounds in these environments (Balows, *et al*., 1992a). Cyanobacteria and members of *Halobacteriaceae* at high salt concentrations may add significant quantities of organic matter from decomposition of their cell walls, which are composed of sugar, proteins, and lipids (Paerl, *et al.*, 2000). Organic osmolytes, which maintain cell turgor pressure under high salt concentration, also contribute to the overall carbon cycle in hypersaline ecosystems (Cummings, *et al*., 1993). Besides potassium, mainly moderately halophilic bacteria accumulate low molecular weight organic compounds (such as glycine betaine) to adapt to osmotic stress (Tanaka, *et al*, 2001; Paerl, *et al.*, 2000).

Martinez-Canovas *et al.* (2004) reported that marine salterns are habitats for a large variety of halophilic or halo-tolerant bacteria that develop throughout the entire gradient of salt concentration. In the first ponds most bacteria are slightly halophilic, whereas in the intermediary ponds, where the seawater is concentrated to a salinity of about 10 to 20% NaCl, most of the bacteria are moderately halophilic. This intermediate environment contains the greatest numbers of organisms. The last ponds are inhabited by extremely halophilic organisms including aerobic numbers of the *Archaea* from the genera *Halobacterium*, *Haloferax*, and *Haloarcula*, in addition to several species pertaining to the *Bacteria* and *Eucarya*. However, only one methanogenic species of the *Archaea* was reported to grow optimally at NaCl concentrations over 20% (Abed *et al.*, 2002b).

Only a few moderately halophilic sulphate reducers have been isolated from different kinds of hypersaline environments including marine salterns. The main characteristics of the isolated sulphate reducers are summarised in Table 2.2. Truper in 1969 isolated a few sulphur reducing bacteria (SRB) from hot brines in the Red Sea (Tinadall, 1992). One of the isolated species tolerated up to 170 g l^{-1} NaCl and seemed similar to *Desulfovibrio halophilus*, and more recently, other SRBs were isolated by a moderately halophilic sulphate reducer was isolated by Caumette *et al.* (1991) from a hypersaline lake in Sinai (Egypt). A second moderately halophilic sulphate reducer was fully described and characterised as a new species of a new genus, *Desulfohalobium retbaense* (Ollivier, *et al*, 1991). It was isolated from the small hypersaline Retba Lake in Senegal. The organism was a nonsporulating motile straight rod. *Desulfovibrio halophilus* and *Desulfohalobium retbaense* represent the only two isolated moderately halophilic species so far reported, Table 2.2 (Abed *et al*, 2002a; Ollivier, *et al*, 1994).

The extreme halophilic bacteria grow best in 200 – 300 g l^{-1} NaCl. These obligate halophiles are red-pigmented organisms, which occur in waters of high salinity such as the *Dead Sea*, for instance (Klein-BenDavid, 2004). The extreme halophilic bacteria adapt themselves to live in high saline environments by having internal concentrations of salt that equal or exceed even the high concentrations in which they

grow. Although the *Halobacteria* have been described as strict aerobes, some grow fermentatively, for example, *Halobacterium halobium* uses arginine as an anaerobic energy source (Hochstein and Tomlinson, 1985). Several extreme halophiles have been isolated by Hochstein and Tomlinson (1985). These halophiles grew anaerobically, but only in the presence of nitrate. It can be concluded that the presence of denitrifying extremely halophilic bacteria in hypersaline waters confirms that brines should favour the presence of such bacteria. The virtual absence of nitrate from hypersaline lakes (e.g. Qabar-Onn Lake, $NO_3 = < 0.8$ mg l^{-1}, Table 4.2, Chapter 4), suggests that active denitrification takes place in the lake.

Table 2.2: Main characteristics of sulphate reducers isolated from hypersaline waters. *(Source: Abed et al., 2002a ; Ollivier, et al, 1994)* .

Property	Sulphate Reducer	
	Desulfovibrio halophilus	***Desulfohalobium retbaense***
Morphology	Vibrio	Rod
Size (width × length), µm	0.6 × 2.5-5	0.7-0.9 × 1-3
Gram stain	Negative	Negative
Motility	1 polar flagellum	1-2 polar flagella
Temp. Optimum, °C	35-40	37-40
Salinity optimum, g l^{-1}	60-70	100
pH optimum	6.5	6.5-7.0
Habitat	Solar Lake	Lake Retba (Senegal)

Bottom sediments of hypersaline water bodies such as the Great Salt Lake, Utah; the Dead Sea; and marine salterns used for the production of solar salt are expected to support a rich community of anaerobic halophilic bacteria, as the solubility of oxygen in hypersaline brines is low and the amounts of organic matter available are usually high (Abed *et al.*, 2002a; Klein-BenDavid, 2004).

Anaerobic halophilic bacteria of the family *Haloanaerobiaceae* have been found in all anoxic hypersaline water bodies and sediments investigated (Abed *et al.*, 2002b). However, quantitative data on the occurrence of members of *Haloanaerobiaceae* in such ecosystems are scarce. *Haloanaerobium praevalens* was reported to be present in the Great Salt Lake (Utah) surface sediment in numbers of up to 10^8 ml^{-1} sediment, while 10^3 -10^5 *Halobacteroides halobius* cells were counted per millilitre of the Dead Sea sediment (Klen-BenDavid *et al.*, 2004).

Five moderately halophilic, obligatory anaerobic chemoorganotrophic species have been described and classified in three genera as follows (Balows, *et al.*, 1992c):

- *Haloanaerobium praevalens*: A non-motile, rod-shaped bacterium growing at salt concentrations from 30-250 g l^{-1} (optimally at 130 g l^{-1}).
- *Halobacteroides halobius*: A very long, rod-shaped motile bacterium, growing at salt concentrations between 80-160 g l^{-1}.
- *Halobacteroides acetoethylicus*: A short, motile, rod-shaped bacterium, growing at salt concentrations between 50-220 g l^{-1} (optimally 100 g l^{-1}).
- *Sporohalobacter lortetii*: Formerly named as *Clostridium lotetii*, a rod-shaped, motile bacterium, producing terminal endospores with attached gas vacuoles, growing at salt concentrations between 60-120 g l^{-1}.
- *Sporohalobacter marismortui*: A rod-shaped motile bacterium, growing at salt concentrations of 30-120 gl^{-1}, sometimes observed to produce endospores without gas vacuoles.

All the five isolates are similar in their DNA (range 27-32 mol%), all stain Gram-negative and have a Gram-negative type of cell wall, and all are mesophilic (optimum growth temperatures around 35-45°C).

Klein-BenDavid *et al.* (2004) carried out an experimental study on growth of extreme halophiles and concluded that halobacteria were eminently suited for aerobic growth under conditions where the concentration of oxygen is extremely low. However, anaerobic growth only would be occurring in the presence of nitrate or nitrite.

Cyanobacteria differ from all other prokaryotes by using a water-oxidising photosynthesis like that of higher plants; in addition, many cyanobacterial strains possess an active nitrogenase enzyme system. Nitrogen-fixing unicellular cyanobacteria combine within the same cell photosynthesis, an oxygenic process; and nitrogen fixation, an oxygen-sensitive process (Balows, *et al.*, 1992a).

Paerl, *et al.* (2000) reviewed several dominant cyanobacterial clostridia living in stressed habitats including hypersaline waters. Among the cyanobacterial genera identified at hypersaline environments are *Microcoleus, Lyngbya, Synechococcus, Phormidium, Calothrix, Scytonema, Schizothrix,* and *Spirulina.* Cyanobacterial-dominated mats may be found in a range of extreme environments, ranging from the tropics to the poles, where they are often the dominant and the only biological communities. The Bahamian islands have many small hypersaline lagoons (salinity range 45-100 g l^{-1}). The microbial mats in this ecosystem are well-developed under nutrient depletion and high temperature (>30°C) conditions. *San Salvador Island, Bahamas* has numerous hypersaline lagoons including *Storr's Lake* (salinity 4.5-9%), which supports microbial mats dominated by the heterocystous cyanobacterial genus *Scytonema,* non-heterocystous *Schizothrix* and coccoid forms *Synechocystis* and *Synechococcus.* Another hypersaline lagoon in the Bahamian islands is the *Salt Creek Pond* (salinity 45-100 g l^{-1}), which contained a non-calcified cyanobacterial mat dominated by the non-heterocystous filamentous genera *Microcoleus, Lyngbya,* and *Oscillatoria.*

Ajaili, *et al* (1984) reported that 19 species of diatoms have been found in Qabar-Onn Lake corresponding to 13 genera. The vertical distribution of the diatoms in the lake water during cold season shows that diatoms were concentrated at the surface (e.g. 0.1 m deep), however, it is interesting that two diatoms species (*Cyclotella meneghiniana* and *Stephanodiscus dubius*), were only found near the lake bottom.

2.2 Biofilm and Biofouling

2.2.1 General

In membrane systems, biofouling represents the bottleneck of the process performance because all other fouling components, such as organic and inorganic dissolved substances and particles can be removed by pretreatment (Flemming, 1997). Biofouling arises from microbial biofilms (Figure 2.2), which are very common in water systems of any non-sterile plant. Undesired effects of biofouling include energy loss, decreased water quality and possible contamination of drinking

water with pathogenic bacteria, plugging of filter systems and causes corrosion or *biodeterioration* of equipment and pipelines.

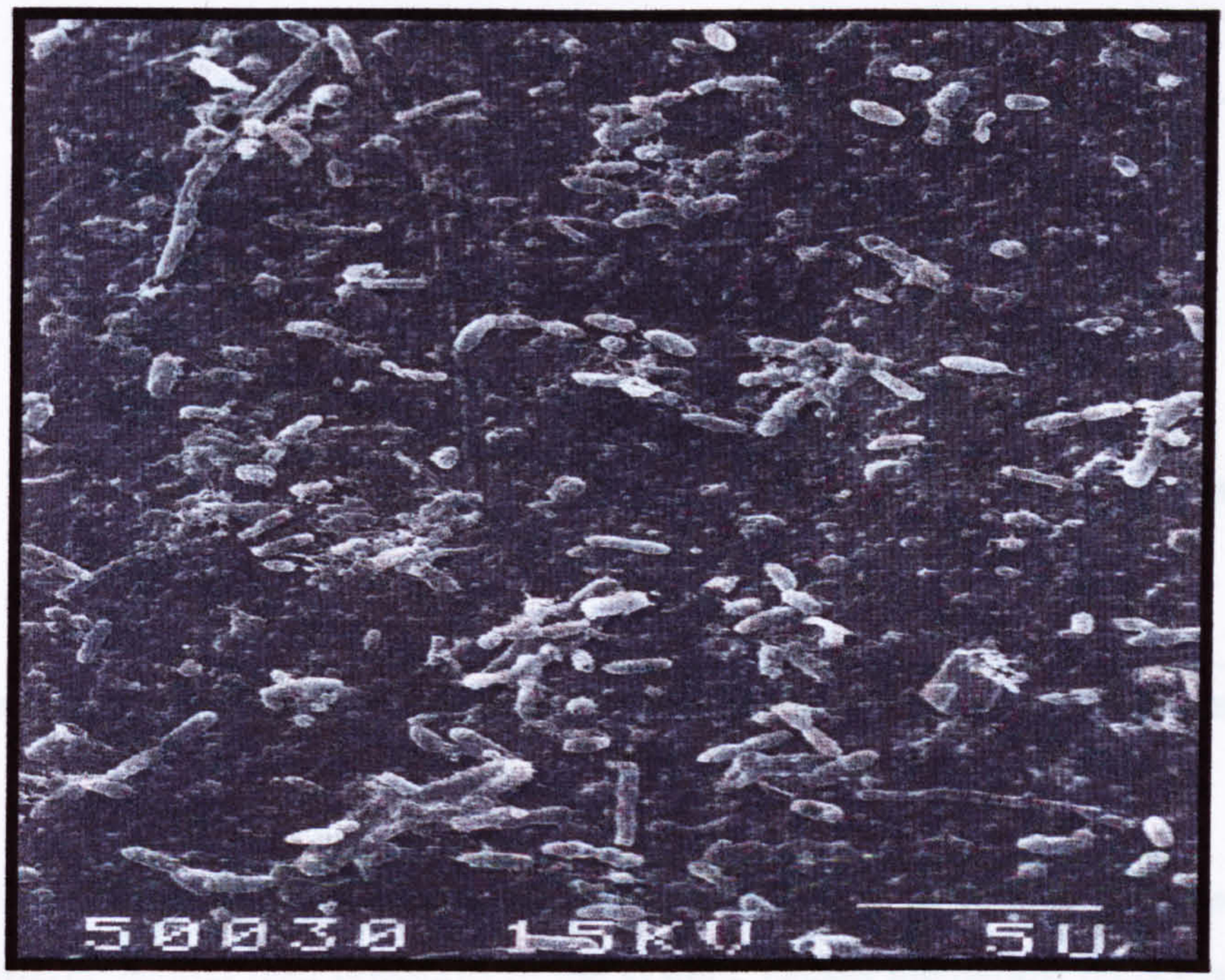

Figure 2.2: Scanning electron micrograph of a biofouled RO membrane surface: (Bar= 5. μm). (*Reproduced from Flemming, 1997)*

In reverse osmosis systems, biofilms are involved from the very beginning (after few hours of operation) and a biofilm develops and participates in the separation process. Biofouling occurs only when biofilm development exceeds a certain level "*threshold of interference*", and this is the case when performance parameters (e.g. permeate flux) fall below given limits (Melo and Bott, 1997).

2.2.2 Detection and Diagnosis of Biofouling

Usually the membrane system responds to biofouling problems by an increase of $\Delta P_{(feed/brine)}$ and $\Delta P_{(membrane)}$ (Figure 2.3). However, this response is very non-specific and can be caused by other fouling mechanisms as well. Unfortunately, there is still no technology available to take biofilm samples non-destructively from an operating membrane assembly. In practice, either a bypass membrane device is

used from which membranes can be removed and investigated destructively, or other representative surfaces are sampled which are accessible, such as cartridge filters (Flemming, 1997).

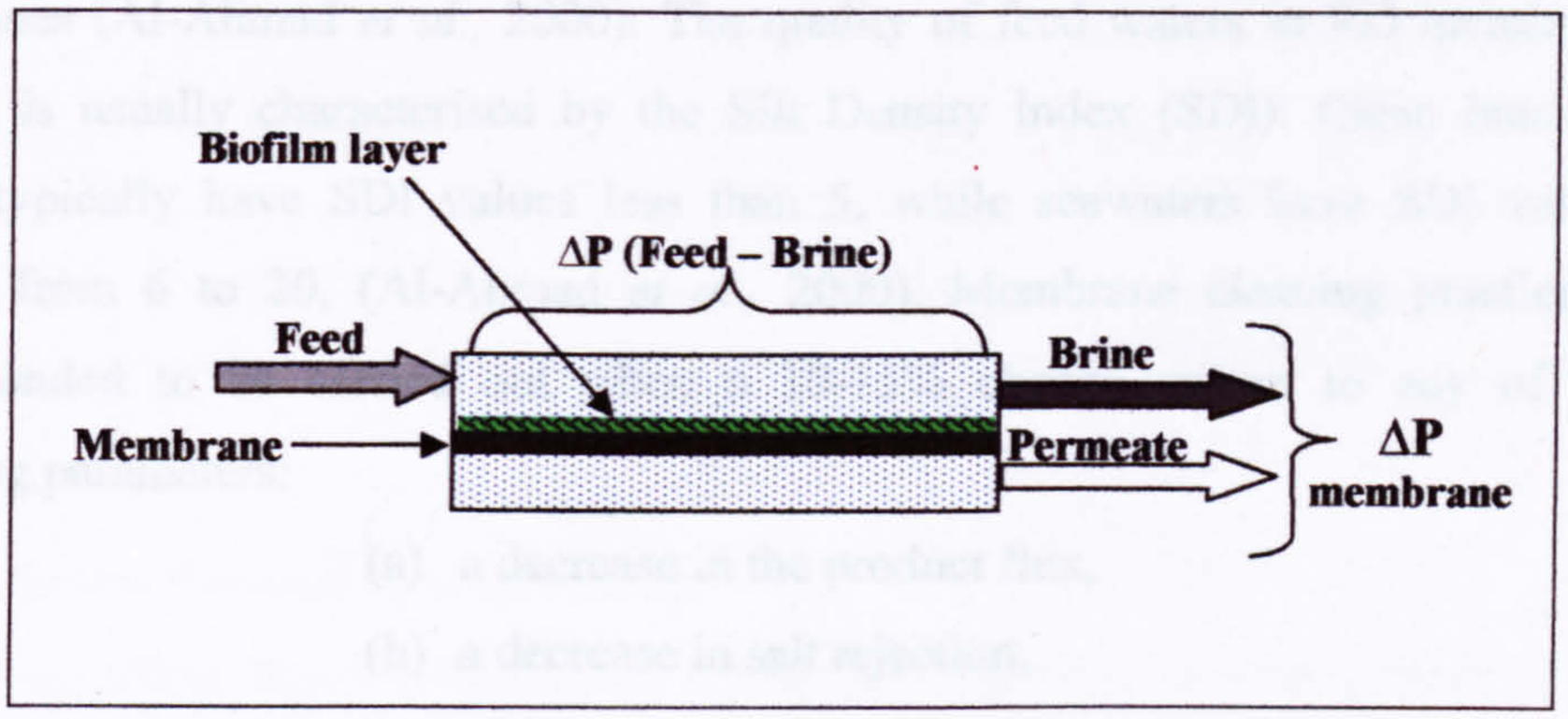

Figure 2.3: A schematic representation of the pressure situation in a membrane system.

In reverse osmosis systems, biofouling causes a decline in membrane flux, increases both differential and feed pressures of the system, causes membrane biodegradation, decreases salt rejection of the membrane, and increases energy requirements for the system (Sheikholeslami, 1999). In addition, there is an interaction between biofouling and corrosion leading to a special type of corrosion known as "microbiological corrosion" (Al-Ahmad, *et al.*, 2000). The later can be attributed to the presence of several factors, which include:

(a) formation of oxygen concentration cells,

(b) formation of ion concentration cells,

(c) acid production (sulphuric acid), and

(d) creation of anaerobic niches.

Biofouling in spiral wound modules occurs because of the different module design of these membranes (Coker and Sehn, 2000). Their design makes them an ideal environment for the growth of microorganisms that form a microfilm on the membrane surface and on spacing material in the narrow feed channels. The growing

biofilm traps the suspended and colloidal particulate matters which quickly build-up as a biomass (Al-Ahmad *et al.*, 2000).

Biofouling can be controlled either by pretreatment of feed waters or by cleaning of membranes (Al-Ahmad *et al.*, 2000). The quality of feed waters in RO membrane systems is usually characterised by the Silt Density Index (SDI). Clean brackish waters typically have SDI values less than 5, while seawaters have SDI values ranging from 6 to 20, (Al-Ahmad *et al.*, 2000). Membrane cleaning practice is recommended to be carried out when a 10-15% change occurs to any of the following parameters:

(a) a decrease in the product flux,
(b) a decrease in salt rejection,
(c) an increase in the pressure drop, or
(d) an increase in the feed pressure of the system.

2.2.3 Biofilm Autopsy Studies

Autopsy (destructive test analysis of membranes after operation) results of hundreds of membranes from around the world reported that the two major components of the biofouling layers were water (80% - 94%) and organic matter (20% - 90% of the remnants), of which 30% - 40% were humic substances. Inorganic compounds common in the biofouling layer were iron (30-39%), silica (0.5-37%), and lower amounts of calcium sulphate and carbonate (3-5%). Microbial species, typically cultured from membrane surfaces, are summarised in Table 2.3 (Baker and Dudley, 1998).

The characteristics of a biofouling layer (biofilm) are dependent on a series of variables, such as organic/inorganic attachment and deposition, microbial attachment and growth, which precede and are concurrent to physico-chemical processes and metabolic activities. It is, therefore, extremely difficult to anticipate and detail the characteristics of such complex matrices and therefore, bench and/or pilot-testing are favoured when a new process or application is being considered.

Table 2.3: Microorganisms cultured from biofouled surfaces of spiral wound elements (Baker and Dudley, 1998).

	Viable Bacterial Counts (CFU cm^{-2})	Fungal Counts (CFU m^{-2})		Common Species (Identified by Phenotype)
Fouled membrane	10^2 - 10^8	0 – 10^3	Bacteria	*Pseudomonas, Corynebacterium, Flavobacterium, Aeromonas.*
Plastic spacer material	4×10^2 - 5×10^5	0 – 10^3	Fungi	*Penicillium, Tricoderma, Aspergillus.*
Permeate carrier	$<10^2$ - 10^6	none	Yeast	Occasionally identified in significant numbers.

2.2.4 Biofilm Formation Mechanism

Biofouling may be considered a "biofilm reactor in a wrong place". The operational development of biofilm on membrane surfaces, as shown in Figure 2.4, can be described in three steps (Flemming, 1997):

(a) ***The induction phase*:** this is the primary colonisation of microorganisms to the membrane surface. It is important to prevent biofilm development. The induction phase refers to the time between two cleaning cycles.

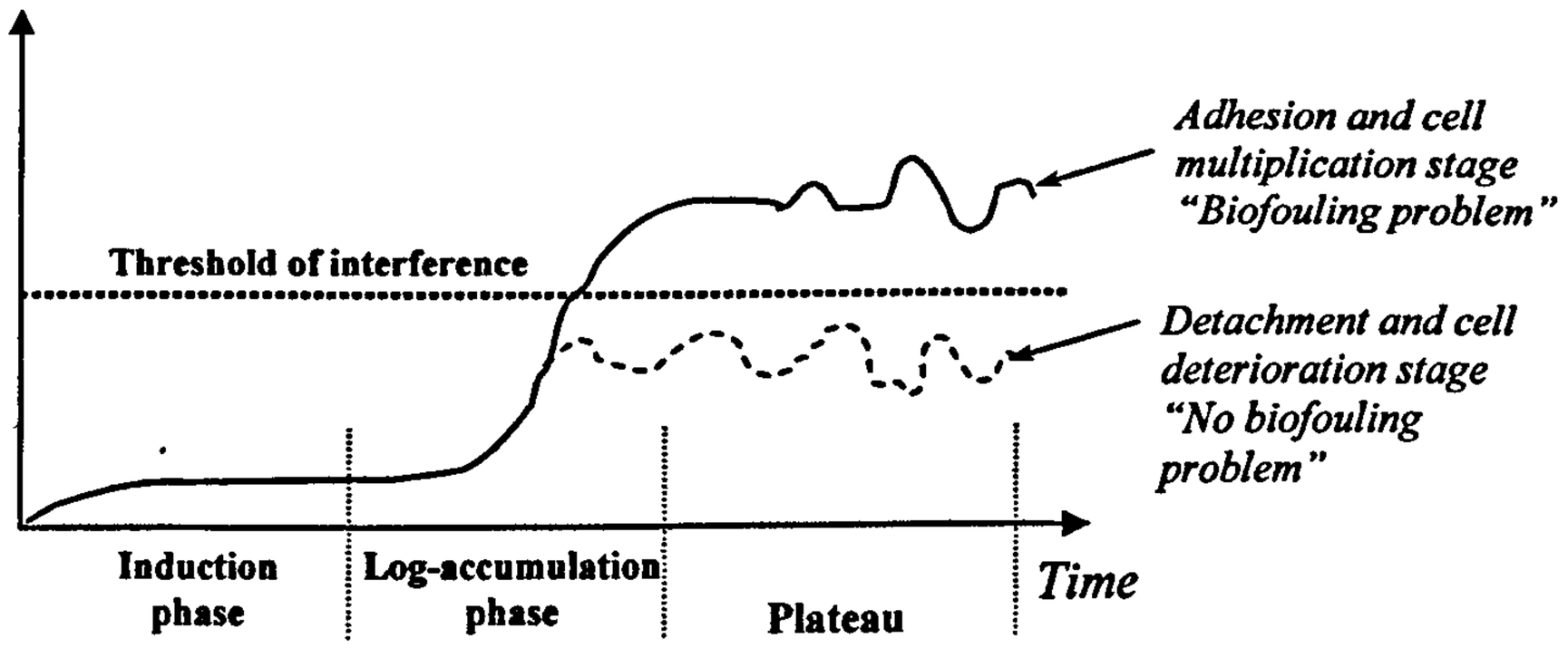

Figure 2.4: Time-dependent development of biofilm accumulation: [Change in biofilm growth parameter (thickness, weight, etc); threshold of interference: arbitrary extent of biofilm development above which biofilm interferes with the performance of a membrane system]. *Source: Flemming, 1997.*

(b) ***The logarithmical growth phase*****:** this second stage occurs when cell growth on the membrane surface contributes more to the biofilm accumulation than does further adhesion of planktonic (e.g. autotrophic) cells.

(c) ***The plateau phase*****:** this is the stage where the biofilm growth (adhesion) and cell detachment are in balance. This phase is mainly controlled by many operational factors and conditions, which include: nutrient concentration, the mechanical stability of the biofilm, and the effective shear forces.

Although adhesion and colonisation of a surface is affected by specific microorganisms, available surfaces and environmental conditions, there are a number of fundamental processes common to all sessile bacteria; they must be able to attach to a substrate or other bacteria, use available resources to grow and reproduce, and to relocate onto new areas when conditions become unfavourable (Flemming, 1997; Percival *et al.*, 2000; Baker and Dudley, 1998). Biofilm formation can be divided in four general stages: formation of a surface conditioning layer, microbial transport and adhesion (reversible and irreversible) to a surface, growth and division of microorganisms (microcolony and biofilm formation), and detachment (Christensen, 1999; Neu and Marchall, 1990; and Percival *et al.*, 2000).

2.2.4.1 Conditioning Layer

A conditioning layer is formed when clean surfaces are exposed to solutions, and interaction between these surfaces and soluble nutrients occur (Percival *et al.*, 2000). The resulting conditioning layer, subsequently, can alter the surface chemistry and change interactions with other molecules and microorganisms (Neu and Marchall, 1990; and Percival *et al.*, 2000).

Percival *et al.* (2000) reported that conditioning "films" of between 30 nm to 80 nm developed after 15 minutes of exposure have been developed, and the researcher also concluded that a conditioning film would most likely exist before microbial

attachment occurs. Conditioning layers change the surface physico-chemical properties usually due to the adsorption of humic substances, polysaccharides, proteins and glycoproteins, which can act as a nutrient source and supply required metal trace elements (Ridgway, 1987; Christensen, 1999; Vrouwenvelder, *et al.*, 2000). Conditioning layers can also suppress the release of toxic metal ions and adsorb/detoxify dissolved inhibitory substances (Percival *et al.*, 2000). Additionally, a conditioning layer can have a serious impact on the initial type and structure of the biofilm, but will not determine its final structure (Boland *et al.*, 2000).

2.2.4.2 Microbial Transport and Adhesion

Basically, microbial transport depends on flow regimes and involves the transport of the microorganisms from the bulk solution to a surface "membrane", which involves mass transport. Microbial mass transport is influenced by many parameters which include: flow regime (laminar or turbulent), thermal effects, gravity effects (differential settling and sedimentation), surface characteristics, and/or intrinsic motility (presence of flagella) (Boland *et al.*, 2000; Percival *et al.*, 2000). Once at a surface, adhesion may be reversible or progress to an irreversible state. The former occurs instantaneously while the later is time dependent, and relies on the molecular and cellular elements present in the system (Christensen, 1999; Vrouwenvelder, *et al.*, 2000; Oliveira, 1992)

2.2.4.3 Biofilm Maturation

Following microbial adsorption to a surface, a certain concentration (sometimes termed a quorum) is reached, where biofilm development starts to occur. This process is governed by several parameters, including, environmental conditions, nutrient availability, surface characteristics, and system hydrodynamics. Several studies have supported the hypothesis that the formation and differentiation of biofilms involved the activation of several genes that are not expressed when cells exist in a planktonic state (Jing *et al.*, 2000; Kievit, 2001). The activation of these genes was believed cell-density dependent and based on cell-to-cell chemical signalling, also termed "quorum sensing" (Jing *et al.*, 2000; Kievit, 2001). Daves, *et al.* (1998) reported that in bench-scale experiments, mutant strains of *Pseudomonas*

aeruginosa lacking one of the quorum sensing systems, formed flatter and undifferentiated biofilms, compared to those formed by a wild-type quorum-competent strain, and were sensitive to the surfactant sodium dodecyl sulphate.

A halogenated furanone was reported to interfere with quorum sensing in *Pseudomonas aeruginosa* at relatively low concentrations (e.g. <1 mg l^{-1}). The presence of this compound did not affect the initial surface attachment; however, it affected the tri-dimensional architecture of the biofilm and increased the bacterial detachment rates from the surface area (Hentzer *et al.*, 2000). In another study, Nys *et al* (1995) reported that halogenated furanones isolated from *Delisea pulchra* significantly inhibited fouling of three major types of organisms, including a marine bacteria (strain SW8), an algae (*Ulva lactuca*) and invertebrate (*Balanus amphitrite*).

Many researchers have reported that Extra-cellular polysaccharide (EPS) production is one of the key factors in biofilm development. (Bachmann and Edyvean, 2006; Flemming, 1997; Baker and Dudley, 1998; Christensen, 1999; and Percival *et al.*, 2000; Vrouwenvelder, *et al.*, 2000; Hentzer *et al.*, 2000; Jing *et al.*, 2000; Kievit, 2001). Biofilms usually contain one or two of the most common saccharides (e.g. D-Glucose, D-Galactose, D-Mannose, Glucosamine, L-Fucose, L-Rhamnose, D-Glucoronic acid, and D-Galacturonic acid) polymerised into a heterogenous matrix (Christensen, 1999).

As the biofilm develops, cells become closer to each other, and this may lead to synergistic interaction among the different microorganisms that start acting in consortium (Percival *et al.*, 2000; Marchall *et al.*, 1994). Finally, this growth results in a complex heterogeneous tri-dimensional structure of cell clusters and organic/inorganic particulate matter and molecules embedded in an EPS matrix. The resulting structures may vary in shape from cylinders, filaments, and mushroom-like structures, and are separated by water channels that allow nutrients and waste products to flow in and out of the biofilm, respectively. Biofilm, in membrane systems, range in thickness from 10 to 100 μm. This thickness is different from one

system to another and is determined by environmental conditions and the degree of shear the system is exposed to (Flemming *et al.*, 1994).

2.2.4.4 Microbial Detachment

Although biofilm attachment mechanisms have been studied by many researchers, microbial detachment from biofilms has only been studied by a few researchers (Percival *et al.*, 2000; More *et al.*, 2000; Stoodley *et al.*, 2001), and this phenomenon is still considered poorly understood. Microbial detachment can result from erosion (single cells), abrasion (due to shear), sloughing (cell clusters), predation, human intervention and self-preservation (Bachmann and Edyvean, 2006; Percival *et al.*, 2000; Moore et al., 2000).

Bacteria have evolved a series of strategies that ensure the release of cells into solution. This mechanism is thought to be part of a survival strategy in which detachment from a depleted surface allows the search and colonisation of new available habitats (Marchall *et al.*, 1994; Stoodley *et al.*, 2001). More *et al.* (2000) summarised the factors known to affect detachment in water systems, which include: environmental parameters (pH, temperature, nutrients and macromolecules), mass transfer of nutrients to the biofilm, growth phase and flow regime (More *et al.*, 2000). Understanding this phenomenon, however, is very important in order to model biofilm behaviour and to avoid public health problems (such as contamination of water distribution systems) that occur due to clusters of microorganisms being randomly released at relatively high concentrations (Stoodley *et al.*, 2001; More *et al.*, 2000, Flemming, 1997; Baker and Dudley, 1998; Christensen, 1999; Percival *et al.*, 2000; Vrouwenvelder, *et al.*, 2000; Hentzer *et al.*, 2000; Jing *et al.*, 2000; Kievit, 2001).

2.2.5 Effects of Biofouling on Membrane Processes

The formation of biofilm on the membrane surface can be a secondary membrane that participates in the separation process. However, biofilm formation in membrane systems leads to the formation of a gel matrix (e.g. a thin film of the deposited particles on the membrane surface, Figure 2.17), which over a conventional mass transport, tends to increase concentration polarisation resulting in scaling problems (Baker and Dudley, 1998). Flemming (1997) summarised the consequences of biofilm development on membrane separation as follows:

(a) Increased membrane resistance by the biofilm which leads to:

- Decrease of permeate production,
- Increase of energy consumption, and
- Increase of membrane pressure drop (ΔP).

(b) Formation of gel phase between water and membrane surface leads to:

- Increase of drag resistance to tangential flow over the membrane,
- Inhibition of convectional transport next to membrane surface,
- Concentration polarisation because these is no tangential flow, and
- Decrease of salt rejection.

(c) Damage to plant and product can be by:

- Microbial attack on membrane material (e.g. cellulose acetate membranes and glue lines),
- Microbial contamination of the permeate, and
- Decrease of module lifetime due to frequent cleaning procedures.

(d) Increased costs of:

- Production loss (less permeate production),
- Product quality loss (e.g. higher salt content, microbial contamination),
- Increased energy costs,
- Increased cleaning demand, and
- Increased replacement costs.

2.2.6 Biofouling In Water Systems

The microbial component of the fouling process (biofouling) is considered as the most critical of the fouling mechanisms, because 99.9% removal of inorganic and/or organic components will extend membrane life longer than similar removals of microorganisms (Al-Ahmed *et al.*, 2000). This is due to the exponential trend in which microorganisms multiply; even small numbers of microorganisms can result in extensive biofilm growth under favourable growth conditions (Flemming, 1997). Biofouling was the most commonly reported fouling problem among reverse osmosis (RO) facilities around the world. In 1991, 58 out of 70 RO plants reported biofouling problems in the United States alone (Ridgway and Flemming, 1996). In plants operating in the Persian Gulf countries, biofouling is an extremely serious problem affecting RO membranes, likely due to high temperatures and nutrient availability in many water sources (Al-Ahmed *et al.*, 2000). Similar problems were reported for NF and RO plants operating in the Netherlands (Vrowenvelder *et al.*, 2000). Biofouling is a difficult problem to diagnose, and it is, therefore, usually assumed to have occurred when measures taken against non-biological foulants fail to produce any improvement in the treatment efficiency. Le Chevallier *et al.* (1988) reported that the inactivation of attached bacteria was not solely related to the biocide oxidising power. Monochloramines inactivate biofilm bacteria more efficiently than chlorine or chlorine dioxide, despite their lower oxidising potential. These results were attributed to the higher penetrating rates of monochloramines into biofilms, which was most likely due to their reduced reactivity with extra-cellular polysaccharides (EPS), providing for increased microbial inactivation. Contrarily, chlorine is known to react with a variety of compounds present in the biofilm matrix, which might have caused its depletion prior to significant penetration into the biofilm layer, resulting in decreased microbial inactivation. Flemming (1997) estimated that biofouling contributed to 30% of the overall operational costs of a 22,7 thousand cubic meters per day RO membrane plant treating wastewater effluent in Orange County, CA, USA.

Biofilm accumulation on a membrane, feed channel, spacer and permeate carrier is highly undesirable because it may block channels, or cause biomass build-up in

between membrane sheets (spiral wound elements). Consequently, water channelling and pressure differentials on the membrane surface may occur. The existence of these preferential paths may cause rapid localised salt accumulation and precipitation of sparingly soluble salts, aggravating fouling. Some of these salts may even contribute to stabilising the biofilm matrix such as iron oxyhydroxides which bond to EPS in the biofilm matrix (Ridgway and Flemming, 1996; Flemming *et al.*, 1994).

In addition, the formation of biofilm on membrane surfaces increases drag resistance, decreasing localised convective flow, and increases concentration polarisation. Biofilms may also provide for local supersaturated areas with crystallisation nuclei, favouring accumulation of precipitated salts in its matrix. As a result, operation and maintenance problems within membrane processes may occur with increases in flux reduction, pressure drop, increase in cleaning frequency, and permeate conductivity. Additionally, biofilms may promote existence of local pressure differentials which may eventually cause a membrane element to crack, a process also known as "telescoping" (Soffer *et al.*, 2004; Ahmed *et al.*, 2001; Flemming *et al.*, 1994; Flemming, 1997).

In summary, biofouling can be a major concern, especially for operators and owners in the Middle East countries due to the hot climate and hard quality of feed water processed (Coker and Sehn, 2000). Many researchers studied biofouling of RO membranes treating seawater and brackish waters (Coker and Sehn, 2000; Baker and Dudley, 1998; Melo and Bott, 1997; Al-Ahmad, *et al.*, 2000). Mitigation measures of biofouling effects can be carried out through two steps: prevention and/or control. Biofilm control can be achieved by either mechanical techniques or chemical methods (Melo and Bott, 1997); however, prevention can only be possible when the biofouling mechanism and its symptoms for a particular water resource are known. As mentioned earlier (Section 2.2), many researchers have carried out mechanistic analyses of biofouling in brackish waters (Al-Ahmad, *et al.*, 2000), however, biofouling of RO membranes in hypersaline water systems has not been investigated. The aim of this study was to investigate the mechanism of biofouling in RO system of hypersaline water (e.g. salinity 60,000 mg/l).

2.3 Classification of Desalination Technologies

During the last two decades, a variety of processes for desalination of brackish water and seawater have been developed and tested. However, some of these technologies have been ignored, due to their uneconomical applications (Noble and Stern, 1995). At present, desalination technologies concentrate on the following three treatment techniques:

(a) Distillation,

(b) Crystallisation, and

(c) Membrane techniques.

The principle of the classification of desalination technologies is based on phase produced (e.g. liquid to vapour, liquid to solid, or remains unchanged: liquid to liquid), Table 2.4 gives some comparative data for the main desalination processes.

Table 2.4: Characteristics of desalination processes.

Process Criterion	Multi-stage Flash Desalination	Multi Effect Desalination	Vapour Compression	Electrodialysis	Reverse Osmosis
Classification	Distillation	Distillation	Distillation	Membrane conversion	Membrane conversion
Type of Energy	Thermal	Thermal	Mechanical	Electrical	Mechanical
Quality of Raw Water (mg/l)	10,000 –100,000	10,000 –100,000	10,000 –100,000	Up to 10,000	Up to 50,000
Quality of Product Water (mg/l)	2 – 50	1 – 50	2 – 50	300 – 500	100 – 500
Energy Required (kwh/m^3)	15.17	-	50	-	8.23
Cost ($/$m^3$)	2.7	1.16	1.6	1.4/1000 gal.	0.65
Application	45,000 TDS Raw	-	-	For Brackish Water	45,000 TDS Raw Brackish water

Reproduced and updated from (Mohsen and Al-Jayyosi, 1999).

The distillation process has been used for a long time for the desalination of both seawater and brackish water. The general principle of this process is that the vapour produced when boiling saline water, which is free from minerals, is condensed to produce pure water (Scott and Hughes, 1996). There are two distillation techniques used in the desalination processes, namely multi-effect distillation (MED) and multi-

stage flash distillation (MSF). Table 2.5 summarises the advantages and disadvantages of each desalination technique.

Table 2.5: Advantages and disadvantages of various desalination processes.

Method of desalination	Advantages	Disadvantages
Multi-effect distillation (MED)	-High production capacity -Low capital cost -High purity (<30ppm) -Minimal skilled operator	-Dependence of output on local power availability -Long construction period -Difficult to control water quality -Low conversion of feed water (30%-40%) -Labour intensive -Large space and material requirements
Multi-stage flash distillation (MSF)	-Flexibility in salinity of fed water -High purity production (<30 ppm) -High capacity production -Low skill requirement -Production of both water and electricity -Low energy input	-Labour-intensive -Low conversion ratio (30%-40%) -Requires pretreatment of feed water -High operating cost -High construction requirements -Limited potential for improvement
Reverse osmosis (RO)	-Suitable for both seawater and brackish water -Flexibility in water quality and quantity -Low power requirement compared with MED and VC -Flexibility in site location -Flexibility in operation start-up and shut-off -Simple operation	-Low quality production (250-500 ppm) -Requires high quality fed water -Relatively high capital and operating costs -High pressure requirements -Long construction time for large plants
Vapour compression (VC)	-High water quality (20 ppm) -High operational load -Short construction period -Small space requirements -Operation and production flexibility	-High operational cost -High energy consumption -Lack of water quality control
Electrodialysis (ED)	-Low operating and capital cost -Flexible energy source -High conversion ratio (80%) -Low energy consumption -Low space and material requirements	-Low to medium brackish water capacity (3000 ppm) -Requires careful pretreatment of feed water -Low production capacity -Purity affected by quality of feed water

Source: Mohsen and Al-Jayyousi, 1999.

During crystallisation, a phase transition from liquid to solid occurs. The ice crystals (freezing process) produced contain only pure water and no mineral salts, so that fresh water is produced when melting the crystals (Noble and Stern, 1995).

In membrane separation techniques, desalination of saline water occurs without any phase transition, in which membranes are employed to produce fresh water. Membrane desalination techniques include reverse osmosis (RO) and electrodialysis (ED).

2.3.1 Membrane Separation Techniques

A membrane may be defined as a "permselective barrier between two homogenous phases" (Mulder, 1996) and can be biological or synthetic in nature. Biological membranes are extremely selective and energy efficient, allowing cells to take up nutrients and excrete waste products, while maintaining their integrity. Synthetic membranes are less complex in nature, less selective and efficient, but more chemically/physically resistant. Membranes can be made of various materials (ceramics, polymers, metals, glass, and liquids); can be symmetric or asymmetric, and can vary in thickness from a fraction of a micrometer to several millimetres.

Membranes used in water treatment processes are pressure driven, and fall into four general classes based on the size and range of the components they are able to reject: microfiltration (MF), ultrafiltration (UF), nanofiltration (NF), and reverse osmosis (RO) (Bilstad, 1997). Table 2.6 shows the general membrane classes as well as applications and competing water treatment processes.

The operation mechanism of the first three techniques (i.e. MF, UF & NF) is to separate molecules according to their size and molecular mass, thus the membranes used are generally defined by their cut-off threshold. Because salt molecules are relatively small (e.g.< 0.001 μm), they can only be captured by RO membranes. Figure 2.5 shows the relationship between each membrane class, the associated molecular weight cut off (MWCO), and molecular sizes of the compounds that they are able to be rejected. MWCO was here defined as the molecular weight of a spherical molecule that is rejected at 90% efficiency (Van der Bruggen *et al.*, 1999), while molecular size is based on the actual size of the molecule.

Table 2.6: Membrane processes applications and comparable water process (AWWARF, 1999; Schafer, 2001; Strathman, 2000).

Membrane Separation Technology	Substances Removed	Comparable Traditional Water Treatment Methods
Microfiltration	Bacteria and larger colloids: separation of precipitates and coagulates	Ozonation-UV radiation, chlorination, coagulation-sedimentation, sand filtration.
Ultrafiltration	All of the above, plus viruses, high molecular weight proteins, organics and pyrogens.	Sand filtration, biotreatment, and activated carbon adsorption.
Nanofiltration	All of the above, plus divalent ions, larger monovalent ions, colour and odour agents, and natural organic matter (NOM).	Lime-soda softening and ion exchange, coagulation-sedimentation, biotreatment, and activated carbon adsorption.
Reverse Osmosis	All of the above, plus monovalent ions.	Distillation and ion exchange.
Electrodialysis/ Electrodialysis Reversal	Dissolved ions.	Ion exchange.

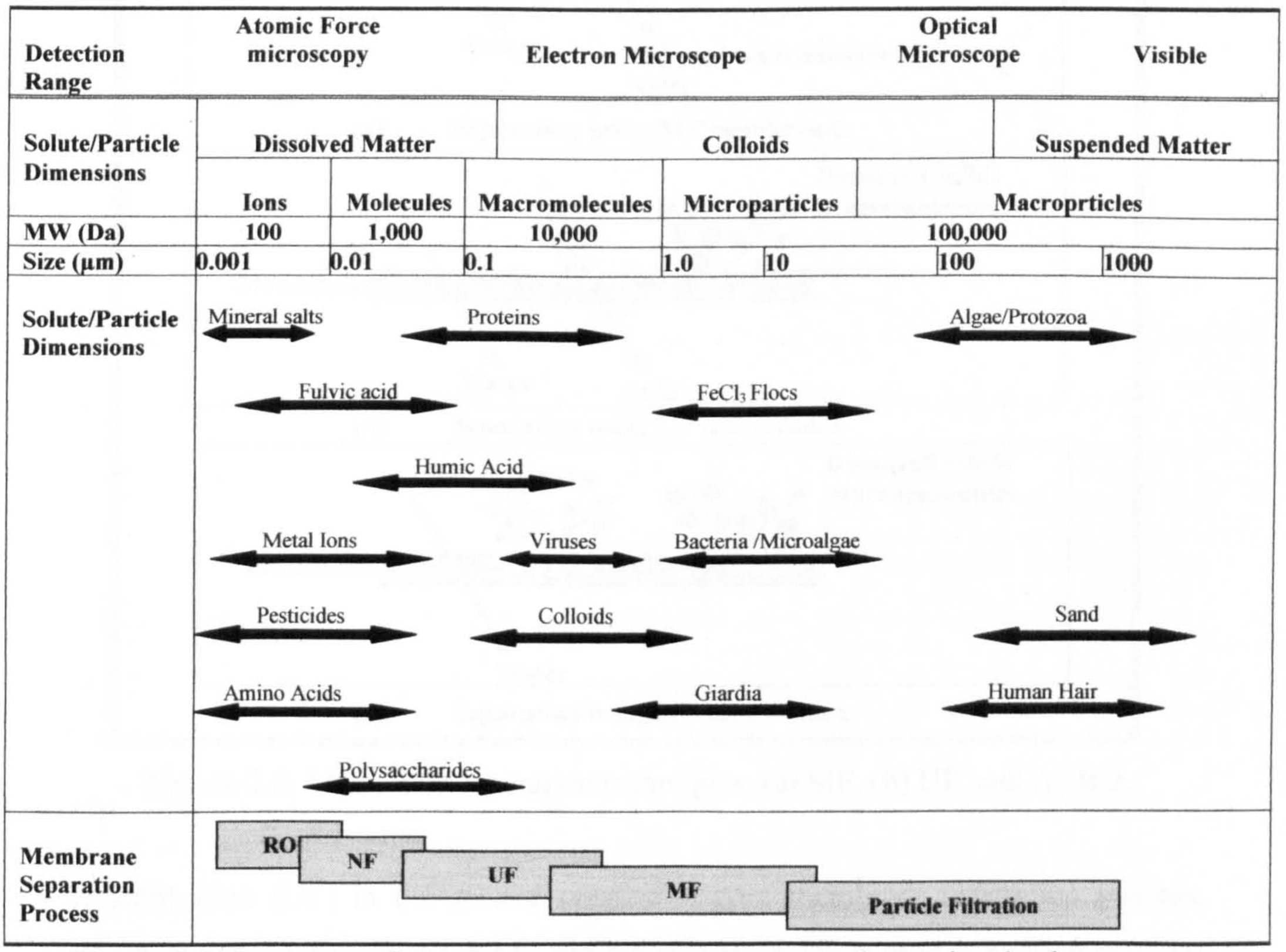

Figure 2.5: Summary of membrane treatment processes and associated solute rejection ranges *(Adopted from Schafer, 2001)*

In membrane microfiltration (MF), the filter is generally made of a thin polymer film with a uniform pore size (0.1μm – 5μm) and high pore density (~ 80%). MF membranes are primarily used to remove turbidity and bacteria, and can serve as a pre-treatment for NF and RO processes. The principle of the MF membrane separation process is shown in Figure 2.6a, which is characterised as a purely physical sieving process (Scott and Hughes, 1996). Due to the high pore density of MF membranes, the later are capable of producing high flow rates of filtrate at modest operating differential pressure of up to 2 bar.

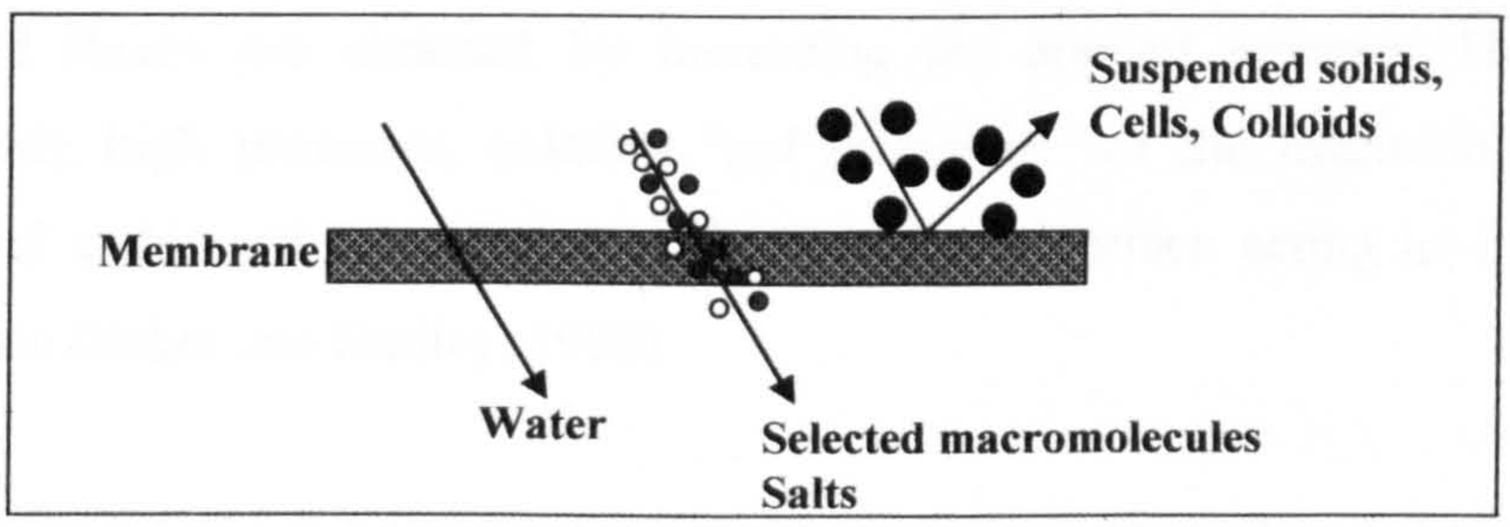

(a) Separation using MF membranes.

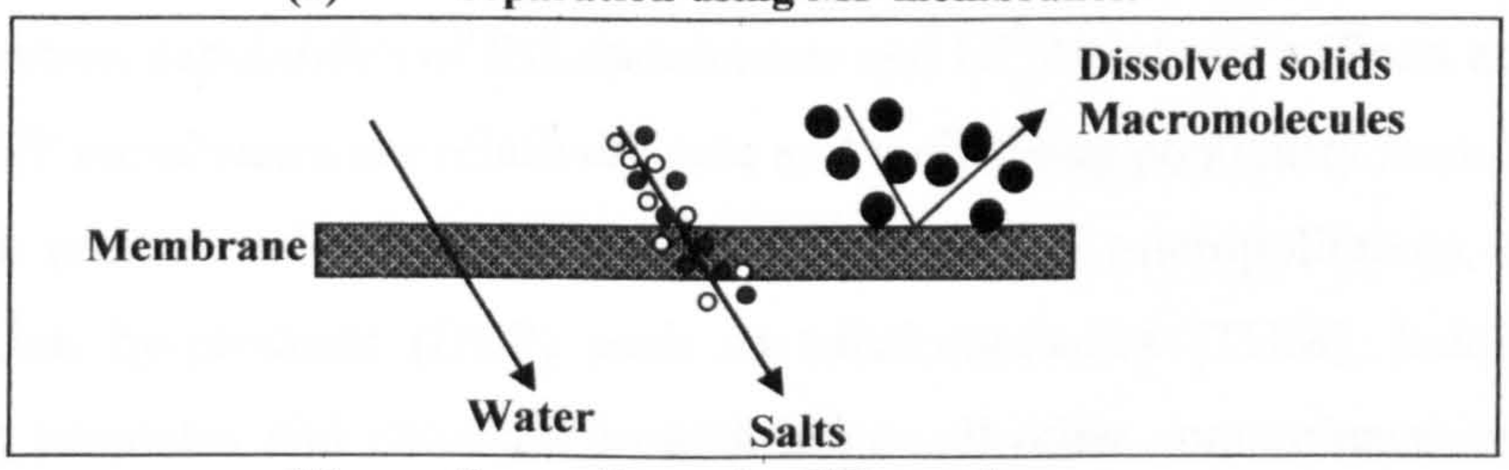

(b) Separation using UF membranes.

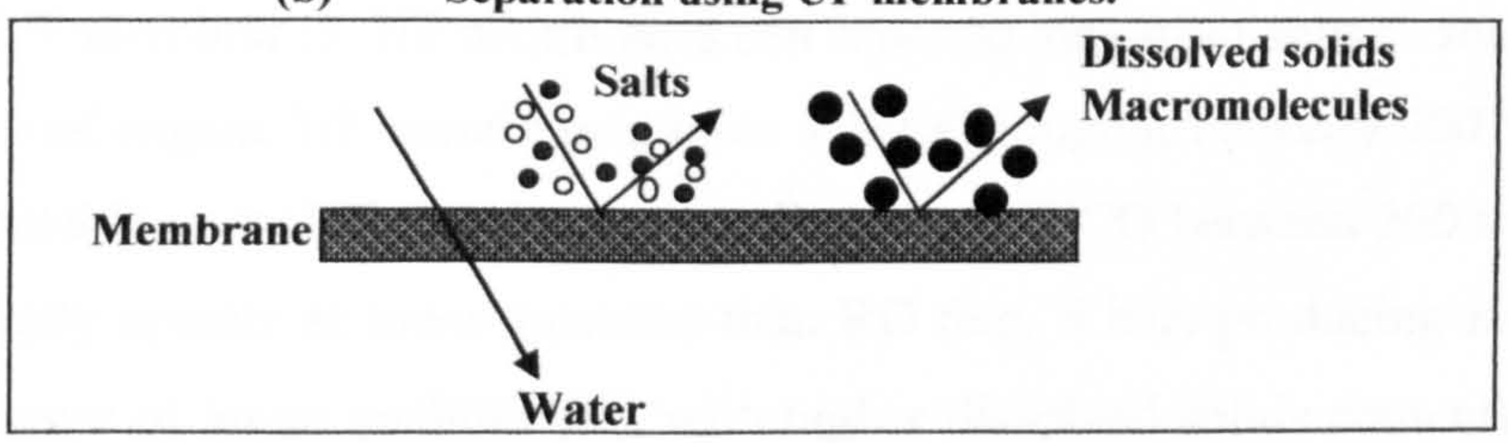

(c) Separation using RO membranes.

Figure 2.6: Membrane separation techniques: (a) MF, (b) UF, and (c) RO.

Ultrafiltration (UF) is the second pressure driven membrane separation process, which covers a region between MF and NF processes. UF is used to remove particles in the size range 0.001μm – 0.02μm. Figure 2.6b shows the solvents and salts of low

molecular weights will pass though these membranes whilst larger molecules are retained (Scott and Hughes, 1996). UF membranes are permeable to molecules, which have molar masses of ≤ 1000 Dalton (Da) and thus exhibit low rejection of salts. Due to their porous matrix, UF membranes cover a wide range of MWCO (from 1,000 Da to >50,000 Da), and are become increasingly popular due to their ability to remove turbidity and viruses. UF membranes with MWCO close to 1,000 Da can be used to remove some organic matter from water resources (Jackangelo *et al.*, 1997). UF membranes are employed under a differential pressure ranging from 1 bar – 7 bar (Noble and Stern, 1995). Similar to MF membranes, the separation mechanism of UF membranes is considered as a physical sieving action, in which increased fluxes are obtained by increasing the applied pressure. However, at sufficiently high pressures, gelation "*gel formation*" of the macromolecules can occur and a thin gel layer forms at the membrane surface acting as a secondary membrane (Baker and Dudley, 1998).

Nanofiltration (NF) is another pressure-driven process applied to the area between the separation capabilities of RO membranes and UF membranes (Scott and Hughes, 1996). NF membranes are relatively new and their rising popularity stems from their ability to remove calcium and magnesium (hardness), micropollutants, colour and disinfection by-products (DBP) such as trihalomethanes (THM), haloacetic acid (HAA5), bromates and chlorites, in addition to all other contaminants removed by MF and UF membranes. NF membranes can separate ions from solutes such as small molecules of sugars. NF membranes have MWCO ranging between 200 Da to 800 Da (for potable water NF membranes usually have MWCO between 200 to 400 Da); and typically operate at lower pressure than RO (e.g. 5 bar) producing higher flow rates of water of lower qualities (i.e. with higher dissolved solids content) than that for RO. The application of NF membranes is ideal when high sodium rejection is not needed, but where other salts such as Mg and Ca (i.e. divalent ions) are to be efficiently removed. The cut-off threshold of NF membranes is 200 (MW), and the typical salt rejections at specific conditions (e.g. 5 bar, 2000 mg l^{-1} solute) are 60% for NaCl, 80% for $CaHCO_3$ and 98% for $MgSO_4$, glucose and sucrose (Scott and Hughes, 1996).

Another membrane desalination process is reverse osmosis (RO). The operating mechanism of reverse osmosis membranes is quite different from MF and UF membranes, (Figure 2.6c). RO membranes use a solubilisation-diffusion technique, making use of a semipermeable membrane, which acts as a barrier to all dissolved salts and inorganic molecules, as well as organic molecules with molecular weights greater than 100 Daltons (Da). Unlike MF and UF membranes, RO membranes have no true pores (Scott and Hughes, 1996).

2.3.2 Types of Membrane Materials

Membranes can be classified according to the materials which are used in manufacturing them, which include cellulose acetate membranes, aromatic polyamide membranes, and thin film composites (Scott and Hughes, 1996).

2.3.2.1 Cellulose Acetate

This category of membranes is manufactured using a cast from cellulose diacetate and cellulose triacetate formulations (Mulder, 1996). Cellulose acetate (CA) membranes have poor chemical stability and tend to hydrolyse over time depending on the operating conditions (i.e. temperature and pH). These membranes have relatively low temperature range (e.g. 0°C to 30°C) and an acidic range (pH 4.0 to pH 6.5). CA membranes are very prone to biological attack (Baker and Dudley, 1998), and hence they show poor performance in water desalination applications. Additionally, and because of their poor chemical stability (El-Saied *et al.*, 2003), these membranes are incapable of withstanding continuous exposure to low levels of biocides (e.g. antifoulants). Due to their poor stability, these membranes tend to decrease in their sensitivity to salt rejection over time. However, CA membranes are still very popular due to their availability and low cost.

2.3.2.2 Aromatic Polyamide (Aramide)

This category of membranes was firstly produced in hollow fine fibre foam, which was produced by solution spinning (Mulder, 1996). The structure of these membranes consists of two layers, a thick outer porous fibre supporting structure of approximately 26 μm thick attached to a dense skin inner film of about 0.1μm to 1.0

μm thick which is responsible for the filtration process. Salt rejection takes place on the dense layer, which is enhanced by post-treating the fibres with polyvinyl methyl ether for brackish waters and polyvinyl methyl ether and tannic acid for seawater applications.

Unlike CA membranes, aramide membranes are highly chemically stable, and can be operated continuously in the temperature range from 0 °C to 35 °C and a pH range from 4 to 11. Aramide membranes are also characterised by their resistance to biological attack (Baker and Dudley, 1998). However, continuous exposure to chlorinated waters by these membranes can cause serious damage to their structures, and thus it is highly recommended to dechlorinate feed waters applied to these membranes (Bilstad, 1997; Baker and Dudley, 1998; Coker and Sehn, 2000).

2.3.2.3 Thin Film Composites

This category of membranes has been produced recently by many different manufacturers. In the mid-1970s, *Fluid Systems Division of Universal Oil Products* (FSDUOP) commercially introduced its TFC® (Thin Film Composite) membranes. *Film Tec Inc.* then introduced its FT-30 composite membranes in the early 1980s. These types of membranes are manufactured by forming an ultra-thin barrier layer (e.g. 0.2 μm) on the surface of a micro-porous polysulfone which has been cast onto a porous fabric supporting layer (Mulder, 1996) as seen in Figure 2.7. The barrier layer on the polysulfone is created by *in-situ* interfacial polymerisation techniques with polyamides or polyureas. This category of membranes has several advantageous

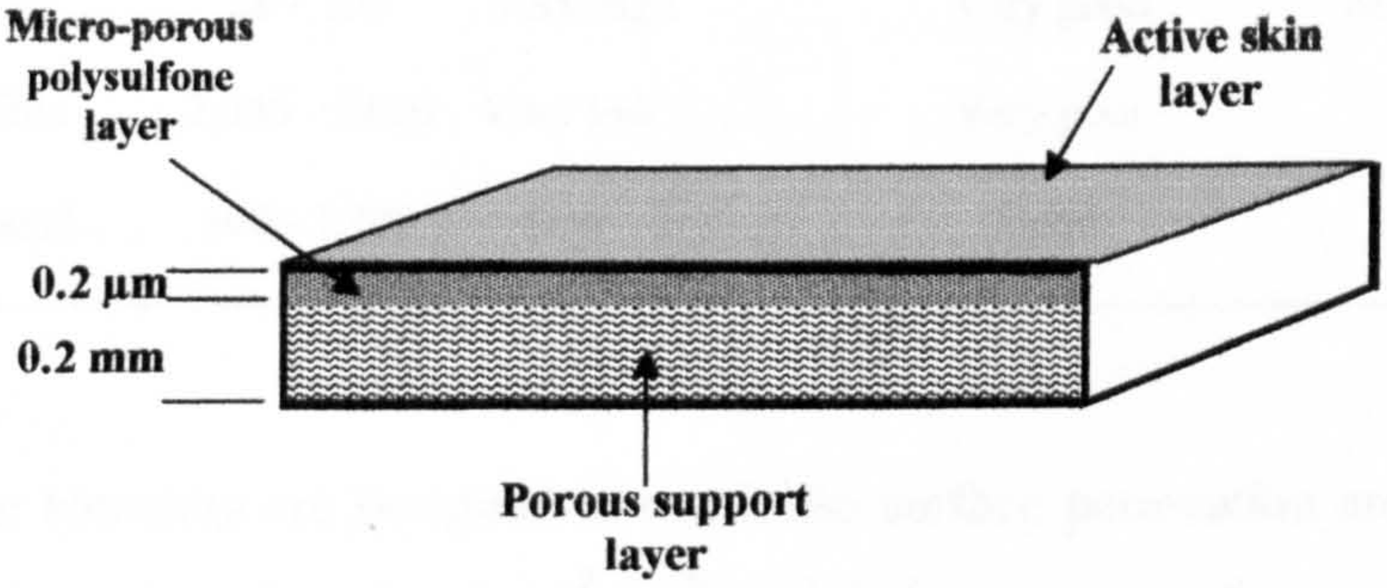

Figure 2.7: A schematic diagram of thin film composite membrane.

features over other membrane types (Mulder, 1996). TFC membranes have higher chemical stability; capable of delivering higher fluxes, have higher salt rejection at moderate pressures, and can provide greater resistance to biological attack (Baker and Dudley, 1998). Additionally, these membranes can be operated at a wider range of operating conditions (e.g. temperature from 0°C to 40°C and pH from 2 to 12). However, these membranes are sensitive to chlorine and other oxidants (Madaeni *et al.*, 2001).

2.3.3 Membrane Configurations

Commonly, the term "membrane" is used to describe the whole membrane assembly which consists of a membrane sheet, a membrane support, flow distribution channels, feed inlets, brine and permeate outlets, and pressure vessels (Noble and Stern, 1995). Reverse osmosis (RO) membranes are commercially available in spiral wound and hollow fibre configurations; however, they are also available in a narrow range in tubular and plate and frame configurations (Noble and Stern, 1995; Scott and Hughes, 1996). Table 2.7 lists some advantages and disadvantages associated with each class.

Table 2.7: Costs and major applications of commercially available membrane modules (Strathman, 2000).

Membrane	Area/Volume ($m^2\ m^{-3}$)	Relative Costs	Control of Concentration Polarisation	Applications
Plate-and-Frame	400 - 800	Medium	Good	MF, UF, NF, RO
Tubular	20 - 100	Very high	Very good	MF, UF, NF, RO
Hollow-Fibre	2,000 - 5,000	Very low	Very poor	RO
Spiral Wound	800 - 1,200	Low	Good	UF, NF, RO

Membrane elements are designed to maximise surface permeation area (membrane surface area per unit volume; $m^2\ m^{-3}$), minimise concentration polarisation (by promoting turbulent conditions in the membrane element) and avoid contamination

between the feed and the permeate streams (Mulder, 1996). In addition, they should be easy to clean, easy to assemble and disassemble and have a low "hold-up" volume (Strathman, 2000).

2.3.3.1 Spiral Wound Module

Figure 2.8 shows a schematic diagram of a spiral wound module. This membrane configuration is the most widely used module for brackish water and seawater desalination applications (Mulder, 1996). These modules have been subjected to numerous improvements since their development in the mid-1960s.

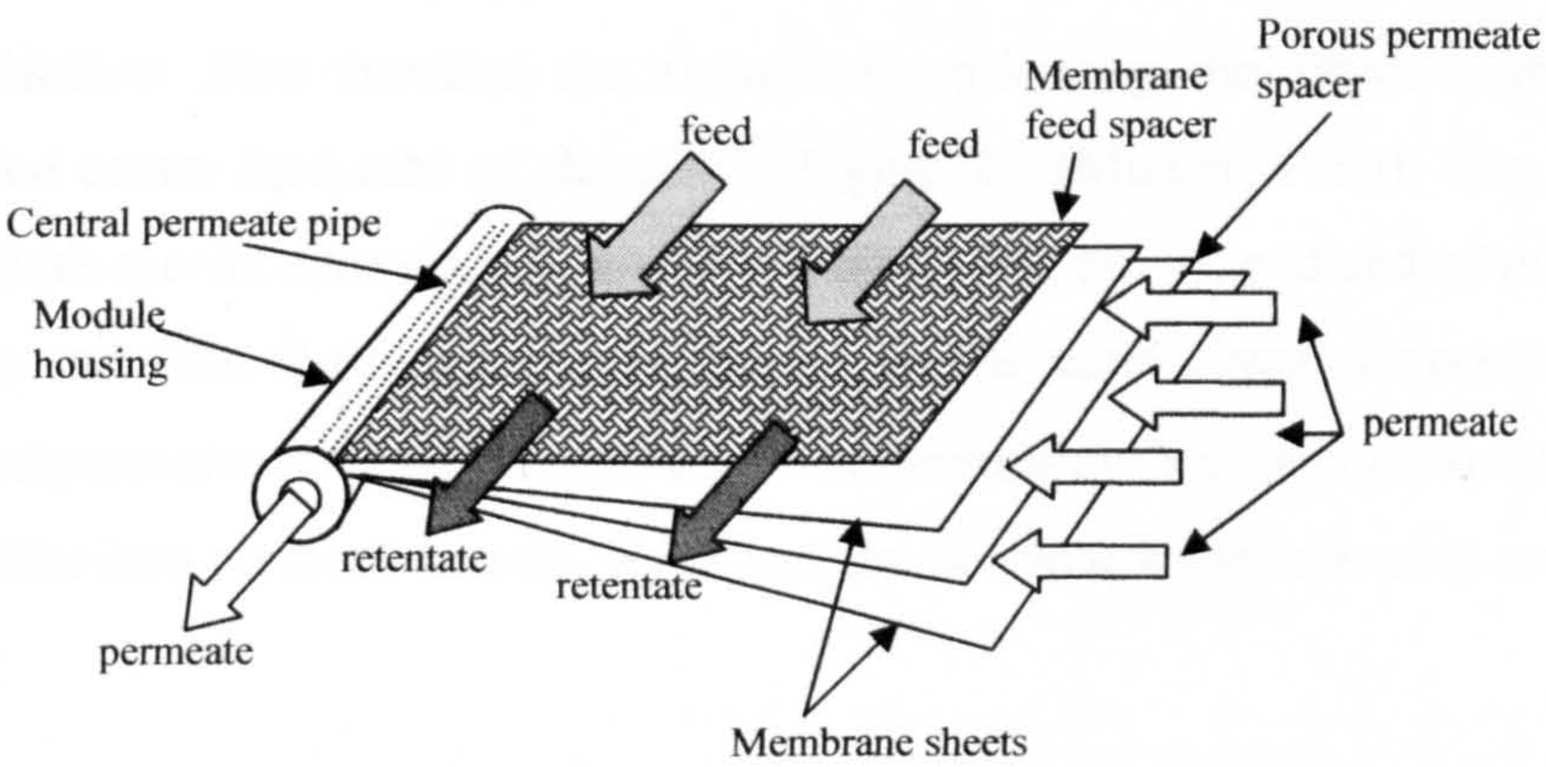

Figure 2.8: Schematic drawing of a spiral-wound module (Geesey, 1987).

These modifications have included increasing applied pressures, improving feed channels and spacer design, and applying improved seals and adhesives (Scott and Hughes, 1996). Originally, the typical spiral wound devices use cellulose acetate membranes, however, today other materials such as cellulose triacetate and polyamide/polysulfone composites are also used (Scott and Hughes, 1996; Sheikholeslami, 1999). Spiral membranes have a lesser tendency towards concentration polarisation than fibre membranes due to the greater control of membrane module design. The aim is to maintain high fluid flow parallel to the membrane surface to promote mixing at the membrane surface to minimise the boundary layer thickness. In spiral-wound modules, the presence of concentrate

spacers helps to create more turbulence of the solution at the concentrate side, and thus reduces the effects of polarisation (Song and Yu, 1999; Al-Bastaki and Abbas, 1999a).

The operation of an individual spiral wound element usually provides 8 to 10% recovery. However, 4 to 7 elements can be connected in series in a single pressure vessel in order to achieve 50% recovery (Baker and Dudley, 1998). The desired system capacity and recovery are achieved by connecting pressure vessels either in series or in parallel and reject staging (e.g. vessels are connected in series and in parallel), as shown in Figures 2.10a and 2.10b.

2.3.3.2 Hollow Fibre Module

Hollow fibre bundles are formed by orienting the fibres parallel to a perforated centre feed tube as showed in Figure 2.9 (Mulder, 1996). The fibres are treated with special epoxy resins to create a tube sheet on one end and a "nub" on the opposite end. The O-ring groove is formed on the sheet circumference to prevent brine and permeate streams from mixing. The permeators are assembled by inserting the bundles into pressure vessels. However, the pressure vessel can only contain one bundle.

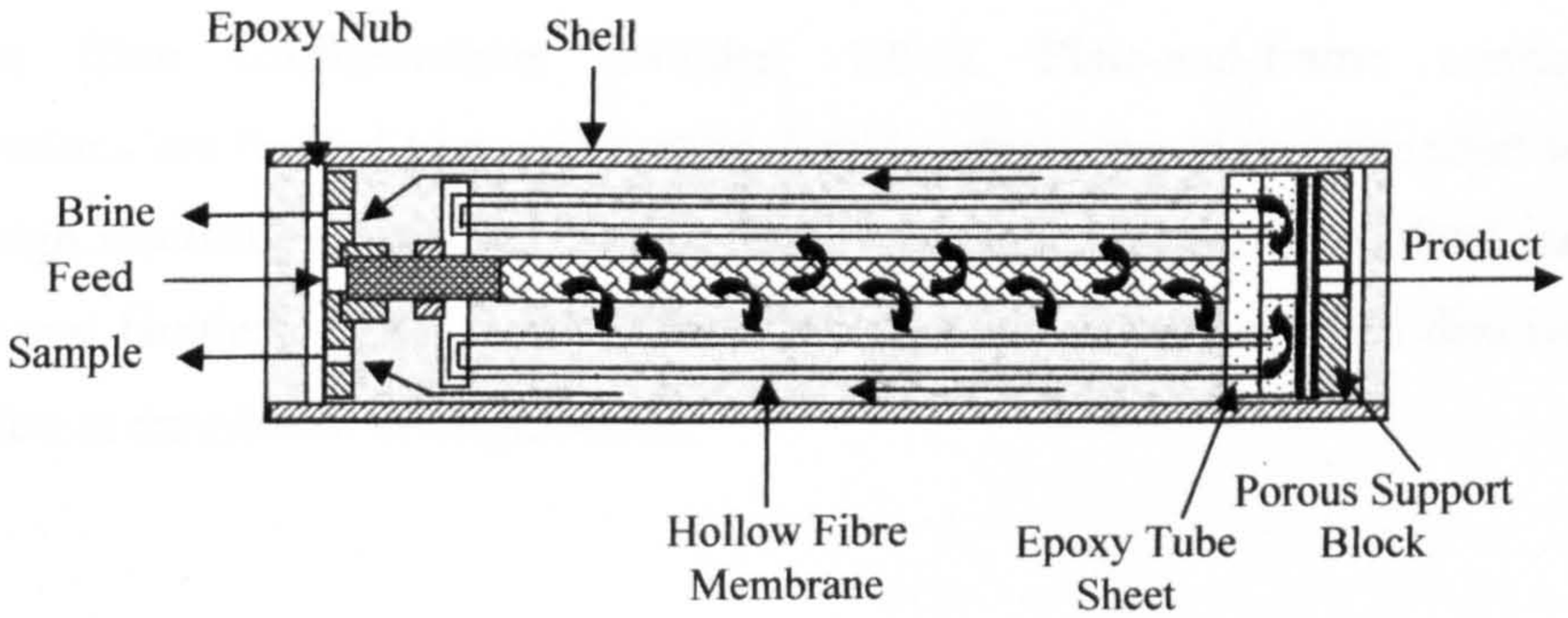

Figure 2.9: Schematic drawing of a hollow fibre device (Geesey, 1987).

The hollow fibre device can be operated by intruding the pressurised feed into the centre tube. Then the centre tube distributes the feed along the outer surface of the permeator followed by feed flow outward of the fibres. The permeate exits the device at low pressure however, the reject (brine) leaves the device at a minimal pressure drop which makes it available to feed successive stages for additional recovery requirements. Individual hollow fibre permeator provides 50% recovery in brackish water applications (Heitmann, 1990). It is possible to operate hollow fibre modules with the feed flowing inside the fibres and the permeate flowing outside the fibres.

2.3.3.3 Tubular Configuration

Currently, tubular configuration devices are very limited in water desalting applications (Mulder, 1996). Water desalters prefer using spiral wound or hollow fibre membranes because they have higher surface area to volume ratios, provide better recovery performance, and are comparatively cheaper. However, tubular membrane devices are still used for water streams with high suspended solids such as waste streams and industrial wastes for food production, as in dewatering of dairy products (Bilstad, 1997).

2.3.3.4 Plate and Frame

Similarly, plate-and-frame membranes are very limited in desalination applications due to high cost and lower recovery rates compared to spiral wound and hollow fibre configurations (Mulder, 1996). Plate-and-frame configuration applications are limited to concentrating liquids containing high suspended solids or with high viscosities, especially in the food, beverage, and pharmaceutical industries (Scott and Hughes, 1996). Table 2.6 summarises the advantages and disadvantages of different membrane configurations.

Table 2.8: Advantages and disadvantages of various membrane configurations.

Membrane Configuration	Advantages	Disadvantages	References
Spiral wound	• Good resistance to fouling, • Easy to clean, • Easy field replacement, • Available in a wide variety of membrane materials, • Available from several manufacturers.	• Moderate membrane surface area/volume ratio, • Some tendency for concentration polarisation, • Difficult to troubleshoot, • Difficult to achieve high recoveries in small systems.	Mulder, 1996; Scott and Hughes, 1996; Sheikholeslami, 1999; Song and Yu, 1999; Al-Bastaki and Abbas, 1999a.
Hollow fibre	• High membrane surface area/volume ratio, • High recovery in individual permeator, • Easy to troubleshoot, • Easy to change bundles in-situ.	• Sensitive to colloidal fouling, • Limited number of manufacturers and membrane materials.	Mulder, 1996; Heitmann, 1990; Geesey, 1987.
Tubular	• Large well-defined flow passages, • Can achieve high flow velocities, • Low tendency to foul, • Easy to clean, • Membranes can be removed and reformed, • Can operate at very high pressures.	• Very low membrane surface/volume ratio, • Comparatively expensive, • Minimal choice of membrane materials.	Mulder, 1996; Bilstad, 1997.
Plate and frame	• Open flow channels • Low tendency to foul, • Easy to disassemble for cleaning and membrane replacement, • Can use several membrane types.	• Low membrane surface area/volume ratio, • Potential for leaks between leaves, • Comparatively expensive.	Mulder, 1996; Bilstad, 1997

2.3.4 Membrane Recovery

The basis of membrane separation processes is illustrated in Figure 2.10. The feed stream is forced through a membrane and divided into a permeate stream, containing species that pass through the membrane, and a concentrate stream, containing all the rejected species (Figure 2.10a). This separation depends on the membrane characteristics, solution chemistry, and environmental conditions (Scott and Hughes 1996).

The typical recovery of each membrane element is less than 15%, which is poor in terms of overall process efficiency. In order to increase the overall recovery of a system to levels between 70-90%, membrane processes are typically staged (Figure

2.10b). A stage consists of several pressure vessels in parallel (each pressure vessel housing two to six elements), in which the concentrate of the up-stream stage is fed to the downstream stage, where additional permeation occurs. As filtration progresses, fewer membrane elements are needed in each stage, because the permeate flow is collected from the previous stages, less volume remains to be filtered. Finally, at the end of a staged array the different permeate streams are combined into one main stream. Recently, the combination of low pressure membranes (MF and UF) with high pressure membranes (NF and RO), termed an

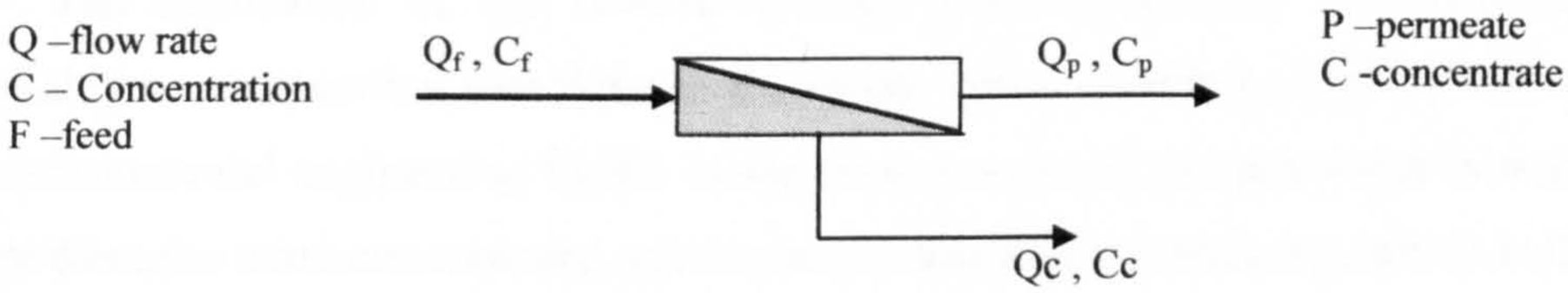

System recovery -10%-15%

(a) Module schematic

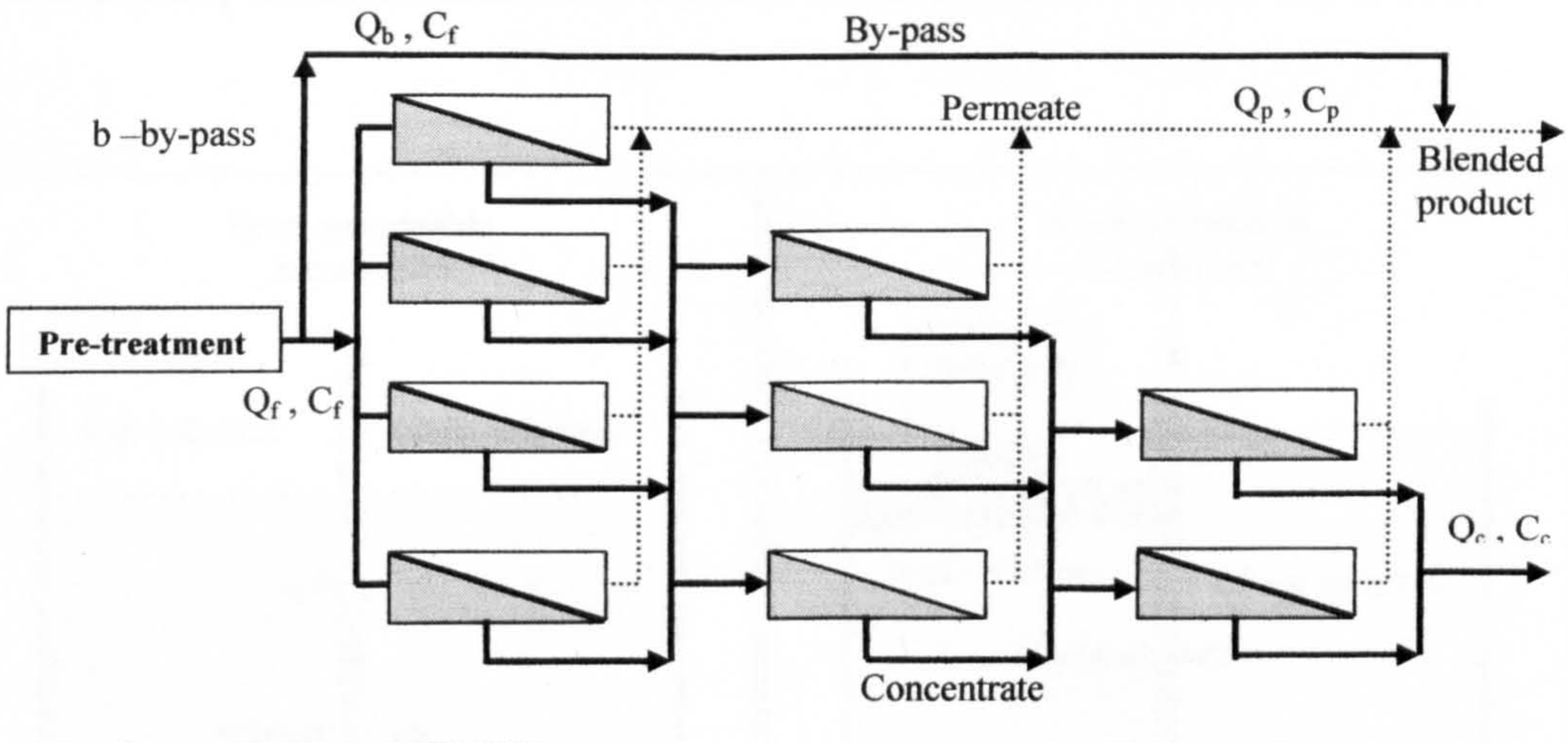

System recovery -70%-90%

(b) Full-scale membrane elements staged array

Figure 2.10: Membrane separation process schematic: a) module schematic, and b) membrane staged array.

integrated membrane system, has been used as an alternative to conventional treatment. The initial set of membranes operate as a microorganism and particulate matter filter (which in conventional processes would require coagulation/flocculation, settling and filtration), relieving the downstream NF/RO membranes of particulate load, and maximising process efficiency in terms of organic matter removal and costs (Kruithof *et al.*, 2001; Van der Bruggen *et al.*, 1999).

2.4 Reverse Osmosis Theory

The application of the reverse osmosis (RO) technology has increased remarkably as a separation technique in the recent years, especially in the chemical and environmental engineering fields. In the reverse osmosis process water is made to pass from the more concentrated solution to the less concentrated one, which is the reverse of the principle of osmosis (Figure 2.11). The force necessary to accomplish this is the application of pressure greater than the osmotic pressure of the saline solution (Scott and Hughes, 1996). When this saline solution, which is in contact with a semi-permeable membrane, is placed under pressure in excess of the osmotic

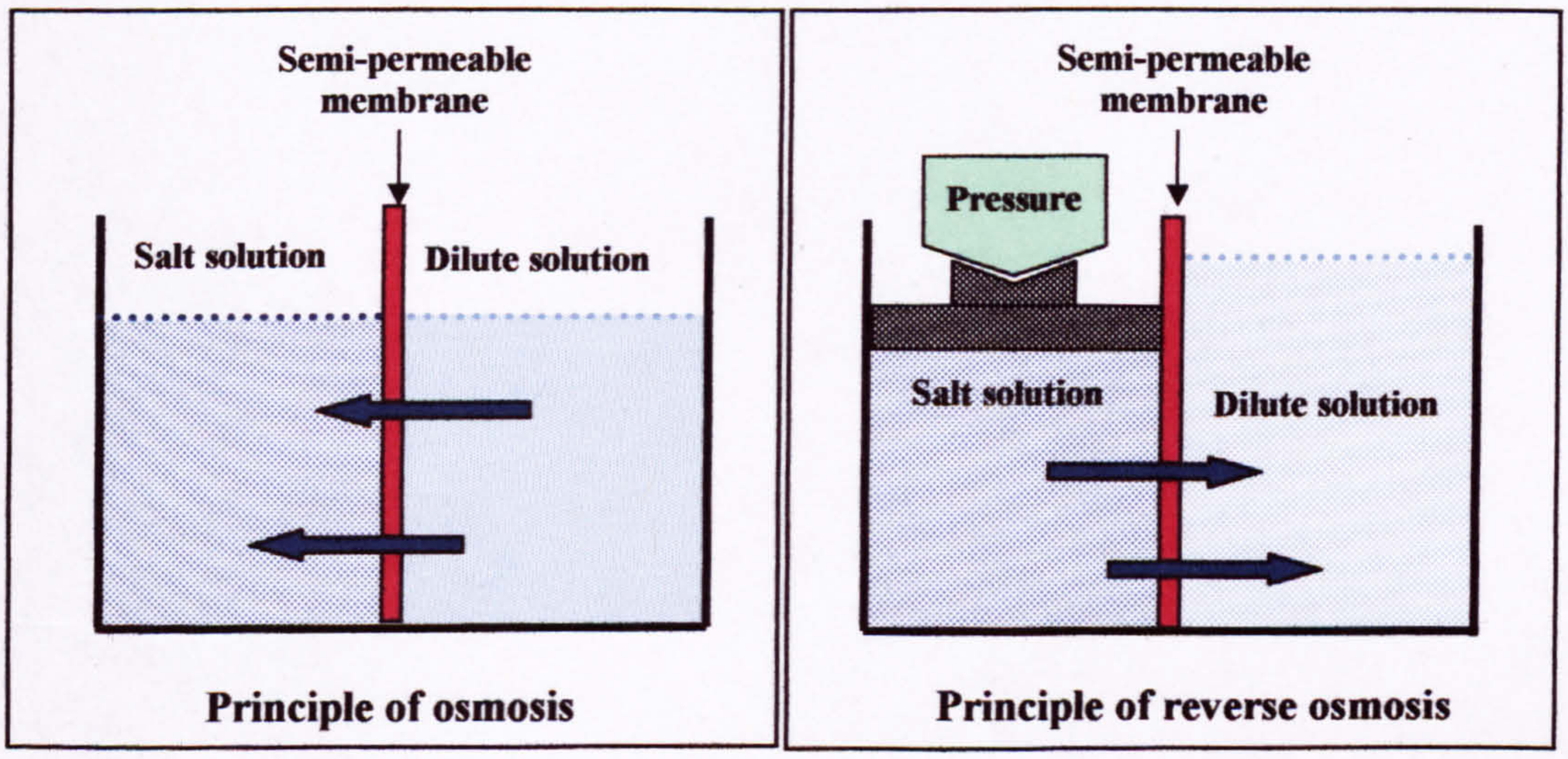

Figure 2.11: Principles of osmosis and reverse osmosis.

pressure of that solution, water from the saline solution will flow through the membrane. Water flow will continue until the pressure created by the osmotic head equals the osmotic pressure of the saline solution (Heitmann, 1990).

The driving force for the water transport across the membrane is the pressure difference between the operating pressure and the osmotic pressure, which is a characteristic of the solution only and not of the nature of the membrane (Bilstad, 1997). In such cases, the permeability of the salt across the membrane depends on the concentration gradient of the solution across the membrane, which frequently exceeds the bulk feed concentration due to polarisation, (see Section 2.4.2.5).

2.4.1 Basic Equations

There are three main concepts, which define the theory of the reverse osmosis process: water transport, osmotic pressure, and salt transport. These concepts are explored in the following subsections (Equations are from Noble and Stern, 1995)

2.4.1.1 Water Transport

The following equation describes water transport through a semipermeable membrane:

$$Qw = Kw \frac{(\Delta P - \Delta\pi) A}{t} \qquad \text{Equation (2-1)}$$

Where

Q_W	= water flow rate through the membrane	($l.s^{-1}$)
K_W	= membrane permeability coefficient for water	($l\ s^{-1}\ Pa\ m^{-1}$)
ΔP	= hydraulic pressure differential across membrane	(Pa)
$\Delta\pi$	= osmotic pressure differential across membrane	(Pa)
A	= membrane surface area	(m^2)
t	= membrane thickness	(m)

2.4.1.2 Osmotic pressure

Osmotic pressure depends on solute concentration, solution temperature, and the type of ions present, (Table 2.9). The van't Hoff equation describes osmotic pressure for dilute solutions:

$$\pi = viciRT \qquad \text{Equation (2-2)}$$

where

π	= osmotic pressure	(Pa)
c_i	= molar concentration of the solute	(g mole^{-1})
v_i	= number of ions formed when a solute dissociates	(Dimensionless)
R	= gas constant	(Pa.mole.g^{-1}.K^{-1})
T	= absolute temperature	(Kelvin)

Table 2.9: Calculated osmotic pressure at 25°C.

Species	Concentration (mg l^{-1})	Osmotic pressure (MPa)
NaCl	35,000	2.79
	5,000	0.39
	1,000	0.12
	500	0.09
Seawater	44,000	3.23
	32,000	2.31
Sucrose	34,000	0.26
	340,000	2.60
Glucose	18,000	0.24
	90,000	1.21

Source: Nobel and Stern, 1995.

2.4.1.3 Salt Transport

Salt transport through a membrane is proportional to the concentration or chemical potential difference across the membrane and can be described by the following equation:

$$Qs = \frac{Ks(\Delta C)A}{t} \qquad \text{Equation (2-3)}$$

where

Q_S	= salt flow through the membrane	(g s^{-1})
K_S	= membrane permeability coefficient for salt	(m^{-1})
ΔC	= salt concentration differential across membrane	(g)
A	= membrane surface area	(m^2)
t	= membrane thickness	(m)

The transport of salt across a membrane is commonly expressed as salt passage or salt rejection. Salt passage is the percentage of the salt in the feed that passes through the membrane into a permeate:

$$SP = \left(\frac{Cp}{Cf}\right) 100 \qquad \text{Equation (2-4)}$$

where

SP = % salt passage	(%)
C_p = salt concentration in product stream	(g l^{-1})
C_f = salt concentration in feed stream	(g l^{-1})

The percentage of salt rejection is 100% minus the percentage of salt passage.

2.4.2 Factors Affecting Membrane Performance

There are several factors that control the performance of RO membranes. These factors include recovery/conversion percentage, temperature, pressure, membrane compaction, and concentration polarisation (Heitmann, 1990).

2.4.2.1 Recovery/Conversion

Recovery/Conversion can be defined as the percentage of the feed water that is converted to permeate, and this can be calculated using the following equation:

$$Y = \left(\frac{Qp}{Qf}\right) 100 \qquad \text{Equation (2-5)}$$

where:

Y = % recovery or conversion	(%)
Q_p = product stream flow rate	(l s^{-1})
Q_f = feed stream flow rate	(l s^{-1})

2.4.2.2 Temperature

The effect of temperature change can result in both osmotic pressure (π) and water flux (Q_w) changes. As indicated in Equation 2-2, the osmotic pressure and water flux (K_w) is directly proportional to temperature (Figure 2.12). Water viscosity can also be affected with variations in water temperature. It is estimated that an increment of one degree Celsius in water temperature can cause an increase of 3% in membrane capacity (Bilstad, 1997).

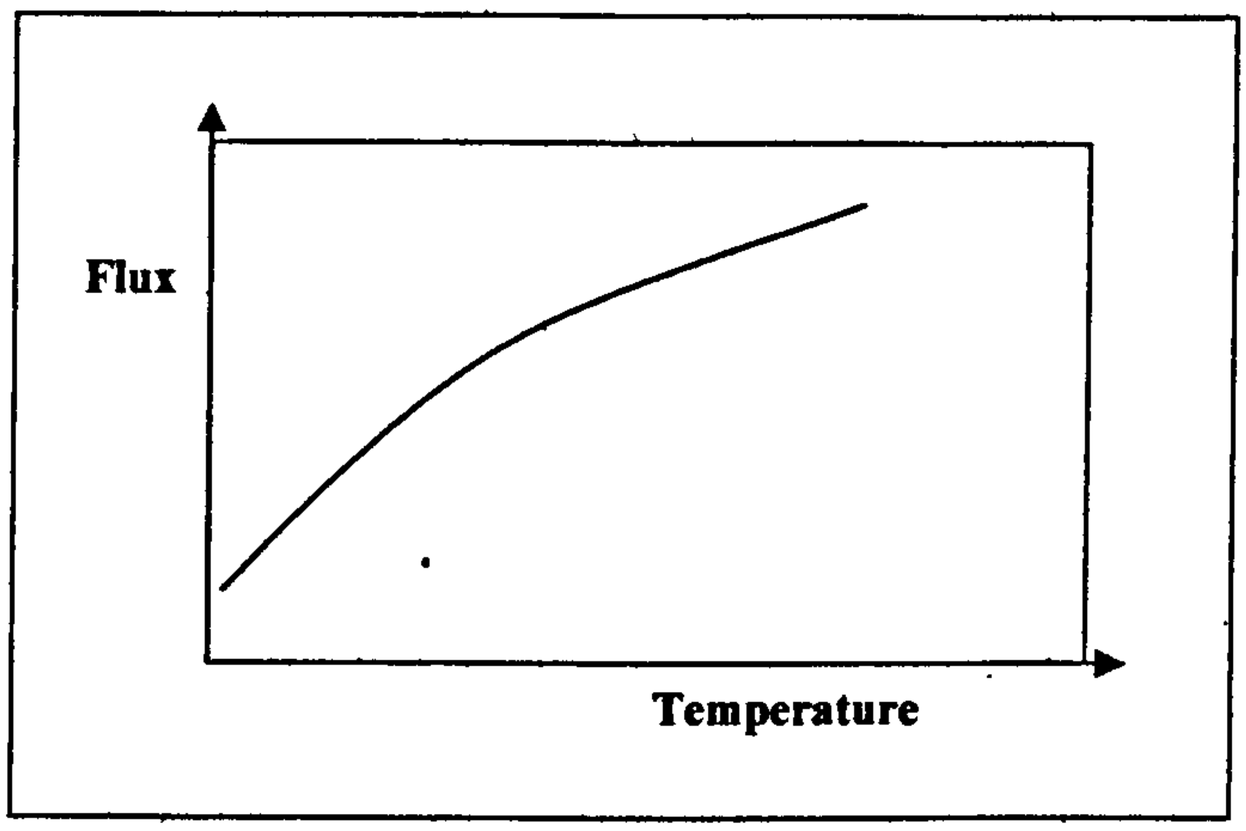

Figure 2.12: Flux and operating temperature relationship in RO membranes.

2.4.2.3 Pressure

As a general rule, any increase in transmembrane pressure (ΔP) results in an increase in water flux (Q_w) of a given set of feed conditions (Figure 2.13). Applied pressure causes creep deformation of membranes, which is referred to as "membrane compaction", this eventually causes decrease in membrane capacity.

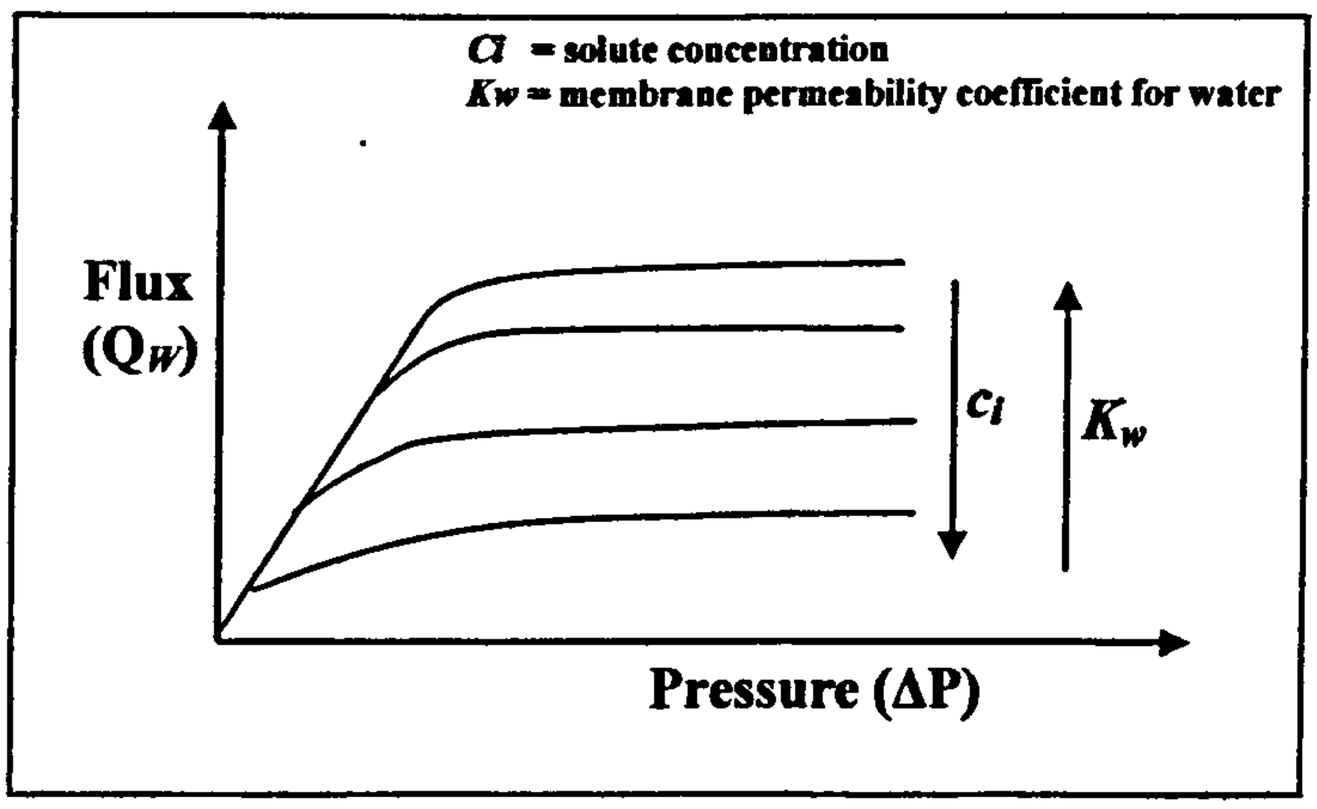

Figure 2.13: Flux as a function of the applied pressure for various bulk concentrations in RO membranes.

2.4.2.4 Membrane Compaction

Membrane compaction is defined as decrease in water flux through a membrane with time (Bilstad, 1997). Compaction is caused by creep deformation of

polymeric membranes over time and its intensity is dependent on membrane material, applied pressure (ΔP), and water temperature. The higher the ΔP and temperature of a membrane system the greater tendency of a membrane to creep (Figure 2.14).

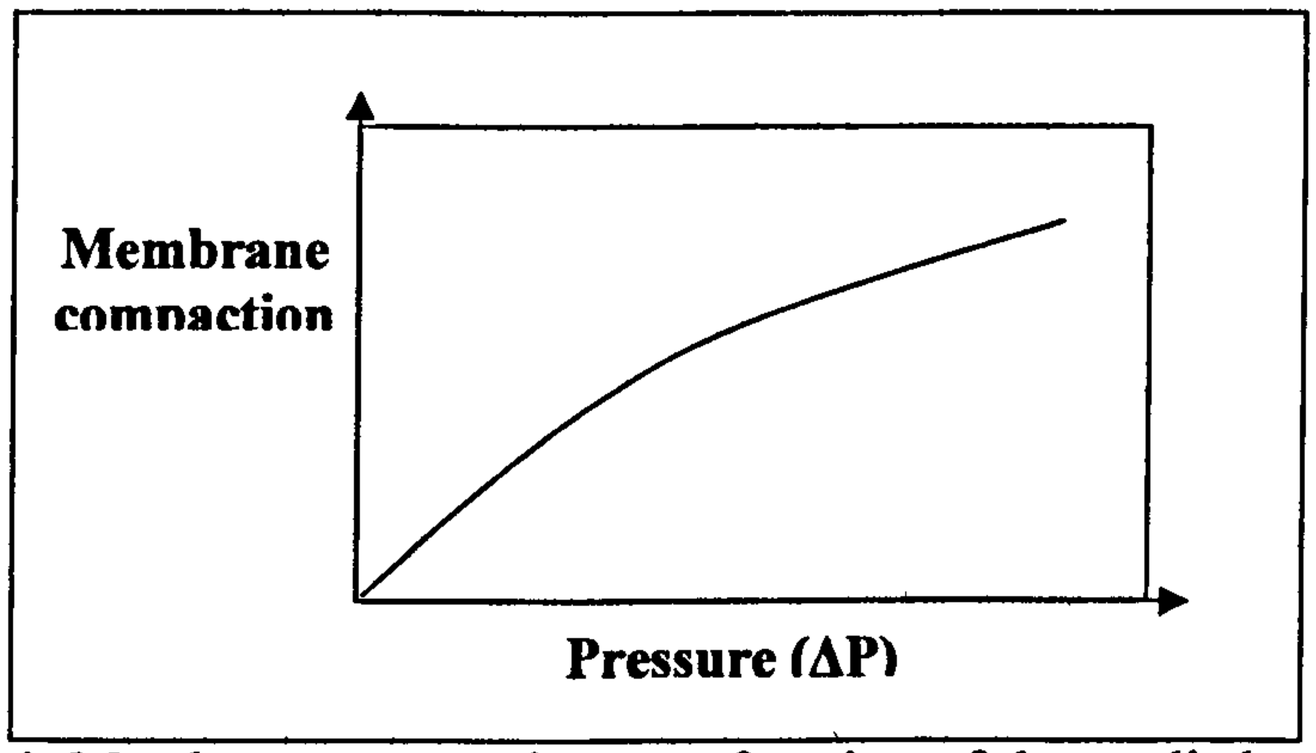

Figure 2.14: Membrane compaction as a function of the applied pressure in RO membranes.

2.4.2.5 Concentration Polarisation

The phenomenon of concentration polarisation is very common in the membrane desalination processes (Bilstad, 1997). It results from the build-up of a boundary layer of more highly concentrated solute on the membrane surface than in the bulk liquid. This phenomenon occurs because water permeation at the membrane surface leaves the more concentrated solute layer which diffuses slowly back into the bulk solution (Bhattacharya and Hwang, 1997). Figure 2.15 represents a schematic diagram of the concentration polarisation phenomenon, which results from the build-up of a boundary layer of more highly concentrated solute on the membrane surface than in the bulk liquid. The polarisation phenomenon is a function of solution concentration and turbulence at the concentrate side. Therefore, more turbulent solutions result in higher permeates fluxes due to thinner boundary layers (Shaalan, 2002).

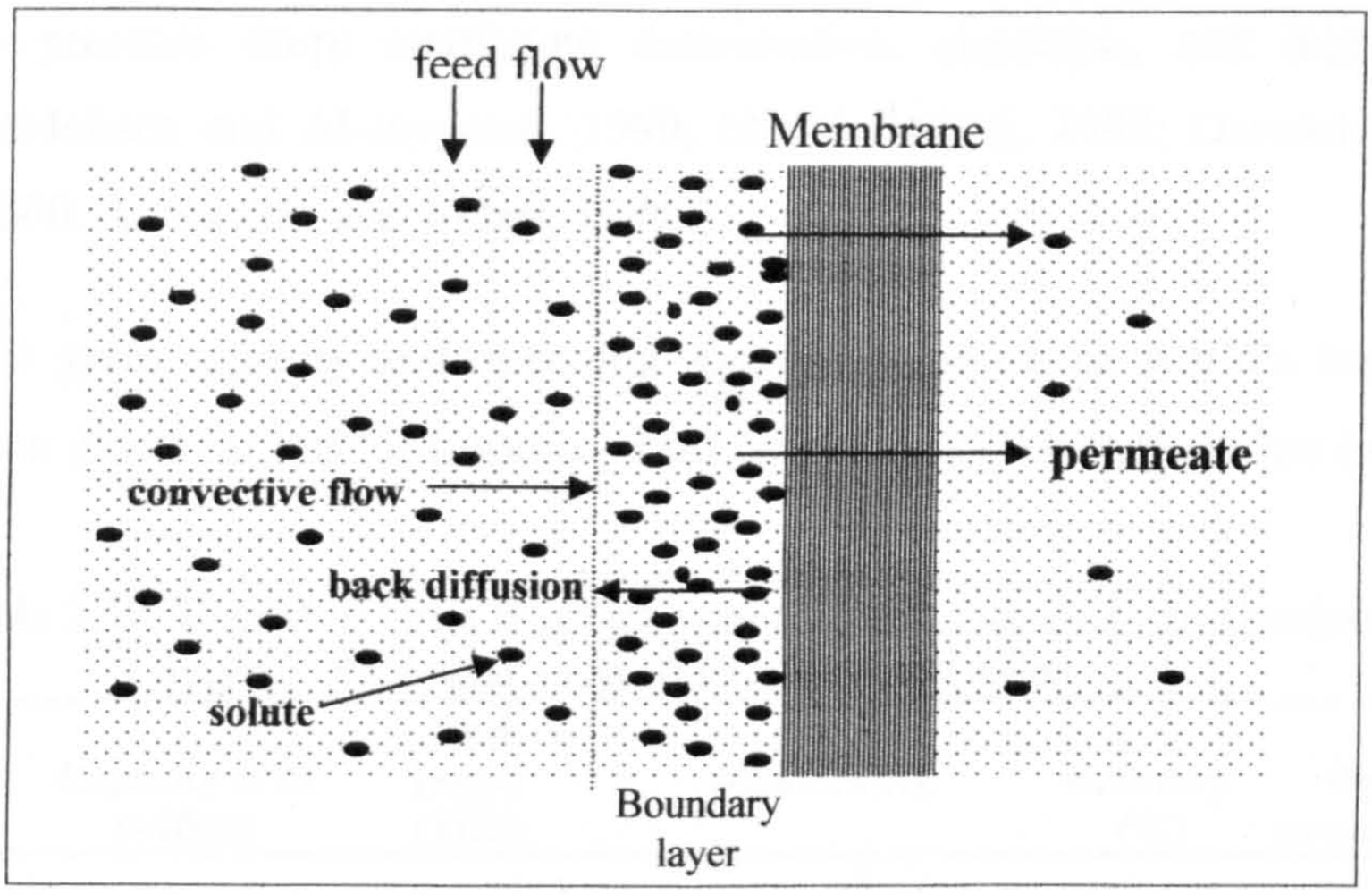

Figure 2.15: A schematic representation of concentration polarisation phenomenon.

2.4.3 Reverse Osmosis Desalination of Brackish Waters

Among the adopted desalination technologies, reverse osmosis has been considered the most attractive technique (Figure 2.16) especially in desalination of brackish waters (Matsuura, 2001). However, many limitations have been encountered for the operation of this method. These operating problems include:

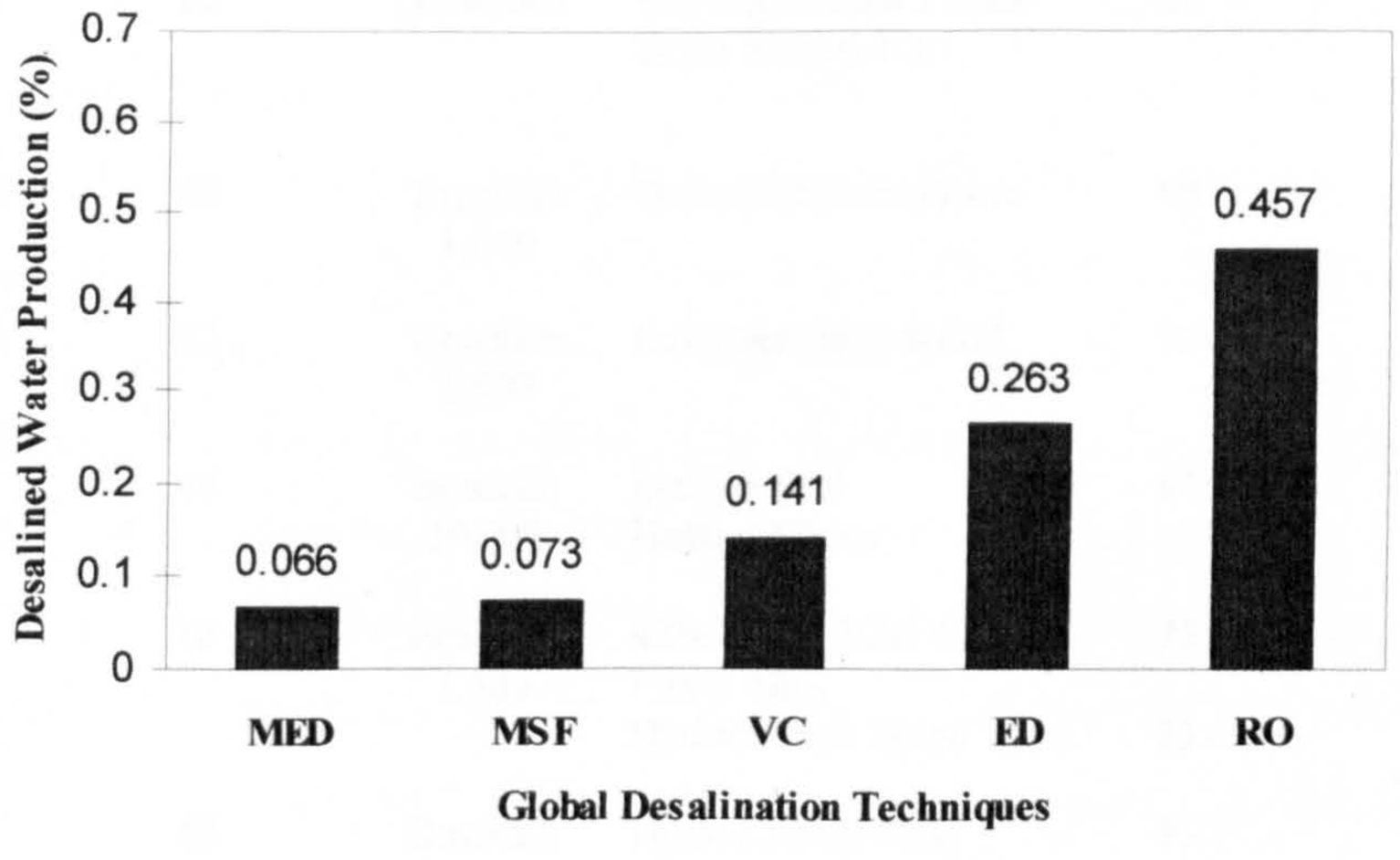

Figure 2.16: Relative global Usage of the Common Desalination Technologies.
Source: (Matsuura, 2001).

membrane fouling, concentration polarisation, high feed pressure requirements, excessive pressure drop, membrane deterioration, corrosion, and inland brine disposal (Mohsen and Al-Jayyousi, 1999; Sheikholesami, 1999; Darwish and Al-Najem, 2000, Al-Bastaki and Abbas, 1999b).

Table 2.10 gives capacity and operating data for some of the world's largest RO desalination plants for brackish waters. With the passage of time, there has been a

Table 2.10: Reported large brackish water reverse osmosis desalination plants.
Source: Noble and Stern, 1995; Jaber and Ahmed, 2004.

Location	Capacity m^3/d (×1000)	Feed (mg/l) (TDS)	Membranes	Recovery (%)	Operating pressure (MPa)
Deir al Balah Gaza (1999)	1.1	Brackish 1300	DuPont Hollow Fibres	75%	1.5
Yuma, Arizona, USA 1990	274	Brackish 3,000	69% Fluid Systems /UOP Cellulose Acetate Blend 31% Hydranautics Cellulose Acetate Blend.	-	70
Daesan, Korea, 1990	95	Brackish	Toray Spiral	-	-
Iraq, 1983-86	64	Brackish	DuPont Hollow Fibres	-	-
Riyadh, Saudi Arabia, 1984	60	Brackish	DuPont Hollow Fibres Brine Staged 4:2:1	90	2.8
Salboukh, Saudi Arabia, 1979	60	Brackish 1,610	DuPont Hollow Fibres	90	-
Unayzah, Saudi Arabia, 1989	52	Brackish 1,500	Envirogenetics Spiral	90	-
Ras Abu Jarjur, Bahrain, 1984	46	Brackish 19,000	DuPont B10 Hollow Fibres	61	5.8
Cape Coral, Florida, USA, 1989	46	Brackish 1,500	42% DOW TCA 0.53 Fibres 58%	75	1.4
			Hydranautics Spiral	85	1.7
Fort Myers Florida, USA, 1989	46	Brackish 400-500	Hydranautics/Nitto Denko Spirals	90	0.7
Bayswater, Australia, 1985	36	Brackish 2,500	Hydranautics Spirals	82	3.0

shift from hollow fibre to spiral wound composite modules, with the module replacement market being dominated by spiral wound units able to operate at lower than original design pressures (Matsuura, 2001).

2.5 Fouling

2.5.1 Types of Membrane Fouling

Even though there have been great advances in the development and application of membrane systems for desalination and water purification, membrane fouling still remains as a major bottleneck (Sheikholesami, 1999). The fouling problem has been considered as the key factor in the economics and operation of membrane plants (Moatty, 2001; Garcia-Rodriguez, *et al.*, 2001).

Figure 2.17 summarises the possible fouling mechanisms that may occur in a membrane. Case A shows the phenomenon where particles may plug smaller pores and cause narrowing of the larger ones, case B indicates particles can plug the narrow pores. Case C shows that particles can form a layer on the membrane surface, which acts as a secondary membrane, and in case D even larger pores can be plugged by debris or larger particles.

Fouling is the loss of throughput of a membrane device as it becomes chemically or physically changed by the process fluid (often by a minor component or a contaminant) (Matsuura, 2001). Fouling can also be thought of as the effect causing a loss of flux which cannot be reversed while the process is running. Fouling is also distinct from "membrane compaction", which results from the irreversible creep in the membrane as a response to stress. This phenomenon is very frequent in RO membranes, but at the pressures used in MF and UF it is usually ignored. Generally, fouling is a term used to describe the undesirable formation of deposits on surfaces, which occurs when rejected solids are not transported from membrane surface back to the bulk stream. Several types of fouling can be caused by the following processes:

- Inorganic deposition (scaling),
- Organic molecules adsorption (organic fouling),

- Particulate deposition (colloidal fouling), and
- Microbial adhesion and growth (biofouling) (Al-Ahmad *et al.*, 2000).

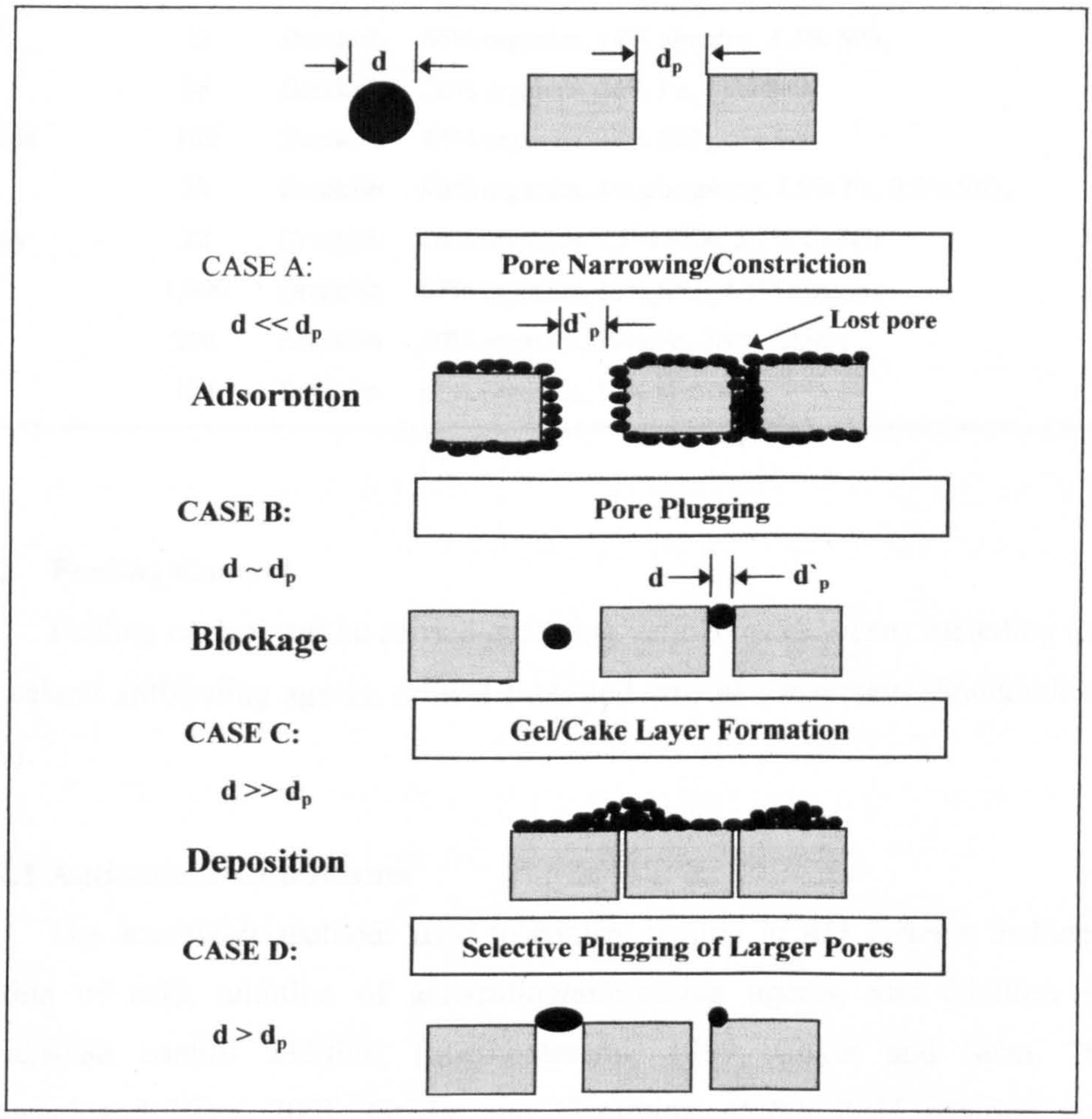

Figure 2.17: Fouling schematics in membrane systems.
Source: Noble and Stern, 1995.

In brackish water treatment, organic fouling is the most common problem (Matsuura, 2001). Table 2.11 summarises percentages of organic foulants at different RO plants treating brackish waters worldwide.

Table 2.11: Summary results of autopsies of membrane system (Matsuura, 2001).

Plant location	Size (m^3/h)	Water source	Major foulants	Water content
Netherlands	18	Brackish	44% organic, 30% Fe, 10% SiO_2	89%
Canary Islands	63	Brackish	63% organics, 4.7% $MgCO_3$, 1.7% $CaSO_4$	92%
Spain	12	Brackish	66% organics, 14% alumina, 3.4% SiO_2	94%
Italy	36	Brackish	26% organics, 36% Fe, 13% SiO_2	85%
Argentina	160	Brackish	44% organics, 37% SiO_2, 5% Fe	93%
Spain	20	Brackish	90% organics, 4% phosphate, 1.9% Fe, 0.5% SiO_2	94%
Germany	22	Brackish	76% organics, 7.1% SiO_2, 5.1% $CaPO_4$	85%
Spain	1,000	Brackish	67% organics, 13% SiO_2, 4.5% alumina	90%
Egypt	200	Brackish	50% organics, 39% Fe, 2.9% $CaSO_4$	92%
USA	125	Brackish	63% organics, 10% alumina	85%

2.5.2 Fouling Control

Fouling control can be carried out using various mechanisms including use of antiscalant/ antifouling agents, critical flux, and critical conversion (Sheikholesami, 1999).

2.5.2.1 Antiscalant/antifoulants

The acceptable methods used to control scaling in RO systems include the addition of acid, addition of antiscaling/antifouling agents, and addition of a hybrid/scale control additive, (Sheikholesami, 1999; Coker and Sehn, 2000; Sadhwani and Veza, 2001; Griebe and Flemming, 1998). Acid addition was a common practice used during the 1960s and 1970s, as it was an effective method to control alkaline scaling (Hamrouni and Dhahbi, 2001). The use of sulphuric acid dosing in the range of (15 – 97 ppm) was found to be more economical (e.g. 1.8 times) compared with other antiscalant additives (Moatty, 2001). However, sulphuric acid addition has led to several operational problems such as corrosion, transport and storage, and safety problems due to the very special handling measures required (Sadhwani and Veza, 2001).

The addition of antiscalant/antifouling agents is another common practice for membrane fouling control in RO systems (Squire, 2000). Small dosing of these chemicals can delay scale deposition in the desalination plant units. The addition of phosphates and polyphosphates, as antiscalants to minimise scaling in RO membranes, exhibits excellent results of inhibiting scale formation, (Al-Rammah, 2000). These substances hydrolyse in short periods of time to form orthophosphates, which are inactive as an antiscalant. Consequently, their application leads to the deposition of Ca and Mg ions as a soft sludge leading to sludge disposal problems (Squire, 2000; Matsuura, 2001; Al-Rammah, 2000).

During the last few years, new antiscalant/antifouling agents have been used including polycarboxylic and phosphoric acids as well as a mixture of polyacrylate and hydroxylidene diphosphate (HEDP), which is highly effective against calcium carbonate scale. Additionally, many RO desalting plant operators prefer the application of polymers as scale inhibitors (Al-Rammah, 2000). These chemicals usually include polyarylic acid with phosphates, which can be used as antiscalants or antifoulants depending on the mode of application of these chemicals (Bremere *et al.*, 2000; Hamrouni and Dhahbi, 2001). In addition, the application of some antiscalants, such as sodium hexametaphosphate (SHMP) and Permatreat-191, into the feed waters showed good scale inhibition. However, their addition cannot prevent scaling but can only retard it until the concentrate leaves the permeator in RO plants (Al-Shammiri *et al.*, 2000). The application of polyphosphates in the RO systems as antiscalants can cause problems due to hydrolysis and euthrophication (i.e. formation of orthophosphates) (Shaposhnik *et al.*, 2001).

Hybrid acid/scale control additives (mixtures of acids and antiscalants) are considered the second most common method used for membrane scale control in RO systems (Sheikholeslami, 1999). This method was introduced to lower the acid dose rates and to employ small doses of antiscalant/antifouling reagents in order to minimize corrosion problems and avoiding the requirements of feed water neutralisation (Shaposhnik *et al.*, 2001).

2.5.2.2 Critical Flux

Figure 2.18 shows that flux (J), a measure for membrane performance, is controlled by two phenomena, concentration polarisation and fouling (Madaeni *et al.*, 2001). The two most important parameters which can combine to cause fouling of membranes in the RO systems are the total flux (J_t) and the cross-flow velocity (v) of feed waters (Al-Bastaki and Abbas, 1999a; Abbas and Al-Bastaki, 2000). Critical flux (J_c) can be defined as the maximum flux below which fouling resistance remains negligible. Figure 2.19 presents the relationship between total flux and cross-flow velocity as a function of particle size. The figure represents a reverse relationship between flux and particle size; however, larger particles have less tendency to deposit on the membrane surface especially at high flow velocities. The relationship between critical flux, other operating conditions, and feed water characteristics has been investigated by many researchers (Al-Bastaki and Abbas, 1999a; Abbas and Al-Bastaki, 2000; Bouhidel and Oulmi, 2000; Coker and Shen, 2000). However, the effect of membrane type on the trend of the critical flux has not been reported (Coker and Shen, 2000).

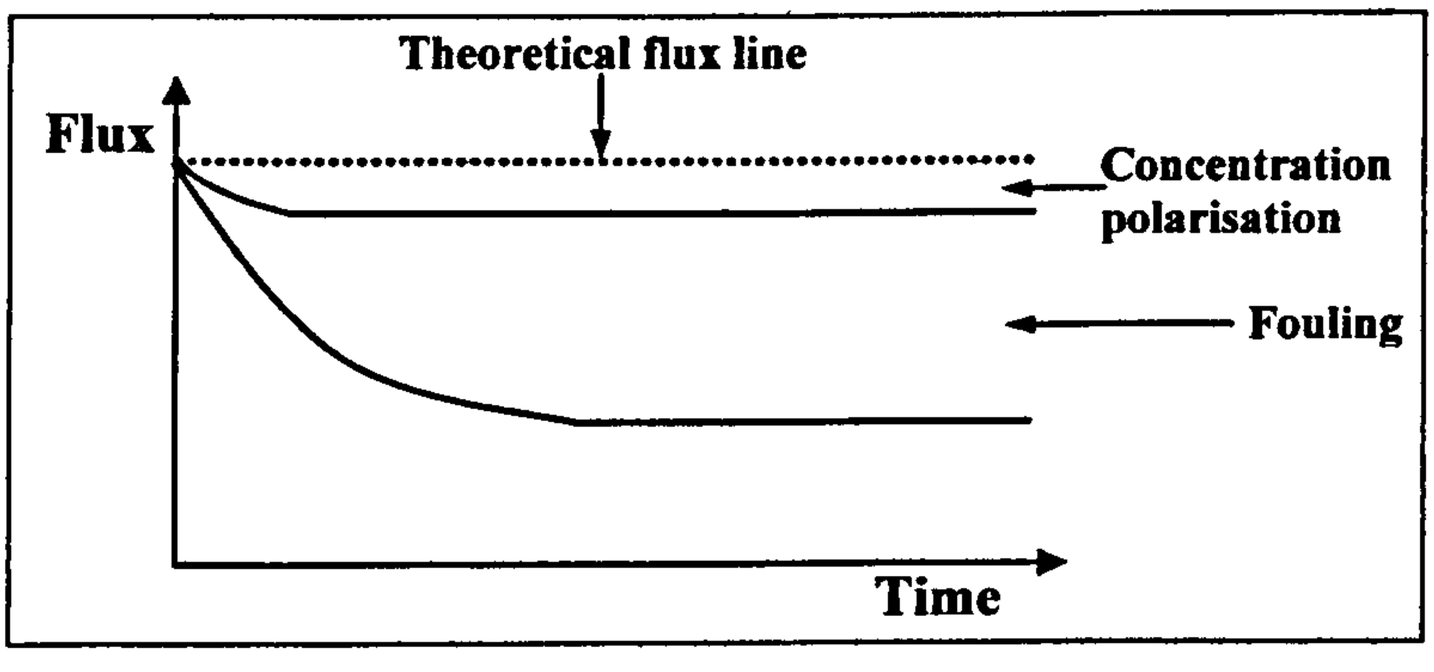

Figure 2.18: Flux as a function of time: concentration polarisation and fouling influences.

The critical conversion of a solution is a function of critical flux, critical flow velocity, and other parameters affecting the stability of the solution such as salinity, pH, temperature, pressure, repulsion forces and type of particles (Al-Bastaki and Abbas, 1999a; Abbas and Al-Bastaki, 2000). A study in the Middle-East (Gulf countries) indicated that almost all the RO plants were designed at above the critical conversion values, and thus they were subjected to fouling (Ahmed, *et al.*, 2000).

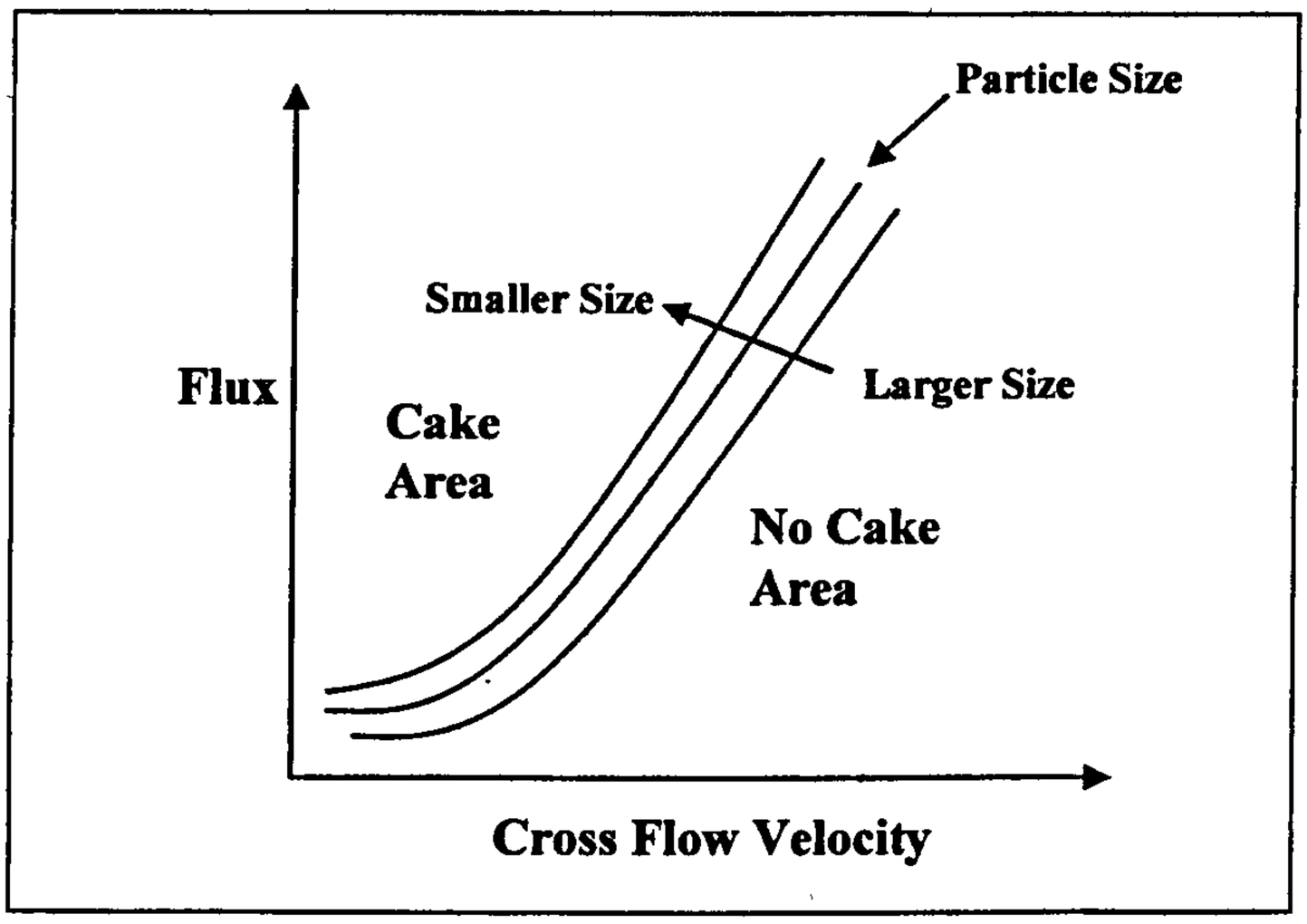

Figure 2.19: Flux as a function of cross flow velocity: critical fluxes for various particle sizes.

2.5.2.3 Antifouling Membranes and Modules

The third option of membrane fouling control in RO systems is to develop membrane modules that are resistant to fouling (Redondo, 1999). Researchers in this area have investigated developments and modifications to membrane module and spacer design.

Investigations on the effect of ultrasound and flow pulsation on the hydrodynamics of flow have been carried out by many researchers (Mairal *et al.*, 2000; Al-Bastaki and Abbas 1999a). The *Mineral Water Development Company* in South Africa developed a novel RO unit that has two advantageous features over conventional RO membrane systems. This unit is capable of reducing membrane fouling and improves hydrodynamic conditions by reducing the boundary layer thickness at the membrane surface enhancing both membrane flux and apparent salt rejection of the system (Sheikholeslami, 1999).

The application of an electromagnetic device, which creates an electromagnetic field around the membrane assembly, has been studied (Mairal *et al.*, 2000). It was

concluded that the presence of such an electromagnetic field on the membrane material could inhibit the precipitation of soluble salts, and also cause the organic materials not to interact with the membrane surface.

Studies on membrane surface modifications have been carried out by many researchers (Ma *et al.*, 2001; Al-Ahmad *et al.*, 2000; Redondo, 1999). These modifications attempt to change certain physical and chemical properties of the membrane surface in order to improve its performance by reducing primary fouling and the adsorption of molecules. The modifications aim to develop membranes with smoother surfaces (Al-Ahmad *et al.*, 2000), have longer cleaning cycles (Sadhwani and Veza 2001), more fouling resistance (Redondo, 1999), high fluxes (Al-Bastaki and Abbas, 1999a), and lower cleaning costs (Sadhwani and Veza, 2001; Matsuura, 2001).

Membrane surface modifications can be achieved by several means, which include change of charge or hydrophilicity, redox radical grafting as well as by application of composite coating to electrodialysis membranes (Shaposhnik *et al.*, 2001; Matsuura, 2001).

Matsuura (2001) reported that enhancement of RO membrane performance can be achieved by improving the membrane surface. They attributed the high water productivity of the newly developed membranes to the increase in the roughness of the membrane surface. In a similar study, Ma *et al.* (2001) found a relationship between flux of RO membranes and their surface roughness. It was found that an increase in membrane surface roughness resulted in a higher water permeation flux. This important increase in the membrane performance and productivity was attributed to the actual expanded surface area, which is almost 40% more than the geometric surface area (based on smooth surface) of the membrane, as well as to the increased mixing rate of feed stream near the membrane surface in cross-flow modules, Figure 2.20 (Bessieres *et al.*, 1996).

However, the increase in the microscopic scale roughness of RO membranes can result in higher fouling of RO systems by colloidal particles (Sheikholeslami, 1999; Mairal *et al.*, 2000; Redondo, 1999). The effects of surface roughness on the interaction forces between particles and membrane surface were investigated by Elimehech *et al.*, (1997). According to their studies, it was concluded that a higher membrane surface roughness results in more interaction between colloidal particles and the membrane, thus leading to more fouling in the membrane system.

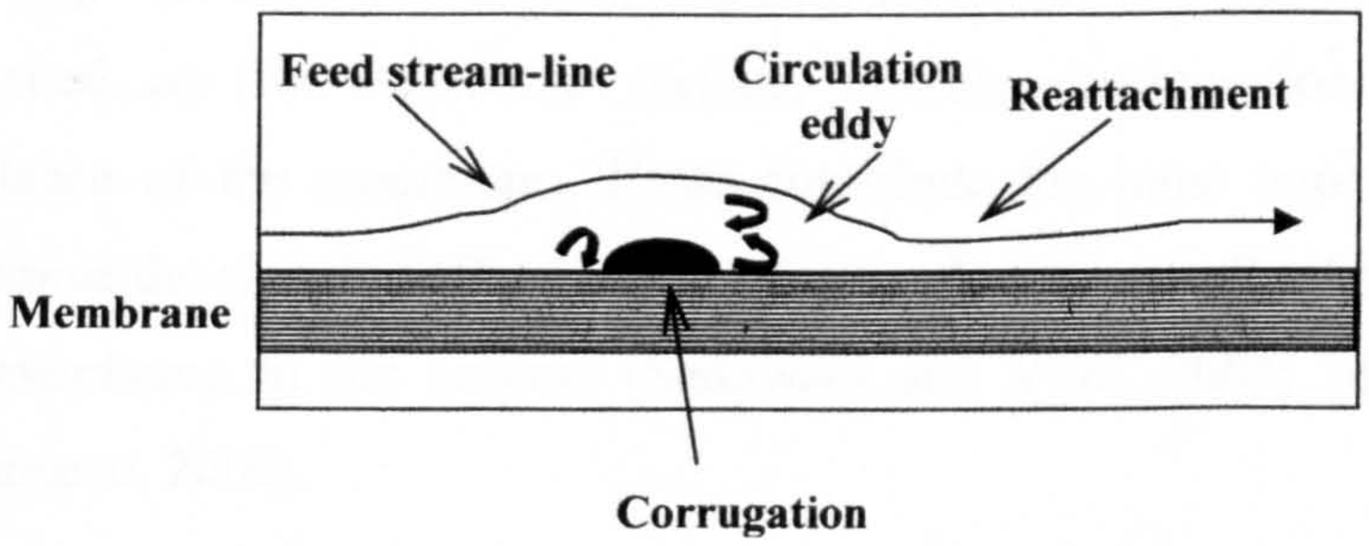

Figure 2.20: Stream-lines in a corrugated membrane.

As mentioned earlier (Section 2.4.2.5), one factor limits mass transfer in membrane processes such as RO and UF, which is a concentration polarization phenomenon (Al-Bastaki, and Abbas, 1999b). This phenomenon was described by the presence of a small thickness film near the membrane surface in which the solute concentration is much higher than that at the bulk of the fluid (Bouhidel and Oulmi, 2000). In an attempt to minimize polarization and fouling, several manufacturers have commercially available low fouling membranes (*FILMTEC, Dow, DuPont, Osmonics, and Trisep*). These novel membranes comprise a commercial heterogeneous membrane with a stable, thin multi-layer composite coating to minimize polarization resistance (Bouhidel and Oulmi, 2000; Sheikholeslami, 1999). On the other hand, several membrane designers and manufacturers (*Dow, DuPont, Osmonics, and Trisep*) have studied the effects of modifications to module and spacer design on membrane performance and productivity. These modifications include reduction in leaf length, spacing adjustments, alternative packing materials and new feed and permeate spacer design.

2.5.3 Membrane Cleaning

Membrane cleaning technology has been of great importance to restore the performance of the membrane. Although all cleaning techniques can only reduce fouling to some extent, cleaning methods will always be employed in practice, Figure 2.21 (Sadhwani and Veza, 2001). The frequency with which membranes need to be cleaned can be estimated from process optimisation (e.g. optimum flux and optimum applied pressure). Membrane cleaning can be classified into four methods, which are hydraulic cleaning, mechanical cleaning, chemical cleaning and electrical cleaning. The choice of the cleaning method mainly depends on the type of foulant deposited on the membrane surface, module configuration, and the chemical resistance of the membrane. These contribute the most important factors, which determine the cleaning effectiveness of a membrane, as well as the economical life of the membrane in the process (Sadhwani and Veza, 2001; Madaeni *et al*, 2001; Duranceau, 2000).

The mechanism of biofilm cleaning can be considered as a two-step process:

1) Weakening of the fouling layer, which can be performed by cleaners that interfere with the dominating physico-chemical interactions, and
2) Removal of the fouling layer, which usually can be performed by shear forces (Flemming, 1997).

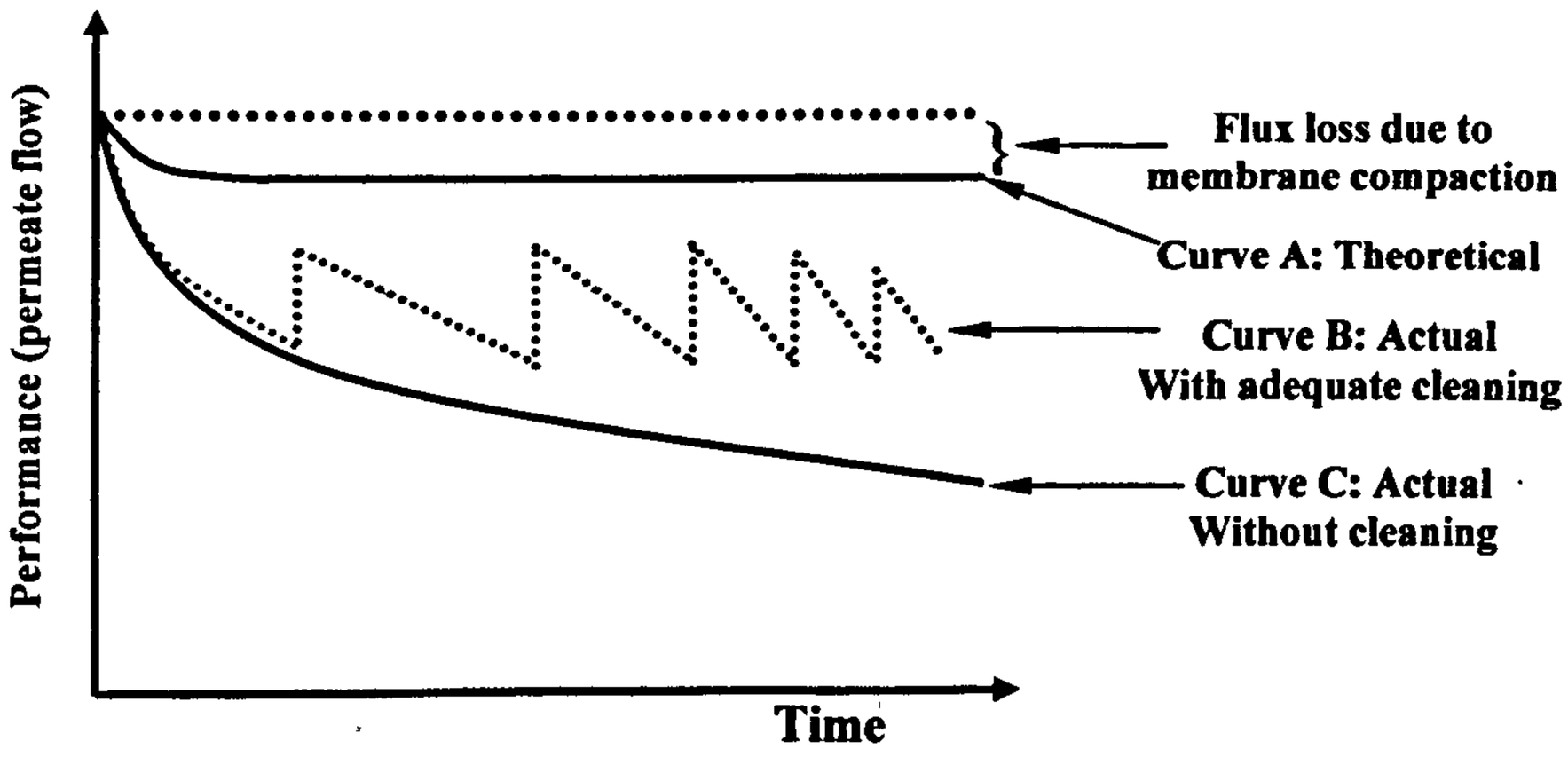

Figure 2.21: Permeate flux in membrane systems: theoretical with and without cleaning.

2.5.3.1 Hydraulic Cleaning

Hydraulic cleaning methods include back-flushing (only applicable for MF and open UF membranes), back-shock treatment (back-flushing for only a fraction of a second), flow pulsation and reversing the flow direction at a given frequency (Noble and Stern, 1995). In practice, flow pulsation and reversing flow direction methods can also be considered to improve the solution hydrodynamics (Duranceau, 2000).

2.5.3.2 Mechanical Cleaning

Mechanical cleaning can only be applied in tubular configuration systems using oversized sponge balls (Noble and Stern, 1995). Mechanical methods may be applied both "online" when the system is operating or "offline" when the system is shutdown.

2.5.3.3 Chemical Cleaning

As mentioned earlier, chemical cleaning is the most important and practical method used to reduce fouling, with a number of chemicals being used either separately or in combination (Bremere, *et al.*, 2000; Al-Rammah, 2000). The most common chemicals used in membrane cleaning include: acids (e.g. HCl, H_2SO_4, H_3PO_4, citric acid), alkali (e.g NaOH), enzymes, and complexing agents (e.g. EDTA), and disinfectants (H_2O_2 and NaCl).

In their studies, Sadhwani and Veza (2001) found that membrane productivity can be increased by using some good cleaning solutions such as a basic solution with detergent, acid solution without detergent, or two-step cleaning (acid + basic) solutions with detergents. However, when increased water quality is needed (e.g. minimum conductivity values), it is recommended to use cleaning solutions in two steps with detergents.

2.5.3.4 Electrical Cleaning

The application of pulsed electric field near the membrane surface, in order to move the charged particles away from the membrane, is another common practice, especially in ED membranes (Noble and Stern, 1995). The cleaning method can be carried out without interrupting the filtration process; however, one drawback of this process is the requirement of electrically charged membranes (e.g. metal membranes).

2.6 Pretreatment Strategies In RO Systems

RO membranes are susceptible to a wide variety of organic and inorganic foulants. To mitigate membrane fouling, RO systems require sufficient, reliable pretreatment to produce superior quality RO feed water that will ensure stable, long-term performance of RO membrane elements; regardless of the turbidity variations of the raw water.

Ineffective or unreliable pretreatment can lead to problems with the RO system including high rates of membrane fouling, high frequency of membrane cleanings, lower recovery rates, high operating pressure, poor product quality and reduced membrane life; all having a direct impact on plant productivity and operational costs (Maartens and Jacobs, 1999). Accordingly, the pretreatment optimisation is the key factor for a successful RO desalination system.

The economic feasibility of RO systems largely depends on maximising the productivity or permeation rate and the membrane life (Bilstad, 1997). In actual operation, membranes tend to become fouled as a consequence of feed water carrying impurities (e.g. organic matter, biomass, etc). If these foulants are allowed to accumulate on the membrane surface, a gradual and serious deterioration of performance will occur (Luo and Wang 2001). In order to restore the performance of the membrane, it must either be cleaned periodically or a pretreatment scheme must be implemented. Figure 2.22 (Maartens and Jacobs, 1999) shows the effect of the pretreatment on the productivity. Curve A indicates the theoretical productivity, assuming ideal feed water free of impurities with no pretreatment. The small initial

decay on curve A is due to membrane compaction, and curve B shows the actual productivity with an adequate pretreatment and the effect of periodic cleaning required restoring the system productivity. Curve C represents the actual membrane productivity with inadequate pretreatment. The frequency of cleaning is higher which results in the membrane not being restored to its initial condition and a reduction in membrane permeability.

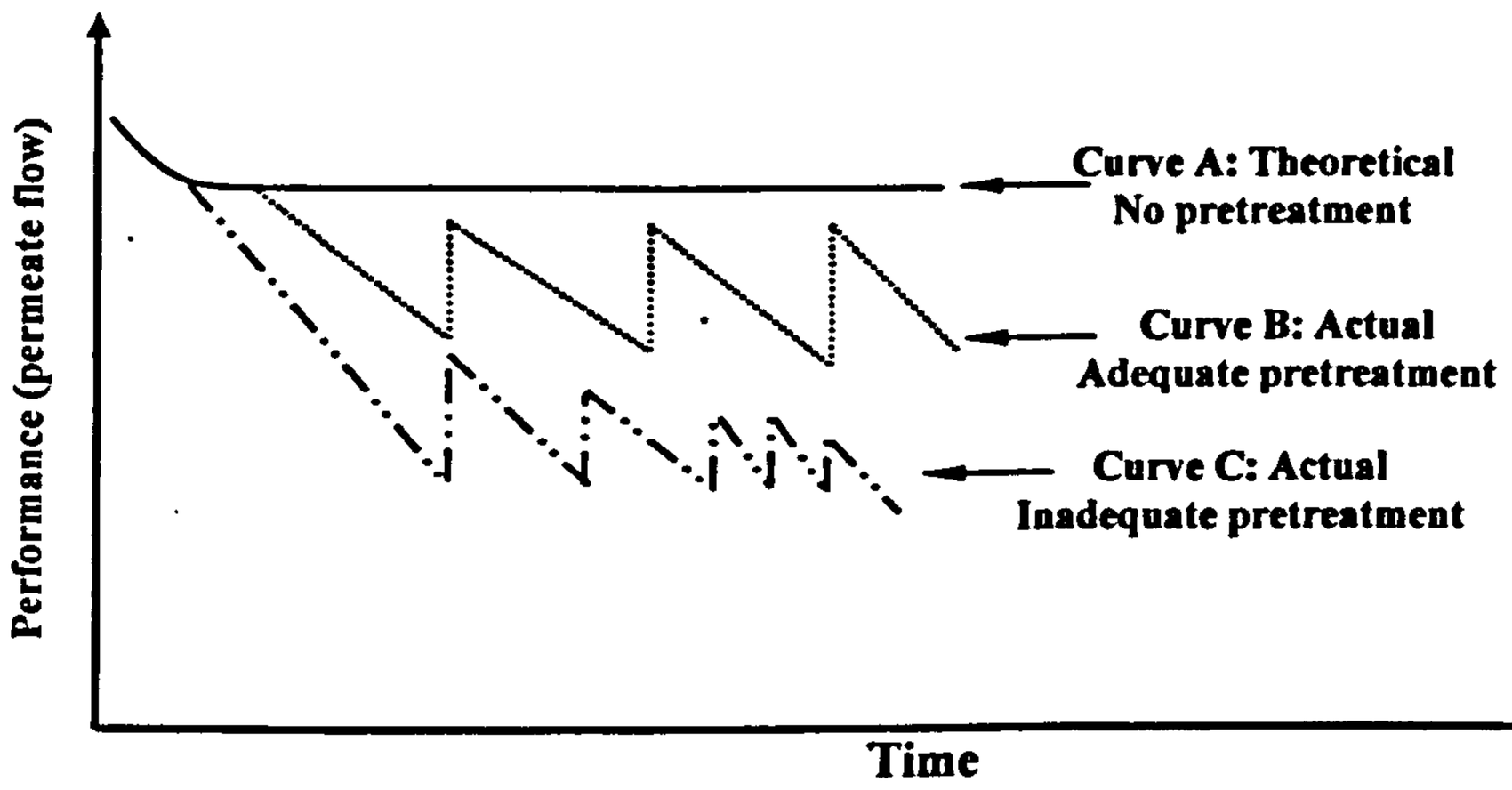

Figure 2.22: Effect of pretreatment on productivity.
(Source: Maartens and Jacobs, 1999)

Since RO fouling mitigation has become necessary, a series of pretreatment technologies has been integrated into the system. Some of these are already implemented in the industry while the rest are still in their infancy. The following are some of the pretreatment technologies that have been investigated.

The pretreatment solutions can be used for both nanofiltration (NF) and RO, which are the top contenders for surface water treatment (Maartens and Jacobs, 1999). These then meet the more stringent water quality regulations. Advanced pretreatment processes, such as conventional MF and UF, become necessary to maintain productivity (Glucina *et al.*, 2000). MF membranes can remove suspended particles, cells, and colloidal particles, whilst UF membranes can remove particles in the range of (0.001–0.02 μm) such as dissolved solids, and macromolecules.

Conventional RO pretreatment (mostly using chemical addition and sand filtration, followed by a security finefilter system) has been widely applied in the past for seawater RO plants to lower the Silt Density Index (SDI) and to remove suspended solids and excessive turbidity. Figure 2.23 shows a classical conventional pretreatment system attached to a small-scale RO plant. The system usually consists of an open seawater intake, screens for coarse prefiltration, chemical additions (break-point chlorination, acid addition, inline coagulation, addition of a flocculation aid) followed by a single- or double-stage sand filtration. The final step of pretreatment is the cartridge- or bag type guard filter with a mesh size of five to ten microns to protect RO membranes, accordingly, particles larger than five microns only are removed.

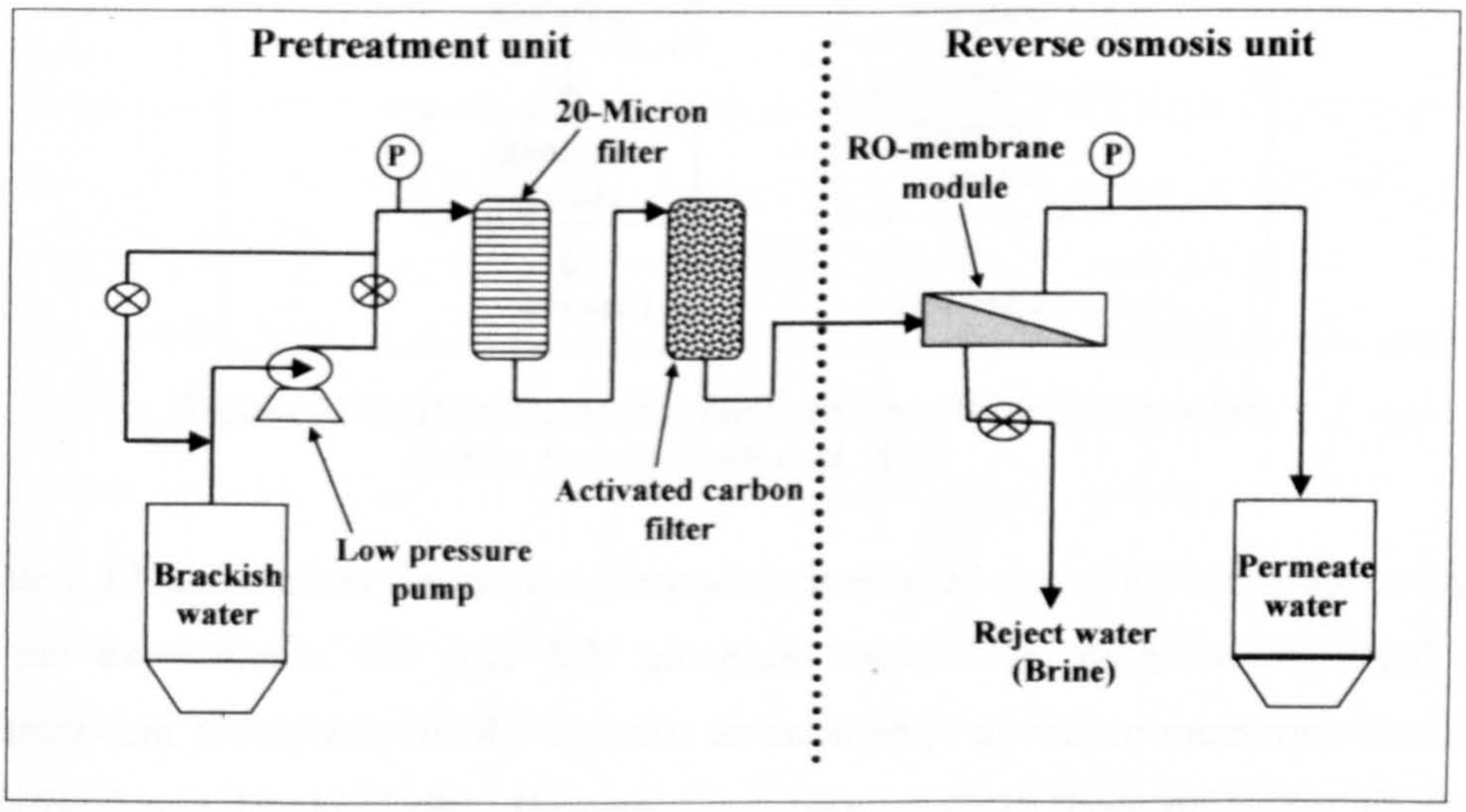

Figure 2.23: Schematic configuration of a classical pretreatment system attached to a small-scale RO plant.

Hybrid systems have also been used in which membranes are joined with other conventional separation processes such as slow-sand filtration and activated carbon filtration (GAC) with UF and MF (Figure 2.24) (Maartens *et al.*, 1999). Griebe and Flemming (1998) carried out experimental work, which shows that introducing a

sand biofilter before and after two RO test cells, equipped with a polyamide composite membrane in the solution, resulted in a decreased biofilm thickness attached onto the membrane. The decline in permeate flux after 10 days of operation was >20% when no sand biofilter was used, however, no flux decline was observed in the test cell with a sand filter ahead the RO membrane.

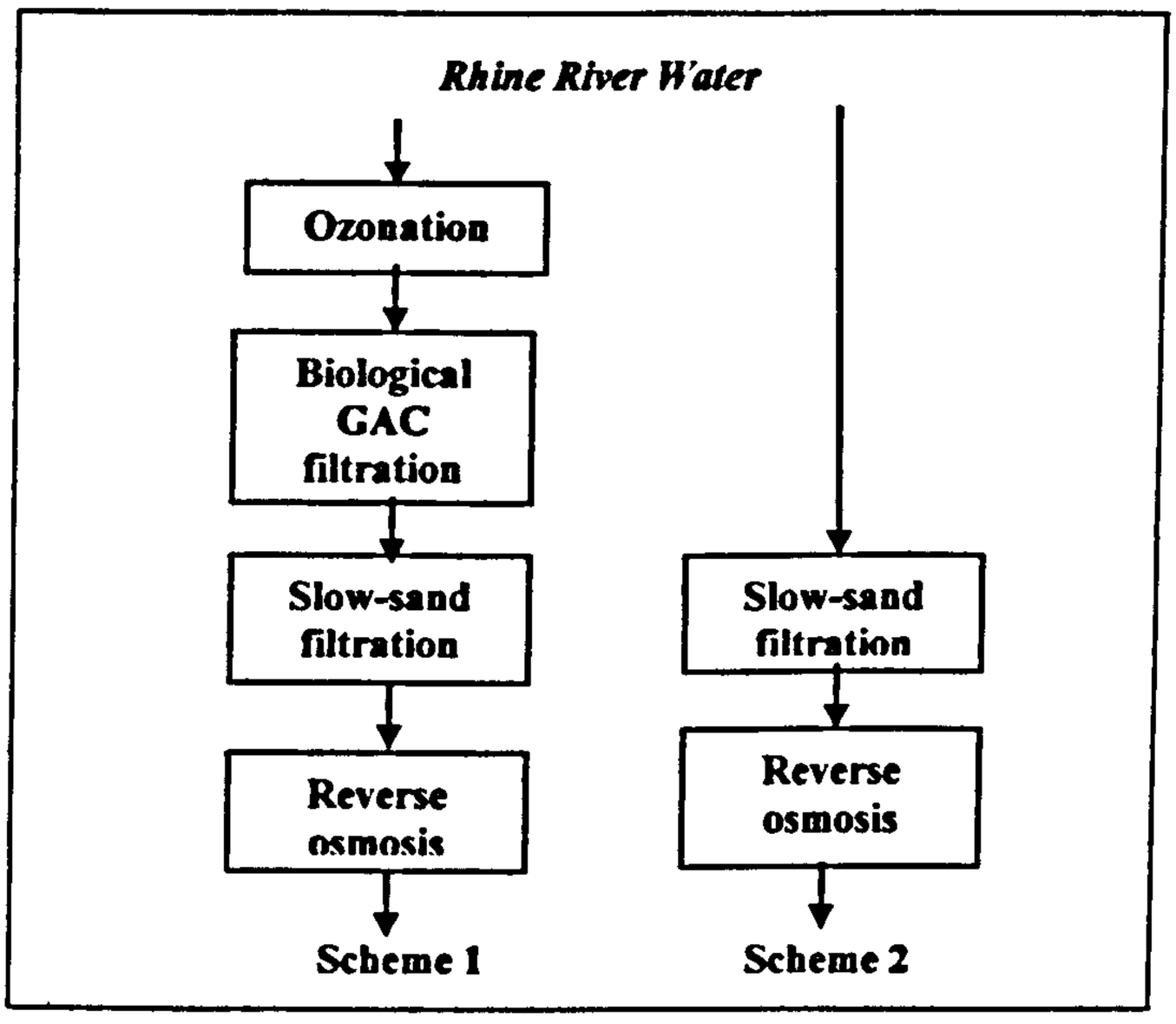

Figure 2.24: Pretreatment options of The Rhine River water.
Source: (van der Hoek, et al. 2000)

Table 2.12 summarises the biofilm parameters measured on the RO membranes used in the experiments. UF and MF processes have been progressively used as pretreatment procedures for RO systems as an attempt to reduce membrane fouling (Maartens and Jacobs, 1999). However, the membranes in these processes are also subjected to fouling, and its control should frequently take place. Fouling control of these membranes is normally achieved by backwashing (Ma *et al.*, 2001) and rarely by using chemical cleaning (Coker and Sehn, 2000; Madaeni *et al.*, 2001). As a general rule, in most RO desalting plants, backwashing is applied on the pretreatment membrane stages every 40 minutes and chemical cleaning every 6 months.

Table 2.12: Biofilm parameters measured on RO membranes before and after a sand biofilter.

Parameter	Before Sand biofilter	After Sand biofilter
Total bacterial number, cm^{-2}	1.0×10^8	5.5×10^6
Colony forming units, $cfu.cm^{-2}$	1.0×10^7	1.2×10^6
Protein content, $\mu g.cm^{-2}$	78	4
Humic substances, $\mu g.cm^{-2}$	41	12
Carbohydrates, $\mu g.cm^{-2}$	26	3
Uronic acid content, $\mu g.cm^{-2}$	11	2
Biofilm thickness, µm	27	3

Source: Griebe and Flemming (1998)

Although the novel pretreatment technology "compact accelerated pretreatment softening" (CAPS) is still in its infancy, experiments have shown encouraging results for the removal of inorganic, colloidal, and organic particles from feed waters (Gilron *et al.*, 2000). CAPS pretreatment technique comprises of a combination softening agents and a MF membrane. However, this method is also subjected to membrane fouling and requires backwashing every 40 min (Ma *et al.*, 2001).

Unlike conventional pretreatment systems, Ultrafiltration (UF) membranes provide a positive barrier to particulates and pathogens and protect the RO membranes by physically separating the solids. This ensures a consistent and excellent RO feed flow quality, regardless of raw water turbidity even during storm events and algae blooms. It is also considered to be the best choice for pretreatment of seawater containing colloidal silica.

2.7 Summary

Based on the literature reviewed on the application of RO technology in the desalination of brackish waters, several conclusions can be made:

(a) In most Middle East countries, fresh water scarcity is threatening water demand and resources and, to some extent, has provoked national development strategies in the region. However, desalination of brackish waters can be an alternative for fresh water resource especially in arid and remote areas (e.g. deep Saharan oases).

(b) A considerable amount of work has been carried out to study the biology and the mechanism of biofilm formation in both seawater and brackish waters; however, little work has been carried out to study the biology of hypersaline waters (e.g. Qabar-Onn Lake) (Ajaili, *et al.*, 1984). In order to investigate biofouling mechanism in such hypersaline water, getting a clear picture of the biodiversity and unique biology of this unexplored water system (i.e. Qabar-Onn Lake) is highly desirable.

(c) Desalination received vast attention during the last decade as a means to alleviate water shortage problems. The desalination technology is based heavily on the use of membranes mainly reverse osmosis (RO) processes for the treatment of both brackish water and seawater for domestic consumption.

(d) Among the desalination technologies available, RO is currently considered as the most attractive process to produce fresh water from both brackish water and seawater. This technology is well established and known for its high quality water product and comparatively low energy requirements.

(e) In membrane processes such as RO desalination systems, the flux, a measure of membrane performance, is controlled by two phenomena: fouling and concentration polarisation. Extensive research has been

carried out to investigate fouling control strategies and mitigation in membrane systems. These activities include pretreatment of feed waters, application of antiscalant/antifoulants, and membrane and spacer design improvement and the development of antifoulant membranes. However, little research has been reported on the concentration polarisation mechanism.

(f) Unlike the inorganic fouling problem, very little research has been carried out to investigate the biofouling phenomenon. However, this phenomenon is more common in the case of desalination of brackish waters in hot climates due to the higher water temperatures and sunlight abundance (e.g. temperature over 45°C). Thus the objective of this work was to fill this gap through *in-situ* investigations on the biofouling phenomenon in more details and to give more insights on the relationship between concentration polarisation and biofouling.

Chapter 3

MATERIALS AND METHODS

3.1 Experimental Apparatus

3.1.1 High Pressure Reverse Osmosis Membrane Test System (HPROMTS)

3.1.1.1 Description of HPROMTS

All membrane tests were performed in a high pressure reverse osmosis membrane test system (HPROMTS), which was designed especially to be safe when operated at high pressure, maintain sterile conditions, being transparent to visualise membrane surface during operation, and have two identical membrane cell modules to allow comparison of different membrane characteristics. Figures 3.1 and 3.2 illustrate a schematic diagram of the HPROMTS system showing the piping and instrumentation set-up, and a photograph of the experimental set-up, respectively.

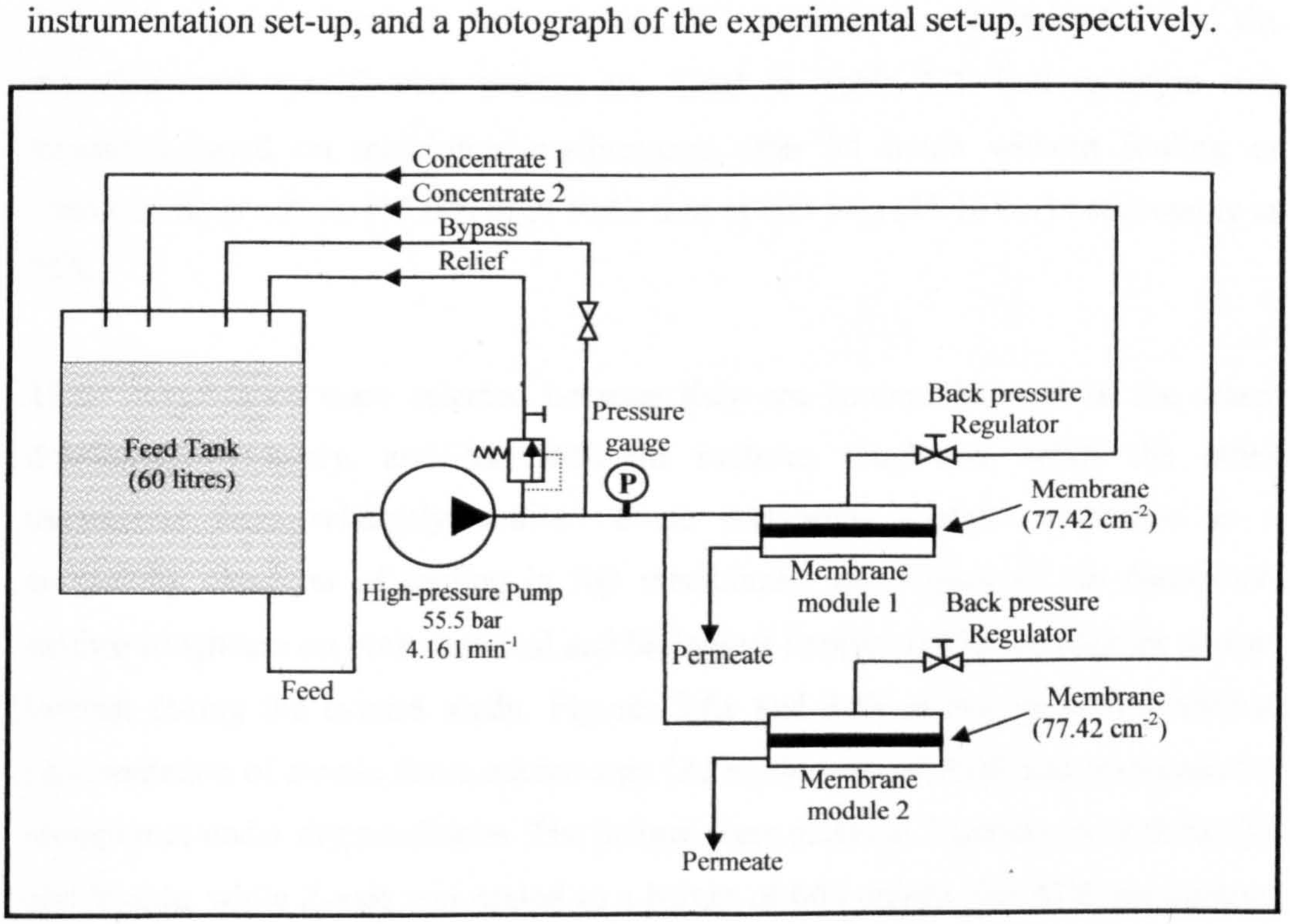

Figure 3.1: Schematic diagram of the high-pressure reverse osmosis membrane test system (HPROMTS).

Missing pages are unavailable

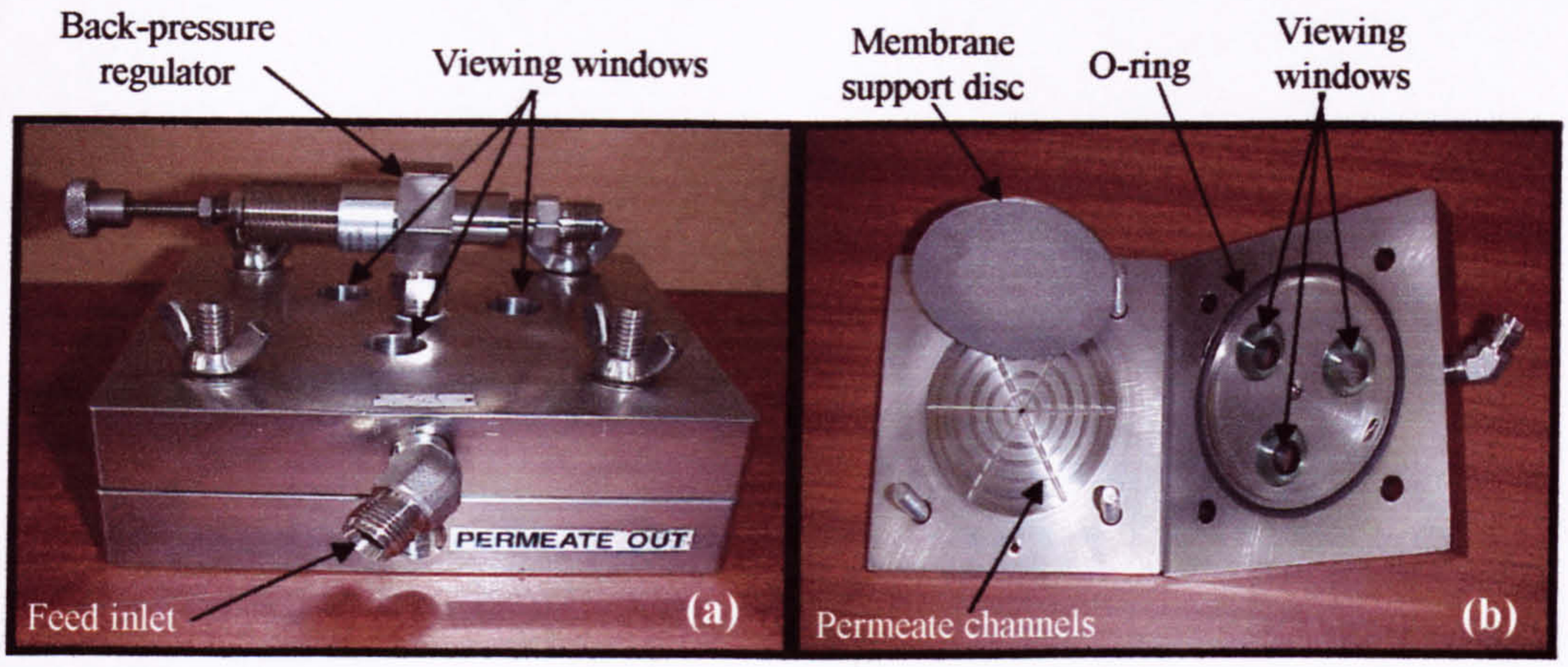

Figure 3.5: Pictures of the membrane module: (a) Complete assembly, and (b) Inside view.

3.1.1.2.4 Selection of RO Membranes

Two different RO membranes were selected for this study. These membranes are ADF (AD–Series, *Osmonics-Desal*, USA) and Nanomax-95 (Millipore, UK). Selected physico-chemical and operational characteristics (obtained from the manufacturers' specification sheets) are listed in Table 3.2. Salt rejection was measured based on membrane performance after 24 hours without fouling or boundary layer effects [32,000 mg/l NaCl feed at 800 psig (55.16 bar) net pressure at 25°C.

These membranes were selected because they are commonly used in the water desalination industry, and had different surfaces roughness, while the other parameters were relatively similar. Since membrane surface roughness is a controlling character of fouling in RO membranes, the impact of the membrane surface roughness on both chemical and biological fouling of RO membranes was of interest during the current study. Figures 3.6a and 3.6b shows three-dimensional representation of atomic force microscopy (AFM) images of ADF and Nanomax-95 membranes under dry conditions. The images were scales at 1 μm/div in both the X- and Y-axis, while Z-axis was scaled to a height of 600 nm/div for ADF membrane, and of 250 nm/div for Nanomax-95 membrane.

Table 3.2: Summary of membrane characteristics.

Parameter	ADF-TFC®	Nanomax-95
• Material	Thin Film Composite	Polyamide
• Configuration	Flat sheet	Flat sheet
• Surface roughness (R_a), (nm)*	46.45	8.77
• Salt Rejection, (%)	99.5	99.2
• Max. operating pressure (bar)	55.16	48.00
• pH range	4.0 – 11.0	4.0 – 10.0
• Temperature range	4 - 55	4 – 50
• Prefiltration Requirements	0.22	0.20

* More details on surface roughness are given in Chapter 6, Section 6.2.1.2.

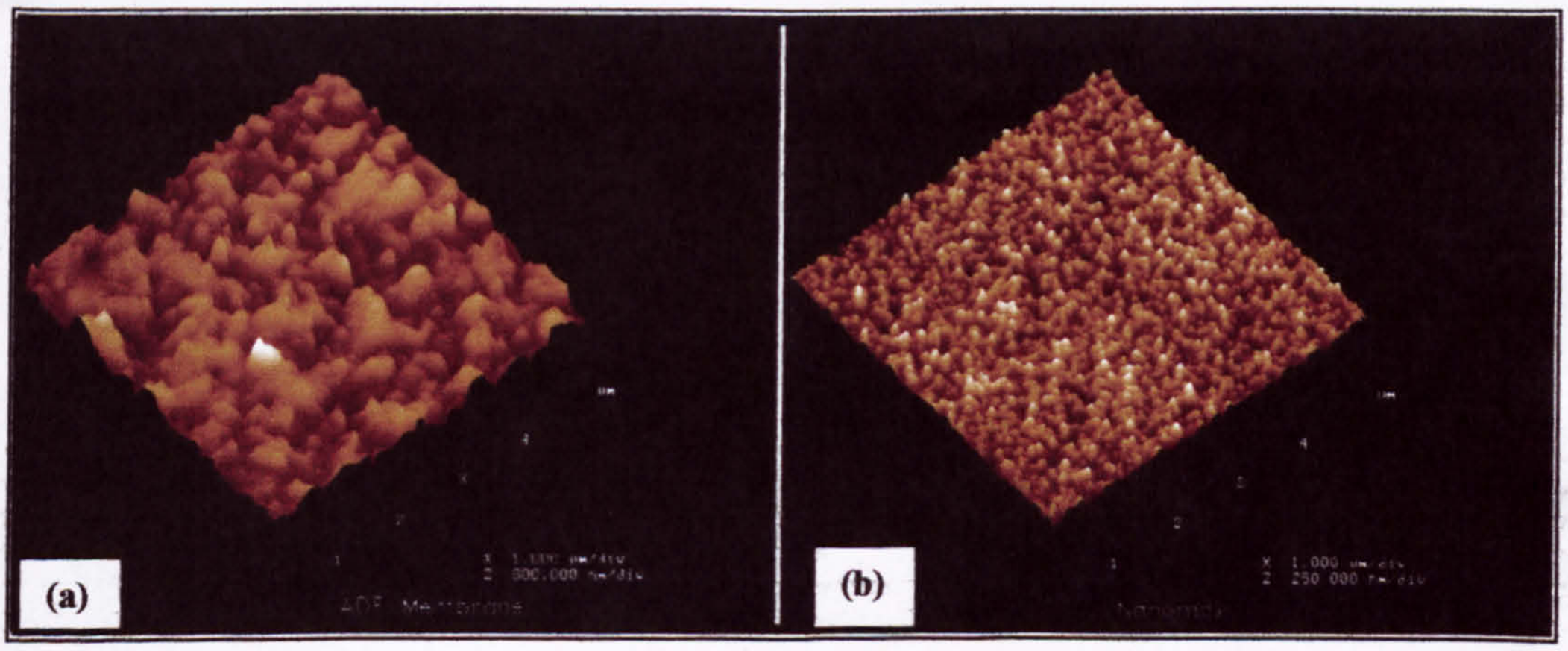

Figure 3.6: Three-dimensional representation of atomic force microscopy (AFM) images of: (a) ADF membrane, and (b) Nanomax-95 membrane, under dry conditions.

The AFM micrographs of the active layer surfaces of the composite (i.e. ADF) and the polyamide (i.e. Nanomax-95) membranes, shown in Figures 3.6a and 3.6b, clearly show the striking differences between the surface morphologies of the two membranes. While the thin-film composite (i.e. ADF) membrane exhibits large-scale surface roughness of ridge-and-valley structure, the polyamide (i.e. Nanomax-95) membrane surface is relatively very smooth. The distinct of the composite membrane is an inherent property of the interfacially polymerised aromatic polyamide

composite membranes (Petersen, 1993). In inspecting the AFM images, one should notice that the scale of the axes (particularly of the vertical Z axes) for the two types of the membranes are quite different (e.g. 600 nm/div. and 250 nm/div. for composite and polyamide membranes, respectively); a much larger scale Z axes was used for the image of the composite membrane because of its marked roughness. The roughness of the polyamide membrane is of the order of a few nanometres, whereas that of the composite membrane is of the order of several hundreds of nanometres. This selection of these two types of membranes was very successful in revealing the impact of surface roughness of RO membranes on the attachment rate of the colloidal and bacterial cells to the membrane surface, presented in Chapter 7.

3.1.1.2.5 Selection of Visualising Device and Membrane Module Modifications

In-situ monitoring of nuclei initiators of crystal formation on the membrane surface during operation was one of the main objectives of this study. The design considerations in this context focused on three tasks: Firstly, to make modifications to the stainless steel top plate of the membrane module in order to view the membrane surface. Secondly, to select a proper videoing device attached to a display device (e.g. computer screen) to detect the start of the formation of crystal initiators (i.e. nuclei formation) in a specific area on the membrane surface, and finally the selection of an appropriate lighting source in order to have a clear view of the membrane surface.

In-situ viewing of the membrane surface during operation required setting a transparent (i.e. glass) window‹s› on the top plate of the membrane module. This window‹s› must stand the system pressure (up to 70 bar), and have enough representative viewing area of the membrane surface. Three identical transparent discs, made of *toughened safety glass*, were evenly set and glued at the pre-cut windows on membrane module as, illustrated in Figure 3.5. The schematic drawing and dimensions of the glass window are shown in Figure (3.7). The glass disc has a diameter of 40 mm with a working diameter of 30 mm and a thickness of 10 mm. A circular (60 W) halogen lamp, with adjustable lighting intensity, mounted around the lens zoom was used to illuminate the membrane surface.

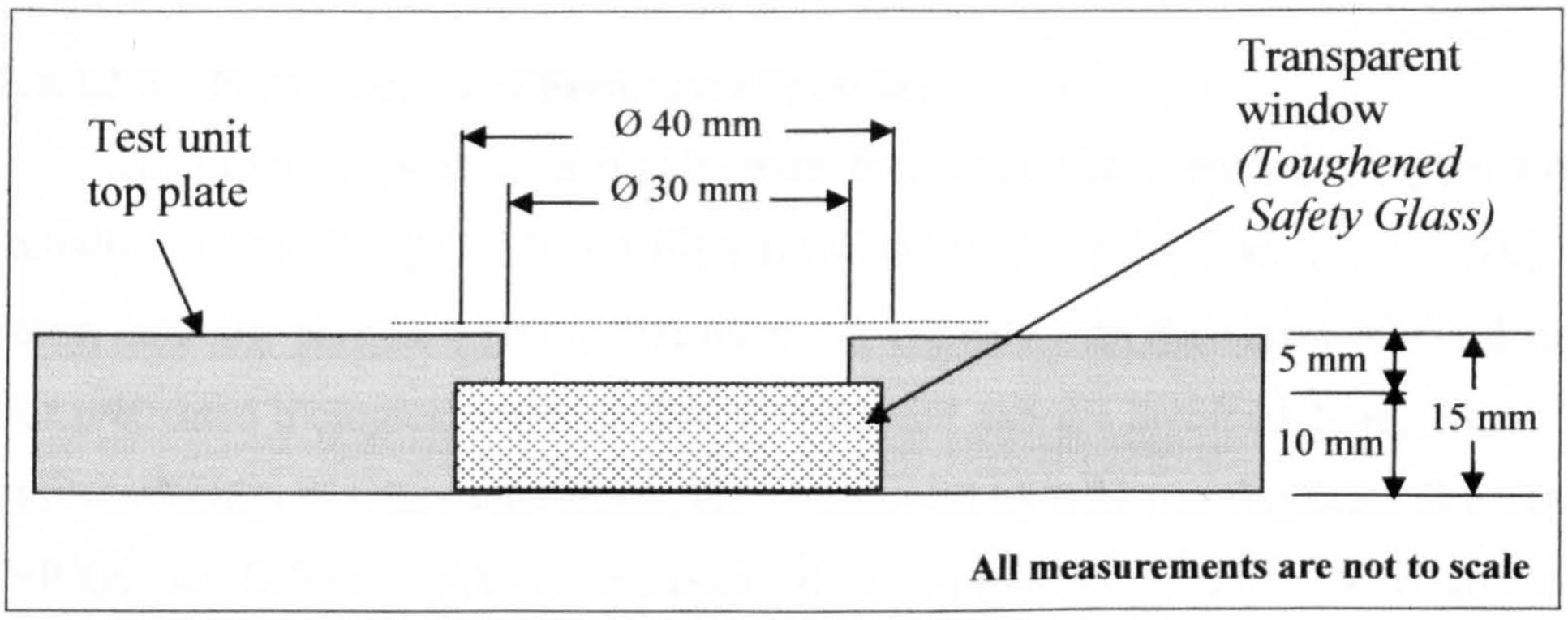

Figure 3.7: Schematic drawing of the viewing window on the top plate membrane module.

A *ZEISS Discovery V12 SteREO* microscope, attached to ZEISS Achromat 1.5× FWD 28 mm objective lens with a maximum magnification of 150× was used to view the membrane surface. Axiovision 4.5 software attached to this microscope was used to view live video and to snap pictures of the formed salt crystals during operation.

3.1.1.3 HPROMTS Procedure

3.1.1.3.1 Membrane Setting

At the beginning of each experimental run, lab grade distilled water was permeated through the membrane under standard conditions. 20 litres of distilled water was placed in the feed tank and was allowed to circulate through the membrane with a gradual increase in the system pressure until the recommended setting pressure by the membrane manufacturer (e.g. 500 psig, ~34.2 bar) was reached. The flux was monitored with time for 30 minutes to 45 minutes. This practice was essential, not only to flush the membrane channels from the preservatives (i.e. glycerine and sodium metabisulphite), which were added to prevent microbial growth in the membrane channels, but also to allow for any compaction to occur due to the pressure effects. The membrane was assumed to reach steady-state when the pure water flux varied less than 4% over a minimum period of 30 minutes.

3.1.1.3.2 Pretreatment of Feedwater Samples

In order to produce a highly pure feedwater, the prepared samples were initially filtered though a 1.2 μm filter (Millipore Glass microfiber filter, GF/C) to retain colloids, particles, and undissolved salt crystals with diameters of ≥ 1.2 μm. For pretreated biological samples, the pretreatment process involved 2-step filtration (1.2 μm Millipore Glass microfilter, GF/C followed by 0.22 μm BioTrace ® PVDF, Pall Gelman Laboratory) to ensure removal of any microorganism cells which were initially added in the preparation step of the biological samples. The filtration process (i.e. pretreatment) was conducted for the freshly prepared samples using apparatus from *Millipore Corporation, Bedford, Massachusetts, U.S.A.* The filtration unit is illustrated in Figure (3.8), and directly poured into the feed tank of the HPMCTS system prior to each experimental run.

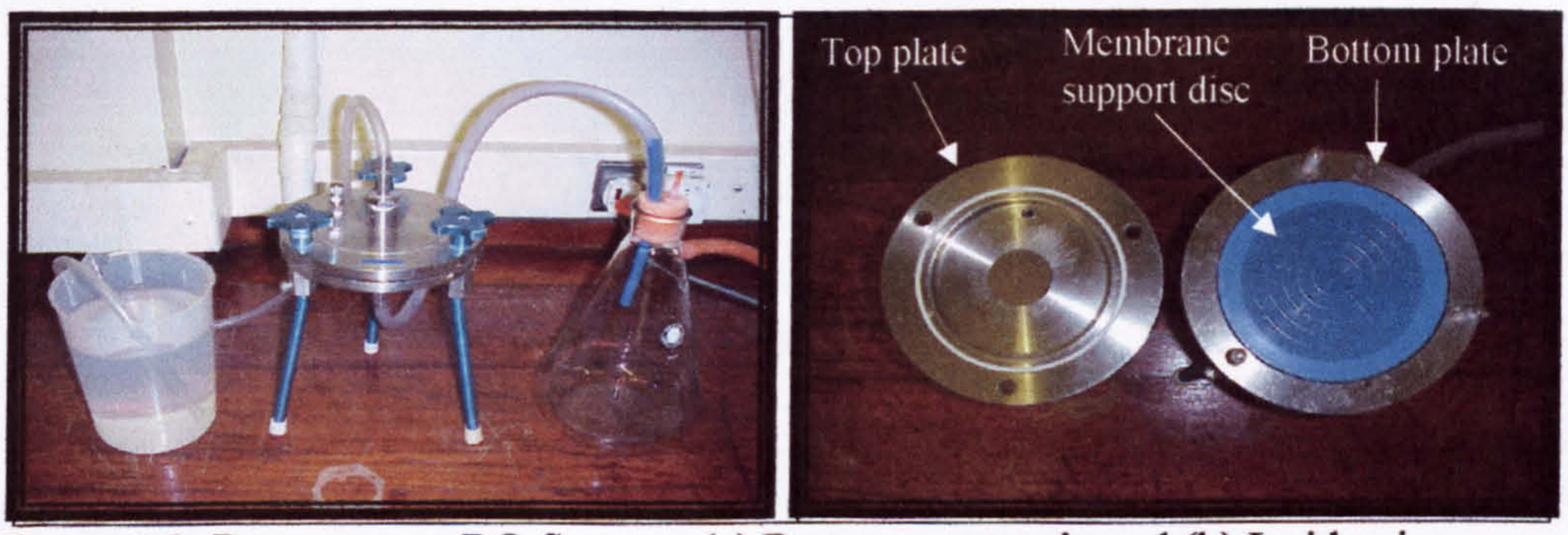

Figure 3.8: Pretreatment RO System: (a) Pretreatment unit, and (b) Inside view.

3.1.1.3.3 The Experimental Procedure

After setting the membrane with distilled water, the system pressure was decreased gradually to the minimal value (e.g. 2-5 bar) and the pressure pump was switched off. The water tank was emptied, and refilled with the prepared pretreated feedwater sample for the designated experimental run. Followed by switching on the pump, the system pressure was increased gradually starting from 100 psig up to 700 psig (6.83 bar to 47.83 bar) with increment intervals of 50 psig (3.41 bar) every step

(see Appendix B for more experimental run conditions). Permeate pressure, permeate volume, cumulative permeate volume, permeate flux, permeate cumulative flux were measured and/or calculated versus time at each pressure increment. The permeate volume was accurately measured using a *Precisa*® scale with an accuracy of 0.01g (i.e. 0.01 ml, assuming that the permeate product is pure water, density = 1 kg l^{-1}). The increase in the system pressure was continued until the system pressure relief valve automatically opened at the maximum pressure for the membrane (e.g. 650 psig to 675 psig = about 44.4 bar to 46.1 bar).

Once the flux behaviour for a designated experiment was finished, the run continued at the maximum pressure for crystallisation and/or biofouling investigation experiment. The microscope was switched on, starting the video monitoring of the membrane surface through the glass window. Once salt crystals started to develop on the membrane surface, they were photographed, and their dimensions were measured using the attached software (Axiovision 4.5).

Having finished the experimental run, the pressure was decreased to the minimum, the pump switch off, and the membrane module was dismantled. If that membrane was to be observed by ESEM, the membrane sheet was taken out using clean tweezers to prevent damage and contamination, by horizontally sliding the membrane sheet out from the module to a clean and sterile Petri-dish without loosing the water droplets on the membrane surface to keep it moist until observation, and finally, the Petri-dish was sealed using Parafilm sealant and kept at 4°C until use.

3.1.2 Rotating Annular Biofilm Reactor (RAB)

3.1.2.1 Description of Rotating Annular Biofilm Reactor (RAB)

In the cyanobacterial adhesion experiment, the biofilm was grown using a rotating annular biofilm (RAB) reactor, Model 1120, *Biosurface Technologies*, USA (http://www.imt.net/~mitbst/); operated at batch mode. The reactor was operated at room temperature (22±2°C) and a slow rational speed of 28 rpm, in order to maintain equity in light exposure and nutrients contact for all exposed slides, as well as to prevent biofilm sloughing and the detachment of the adhered bacterial cells. Details

of the reactor dimensions, as obtained from their manufacturer specifications sheets, are given in Table 3.3, and the reactor shown in Figure 3.9.

Table 3.3: Physical characteristics of the RAB reactors used in the study

Parameter	Reactor dimensions
Diameter of rotating cylinder	140 mm
Diameter of inner glass cylinder	157 mm
Width of annular gap*	8.5 mm
Height of rotating cylinder	155 mm
Height of inner glass cylinder	176 mm
Diameter : height ratio inner glass cylinder	0.892
Wet height of reactor	160 mm
Working volume	1000 mL
Surface area of one slide	1875 mm^2
Diameter of draft tube	12.5 mm
Length of draft tube	160 mm
Number of draft tubes	4
A/V ratio	2.3

* Distance between inner and outer cylinder.

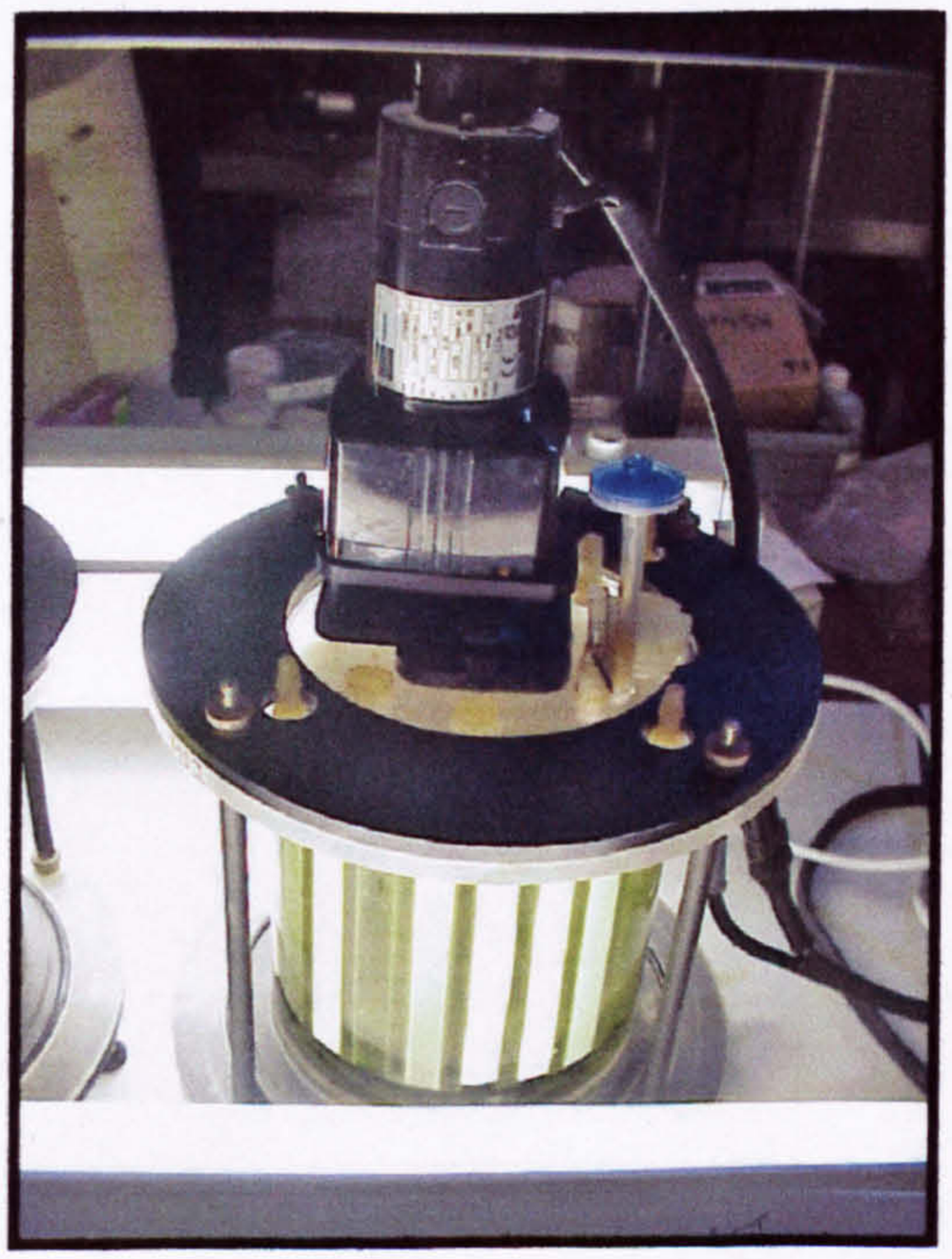

Figure 3.9: A photograph of the Rotating Annular Biofilm (RAB) Reactor.

The reactor shown in Figures 3.9, 3.10a and 3.10b consists of two concentric cylinders; a stationary outer transparent (Toughened glass) cylinder and a rotating inner drum, which accommodates 24 removable slides.

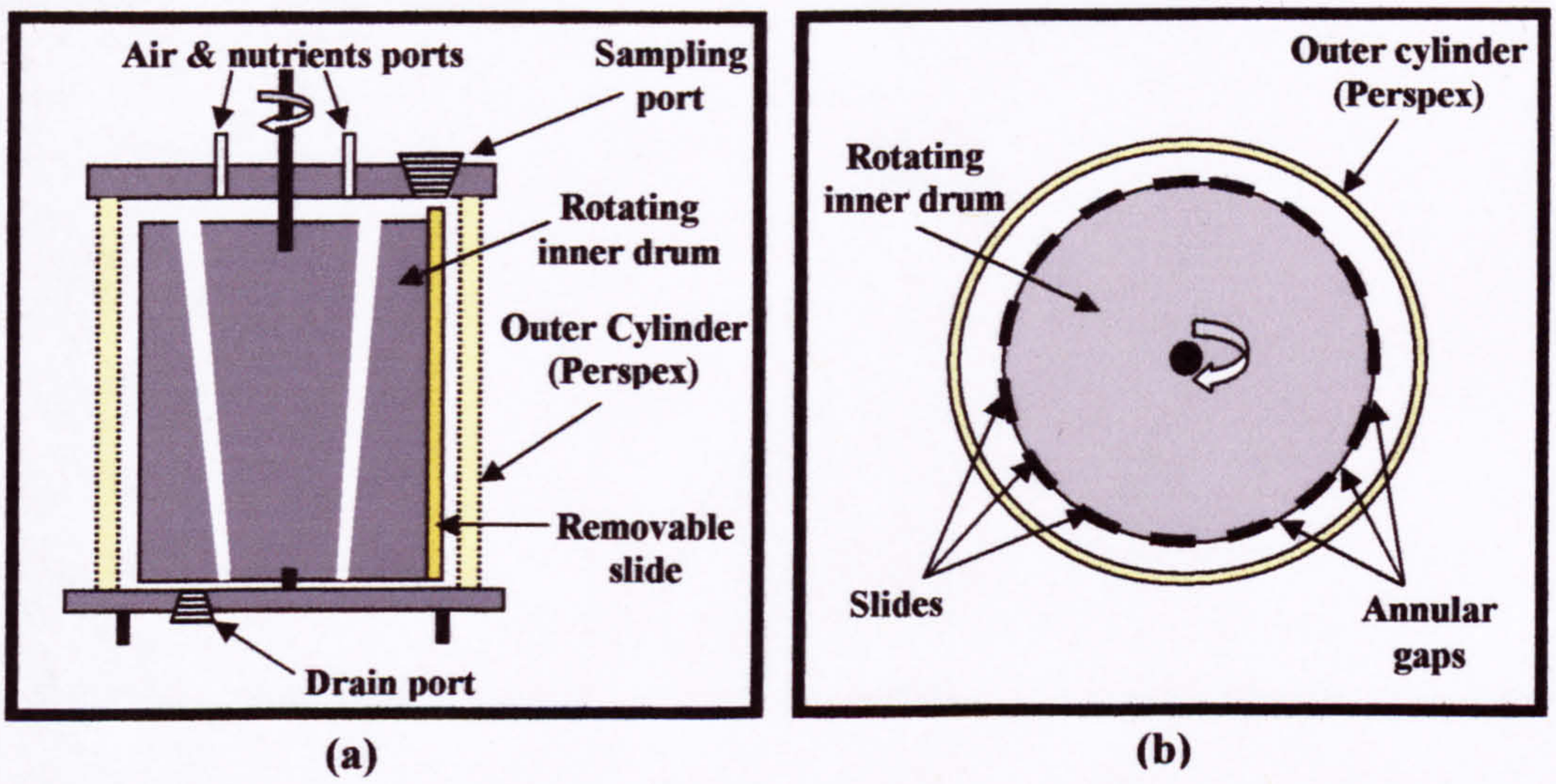

Figure 3.10: Schematics of the Rotating Annular Biofilm Reactor (RAB): (a) Side view and (b) Top view.

The bioreactor can fit removable slides (15 cm × 1.5cm) of different materials (Figure 3.11), providing for removable experimental surfaces for biofilm growth. In this study, four different substrata were investigated, ADF (thin film composite) membrane, stainless steel (EN1.4307), Perspex glass, and Teflon. The rotational speed of the inner drum was controlled by a variable speed motor, allowing control of different shear stresses to be applied to the slides. The reactor was equipped with an air filter (Millipore, 0.22 μm) inlet that allowed the air exchange, a slide removal port and an outlet drain that was used to drain the system after completion of the experimental run.

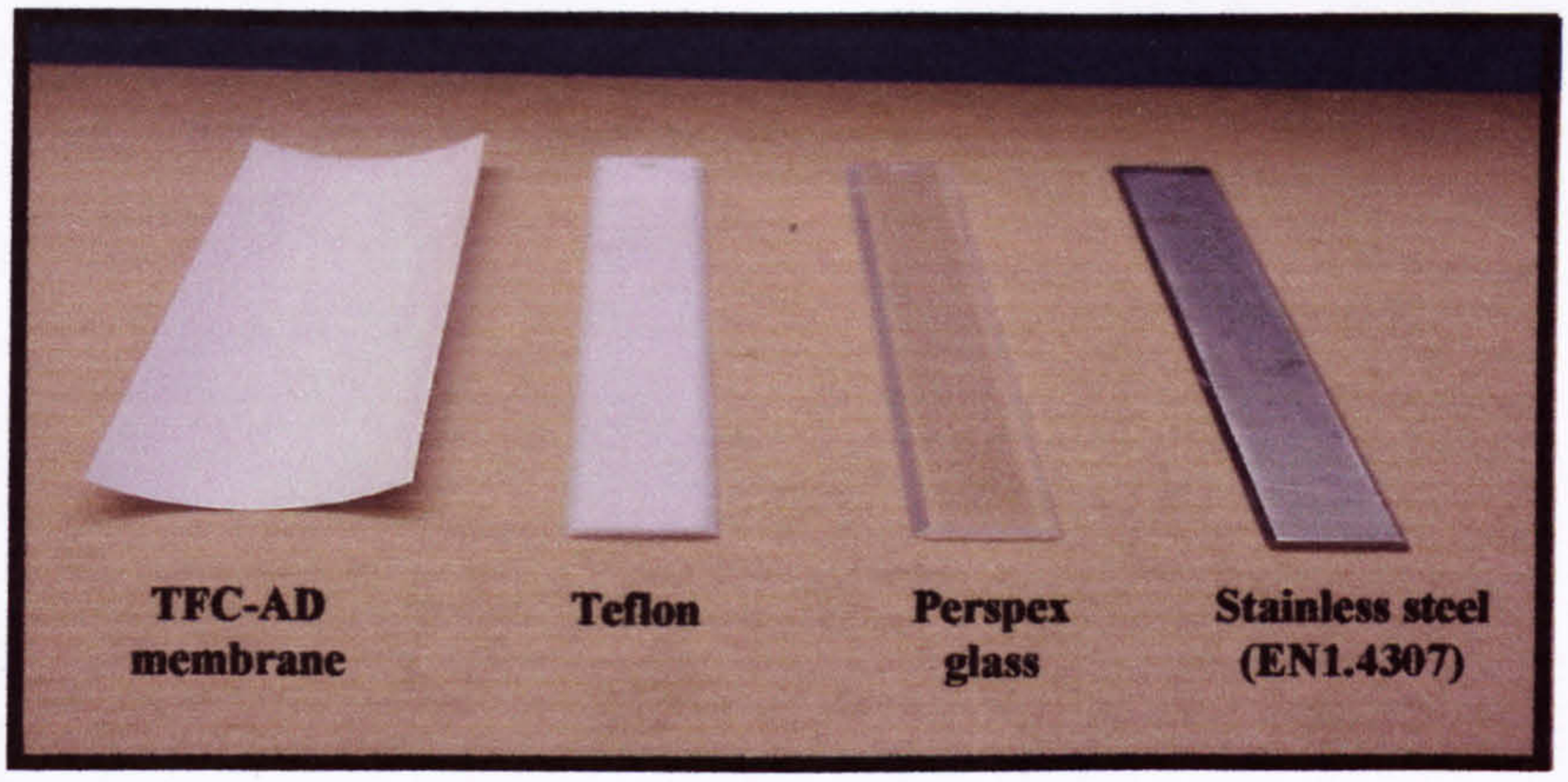

Figure 3.11: Slides of various materials used in the bacterial adhesion experiment.

3.1.2.2 RAB Inoculation and Experimental Conditions

At the beginning of the experiment, two annular reactors and a set of four slides of each material for each reactor were used. Four slides of each material were firstly, degreased with benzene in an ultrasonic bath for 30 minutes, soaked in 1% (w/v) solution of Virkon powder (VWR International Ltd., UK) for overnight, and rinsed in distilled water for several times. Finally, the slides were installed on the inner drum of each reactor and sterilised by autoclaving. Under sterile conditions (inside a laminar flow cabinet), the membrane sheets were mounted on Perspex glass holders in order to stretch them flat in the solution. The reactors, were then inoculated with 800 ml pre-grown cyanobacterial cultures: one was grown in BG11 medium (described later in Section 3.3.1.3) with no added salt, and the other culture was grown in BG11 medium with 60 g/l of NaCl. The experiment was operated in a batch mode at 28 rpm (corresponding to a shear stress of about 0.1 N m^{-2}), under a 12 h light/dark cycle during the experiment period until bacterial attachment started to develop, which was confirmed by eye (more details on culturing and the experimental conditions are presented in Chapter 6, Section 6.2.2).

After inoculation, the two-reactor system was run under semi-batch conditions as 200 ml of fresh media aliquots were fed to each reactor every week in order to maintain a sustainable nutrient flow in the system at a constant shear rate (0.1 N m^{-2}). These conditions were selected based on evidence on washout conditions selected for

microorganisms that are able to form biofilms, and that intermediate shear rates increase nutrient transport from the bulk solution into the biofilm without excessively decreasing its thickness (Bachman and Edyvean, 2006).

3.1.2.3 Biofilm Growth, Detection and Sampling of Slides

Having all slides submerged in the cyanobacterial culture media; the attachment of biomass cells on the provided slides was visually monitored and regularly photographed. The biomass concentration in the bulk solution was regularly monitored in order to maintain a sustainable biomass concentration in the solution to avoid detachment of biofilm from the slides. In order to analyse the attached biofilm, the slides were removed from the bioreactor (through the sampling port, Figure 3.10a) under sterile conditions, were placed in sterile air-tight glass containers, and were kept at 4°C until further analysis.

3.2 Sample Collection and Preparation

3.2.1 *In-situ* Determinations

In-situ analyses, such as water temperature, pH, dissolved oxygen and water salinity at various depths of the lake were carried out on the day of sampling. These data are reported in Table 4.1 (Chapter 4). The methodology of carrying out these measurements is presented in following Section 3.2.3. In addition, further information and data from some reported research work on this lake have been obtained from organisations involved (*e.g. The Faculty of Engineering and Technology, University of Sebha, Brack, Libya*), are presented in Table A-2, Appendix A.

3.2.2 Sampling Procedure

Due the remoteness and the transportation difficulties of regularly visits to Qabar-Onn Lake, water sampling was carried out only three times throughout the research period. The sampling season, time, and locations were considered due to the large seasonal and time variations of the water composition. Water sampling was carried out in May (beginning of warm season) in years 2003, 2004, and 2005 at 1000 and 1200 hrs. Since Qabar-Onn Lake represents a stratified lake profile (i.e.

phytoplankton, thermocline and anaerobic, respectively), three sets of samples were collected from three depths (0.2 m, 4.0 m and 8.0 m), which represent these lake stratification layers (Figure 3.12). Water samplings were collected from 6 locations distributed over the lake.

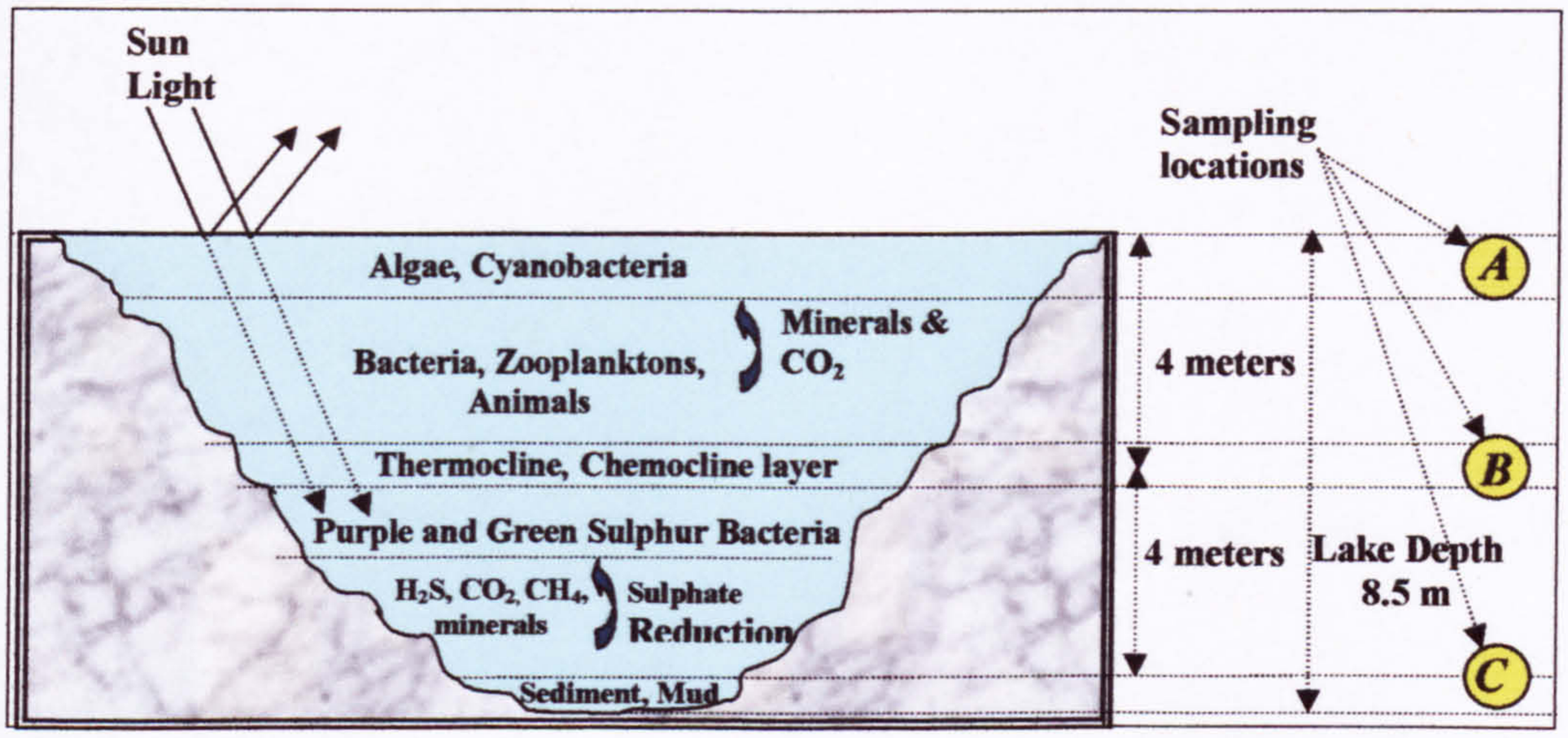

Figure 3.12: Water sampling locations at Qabar-Onn Lake.

Water samples were collected in pre-autoclaved 500 ml Pyrex glass bottles using a Casella water sampler shown in Figure 3.13. Three sets of samples were collected from each sampling location, of which one set was used for *in-situ* determinations (e.g. temperature, pH, dissolved oxygen, conductivity, and salinity), while the other 2 sets were kept in a special cool box at about 8°C – 12°C. Afterwards, the samples arrived at the laboratory approximately 10 hours after collection and were stored at 4°C.

A digital thermometer was used for measuring the temperature of the collected samples (±0.05°C). Water temperature for the samples taken from the surface (i.e. 0.2 m depth) was measured directly before taking the samples, however, for the other samples, which were taken from deep depths (i.e. 4.0 m and 8.0 m), water temperature was measured directly after sample collection took place. A *Horiba* pH/conductivity meter (model HB 3500) (± 0.05) was used to determine both the pH and conductivity values of the collected water samples in the field , while a *Horiba*

dissolved oxygen meter (model HB 3311) (± 0.05) was used for *in-situ* determinations of the dissolved oxygen values of the collected water samples. Direct salinity determinations were carried out *in-situ* using a salinity refractometer (Model *ECO7212*, based on percent NaCl, range 0 to 26%) with an accuracy of 2%. Although, this instrument could only give rough estimates of salinity profile in the lake, these estimates were very useful in selecting representative sampling locations in the lake.

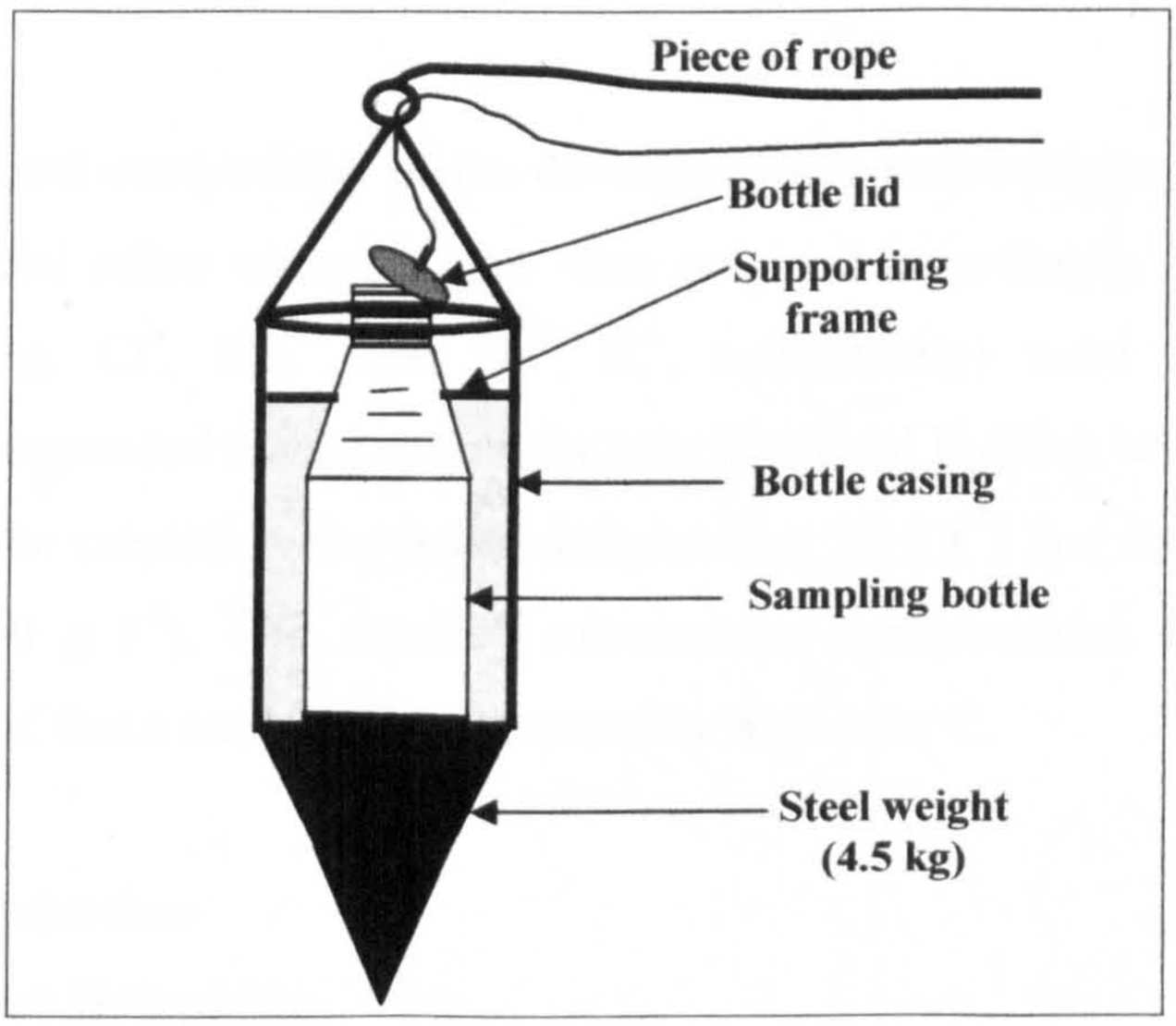

Figure 3.13: Casella water sampler used at Qabar-Onn Lake.

3.2.3 Preparation of Artificial Samples

Due to the relatively large quantities of saline water samples required for each run (20 litres/run) and the large number of experiments required (e.g. 30 runs), all experiments were conducted on artificial saline water samples. The ingredients of the prepared water samples were based on the physico/chemical and biological analyses of Qabar-Onn Lake water. The prepared water samples were categorised into three main types: chemical water samples, biological water samples, and pretreated biological water samples.

In chemical water samples, only chemical ingredients were added to pure distilled water at a designated ionic type and concentration. Whereas, preparing biological water samples involved inoculating chemical water samples with biomass of specific type and concentration. The third type of water samples (i.e. pretreated water samples) have been prepared by performing a 2-step filtration of the biological water samples (1.2 μm followed by 0.22 μm) to ensure the removal of any microorganisms cells which were initially added in the preparation step of the biological samples. The type of the water sample required for a particular run was dependent on the main objective of that experiment.

Based on chemical composition of the dominant ionic concentrations in Qabar-Onn Lake, the artificial saline water samples were prepared accordingly. Two anions and two cations (e.g. Cl^-, SO_4^{2-} and Na^+, K^+, respectively) were selected. These ingredients corresponded to two main salts (*viz:* NaCl and K_2SO_4), which were added in combination to prepare saline water samples (i.e. 30 g l^{-1}) and hypersaline water samples (i.e. 60 g l^{-1}). The detailed calculations, compositions and preparation methodologies of these samples are presented in Appendix C.

3.3 Media Selection

3.3.1 Media for Halophiles

Halophiles are the easiest group of Archaea to culture in the laboratory. A variety of complex media have been described in the literature and a representative collection of media are presented in Tables 3.4 and 3.5. Many, if not most, halophiles will grow in "typical" complex media, e.g., DSM 97 and DSM 372. Some species have the capability of utilising sugar, whereas most require an amino-acid-rich broth.

Unless otherwise indicated, all media components are listed in grams per litre of medium and the final pH is adjusted to 7.2 with 1M NaOH. To avoid precipitation, nutrients and salts were autoclaved separately, although this is not absolutely required. For agar plates, 2% (w/v) agar was added before autoclaving. Due to unavailability of the *Casamino acids*, tryptone water was used as a substitute at the same indicated values and sodium glutamate was deleted from the ingredients list.

Table 3.4: Composition of the DSM 97 medium.

Additive	Concentration/litre
Tryptone H_2O	7.5 g
Yeast extract	10.0 g
Trisodium citrate	3.0 g
KCl	2.0 g
$MgSO_4$, $7H_2O$	20.0 g
$FeSO_4$, $7H_2O$	0.05 g
$MnSO_4$, H_2O	0.20 g
NaCl	250 g
Agar	20.0 g
Distilled H_2O	1000 ml

The pH was adjusted to 7.4, and agar was added after dissolving all ingredients in distilled water.

Table 3.5: Composition of the DSM 372 medium.

Additive	Concentration/litre
Tryptone H_2O	5.0 g
Yeast extract	5.0 g
Sodium glutamate	1.0 g
KCl	2.0 g
Trisodium citrate	3.0 g
$MgSO_4$, $7H_2O$	20.0 g
$FeSO_4$, $7H_2O$	36.0 g
$MnSO_4$, H_2O	0.36 g
NaCl	200.0 g
Agar	20.0 g
Distilled H_2O	1000 ml

Distilled water was added to give 1000 ml, and the pH was adjusted to 7.0-7.2.

3.3.2 Media for Moderately Halophilic Bacteria

The *complex* medium prepared by Rosenberg (Cummings *et al.*, 1993) was successfully used for growing and isolating *Halomonas* bacteria from seawater. A small volume of the artificial seawater (e.g. 26 ml) was replaced by Qabar-Onn Lake water in an attempt for the medium to match the lake water conditions (e.g. chemical composition and nutrients). The ingredients and their concentrations of the Complex medium are presented in Table 3.6.

Table 3.6: Composition of the Complex medium.

Additive	Concentration/litre
Peptone	1.0 g
Yeast extracts	1.0 g
NaCl	178.2 g
Lake water	26 ml
Agar*	15.0 g
Distilled H_2O	1000 ml

* pH was adjusted using 1m NaOH and NaCl was added to adjust the required salinity. Agar was added, after pH and salinity adjustments, when a solid medium was needed.

3.3.3 Media for Cyanobacteria

Most media, and especially the synthetic media, were developed for planktonic unicellular algae, although benthic species have been cultured successfully in some of them (Paerl *et al.*, 2000). It is stated that a particular medium is best for certain species, but this is rarely supported by comprehensive, quantitative comparisons.

The purpose of marine media, however, to grow marine algae, is that a medium should be as simple as possible in composition and preparation. There is considerable variability amongst synthetic media, especially with respect to salinity and concentration of calcium and magnesium (Garcia-Pichel, *et al.*, 1998)). These media are generally buffered, contain mixtures of vitamins and chelated trace metals and may be autoclaved or sterile filtered.

In this experiment, three media types were used to grow unicellular cyanobacteria which include Muller, the defined, and BG11 media. Muller has been used for growth of unialgal cultures successfully (Stein, 1979). *Dinoflagellates*, several red and brown algae and *coenocytic* green species have been grown successfully. The medium was unbuffered and some precipitation resulted from autoclaving, but the pH returns to normal about 36 h after sterilisation. The composition of the medium consists of nutrients, trace elements and vitamins as shown in Table 3.7.

Table 3.7: Composition of the enriched Muller medium.

Additive	Concentration/litre
Nutreints:	
NaCl	457 mM
KCl	9.8 mM
$MgSO_4$	26.6 mM
$MgCl_2$	23 mM
$CaCl_2$	13.5 mM
$NaHCO_3$	2.4 mM
$NaNO_3$	1.18 mM
Na_2HPO_4	140 µM
Na_2SiO_3	0.07 mM
Trace metal solution:	M-I + M-II (Tables: 3.5 & 3.6)
Vitamins:	
Cyanocobalamin	0.5 µg
Biotin	0.5 µg
Thiamine.HCl	100 µg
Distilled H_2O	1000 ml

The defined medium described below has been used to grow *Halomonas* SPC1 which was a contaminant of a culture of the halotolerant green algae *Dunaliella prava* CCAP19/9 by Cummings *et al* (1993). The ingredients of the medium are listed in Table 3.11.

Table 3.8: M-I (Trace metal additives for Muller medium)

Element	Conc. µM/l of medium
Zinc	14
Manganese	3.8
Molybdenum	0.83
Cobalt	0.04
Copper	0.008
Iron	1.2
EDTA	53.7
Chelate : metal	2.7 : 1
Boron	32

Table 3.9: M-II (Trace metal additives for Muller medium)

Element	Conc. µM/l of medium
Bromine	185
Strontium	14
Aluminium	0.21
Rubidium	0.13
Lithium	0.14
Iodine	0.12

Table 3.10: Composition of the Defined medium.

Additive	Concentration/litre
$MgSO_4$	50 mM
Tris-HCl (pH 7.6)	50 mM
KCl	10 mM
NH_4Cl	19 mM
Na_2SO4	0.1 mM
FeEDTA	0.025 mM
$K_2HPO_4, 3H_2O$	0.33 mM
Trace element mix*	1 ml
Distilled H_2O	1000 ml

*** pH was adjusted using 1m NaOH and salinity was adjusted to match the lake water. 1 ml of trace element mixtures M-I (Table 3.8) and M-II (Table 3.9) were added to the medium.**

BG11 medium described below has been used to grow most unicellular blue-green algae (cyanobacteria) (Balows et al, 1992a; Flemming *et al.*, 1987; and Flemming *et al.*, 1994). The ingredients of the medium are listed in Table 3.11.

Table 3.11: Composition of BG11medium.

Additive	Concentration/litre)
$NaNO_3$	15 g
K_2HPO_4	0.04 g
$MgSO_4 . 7H_2O$	0.075 g
$CaCl_2 . 2H_2O$	0.036 g
Citric acid	0.006 g
Ferric ammonium citrate	0.006 g
EDTA	0.001 g
Na_2CO_3	0.02 g
Trace element mix*	1 ml
Distilled H_2O	1000 ml
Agar	10 g

*** pH was adjusted using 1m NaOH and salinity was adjusted to match the lake water. 1 ml of trace element mixtures M-I (Table 3.8) and M-II (Table 3.9) were added to the medium.**

3.4 Microbiological Procedures

3.4.1.1 Gram's Staining

Gram's staining experiment was carried out on the halotolerant bacterial species, isolated fro Qabar-Onn Lake, in order to characterise them for the purpose of identification. A Gram's Staining Kit (Catalogue No. PL8055/25, which contains 250 ml Crystal Violet, 250 ml PL7000/25; 250 ml Gram's Iodine, PL7003/25; 250 ml Gram's Differentiator, PL7006/25; 250 ml Safranin, PL7012/25) was used for both Gram-positive and Gram-negative staining of the isolated halobacteria in this experiment.

The staining procedure was carried out as described in the protocol of this product (a detailed staining procedure is presented in Appendix B). 100 µl of the thick centrifuged halobacterial culture was used to prepare a smear on a microscope slide. Having the staining process was done, the stained slides were observed under a light microscope (OLYMPUS, reflected light/fluorescence attachment, Model BH2-RFCA, Japan) using oil immersion objective ×100 magnification. When the Gram's stain procedure is performed correctly, organisms or cells that retain the primary stain/mordant complex will appear as blue to purple in colour and are termed Gram-positive. Organisms and cells that are decolourised by the Differentiator and take up the counter-stain will appear as pink to red in colour and are termed as Gram-negative.

3.4.2 Colony Forming Units

Colony forming units (CFU) were used to measure the number of culturable microorganisms (viable) present in solution and harvested from various substrata surfaces. Samples were serially diluted on sterile Complex medium aliquots (in order to obtain between 30 and 300 colonies per plate), and triplicate samples were plated in agar media containing Complex medium, using a spiral plater (Spiral Biotech, Inc, Bethesda, MD). Colonies were counted after 48 hours of incubation at 37°C. This method provided information regarding numbers of living microorganisms that were

capable of growing on this media, more detailed methodology presented in Chapter 6, Section 6.2.1.4.

3.4.3 Direct Microscopic Counts

Direct counts of the living and dead halobacterial cells, attached to various substrata surfaces, were performed and compared using epifluorescence microscope Model Leitz DIALUX 22EB, equipped with UV gun Ernst Leitz Wetzlar GMBH (type 307-143.004 514662, 100 W, Germany). The coupons surfaces were stained using the (LIVE/DEAD *Bac*Light Bacterial Viability Kit L7007; Molecular Probes Europ BV; The Netherlands) (Biggerstaff *et al.*, 2006). The staining procedure was performed, as stated in the staining protocol described in Appendix B, by direct application of 3 µl of the dye mixture to the attached bacterial cells on various substrata surfaces. Then, the coupons were incubated in a dark place at room temperature for 15 minutes. The coupons were then covered with cover slips and observed under the epimicroscope, using a oil immersion lens, giving a total magnification of ×1000. At least 5 fields of view were counted on each coupon. Bacteria with intact cell membranes fluorescing green and were counted with the intention of enumerating viable bacteria, whereas cells with damaged membranes stain fluorescent red and were counted dead. More detailed methodology presented in Chapter 6, Section 6.2.1.5.

3.5 Physical-Chemical Measurements

3.5.1 Pressure, Temperature, Flow Rates, Conductivity and pH

Table 3.12 characterises the equipment used to monitor physico-chemical parameters. Instrument calibrations were performed according to the manufacturers' guidelines. The pH/conductivity meter was calibrated with standard solutions. The pH probe was calibrated using pH 4, 7 and 10 standard buffer solutions (Fisher Scientific), and the conductivity was calibrated using a 1409 µS/cm NaCl standard solution (Fisher Scientific).

Table 3.12: List of equipment used in physico-chemical parameters determinations.

Parameter	Equipment	Manufacturer/Vendor
Pressure	Pressure relief valve Pressure meter	Desal OSMONICS
Temperature	Temperature probe Thermometer	Cole Parmer Instruments
Flow rate	Precisa scale Class A cylinder	Model XB1600, Swaziland. Scientific Laboratory Supplies SLS
pH/conductivity	Portable pH meter pH/conductivity meter	Hanna instruments (model HI 9145), Sartorius (model PY-P10)
TDS	TDS meter	Sartorius (model PY-P10)
Dissolved oxygen	DO meter	Horiba dissolved oxygen meter (model HB 3311)
Turbidity	Turbidity meter	Hanna instruments (model LP 2000)
Light intensity	Light probe	Fluke Instruments

3.5.2 Silt Density Index (SDI)

The feed water pressure was set to 2.0 bar. Before inserting the membrane filter, 1 l of water sample to be tested was allowed to flow through the testing device, and the temperature was measured during this run. The temperature was between 22°C and 24°C, and was constant during the test run within ±1°C. The membrane filter was then inserted using tweezers to prevent damage, and after having removed any air enclosed, the testing unit was tightly closed. The ball valve was then opened and the time required to filter 500 ml (T_i) was measured using a stopwatch. A graduated measuring cylinder (Class A) was used to measure the volume. After 15 minutes (T_i), the filtration time (T_f) i.e. the time required to filter a further 500 ml of water, was measured and recorded.

3.5.3 Metal Composition

Metal concentration was measured by inductive coupled plasma (ICP)-optical mass spectroscopy (EPA method 200-7), at the AlControl Laboratory, Rotherham,

UK. Undiluted sample volumes of 5 ml were used to measure up to 10 different metals. Method detection limits and more details are shown in Appendix B.

3.5.4 Protein Analysis

Protein analysis in the halobacterial cell-free extract was measured using the Bradford assay (BioRad Laboratories, Sigma® UK). 50 ml of solution was thoroughly mixed with 2.5 ml of protein dye (BioRad Laboratories, Sigma® UK), and colour allowed to develop for 5 minutes, after which the absorbance was measured at 595 nm. A Thermo Spectronic spectrophotometer (MODEL Helios Epsilon) was used. The obtained absorbance were compared to a calibration curve, developed with serum bovine albumin (SBA) solutions (BioRad Laboratories, Sigma® UK), ranging in concentration between 100 µg/ml to 900 µg ml^{-1} with a calculated MLD (minimum detection limit) of 15 µg ml^{-1}.

For the cyanobacterial isolates, the cell-free extract protein analysis was measured using RC-DC Protein Assay (Bio-Rad). The detailed analysis procedure is described in the Protocol stated in Appendix-B.

3.5.5 Compatible Solutes Analysis

NMR analyses were carried out on a Bruker DRX-500 spectrometer operating at 500 MHz for ^{1}H and 125.8 MHz for ^{13}C. All spectra were obtained at a sample temperature of 25°C using a 5 mm tube. Sodium trimethylsilylpropionate (TSP) was used as an internal standard for both chemical shift referencing and concentration. Chemical shifts are listed in ppm (frequency relative to TSP × 10^{6}). For ^{1}H, spectra were acquired using a 90° pulse width (9-20 µs, depending on salt concentration) into 4k complex points over a spectral width of 12500 Hz. This gave an acquisition time of 330 ms, and a 1s relaxation delay was used between scans, typically acquiring 128 transients depending on signal intensity in the sample. The two-dimensional TOCSY (total correlation spectroscopy) spectrum was acquired on a Bruker DRX-600 at 600 MHz, using an 80 ms spin-lock mixing time, a spectral width of 15015 Hz in the direct dimension and 7507.5 Hz in the indirect dimension, 4k complex points in the direct dimension and 400 in the indirect dimension, and a

spin-lock field of 8.4 kHz. Two-dimensional ^{13}C, ^{1}H correlated spectra (C-HSQC) were acquired using 2k real points over a spectral width of 6266 Hz, with a relaxation delay of 2s. ^{13}C garp decoupling was applied during the acquisition time. The magnetisation pathway was selected using gradients, and the magnetisation transfer delay was optimised for a $^{1}J_{CH}$ coupling constant of 145 Hz. In the indirect (^{13}C) dimension, 64 complex points were acquired over a spectral width of 8818 Hz. All spectra were transferred to a Unix computer and processed using FELIX (Accelrys, San Diego, CA). Assignments were made by spiking the sample with authentic samples, and by comparison to published data (e.g. Nagata *et al.*, 1996).

3.6 Environmental Scanning Electron Microscope (ESEM)

Six membrane samples were selected for environmental scanning electron microscope (ESEM) observation. These samples represent one chemical, one biological, and one pretreated run for two types of membranes. ESEM observations were carried out on fresh membranes over three separate run sessions (2-4 hours after the experimental runs finished). As mentioned earlier in experimental procedure (Section 3.1.1.3.3), fresh membrane samples were prepared for ESEM observations by cutting membrane disks (6mm diameter) using a 6 mm cork bore, then the specimens were mounted on adhesive carbon disks on brass studs using clean and sharp tweezers.

All ESEM observations were carried out using Philips XL30 ESEM FEG (FEI/Philips Electrin Optic) equipped with a Schottky Field-emission electron gun, at Hallam University, Sheffield, UK (Figure 3.14). Two PLAs separated the microscope chamber from the FeG column, thereby creating three regions that were separately pumped. The actual chamber pressure and the temperature of the specimen were controlled from a MS Windows graphical user interface and regulated to bring liquid water into thermodynamic equilibrium with the vapour phase.

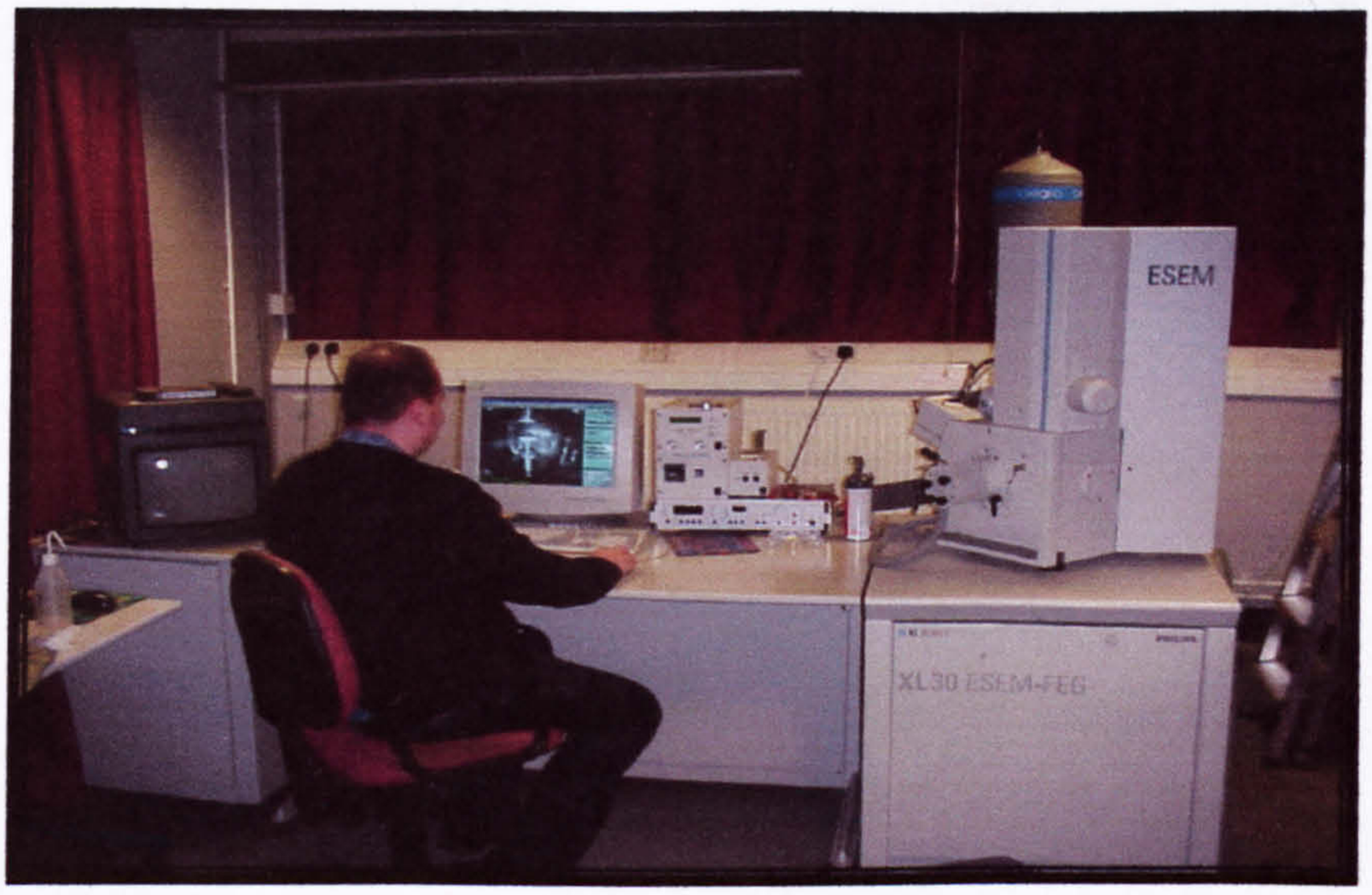

Figure 3.14: A picture of the Philips XL30 ESEM FEG (FEI/Philips Electrin Optic).

The instrument settings were constant for all the three sessions. All specimens were directly viewed in environmental "wet" mode and the specimen temperatures were set to 4°C. When working at a temperature of 4°C, a gas pressure of 4 torr, and maintained the specimen (membrane) surface wet before pump-down procedure. Optimal conditions to maintain a relative humidity of 80% to 85% were experienced. However, specimens with intensive salt crystallisation were prone to dry before observation and photography were completed.

A peltier-cooled specimen stage (Figure 3.15) allowed specimen temperature regulation before and during the observation. A gaseous secondary electron detector (GSED) was mounted below the final lens assembly to permit secondary electron imaging in a gaseous environment. All observations were conducted at beam energies of 10-15 kV, and within a working distance of 10-15mm.

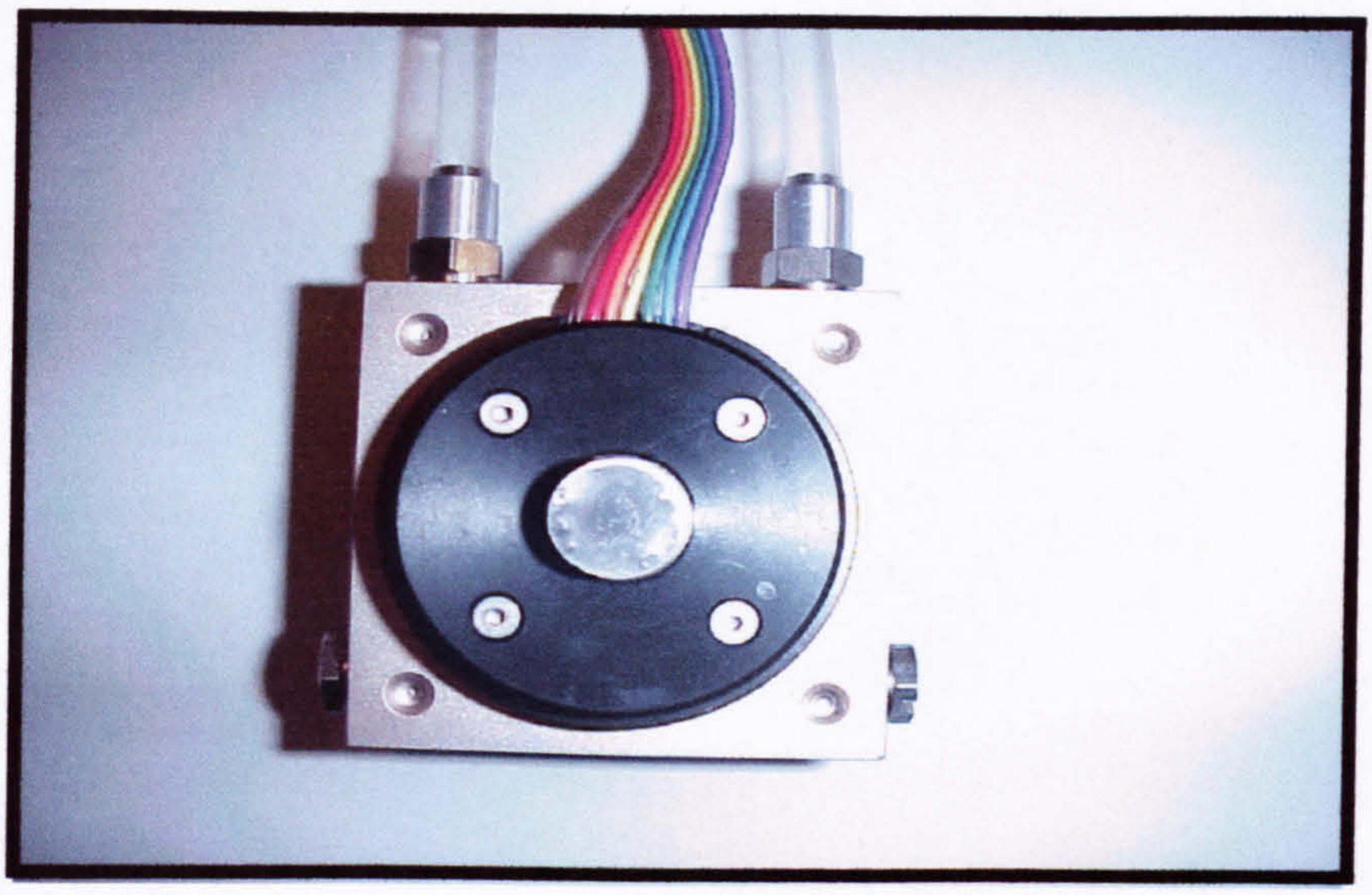

Figure 3.15: A picture of a peltier-cooled specimen stage Philips XL30 ESEM-FEG.

3.7 Atomic Force Microscopy (AFM)

Surface images of the RO membranes (e.g. ADF and Nanomax-95), stainless steel, Teflon and Perspex glass substrata, used in this experiment, were obtained using a NanoScope® IIIa AFM (Digital Instruments, USA), using tapping mode and Etched Silicone Probes with flexible Si_3N_4 cantilever tips (Resonant Frequency 300 kHz; Spring Constant of 40 Nm^{-1}). For RO membranes preparation, the membranes were set up in the high pressure reverse osmosis membrane test system (Figure 3.2), washed for 30 minutes (at pressure 34 bar) with lab grade distilled water, in order to wash out the organic preservative materials from the membrane surface, and left for air-dry for 24 h at 30°C. The AFM technique allows measurement of R_a, R_{ms}, R_{max}, and the Z range. The R_a value is the arithmetic mean surface roughness, while the R_{ms} value is the geometric mean of the surface roughness. R_{max} is the maximum height of the profile above the mean line, whereas the Z-value donates the maximum peak-to-valley height of the profile in the assessment line. In addition, The NanoScope software (Version 4.43) was used to measure length, width, and height of selected objects.

3.8 Experimental Design and Statistical Analysis

Table 3.13 shows the experimental design and the experimental runs conducted during various experimental activities in this study. In the bacterial growth measurements for halobacteria and cyanobacteria (Chapters 4 and 5), the experimental runs were conducted in triplicate, with 2-3 times per week sampling frequency.

Table 3.13: Experimental design and sampling frequency at various research stages.

Scope	Parameter	Number of replications	Sampling Frequency	Reproducibility
In-situ water Sampling	- water sampling/location	3	3	90-95%
	- physico/chem. analyses	3	1	95%
Bacterial Culturing & Growth	- Chlorophyll-a	3	2-3×/week	90-95%
	- Optical density	3	2-3×/week	95-97%
	- pH	1	once/week	98%
	- Temperature	1	continuous/run	99%
	- CFU	3	once/sampling	50-90%
	- Total bacterial count	3	once/sampling	70-90%
Bacterial Adhesion Experiment	- Chlorophyll-a	3	once/week	90-95%
	- Proteins "Qualitative"	2	once at start + once at end	97-99%
	- Proteins "Quantitative"	2	once at start + once at end	97-99%
	- Biofilm similarities /single material	4	1	85-95%
Flux Behaviour & Biofouling Monitoring	-Temperature	Twice/setting	Once/start + Once/end	99%
	- pH	Once/setting	Once/run	99%
	- Conductivity	1	Once/run	98%
	-Membrane micrographs	4-6	Once /run	70-80%
	-Pressure	Once/setting	Once/setting/run	98%
	- Permeate Flux	Once/setting	Once/setting/run	99%

The cyanobacterial adhesion experiment (Chapter 6), which was conducted in two identical biofilm reactors, was conducted for six consecutive weeks. During the experimental run, the cyanobacterial growth in the bulk solution was monitored and carried out in triplicate samples twice a week. Qualitative protein analyses in the cyanobacteria suspended in the bulk solution and of those attached to the biofilm were conducted at the beginning of the experiment (for suspended biomass) and at the end of the experiment (for both suspended and attached biomass). In the flux behaviour and biofouling monitoring study (Chapter 7), due to the large number of water samples required for each run, the ingredients cost, and time needed, single-run experiments were conducted in this study. Although, one sample was taken from the membrane after each run, the microscopic views and ESEM observations taken for each sample were 4-6 and 2-3, respectively.

Statistical analysis was executed using standard ANOVA (Microsoft EXCEL 5). Statistical analysis was always performed using a confidence interval of 95% ($P<0.05$). Test reproducibility was determined based on the relative standard deviation (standard deviation divided by the average value) obtained for all samples collected during and at the end of each run.

Chapter 4

CYANOBACTERIAL STUDIES OF A HYPERSALINE LAKE IN THE LIBYAN SAHARA

4.1 Introduction

Cyanobacteria, also known as blue-green algae, are a common and naturally occurring component of most aquatic ecosystems and occur in freshwater, estuarine, marine, and hypersaline environments. Cyanobacteria are dominant primary producers in hypersaline environments, especially in hot climates (Pearl, *et al.*, 2000). The increasing interest toward this group of phototrophic microorganisms is acknowledged because of both their substantial role in the primary productivity of the hypersaline habitats and the perspective of their biotechnological exploitation. The production of specific metabolites, such as new exopolysaccharides (EPS) of industrial interest, could be a promising field of application of halotolerant cyanobacterial species (Pflüger and Muller, 2004; Rothrock Jr. and Garcia-Pichel, 2005).

For accurate ecological studies and safe biotechnological exploitation of these cyanobacteria, the precise assessment of their taxonomic position is necessary (Abed, *et al.*, 2002b). Coccoid cyanobacteria of hypersaline habitats, characterised by transversely dividing cells, which occur singly or in pairs, and either irregularly distributed in colonies surrounded by mucilage, have been mostly identified as *Aphanothece halophytica* Freèmy (Svenning, *et al.*, 2005), although other generic names, *Coccochloris*, *Aphanocapsa*, *Cyanothece*, or *Synechococcus* have been also used to indicate similar organisms growing in different hypersaline environments (Svenning, *et al.*, 2005; Pearl, *et al.*, 2000; and Garcia-Pichel, *et al.*, 1998).

Microorganisms are naturally adaptable to their environment to cope with changing conditions of various kinds. Apart from the availability of nutrients, varying

temperatures and pH, another frequently changing factor is the osmolarity. This is not only the case in saline environments, but also common in hypersaline lakes, in which, usually salinity increases causing drastic changes in the environmental osmolarity (Pearl, *et al.,* 2000; and Incharoensakdi and Kamchanatat, 2003). Basically, there are two general strategies cells can use to reset turgor pressure and to avoid the detrimental consequences of water loss, when exposed to increasing osmolarity (Tanaka, *et al.*, 2001). One is the so-called "salt-in cytoplasm" type, where inorganic ions, mainly K^+ and Cl^-, are accumulated in the cytoplasm to a level which resembles the external salt concentration; however this strategy limits growth to certain osmolarities. The second strategy is the accumulation of compatible solutes, which are defined as small, soluble, organic molecules that do not interfere with the central metabolism of the cell, even if they are accumulated to high concentrations (da Costa, *et al.,* 1998). This strategy is widespread and is used by the majority of the living cells, (da Costa, *et al.,* 1998; Pfüger and Müller, 2004; and Maskow and Babel, 2001). Compatible solutes accumulation in halophilic cells can basically preserve the same fundamental enzymatic functions as nonhalophiles and, therefore, makes them more flexible than cells using the former strategy (i.e. salt-in-cytoplasm). Qabar-Onn Lake is mainly very rich in K^+ and Cl^- ions concentrations (i.e. $K^+ \cong 16$ g l^{-1} and $Cl^- \cong 79$ g l^{-1}), and the question which may arise is whether the indigenous microorganisms in Qabar-Onn Lake use either the first or second strategy for their osmoadaptation?

In this Chapter, the research focused on exploring Qabar-Onn Lake located in the Sahara (south of Libya) and mainly investigates the cyanobacterial mat using amplified ribosomal DNA restriction analysis to describe the genetic diversity of the new strains belonging to the *'Euhalothece'* cluster. Results also present their morphological similarities and their growth responses to salt and pH, as well as the study extended to cover analyses of the compatible solutes synthesised by the cyanobacterial mat in this lake. A phylogenetic reconstruction analysis based on 16S rRNA gene sequences is also discussed to clarify their systematics.

4.2 Materials and Methods

4.2.1 Sampling Procedure

Three sets of water samples (A, B, and C) were collected from three depth intervals (i.e. 0.2 m, 4.0 m and 8.0 m) in Qabar-Onn Lake, which represent the lake stratification layers (e.g. phytoplankton, thermocline and anaerobic, respectively). The sampling procedure was performed as described earlier in Chapter 3, Section 3.2.3.

4.2.2 Media Selection and Cyanobacterial Isolation

Three growth media were selected to isolate as many cyanobacterial strains as possible from the lake water. The media were Muller, BG11 and The Defined medium, as described by Cummings, *et al.*, 1993; Garcia-Pichel, *et al.*, 1998 and Stein, 1979; respectively (more details about compositions and preparations of these media are described in Chapter 3, Section 3.3.3). The selection of the appropriate medium for isolation and culturing of cyanobacteria was considered based on their support for the best growth under similar growth conditions.

Due to the low concentration of the cyanobacterial cells in the lake water and to speed up the growth process a designated isolation strategy was followed. In this experiment, 100 ml aliquots of three selected media were inoculated with 50 ml portions of water samples taken from the upper layer of the lake (e.g. sample A, depth = 0.2 m, Figure 4.1). The cultures were incubated in a thermostatic incubator set at 27°C under illuminated conditions (75-80 μEinsteins m^{-2} s^{-1}). Fluorescent tubes were used on a 12 h light/dark cycle during the incubation period.

Monitoring of any cyanobacterial growth in the incubated cultures was carried out by regular measurement of the chlorophyll-a (*Chl-a*) values of these cultures. As soon any cyanobacterial growth was detected, a microscopic check of the grown morphotype was carried out. This process was performed by withdrawing 1 ml aliquots from the growth flask, centrifuge at 13,000×g for 5 minutes, and discard the supernatant, then a slide was made from the thickened pellet and viewed under microscope. In most of the cases, a monomorphotype was detected in a single check.

Cyanobacterial isolates culturing was carried out by withdrawing 5-10 ml of the grown cyanobacterium and inoculating it in a pure previously selected medium for this particular organism. The inoculum-to-medium ratio was 1-1.5:10. The isolated cultures were incubated in a thermostatic incubator set at 27°C under illuminated conditions (75-80 μEinsteins m^{-2} s^{-1}) at a 12 h light/dark cycle. Continuous orbital shaking, at 120 rpm, was also maintained throughout the culturing period.

4.2.3 Growth Media

BG11 medium was used for blue-green algae (cyanobacteria). The hypersaline BG11 medium was prepared by dissolving the designated amount of sodium chloride in distilled water to which nutrients, trace elements, and vitamins were added (Garcia-Pichel, *et al.*, 1998). The medium contained 1.5 g $NaNO_3$, 0.04g K_2HPO_4, 0.075 g $MgSO_4$ $7H_2O$, 0.036g $CaCl_2$ $2H_2O$, 6.0 mg citric acid, 6.0 mg ferric ammonium citrate, 1.0 mg EDTA, 0.02 g Na_2CO_3, and 1 ml trace metals mixture (see Section 3.3.3, Chapter 3 for more details).

4.2.4 Strains and Growth Conditions

Cyanobacterial cells, isolated from the lake water, were axenically grown in 250 ml Erlenmeyer flasks with bug stoppers (Bug stopper™, Erlenmeyer vent, Whatman®, Whatman Inc., Clifton, NJ, USA). 15-20% of well-grown cultures (e.g. OD = 1.25) were inoculated into 100 ml of fresh BG11 media in each flask. The cultures were then kept in a thermostatic incubator set at 27°C under illuminated conditions (75-80 μEinsteins m^{-2} s^{-1}). Fluorescent tubes were used on a 12 h light/dark cycle during the incubation period. Continuous shaking, using an orbital shaker at 120 rpm, was also maintained throughout the culturing period. The grown cultures were regularly regenerated (e.g. every 6-8 weeks) by centrifuging cultures and inoculating the thick biomass into fresh BG11 media.

Morphological characteristics of the strains were determined by observations under a light microscope (OLYMPUS, reflected light/fluorescence attachment, Model BH2-RFCA, Japan) during the different growth phases. Salinity requirements were investigated by measuring cell growth in a range of salinities from BG11 medium

with no added salt (NaCl) to BG11 medium supplemented with 2 M NaCl (i.e. 120 gl^{-1}, NaCl).

4.2.5 Measurement of Instantaneous Growth Rate

The growth rate of the cyanobacterial cultures was measured based on two techniques: the optical density (OD) and *Chl-a* concentration. The measurements were always taken during the same period of the light/dark cycle. Typically, growth was followed in triplicate cultures for each condition during periods of 8-10 weeks, and all measurements were carried out on undiluted samples. Growth was exponential in most conditions; however, in some conditions it was steady and slow. The average values of three independent specific growth rate estimates, (μ, day^{-1}), are presented here.

Thermo Spectronic spectrophotometer (*MODEL Helios Epsilon*) was used to measure the OD absorbance of 1 ml culture at 530 nm. *Chl-a* was measured by centrifuging 1 ml portions at 13,000×g speed for 5 minutes followed by resuspending the biomass pellets at 90% methanol overnight and measuring the absorbance at 664 nm. Although the total chlorophyll (*Chl-t*) equals the summation of both values of *Chl-a* and *Chl-b*, according to the following equation:

Chl-t (μg/ml) = 7.04 $Ab_{664\ nm}$ = 20.27$Ab_{647\ nm}$ (Moran, 1982) ⟶ equation 4.1

however when measuring very low chlorophyll concentration, as in cyanobacteria, and because of the much higher *Chl-a* : *Chl-b* concentration ratio, only *Ch-a* value is considered with a slight amendment of equation 4.1 as follows:

Chl-a, (μg/ml) = $Ab_{664\ nm}$ × 12.7 (Moran, 1982). ⟶ Equation 4.2

4.2.6 DNA Extraction

Cyanobacterial cells were harvested from mid-exponential cultures by centrifugation at 13,000×g for 10 min at room temperature, washed three times with a buffer washing solution [(50mM Tris (pH 7.4), 100mM EDTA (pH 8) and 25% Sucrose)] for exopolysaccharide (EPS) removal, and frozen at -20°C until use. 1.8 ml of the thick biomass pellet was used in this experiment following the procedure stated in the protocol of the UltraClean™ Microbial DNA Isolation Kit (MO BIO

Laboratories, Inc.). Only minor modifications in step 4 of the procedure were made (see detailed procedure in Appendix A). About 50 µl of the DNA yield was obtained in this experiment, and then the DNA concentration was checked, using a spectrophotometer to measure the absorbance at (λ = 260 nm and 280 nm) of 5 µl DNA diluted in 65 µl DNA-free deionised water (a detailed procedure is included in Appendix A).

4.2.7 PCR Amplification and Cloning of 16S rRNA Genes

A partial sequence of the 16S rRNA gene was determined following PCR amplification using cyanobacterial primers CYA106F and CYA781R, and aligned with the sequences in the Blast database (Nübel, *et. al.*, 1997). In this experiment, the selection of PCR primers was based on a previous study (Nübel, *et. al.*, 1997) on primer design, which was based on an alignment of all 16S rRNA sequences from cyanobacteria available from Ribosomal Database Project and GenBank. The selected primer sequences and their target regions within the 16S rRNA gene are listed in Table 4.1. The primers were synthesised and are commercially available from Sigma, UK.

The forward primer CYA106F matches a number of published 16S rRNA sequences from prokaryotes with various phylogenetic affiliations outside the phylum of the cyanobacteria. Additionally, this primer was selected for this study because it proved useful in the generation of sequence data from unicellular cultures. Despite its limitations, the forward primer might be preferred, because compared to CYA359F, its use generates longer amplification products (approximately 700 base pairs instead of 450), therefore enabling the determination of more informative sequence data (Nübel, *et. al.*, 1997).

Table 4.1: Primer sequences and their target sites

Primer	Sequence (5' to 3')	Taget Site
CYA106F	CGG ACG GGT GAG TAA CGC GTG A	106 - 127
CYA781R	GAC TAC TGG GGT ATC TAA TCC CAT T	781 - 805

Reported from Nübel, *et. al.*, 1997.

The reaction was performed in a final volume of 50 µl by the Applied Biosystems Model GeneAmp® PCR System 9700, using the following amplification mixture: 6 mM Tris HCl, pH 8.8, 8 µl $MgCl_2$, 1.25 µl of dNTP, 2 µl of each primer, 0.5 µl of Taq DNA polymerase, 3 µl of DNA sample and 27.25 nuclease-free water. The temperature programme was composed by an initial denaturation at 95°C for 3 min, 35 cycles at 94°C for 0 s, 58°C for 20 s, 72°C for 2 min, a final extension at 72°C for 5 minutes. All reactions were repeated at least twice, always including both negative (DNA free) and positive controls. The successful amplification of the expected fragment (approximately 700 bp) was checked by electrophoresis in 1% (w/v) agarose gel at 4 V cm^{-1} for 1 h, stained with addition of 2 loading dye in each PCR tube and observed under UV light (more detailed PCR procedures and results are presented in Appendix A).

4.2.8 Alignment and Phylogenetic Analyses

The new 16S rDNA sequences were multiple-aligned using CLUSTAL W, version 1.83 (Svenning, *et.al* 2005) with a selection of cyanobacterial reference sequences. These sequences were obtained from the GenBank® genetic sequence database under accession numbers (AJ000709, AJ000717, AJ000710, AJ000712, AJ000713, AJ000722, AJ000720, AJ000719, AJ000718, DD086632, AY695346, DD083887, AY768411, AF296872, and AJ000721).

The alignment was corrected using Jalview Multiple Alignment Editor software version 1.8 (Clamp *et al.*, 2004). A phylogenetic tree was constructed from the distance matrix data by applying the algorithm of the neighbor-joining (NJ) method (Tamura *et al.*, 2004) to *K*nuc values with multiple substitutions corrected and positions with gaps excluded. To evaluate the robustness of branches in the inferred tree, the bootstrap resampling method of Felsenstein with 1000 replicates was used. Maximum likelihood (ML) analysis was also carried out using the OMEGA program, version 3.1 (http://www.megasoftware.net/) based on the same alignment data after positions with gaps were excluded. The ML distance matrix was calculated using NucML, and the initial NJ tree was reconstructed by NJdist in the OMEGA package. The ML tree was finally obtained using NucML with the local

rearrangement method from the NJ tree, and local bootstrap probabilities were estimated by a resampling of the estimated log-likelihood method (Kumar *et al.*, 2004).

4.2.9 Electronic Microscopy

2.4.9.1 Preparation of Cells For Transmission Electron Microscopy (TEM)

20 ml of cells in the mid stationary-state growth phase were harvested by pelleting them in 50 ml centrifuge tubes at 1,200 ×g for 10 min. Approximately 20 µl aliquots of the moist cell paste were placed into tightly fitting, interlocking brass planchets (Swiss Precision, Inc., Palo Alto, CA, USA) (Toole *et al.*, 2003). Cryoprotectants such as dextran, mannitol or sucrose were not used. The cells were immediately frozen with liquid nitrogen under high pressure (2,100 bar) using a Bal-Tec HPM 010 high pressure freezing machine (Bal-Tec Products, Middlebury, CT, USA). Following cryofixation, the samples were freeze-substituted at −85°C in 1% glutaraldehyde (Electron Microscopy Sciences, Washington, PA, USA) and 1% tannic acid in HPLC grade anhydrous acetone for 72 h. After this time the samples were rinsed thoroughly in three changes of anhydrous acetone at −85°C for a total of 45 min. Cells were infiltrated with 1% OsO_4 in acetone for 1 h at −85°C before being slowly warmed over 2 h to −20°C, then to 4°C over a further 2 h, and finally to room temperature over 1 h. The cells were then rinsed in acetone and slowly infiltrated with and polymerized in Spurr's resin.

2.4.9.2 Scanning Electron Microscopy (SEM)

Cyanobacterial samples were fixed in glutaraldehyde. Dehydration was carried out in a water:ethanol series, followed by 100% acetone, then liquid CO_2 using a critical point dryer (BioRad Microscience, Watford, UK). The dried samples were spread onto Teflon discs of a suitable size and mounted on bronze stubs with a shallow layer of silver paint, then coated with 2 nm of chromium using a sputter coating device (Xenosput 2000: Dynavac, Australia). Membranes were then examined using a Hitachi S-900 FESEM, at 2 kV accelerating voltage.

2.4.9.3 Transmission Electron Microscopy (TEM)

Embedded cells were cut into serial 70 nm thick sections with an Ultracut R Microtome (Leica, Vienna, Austria) and collected on formvar-coated copper slot grids. Sections were post-stained with 2% uranyl acetate in 50% ethanol for 5 min followed 5 min with Reynolds' lead citrate. The grids were carbon-coated and viewed at 80 kV using a CM12S transmission electron microscope (Philips Electronic Instruments, Co., Mahwah, NJ, USA). Forty-eight cells at various stages of the cell cycle were followed through by serial sectioning. Images of these sections were captured digitally with 1,024×1,024 pixel charged-coupled device (CCD) camera (Gatan Inc., Pleasanton, CA, USA) using Digital Micrograph software (Gatan).

4.2.10 Compatible Solutes Analysis

100 ml of mid exponential phase of each cyanobacterial culture grown in zero salinity and 1M added salt as NaCl were harvested and centrifuged at 4000×g. The resulting pellets were washed twice in 5 ml aliquots of NaCl solution with identical salinities of the original cultures (i.e. 30mM and 1M, respectively). During washing process the mixtures were vortexed for 1 minute followed by centrifugation for 5 minutes at 4000×g. The washed cells were then suspended in 10 ml aliquots of 80% (v/v) ethanol and were thoroughly vortexed for 8-10 minutes at room temperature. The mixtures were allowed to stand overnight at 65°C until dryness. The dried samples were dissolved in 2 ml Milli-Q water, and the resulting solutions were freez-dried at -80°C. Finally, the dried cells were re-dissolved in 1-2 ml of Milli-Q water with 10% D_2O, and were sent for NMR determinations. NMR analyses were carried out as described earlier in Section 3.4.5, Chapter 3.

4.3 Results and Discussion

4.3.1 Physical/chemical analyses

Based on the reported data (Ajaili, *et al*, 1984 and El-Saedi, 2002) and the salinity determinations for the lake water, it can be seen that the salinity has increased steadily during the last two decades. This increase is likely due to the fast evaporation rate from the lake surface (Ajaili, *et al*, 1984). Figure 4.1 shows a comparison of the water salinity in 1984 and in 2001. In 1984, the salinity was reported in the range of 120,000 mg l^{-1} at the water surface and 149,000 mg l^{-1} at the bottom, whilst in 2001, the salinity has been increased by 25% and 8.5%, respectively, with an average of 17% throughout a 17 year-period, which represents an increase 10 g.l^{-1}/year. The effects of high evaporation have also been seen in the temperature of lake water at the water surface decreasing over time. The slightly lower salinity at the water surface of the lake is likely to be a sign that feed water inflow must occur near the surface (Ajaili, *et al*, 1984).

The main physical/chemical analyses and the determinations of the main ions (e.g. cations and anions) of Qabar-Onn Lake water at various depths are shown in Table 4.2. On the contrary, pH values are slightly higher (i.e. 10.3 and 9.8) at the surface than that for the main water body of the lake, which could be because of the slightly higher temperature at the surface compared to the main water body of the lake (i.e. 29.7 and 23.6°C). Furthermore, dissolved oxygen (DO) concentrations showed very low values ranging from 0 mg/l at the bottom of the lake and 1.9 mg/l at water surface, these low DO values can be anticipated to the lower oxygen solubility in waters containing high solutes concentrations. However, these low DO concentrations are necessary to support obligatory an aerobic and facultative microorganisms in such ecosystems (Olliver, *et al*., 1994).

It can be seen that the lake has poor nitrogen content as all samples showed low ammonical nitrogen values (e.g. 0.6 mg l^{-1} - 5.19 mg l^{-1}) as well as the nitrate and nitrite concentrations (0.4 mg l^{-1} and 0.08 mg l^{-1}, respectively). The low nitrogen level in the lake water can be attributed by the poor mineral composition of the soil surrounding the lake, as well as poor vegetation coverage of the Saharan terrains (El-Saedi, 2002).

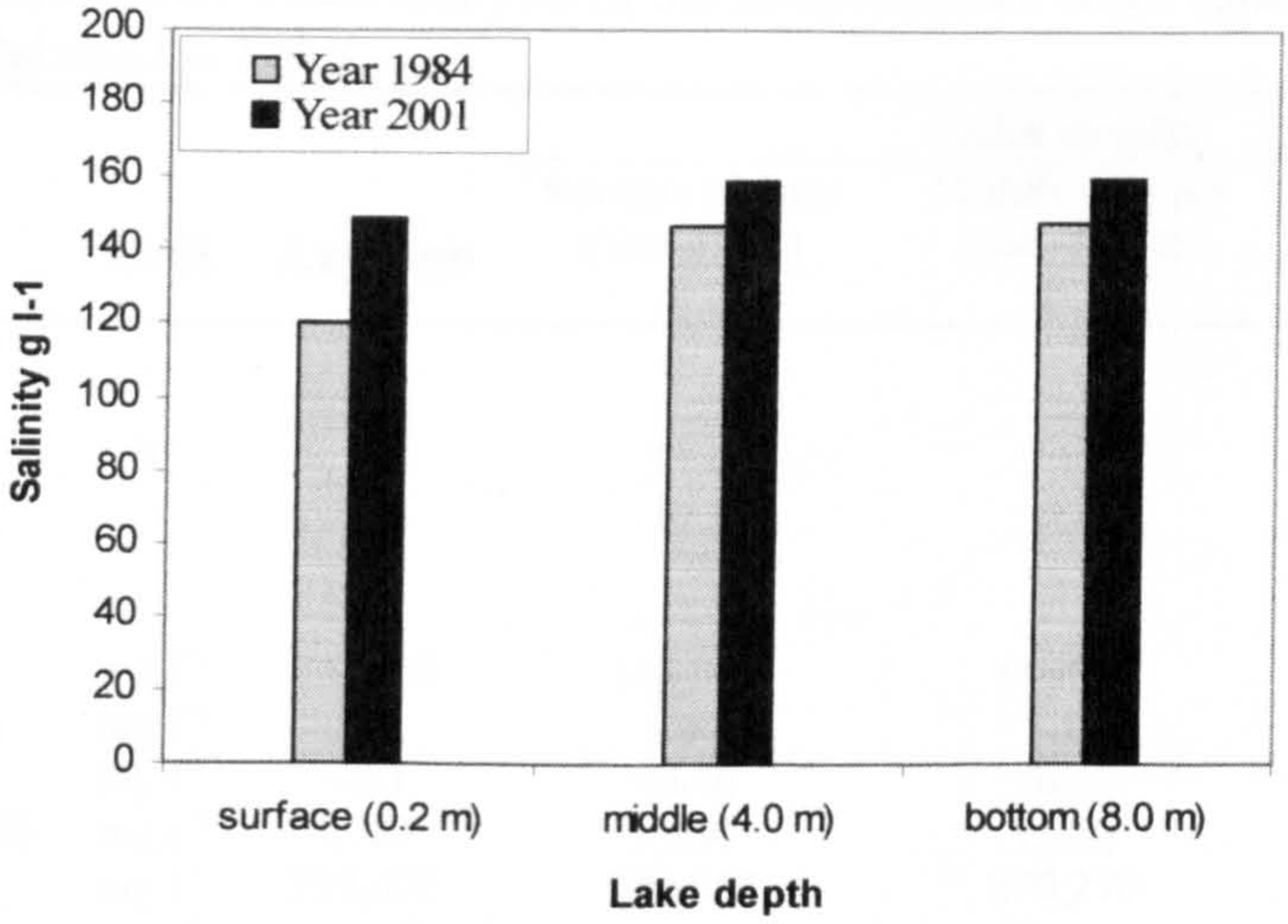

Figure 4.1: Comparative results for the reported salinity values in Qabar-Onn Lake.
Source of data: (Ajaili, et al; 1984 & El-Saedi, 2002)

Values of the concentrations of the major anions and cations are presented in Table 4.2. Four major anions, (i.e. Cl^-, SO_4^{2-}, NO_3^-, and NO_2^-); and five major cations, (Na^+, K^+, Mg^{2+}, Ca^{2+}, and Fe^{3+}), were measured. Figure 4.2 shows that only two anions and two cations (i.e. Cl^-, SO_4^{2-} and Na^+, K^+, respectively) are apparently dominant in this environment and contribute most to the solute concentration in this lake. The low concentration of calcium can be attributed to the remoteness of this lake (approximately 1200 km) from the sea as well as to the geological composition of the surrounding environment (Ajaili, *et al*, 1984).

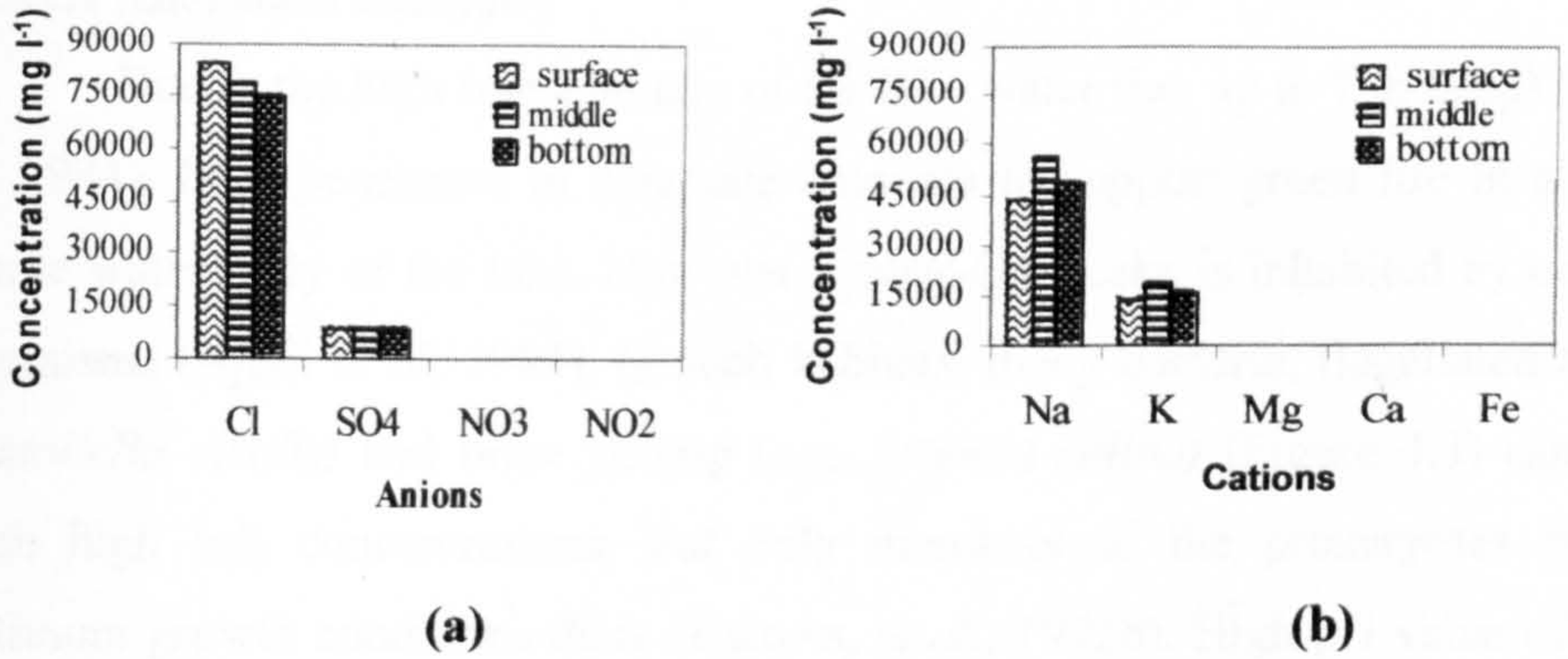

Figure 4.2: Chemical composition against depth at Qabar-Onn Lake:
(a) Anions, and (b) Cations.

Table 4.2: Physical/chemical analysis of the samples taken from various depths at Qabar-Onn Lake.

Parameter	Unit	Average	Lake depth		
			Surface (0.2 m) (Sample A)	Middle (4.0 m) (Sample B)	Bottom (8.0 m) (Sample C)
Physical Analyses:					
Temperature	°C	27	23.6	29.7	27.9
pH	-	10	10.3	9.8	10.1
Chemical Analyses:					
Salinity	mg l^{-1}	150000	146.000	148000	156000
Ammonical-nitrogen	mg l^{-1}	2.8	1.90	5.19	0.60
Total Alkalinity	mg l^{-1}	<0.4	<0.40	<0.40	<0.40
Suspended Solids (SS)	mg l^{-1}	1,767	1,680	1,780	1,840
Total Solids (TS)	mg l^{-1}	323,673	383,580	279,270	308,170
COD	mg l^{-1}	31,233	29,300	32,200	32,000
TOC	mg l^{-1}	17.0	17.0	17.0	17.0
Dissolved oxygen	mg l^{-1}	0.5	1.3	0.2	0
Anions:					
Sulphate	mg l^{-1}	8,573	8,100	8,880	8,740
Chloride	mg l^{-1}	79,000	83,900	78,600	74,400
Nitrate	mg l^{-1}	<0.40	<0.40	<0.40	<0.40
Nitrite	mg l^{-1}	<0.08	<0.080	<0.080	<0.080
Cations:					
Sodium	mg l^{-1}	49,333	43,200	56,100	48,700
Potassium	mg l^{-1}	16,533	14,300	19,000	16,300
Magnesium	mg l^{-1}	30.9	33.0	30.8	28.9
Calcium	mg l^{-1}	1.61	1.31	2.33	1.19
Iron	mg l^{-1}	<0.5	<0.50	<0.50	<0.50

4.3.2 Microbiological Studies

4.3.2.1 Microbial Diversity

Due to the high transparency of the lake water (i.e. up to 7 m deep) (Ajaili, *et al*, 1984), light penetrates in adequate amounts to support green life in almost the whole water body of the lake. However, Qabar-Onn Lake is inhabited by only a few organisms (Ajaili *et al*, 1984). In such habitats, many bacteria, flagellated alga (e.g. *Dunaliella viridis)* and brine shrimp (e.g. *Artemia salina)* (Figure 4.3) can tolerate such high salt concentrations, but only members of the prokaryotes find their optimum growth conditions there (Balows, *et al.*, 1992b). High pH value of the lake water (i.e. pH 10.3) may also has a detrimental impact on the microbial diversity, as only few members of alkalihalophiles find their optimum pH in this lake.

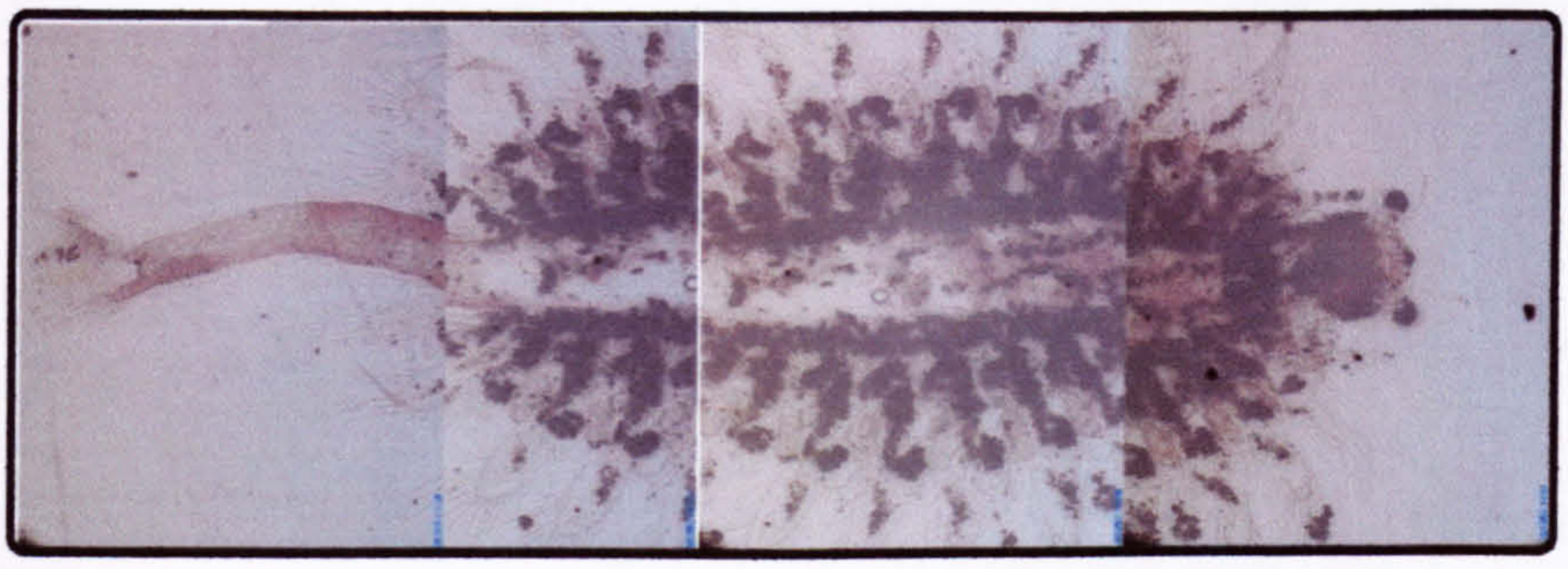

Figure 4.3: A micrograph of the brine shrimp (i.e. *Artemia salina)* isolated from Qabar-Onn Lake. *(Picture taken at 40× magnification and not to scale).*

4.3.2.2 16S rRNA Gene Sequences and Phylogeny

16S rRNA gene sequencing was carried out for two cyanobacterial morphotypes, recently isolated from Qabar-Onn Lake. The gene sequences of these isolates were deposited in GenBank under accession numbers (AY457568 and DQ457013). Similarities between the complete 16S rRNA sequences from the isolated unicellular halotolerant cyanobacteria and other selected strains are presented Table 4.3. The *Euhalothece* sp. strains BAA001 and BAA002 were identified based on microscopy (ultrasructure using SEM and TEM) (Figures 4.5 and 4.6), and 16S rRNA gene sequences analyses. Based on the 16S rDNA distance tree (Figure 4.4), the *Euhalothece* sp. MPI 95AH10 is a near relative of 90% and 99% similar to strains BAA001 and BAA002, respectively (Table 4.3).

Based on the 16S rRNA sequences and the phylogeny distance tree (Fig 4.4), the isolated species (e.g. BAA001 and BAA002) are clearly affiliated with the genus *Euhalothece*. However, their sequences differences from the validly described *Euhalothece* species suggest that these two isolated strains tentatively represent new species.

Although the sequence divergence between the two isolated *Euhalothece* species (e.g. BAA001 and BAA002) is relatively big (e.g. 10%), these sequences have smaller diverges compared to other *Euhalothece* species (e.g. MPI 95AH10) (Table

4.3). Table 4.3 also shows that the two *Euhalothece* species (MPI 95AH10 and MPI 95AH11) are 100% similar (e.g. zero divergence), but in fact they are completely different species, and this may be due to a number of factors such as sequence size and stressed conditions of growth for a particular species.

By using 16S rRNA sequence analysis, Garcia-Pichel *et al.* (1998) subdivided the strains belonging to the '*Halothece*' cluster into a tight subcluster named the '*Euhalothece*' subcluster, and a deep-branching strain phenotypically inseparable from the others. In this experiment, phylogenetic reconstructions of both the cyanobacterial isolates (i.e. strains BAA001 and BAA002) and known strains of halotolerant coccoid cyanobacteria based on both ARDRA patterns (ARDRA results are presented in Appendix A) and the dendrogram (Figure 4.4) showed that the novel species examined in this work and all the *Euhalothece* selected strains made up a unique cluster. Therefore, referred to both phenotypic and genotypic similarities that our isolates have, both BAA001 and BAA002 strains are affiliated to the subcluster *'Euhalothece'*, and hence these results would fill the gap between the species *Gloeothece* sp. strain PCC 6909 and the *Euhalothece* group.

Table 4.3: Similarity matrix for 16S rRNA gene fragments comparing the environmental strains (*Euhalothece* sp. BAA001), (*Euhalothece* sp. BAA002) and some most closely related cyanobacteria.

	Euhalothece sp. (BAA001)	*Euhalothece* sp. (BAA002)	*Euhalothece* sp. MPI 95AH10	*Euhalothece* sp. MPI 95AH11	*Euhalothece* sp. MPI 95AH13	*Euhalothece* sp. MPI 96N303	*Euhalothece* sp. MPI 96N304	*Euhalothece* sp. MPI 96P402	*Euhalothece* sp. Syn CIP22	*Euhalothece* sp. MPI 96AL03	*Euhalothece* sp. MPI 96AL06	*Nostoc* sp. PCC 7120	*Nostoc* sp. PCC73102	*Synechocystis* sp. PCC 6803	*Gloeothece* sp. PCC 6909	*Cyanothece* sp. PCC 7418	*Aphanothece* sp. ATCC 43922
***Euhalothece* sp. BAA001**	100																
***Euhalothece* sp. BAA002**	90	100															
***Euhalothece* sp. MPI 95AH10**	90	99	100														
***Euhalothece* sp. MPI 95AH11**	88	98	100	100													
***Euhalothece* sp. MPI 95AH13**	89	97	97	96	100												
***Euhalothece* sp. MPI 96N303**	89	97	97	97	97	100											
***Euhalothece* sp. MPI 96N304**	89	97	97	97	97	99	100										
***Euhalothece* sp. MPI 96P402**	86	95	95	95	97	97	97	100									
***Euhalothece* sp. Syn CIP22**	87	96	97	97	97	99	99	97	100								
***Euhalothece* sp. MPI 96AL03**	87	96	96	96	97	96	96	96	96	100							
***Euhalothece* sp. MPI 96AL06**	87	0.96	97	97	97	97	97	97	97	96	100						
***Nostoc* sp. PCC 7120**	75	84	85	86	85	85	85	85	85	85	85	100					
***Nostoc* sp. PCC73102**	78	84	87	84	87	87	87	84	84	83	84	93	100				
***Synechocystis* sp. PCC 6803**	80	87	88	86	88	88	88	86	86	85	86	86	87	100			
***Gloeothece* sp. PCC 6909**	77	85	88	88	88	88	88	88	88	87	88	87	86	91	100		
***Cyanothece* sp. PCC 7418**	89	97	96	96	96	97	97	96	97	96	98	86	87	88	89	100	
***Aphanothece* sp. ATCC 43922**	88	98	99	99	96	97	97	95	97	96	97	86	84	86	88	97	100

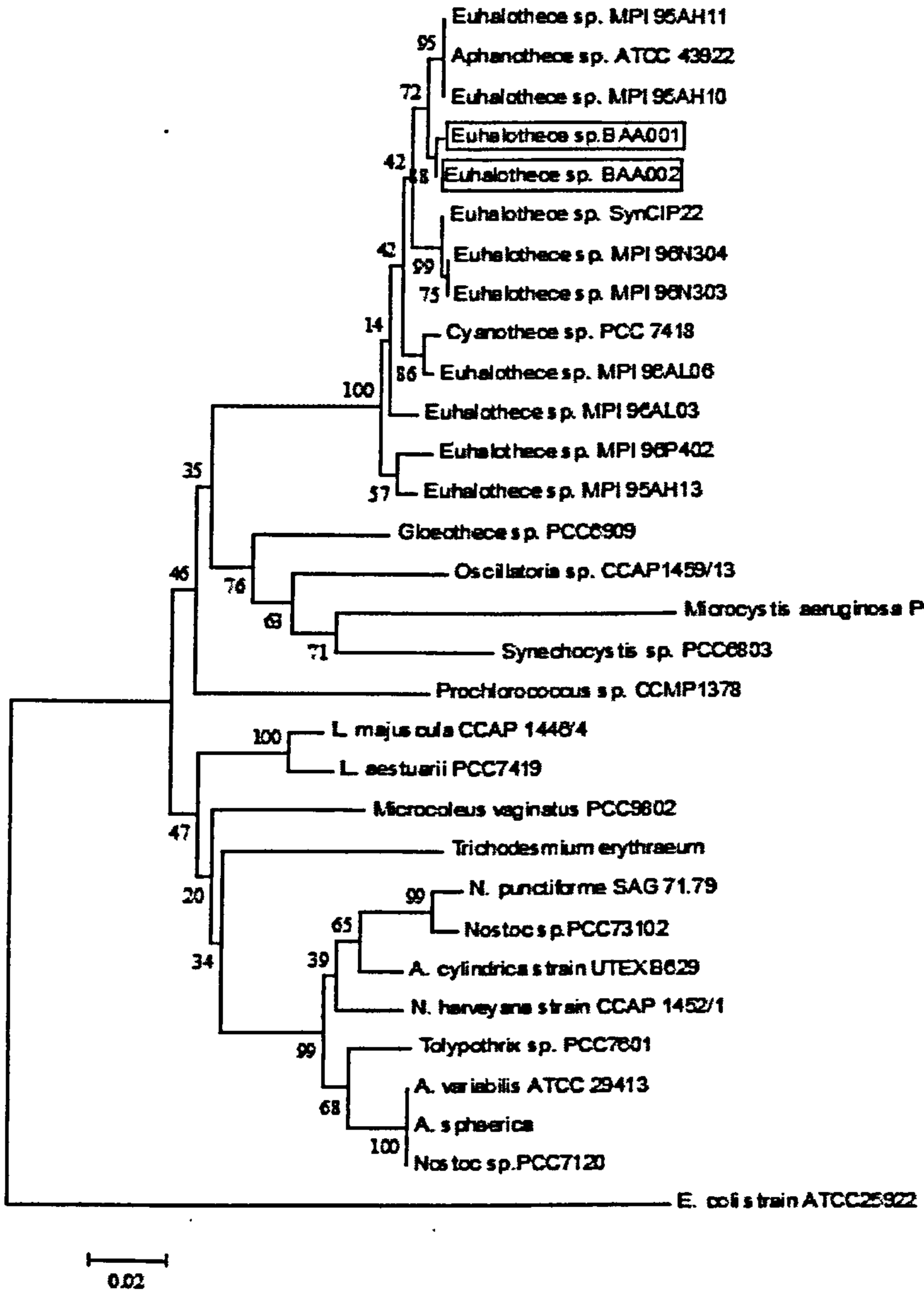

Figure 4.4: 16S rRNA Distance Tree for the *Euhalothece* species (BAA001 & BAA002) Cyanobacteria: [16S rRNA distance tree constructed with the Neighbor-joining method (Saitou and Nei, 1987) using the Tajima-Nei calibration to calculate the evolutionary distances as implemented in the software package Mega3 Version 1.5. A bootstrap analysis involving 1000 resamplings was performed. Outgroup used in this case is *Escherichia coli* strain ATC25922 and both of the *Euhalothece* sp. (BAA001 and BAA002) are framed.]

4.3.2.3 Cyanobacterial Traits

Although cyanobacterial growth occurred in all cultures incubated in BG11 medium, the cultures inoculated with samples taken from the surface layer of the Lake water (e.g. sample A in Figure 4.1), showed faster and denser growth compared to the other samples. Most of the incubated cultures showed similar characteristic isolates. Cell shapes ranged from coccoid to clearly bacilloid (Figures 4.5a & 4.5c). However, in some cases sheaths containing cells were observed in some higher salinity conditions (Figure 4.5b).

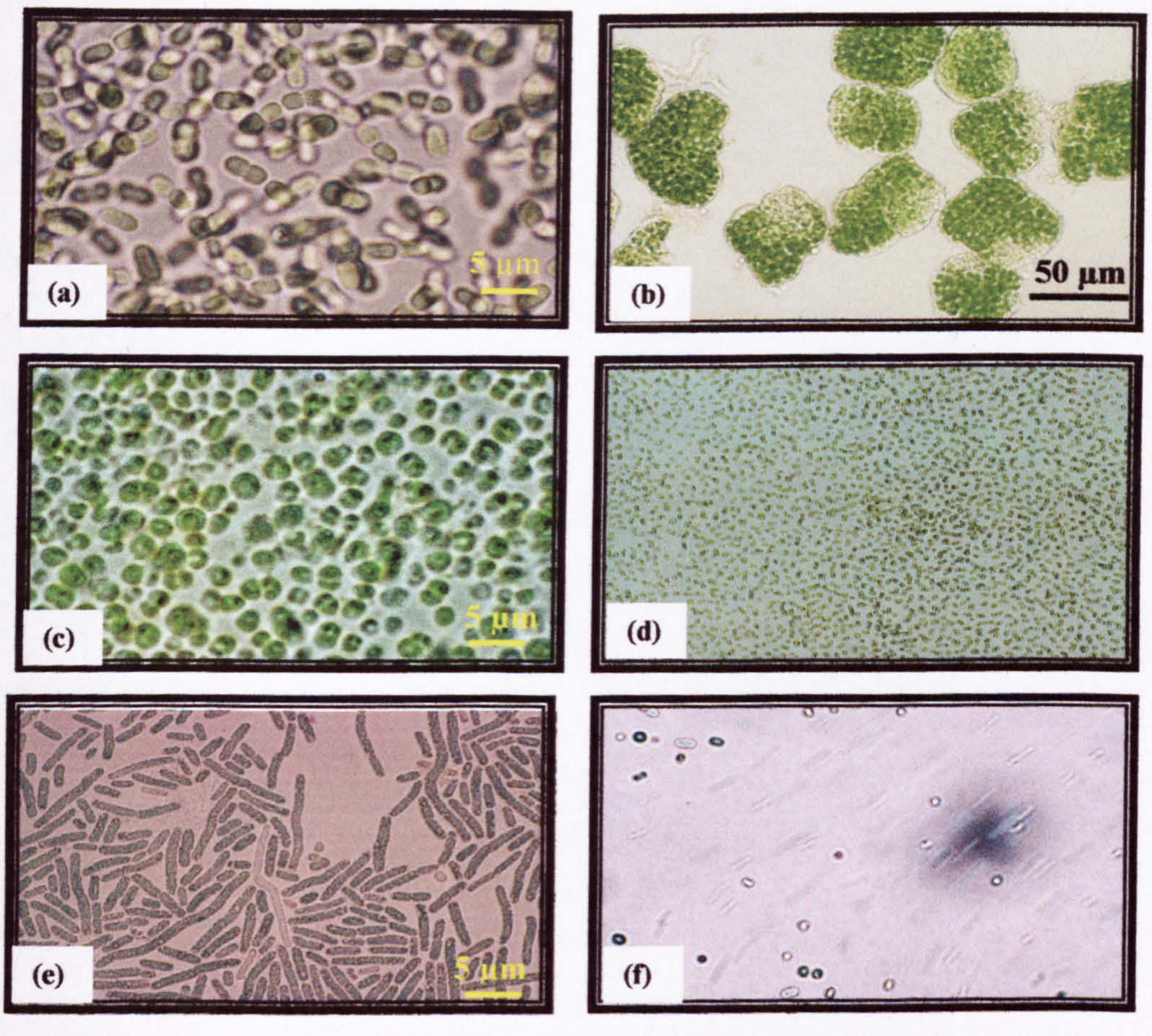

Figure 4.5: Micrographs of the *Euhalothece* species and other unidentified morpholytes:
(a): BAA001 strain (bar= 5µm) (b): BAA001 strain (bar= 50µm)
(c): BAA002 strain (bar= 5µm) (d): BAA002 strain magnified (at 400×)
(e): Unidentified morphotype (*Oscillatoria*-like species, bar = 5µm)
(f): Unidentified morphotype (*Microcystis aerogenosa*-like species, at 1000×).

Microscopic observations of the cultured isolated microorganisms from Qabar-Onn Lake samples revealed the presence of at least four morphotypes of cyanobacteria with different cell shape and size. However, only two morphotypes have been characterised and identified. One of the identified morphotypes (strain BAA001) is a cyanobacterium with a clear coccoid-like morphology (cell diameter 2.5µm - 5.0µm) with an average size of 3.8 µm (Figures 4.7a and 4.7b). The second morphotype (strain BAA002) is cocci to slightly rod-like morphotype (cell length 2 µm – 3.5 µm) with an average size of 2.8 µm (Figures 4.5c & 4.5d), with apparently uneven cell wall compared to strain BAA001.

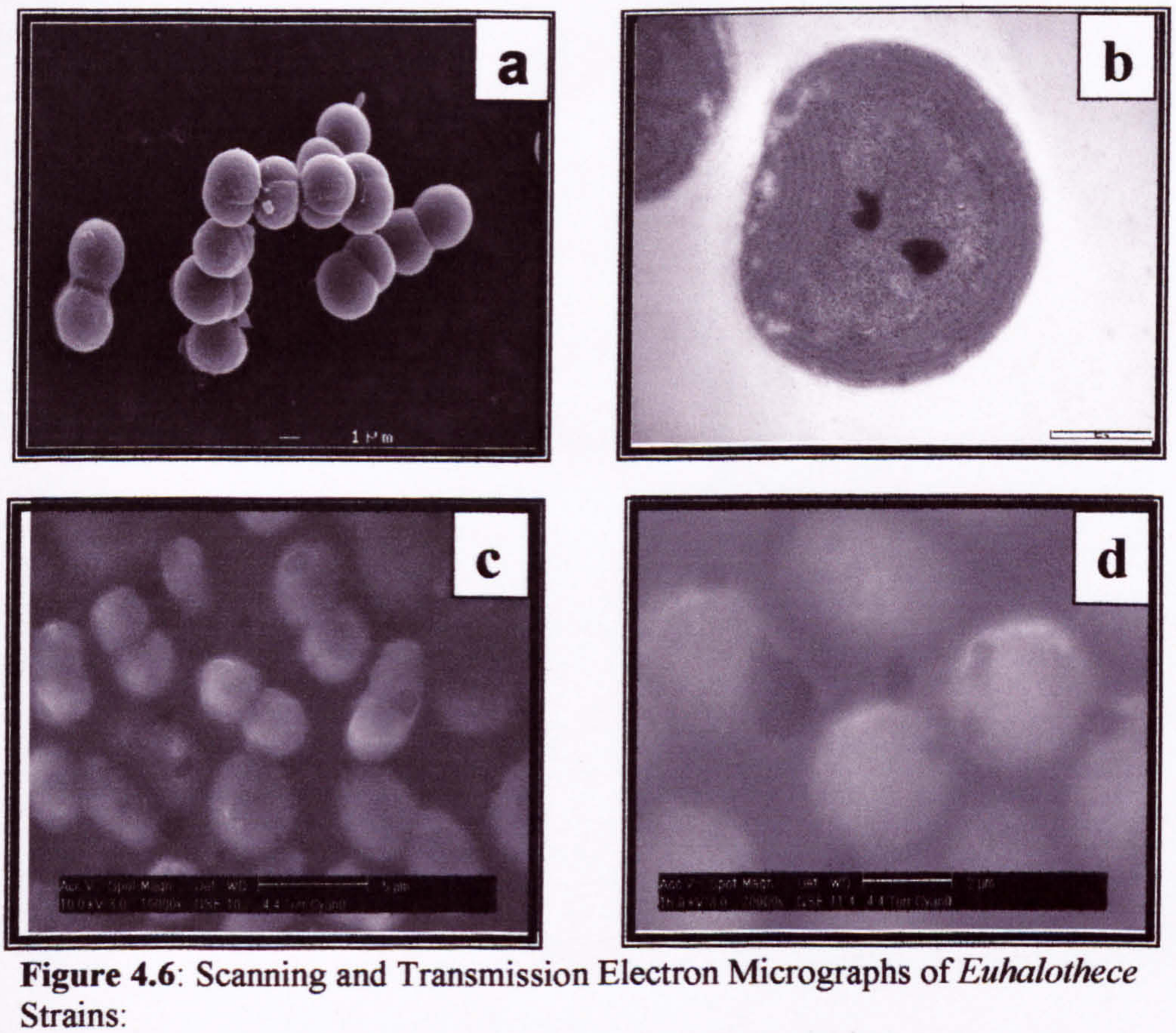

Figure 4.6: Scanning and Transmission Electron Micrographs of *Euhalothece* Strains:
(a) SEM for BAA001 sp. (bar= 1µm) (b) TEM for BAA001 sp. (bar= 500nm)
(c) SEM for BAA002 sp. (bar= 5µm) (d) SEM for BAA002 sp. (bar= 2µm)

The isolated cyanobacterial cells divide in symmetric division in two identical planes in a clear order (Figures 4.6a and 4.6c). In BAA001 strain cultures, the resulting cocci to slightly rod-shaped cells grow to clearly mature bacilli cells during the division process. Cell length varies from 2.5 µm to 5.0 µm for the well-grown cells, whereas cell width was less different in character as it ranges between 2.0 µm to 2.5 µm as seen in Figures 4.6a and 4.6b. Furthermore, growing these cells under stressed conditions (e.g. high salinities and extreme pH values) can produce irregularly shaped and sized cells, however in this experiment, cultures grown in the original lake water, BG11 medium without added salinity, or BG11 with added salinity 60 g/l as NaCl, only were considered for morphological investigations.

Table 4.4: Morphological Traits of the Studied and Reported Cyanobacterial Strains.
[B : bacilloid, CB : Coccobacilloid, C : coccoid, F : fusiform elliptical, and I : irregular]

Strain	Cell			Division				Taxonomy	References
	Width (µm)	Length (µm)	shape	Planes	Asymmetry	Colonies	Gas vesicles		
BAA 001	2.5 (0.3)	4.0 (0.5)	C-CB	1	+	–	?	*Euhalothece*	This study
BAA 002	2.0 (0.4)	2.6 (0.6)	C-CB	1	–	–	?	*Euhalothece*	This study
MPI 95AH10	3.1 (0.3)	4.2 (0.7)	B-CB	1	–	(+/–)[a]	–	*Euhalothece*	Pichel, *et.al.* (1998)
MPI 95AH11	2.8 (0.5)	4.0 (1.0)	B-CB	1	–	(+/–)[a]	–	*Euhalothece*	Pichel, *et.al.* (1998)
MPI 95AH13	10.3 (0.3)	15.9 (1.6)	F-CB	1	+	+	–	*Euhalothece*	Pichel, *et.al.* (1998)
MPI 96N303	variable	variable	C-I	>2	–	–	–	*Euhalothece*	Pichel, *et.al.* (1998)
MPI 96N304	variable	variable	C-I	>2	–	–	–	*Euhalothece*	Pichel, *et.al.* (1998)
MPI 96P402	3.7 (0.6)	7.8 (2.4)	B-CB	1	–	+	–	*Euhalothece*	Pichel, *et.al.* (1998)
MPI 96AL03	5.8 (0.7)	11.6 (1.6)	CB-F	1	+	+	–	*Euhalothece*	Pichel, *et.al.* (1998)
MPI 96AL06	3.5 (0.6)	4.5 (1.0)	C-CB	1	–	–	–	*Euhalothece*	Pichel, *et.al.* (1998)
Syn CI P22	2.6 (0.4)	4.5 (1.0)	B-CB	1	–	–	–	*Euhalothece*	Pichel, *et.al.* (1998)
PCC 7418	5.0 (0.7)	7.4 (1.7)	B-CB	1	–	–	+	*Cyanothece*	Pichel, *et.al.* (1998)
ATCC 43922	3.3 (0.5)	6.8 (3.3)	B-CB	1	–	–	–	*Aphanothece*	Pichel, *et.al.* (1998)

[a] Only at high salinities

Reproduced and updated from Pichel, *et.al.* (1998)

4.3.2.4 Salt Tolerance and Growth Rate

Salt tolerance and growth rate are two interdependent factors. In this experiment, growth rate was used as an indicator for salt tolerance of the cultures grown under various conditions. Salt tolerance and requirements were determined by monitoring the growth of triplicate cultures with zero, 20, 40, 60, 100, and 120 g l^{-1} added salinities as NaCl at various pH values (e.g. pH 4.5, 7, 9, and 10.5). All experiments were carried out in triplicate under

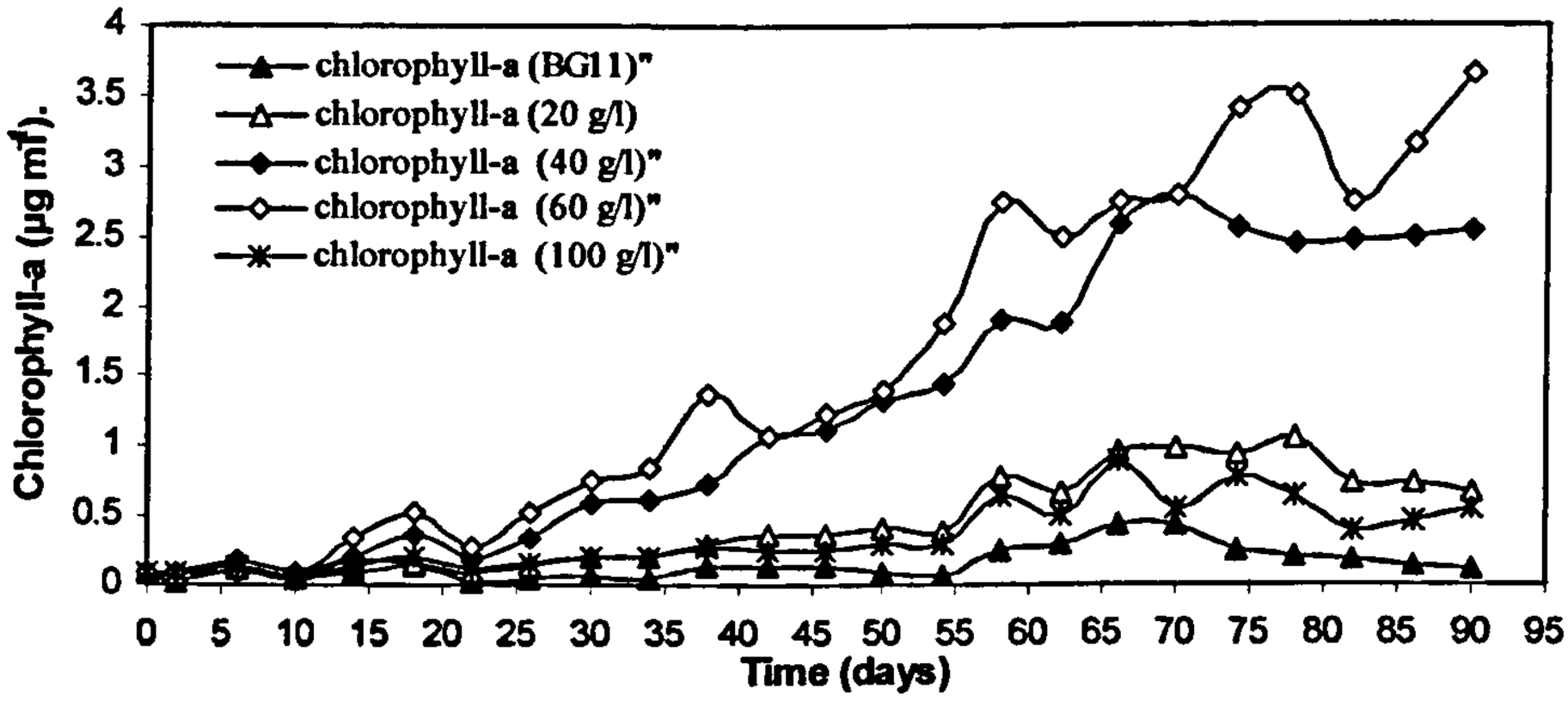

Figure 4.7: Growth profile of *Euhalothece* sp. strain BAA001 grown in BG11 medium with a series of salinities at pH 7

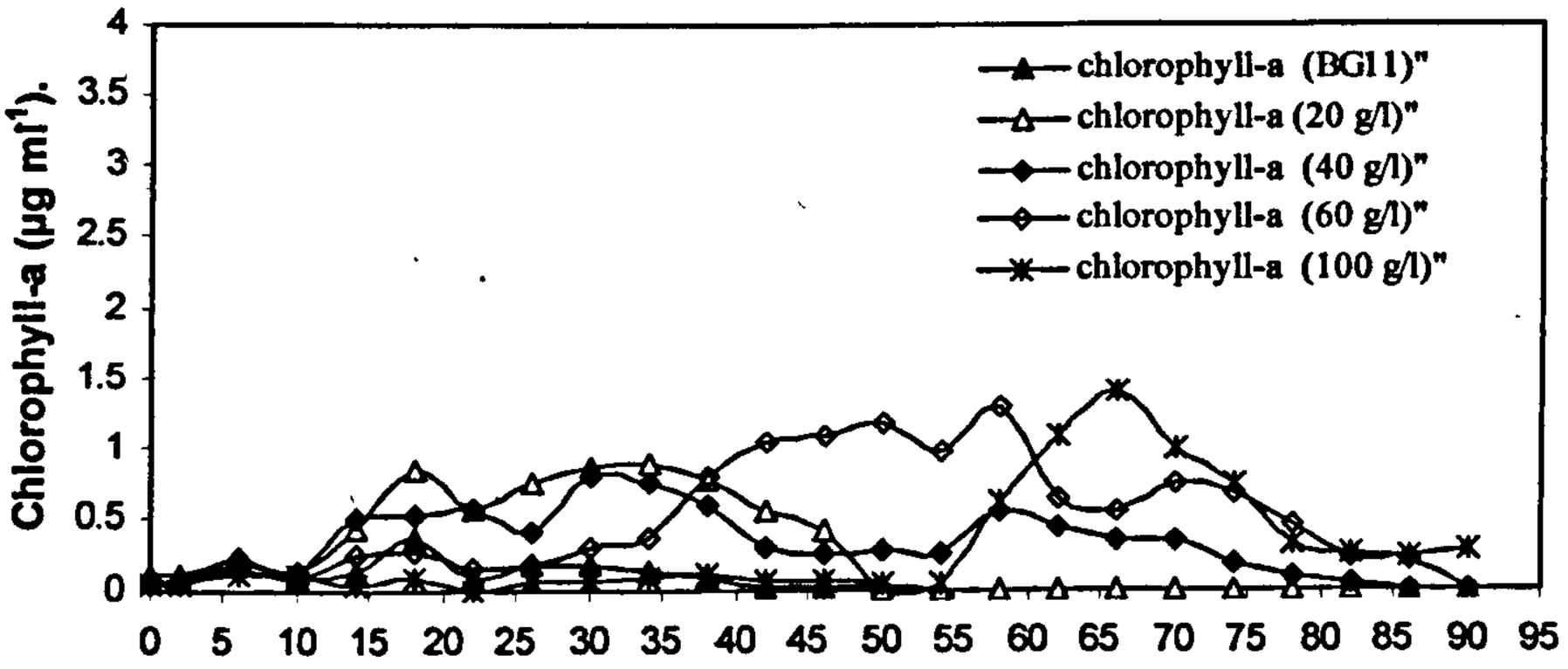

Figure 4.8: Growth profile of *Euhalothece* sp. strain BAA001 grown in BG11 medium with a series of salinities at pH 9

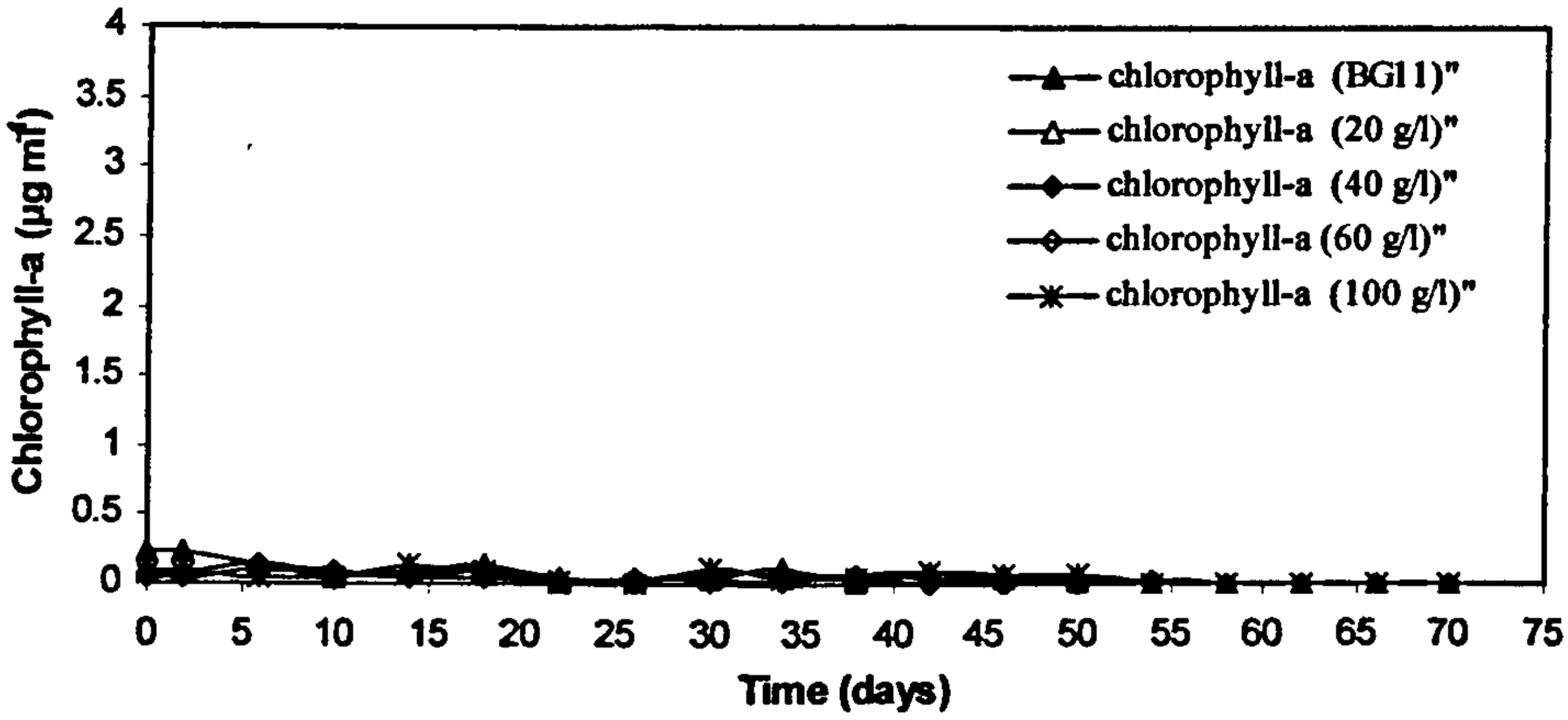

Figure 4.9: Growth profile of *Euhalothece* sp. strain BAA001 grown in BG11 medium with a series of salinities at pH 10.5

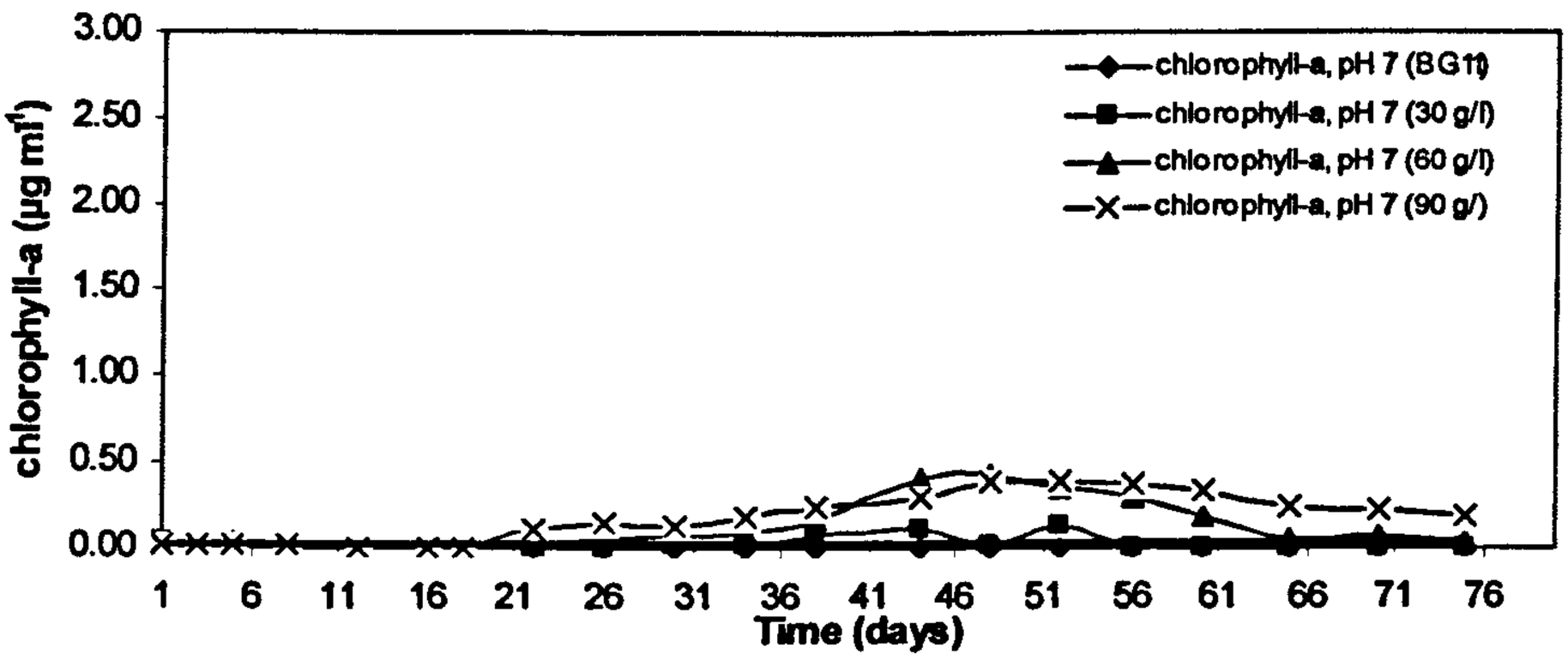

Figure 4.10: Growth profile of *Euhalothece* sp. strain BAA002 grown in BG11 medium with a series of salinities at pH 7

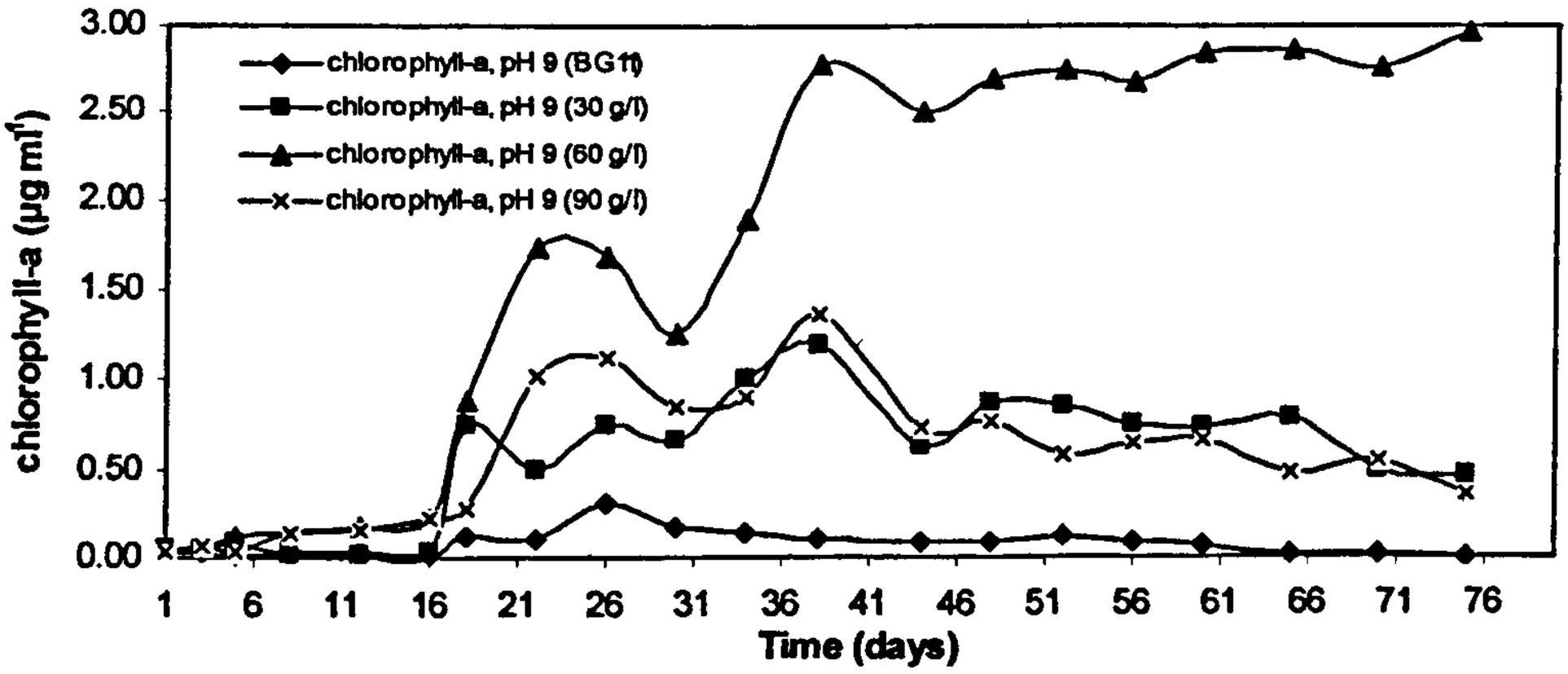

Figure 4.11: Growth profile of *Euhalothece* sp. strain BAA002 grown in BG11 medium with a series of salinities at pH 9

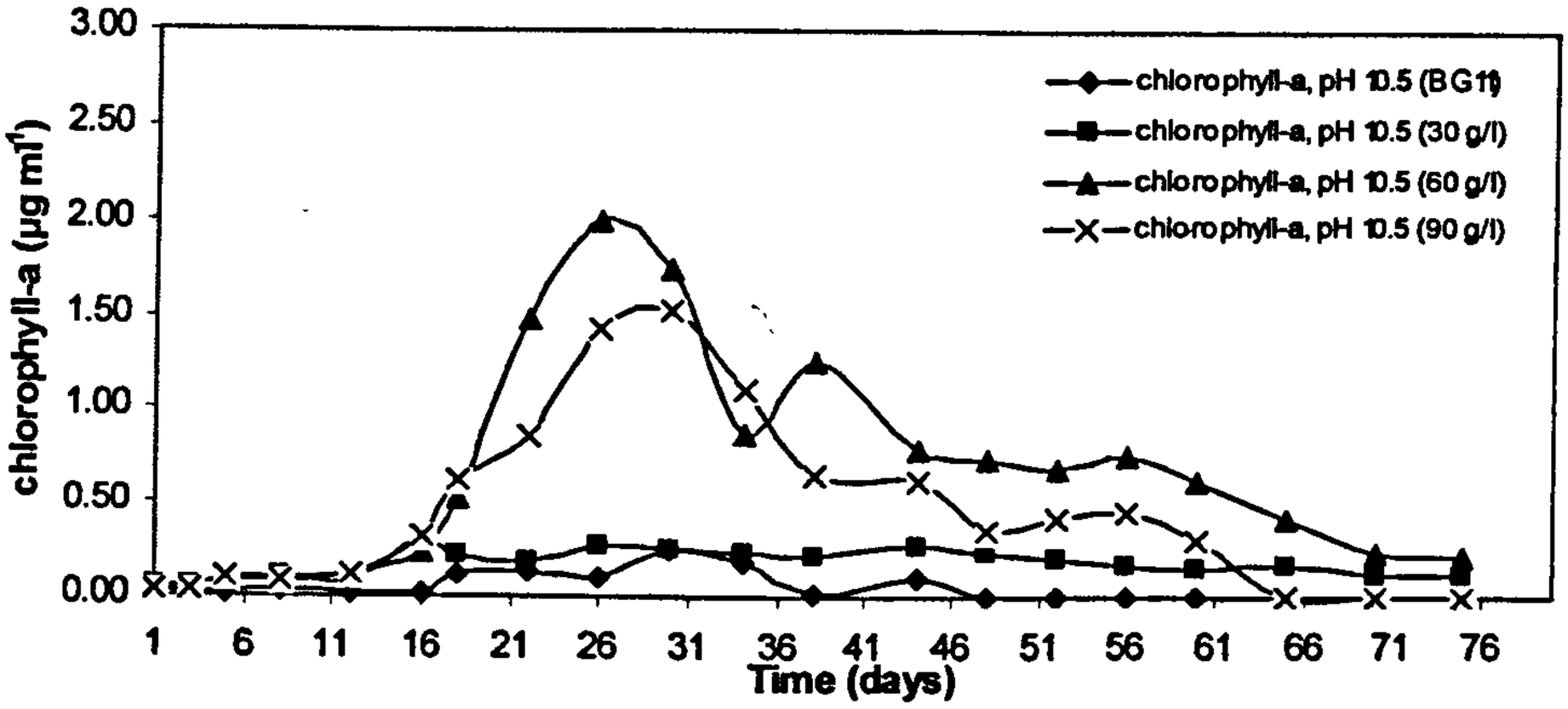

Figure 4.12: Growth profile of *Euhalothece* sp. strain BAA002 grown in BG11 medium with a series of salinities at pH 10.5

(12h light/dark cycle) at room temperature (i.e. 21°C – 25°C). 10% premature inocula grown for about 4 months in BG11 medium at pH 7.2 were used to inoculate 100 ml BG11 cultures with adjusted salinities and pH values under sterile conditions. The growth profiles of these determinations for strains BAA001 and BAA002 are depicted in Figures 4.7-4.9; and Figures 4.10-4.12, respectively.

For BAA001 sp., the effect of varying salinity and pH values on the growth rate can be seen clearly in Figures 4.7-4.9. No growth was observed at pH values below 7 and above 9. At pH 9, the growth profile of all cultures exhibited high uncertainty for the first 50 days before resulting in failure at the experiment end (e.g. 90 days). However, at pH 7, all cultures showed sustained growth which highly dependent on the salinity gradient of each culture. The experiment showed that the maximum growth occurred in cultures containing 6% salinity. Hence, it is the optimal salinity for this organism.

Similarly, strain BAA002 showed no growth at all at any condition at pH below 7, however, it is surprisingly the showed some uncertain growth, especially at high salinities (pH 10.5) (Fig. 12). On the other hand, this experiment showed the maximum growth for this strain (e.g. BAA002) was at 60 g/l salinity.

Thus, the isolated *Euhalothece* strains (BAA001 and BAA002) can be considered as halotolerant and not strictly halophilic species (Garcia-Pichel *et al.*, 1998), as they showed sustainable growth with various salinity gradients. Unlike salinity, pH variations showed detrimental affects on the growth rate for both isolates, and hence these isolates are very sensitive to pH changes.

In order to determine the optimal growth conditions more accurately, the specific growth rate of each organism for each condition was determined. These results are summarised and presented in Figure 13 for stains BAA001 and BAA002. Here it can be seen that no growth was observed in BAA001 strain cultures grown at pH 4.5 and pH 10.5. Differences among cultures in salinity-dependent growth were significant at pH values 7 and 9. At pH 9, only cultures grown with 60 g/l salinity showed moderate growth (e.g. μ= 0.0284 day^{-1}). However, all cultures grown at pH 7, with various salinity gradients showed sustained growth (e.g. μ = 0.01 – 0.05 day^{-1}). Additionally, cultures grown at pH 7, with 60 g/l salinity reached much higher growth rates (μ = 0.05 day^{-1}) than other cultures grown at different salinities.

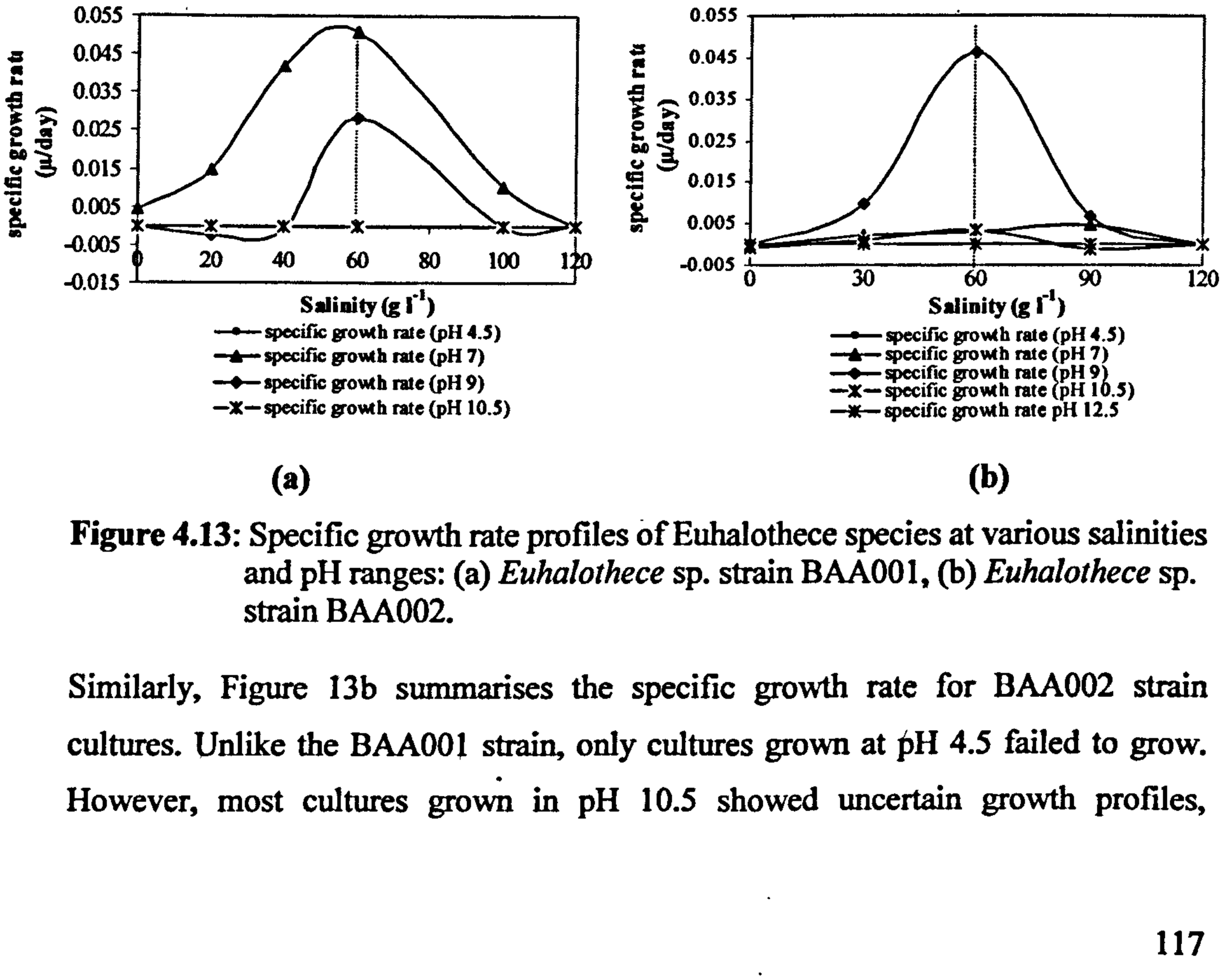

Figure 4.13: Specific growth rate profiles of Euhalothece species at various salinities and pH ranges: (a) *Euhalothece* sp. strain BAA001, (b) *Euhalothece* sp. strain BAA002.

Similarly, Figure 13b summarises the specific growth rate for BAA002 strain cultures. Unlike the BAA001 strain, only cultures grown at pH 4.5 failed to grow. However, most cultures grown in pH 10.5 showed uncertain growth profiles,

especially at high salinities (e.g. 60 and 90 g/l) (Fig 4.12). This growth profile is likely attributed to the optimality of the salinity which likely increases the organism's tolerance to adapt to other conditions (e.g. high pH). On the other hand, this strain also shows another interesting result that being, the optimal pH value for growth is pH 9 and not the neutral pH as seen for strain BAA001.

4.3.2.5 Compatible Solutes Determinations

Figure 4.14 reports ^{1}H spectra of *Euhalothece* sp. strain BAA001 cells grown in BG11 media with no added salt and with 60 g/l salinity added as NaCl. In particular, the signals at 3.40 and 3.85 ppm originate from the methyl and methylene signals of betaine, respectively. Figure 4.14 also barely shows that the *Euhalothece* sp. strain BAA001 use only betaine as an osmoprotectant when grown in these growth conditions (e.g. growth medium, salinity and pH). No other signals of other osmolytes were observed in this experiment. The effect of salinity increase on the qualitative and quantitative responses is also clearly depicted in Figure 4.15. With increasing salinity in the growth medium from zero to 60 g/l, no signals of other osmolytes were detected and betaine concentration increased by 3-4 folds. Interestingly, the obtained results also showed that there is a threshold concentration of betaine even when cells were grown in BG11 medium with zero salinity. This might be explained by the fact that the ability to synthesise betaine *de novo* is very common in both oxygenic and anoxygenic phototrophic eubacteria and methanogens, displaying moderate or high salt tolerance (da Costa, *et al.*, 1998).

In a similar study on a cyanobacterium isolated from a moderately hypersaline environment (Mono Lake, USA), Daiz and Taylor (1996) found that the addition of glycine betaine to the growth medium relieves or restores the growth of bacteria inhibited by excessive salinity. Exogenous additions of glycine betaine enhanced the growth of bacteria at moderate bacteria and allowed a higher maximal salinity for growth. Only glycine betaine permitted growth of the bacterial strain ML-D at 3.5M NaCl (Daiz and Taylor, 1996).

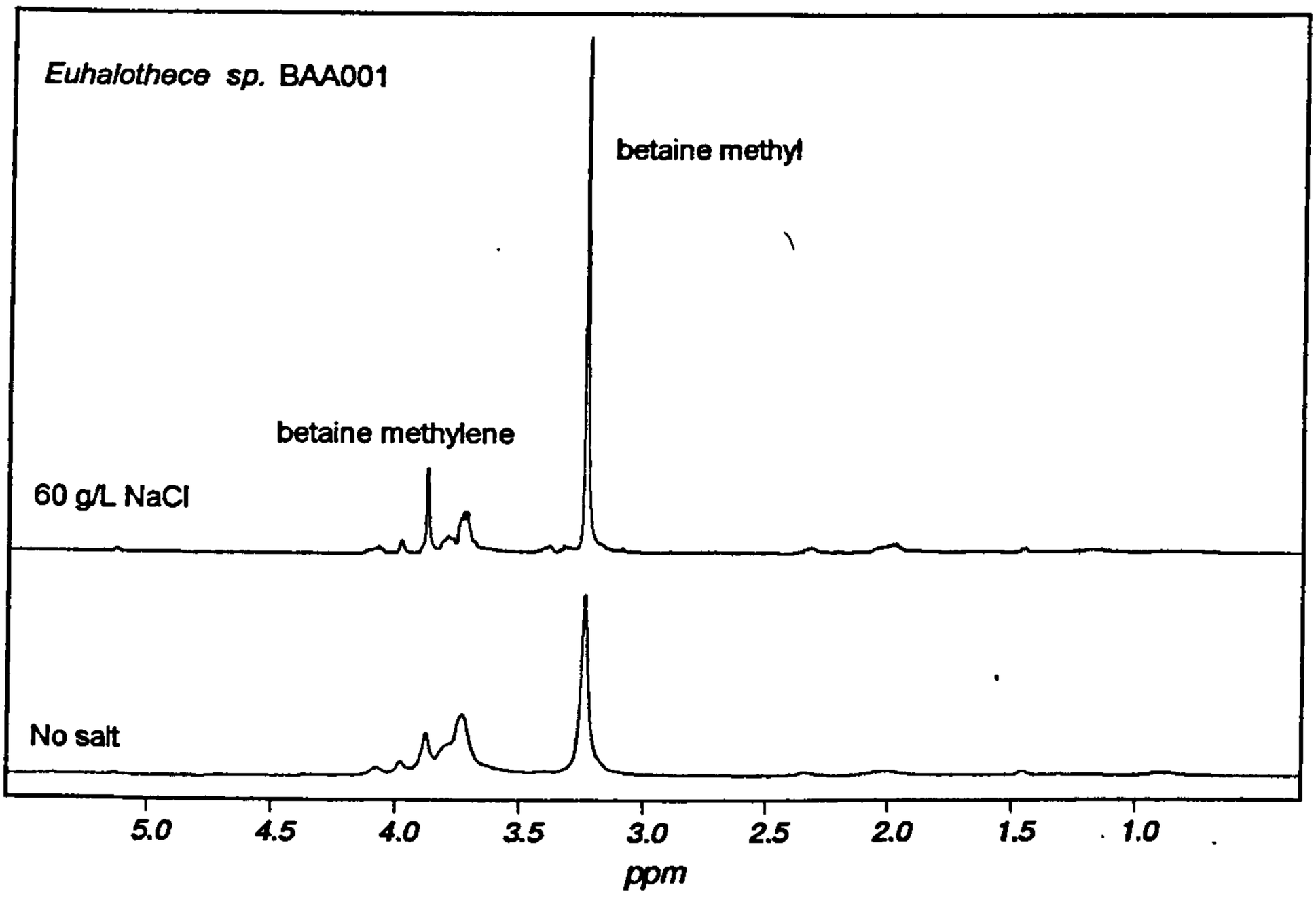

Figure 4.14: 1D 500 MHz ^{1}H spectra of cell extracts from *Euhalothece* sp. strain BAA001. The cells were grown in BG11 medium with no added salt and at 60 g l^{-1} salinity as NaCl. The peaks are labelled with the compounds that give rise to the peaks. Most of the other unlabelled peaks are presumed to be normal cellular metabolites.

NMR analyses of compatible solutes in the isolated *Euhalothece* sp. strain BAA001 indicated that accumulation of glycine betaine is important for osmotic adaptation of this isolate in presence of high NaCl concentrations. The fact that the accumulation of betaine as a sole osmoprotectant in *Euhalothece* sp BAA001 was independent of the medium composition (i.e. BG11 medium does not contain any yeast extract) indicates that the presence of betaine in the cells was definitely synthesised by the cells (e.g. *de novo*) and might be betaine is absolutely required as a compatible solute for this isolate grown under stressed conditions. Unlike other cyanobacteria and halobacteria isolated from similar hypersaline environments, *Euhalothece* sp. strain BAA001 accumulates only betaine as a sole osmoprotectant to adapt to high salinities. As a moderate halotolerant, *Euhalothece* sp. strain BAA001 should accumulate glucosylglycerol and not betaine. Only extreme halotolerant cyanobacteria are expected to accumulate glycine or glutamate betaine (Page-Sharp, *et.al.*, 1999).

4.4 Conclusions

The indigenous microorganisms inhabiting the hypersaline environment in Qabar-Onn Lake seem to have a strong potential to adapt to the rapid increase in the lake salinity (Ajaili *et al.*, 1984). However, the later highly restricts their growth and reproduction. The hypersalinity of this lake partially inhibits the photosynthesis and, to some extent, the nitrogen fixation (Rothrock and Garcia-Pichel, 2005). In addition to salinity, pH also seems to be a limiting factor to the biodiversity and dominance of microorganisms.

Qabar-Onn lake microbial mats are apparently rich in species. Direct microscopic observations revealed that a high diversity of phototrophic organisms since four morphotypes could be distinguished. It should be realized, however, that the biodiversity estimation in our study was based primarily on culture-based techniques. Since many organisms resist culturing in standard media (Svenning *et. al.*, 2005), the actual biodiversity is likely to have been much higher. The poor concentration of nitrogen in Qabar-Onn lake water, (e.g. $NO_3^- < 0.4$ mg l^{-1} and $NO_2^- < 0.08$ mg l^{-1}, Table 4.2), apparently did not restrict microbial diversity to a major extent. Either the poor nitrogen concentration, or the high concentration of other elements (e.g. S, Cl, Na, and/or K), that are thought to be inhibitory for many microorganisms, resulted in a genetically different community composition of Qabar-Onn Lake. Currently, a clone library of 16S rDNA genes amplified from environmental DNA extracted from the Qabar-Onn Lake microbial mat is under construction for further investigations.

The structural community analysis of the Qabar-Onn Lake microbial mat, however, revealed apparent characteristics. Although the water samples were collected from three stratified layers in Qabar-Onn Lake (Fig 4.1), the cyanobacterial mats were only found on the surface layer. The richness of the cyanobacterial mats at the water surface would be referred to the slight decrease in salinity, which contributes a major limiting factor for the isolated cyanobacteria. Light penetration is definitely not the case as the lake has a transparency of about 7 meters depth (based on Sechi disc; Ajaili *et al.*, 1984), so light penetrates in adequate amounts to support

photosynthesis. Also, in their study, Ajaili, *et al.* (1984) have found that 3 from 19 species of diatoms identified in Qabar-Onn Lake, were collected at 7.8 meters depth, this gives another indication of light sufficiency to support photosynthesis processes in the lake. pH also plays a significant factor for cyanobacterial diversity and growth in this lake. pH has a uniform distribution throughout the lake profile, with a very slight increase at the surface layer (e.g. from pH 10.25 to pH 10.40). This change, however, is considered insignificant in this instance as specific growth profiles of both *Euhalothece* isolates (e.g. BAA001 and BAA002) showed that pH 7 and pH 9 are the optimal pH values for these isolates, respectively.

Unicellular cyanobacteria are common constituents of the laminated mat communities which develop in marine and hypersaline ecosystems throughout the world. They are prevalently distributed in the upper photic zone of the mat, where they are closely associated with a restricted number of filamentous cyanobacteria belonging to the form-genera *Microcoleus*, *Phormidium*, *Spirulina* and *Oscillatoria*, and contribute to the bulk of intercellular gelatinous matter (Paerl, *et al*, 2000). At salinities higher than 10% and this is the case for Qabar-Onn Lake, coccoidal cyanobacteria are more abundant than filamentous ones and can still be found in NaCl-saturated brines. However, not all the isolated cyanobacterial mats are identified and characterised, therefore filamentous cyanobacteria may exist in this lake.

Understanding the dynamics of microbial communities, even for relatively small systems like Qabar-Onn Lake, is not an easy task. Further research involving extended time and biological analysis distribution in Qabar-Onn Lake is required. Although molecular techniques will remain the major tool for description of the complexity of microbial communities, novel culturing techniques such as dilution to extinction method (Benlloch, *et al.*, 2002) should also be applied. Efforts should therefore be undertaken to protect the unique Qabar-Onn Lake ecosystem in order to conserve its still largely unexplored biodiversity.

Chapter 5

HALOBACTERIAL STUDIES OF A HYPERSALINE LAKE IN THE LIBYAN SAHARA

5.1 Introduction

Hypersaline environments are generally defined as those containing salt concentrations in excess of seawater (e.g. > 35 g l^{-1} TDS) (Burns, *et al.*, 2004). Most of the currently existing hypersaline bodies derive from the evaporation of seawater and are called thalassic. Athalassic waters are those in which the salts are of nonmarine proportion, found for example after the concentration of sea water leads to precipitation of NaCl, leaving a high concentration of potassium and magnesium salts (Burns, *et al.*, 2004).

The Great Salt Lake (in the western US) and the Dead Sea (in the Middle East) are the two largest and best-studied hypersaline lakes (Paerl, *et al.*, 2000). The Great Salt Lake has the larger area (3,900 km^2) and is shallower (10 m deep), and has a salt composition equivalent to concentrated seawater. The Dead Sea is comparatively smaller (800 km^2) and deeper (340 m), and contains a very high concentration of salts (~ 31% TDS), especially magnesium salts. Both lakes have nearly neutral pH values; however, it is slightly alkaline in the Great Salt Lake and slightly acidic in the Dead Sea (Ollivier, *et al.*, 1994).

Many small evaporation ponds or sabkhas are found near the coastal areas, these ponds are usually formed when seawater penetrates through seepage or via narrow inlets from the sea (Paerl, *et al.*, 2000). Examples of these ponds include: The Great Solar Lake in the western United States, Gavish Sabkha and Ras Muhammad Pool near the Red Sea coast, Guerrero Negro on the Baja California coast, Lake Sivash near the Black Sea, and Sharks Bay in Western Australia. In addition, many hypersaline soda brines also exist, these include: the Wadi Natrun lakes of Egypt,

Lake Magadi in Kenya, and the Great Basin lakes of the western United States. Soda brines are lacking in magnesium and calcium divalent cations because of their low solubility at alkaline pH (Paerl, *et al.*, 2000).

Hypersaline environments also include closed drainage basin (endorheic) lakes where evaporation exceeds precipitation. This is the case in a group of ten relatively small lakes in Ramlat Az-Zallaf, Libyan Sahara. Qabar-Onn Lake is the biggest among these lakes, which supports a unique hypersaline environment for many organisms (Ajaili *et al.*, 1984). This lake is addressed in more detail in Chapter 4, Section 4.2.

Halophiles are salt-loving organisms that inhabit hypersaline environments. They include mainly prokaryotic and eukaryotic microorganisms with the capacity to balance the osmotic pressure of the environment and resist the denaturing effects of salts (Ventosa, *et al.*, 1998). Generally, halophiles can be loosely classified as slightly, moderately and extremely halophilic, depending on their tolerance and requirement of NaCl. Halophiles are found distributed all over the world in hypersaline environments, many in natural hypersaline brines in arid, coastal, and even deep-sea locations, as well as in artificial salterns used to mine salt from the sea (Kushner and Kamekura, 1988).

Moderately halophilic bacteria are those which grow best in media containing 30 g l^{-1} to 150 g l^{-1} (w/v) NaCl (Kushner and Kamekura, 1988). These extremophiles inhabit a wide range of hypersaline environments and play an important role in the microbial diversity and community of saline environments (Llamas, *et al.*, 1997). In order to overcome the extreme osmotic pressure of the hypersaline environments, halophilic bacteria and eukaryotes accumulate mostly neutral organic compatible solutes and exclude most of the inorganic salts. In contrast, the halophilic archaea balance the external high salt concentration by intracellular accumulation of inorganic ions (in particular K^+) to concentrations that exceed that of the medium. Therefore, all the cellular components of the halophilic archaea must be adapted to function at the extremely high intracellular salt concentration (Imhoff, 1986).

In this chapter, a new species of the genus *Halomonas* was proposed based on conventional morphological, physiological, biochemical and chemical characteristics and through phylogenetic analysis based on 16S rRNA gene sequencing approach. Results also include the phylogenetic reconstruction analysis based on 16S rRNA gene sequences in order to clarify its systematics.

5.2 Methodology

5.2.1 Sampling Procedure

Water samples collection from Qabar-Onn Lake was conducted as described earlier in Chapter 4, Section 4.2.1. Three sets of water samples were microbiologically screened, which were collected from surface, middle, and bottom layers of the lake (Figure 4.1, Chapter 4).

5.2.2 Media Selection and Culturing

The isolation procedure was conducted by inoculating fresh lake water samples into various selected media at various salinity and pH values, with a water sample-to-medium ratio of 1 : 2. Growth was followed by measuring the optical density (OD) at 530 nm. As soon as bacterial growth occurred in a medium, the culture was centrifuged at 4000×g for 10 minutes and the biomass pellets were resuspended in fresh designated media under controlled conditions. Aliquots from the new grown cultures were then used for further experimental investigations.

The halobacterial species (BAA003), isolated from the lake, was grown in Complex medium. This medium was prepared by dissolving the designated amount of sodium chloride in distilled water to which nutrients, trace elements, and vitamins were added (Garcia-Pichel, *et al.*, 1998). The medium contains 1 g l^{-1} peptone, 1 g l^{-1} yeast extract and 26 ml/l of the lake water was added as a supplement of nutrients and trace elements. Solid Complex medium was prepared by the addition of 15% (w/v) agar to the liquid medium (see Chapter 3.3.1.2).

Maintaining the desired pH during experiments was achieved by addition of biological pH buffers: MOPS, pH 7.2; CHES, pH 9; and CAPS, pH 10.5 (Sigma, UK). The pH buffers were added to the prepared cultures at 50 mM concentration after adjusting to the desired pH using 1M NaOH. The grown bacterial colonies were stored in sealed Petri dishes at 4°C for regeneration into fresh Complex medium aliquots for further use.

The experimental cultures for the halobacterial species were conducted in 250 ml conical flasks with bug stoppers (Bug stopper™, Erlenmeyer vent, Whatman®, Whatman Inc., Clifton, NJ, USA). The cultures were kept in a thermostatic incubator set at 30°C, with continuous shaking using an orbital shaker set at 225 rpm.

5.2.3 Measurement of Instantaneous Growth Rate

The growth rate of the isolated halobacterial cultures was measured based on the optical density (OD) at 530 nm. Typically, growth was followed in triplicate cultures for each condition and all measurements are carried out on undiluted samples. The average values of three independent specific growth rate estimates, (μ, day^{-1}), are presented here. Thermo Spectronic spectrophotometer (MODEL Helios Epsilon) was used to measure the OD absorbance in1 ml cuvette at 530 nm using medium as blank.

5.2.4 DNA Extraction

50 ml aliquot of well-grown (e.g. OD = 1.0-1.2) halobacterial culture was concentrated to 10 ml by centrifugation at 4000×g for 10 minutes, washed three times with a NaCl based saline solution of identical salinity to the original culture for exopolysaccharide (EPS) removal, and frozen at -20°C until use. 1.8 ml of the thick biomass pellet was used in this experiment following the procedure stated in the protocol of the UltraClean™ Microbial DNA Isolation Kit (MO BIO Laboratories, Inc.). Only a minor modification in step 4 in the protocol procedure was made (see detailed procedure in Appendix B). About 50 µl of DNA was obtained in this experiment, and then the DNA concentration was checked, using a spectrophotometer to measure the absorbance (at λ = 260 nm and 280 nm) of 5 µl

DNA diluted in 65 µl DNA-free deionised water (a detailed procedure is included in Appendix B).

5.2.5 PCR Amplification

A partial sequence of the 16S rRNA gene was determined following PCR amplification using universal primers (Forward 5' CCG AAT TCG TCG ACA ACA GAG TTT GAT CCT GGC TCA G 3') and (Reverse 5' CCC GGG ATC CAA GCT TAC GGC TAC CTT GTT ACG ACT T 3'), and aligned with the sequences in the Blast database (Lane, 1991). In this experiment, the selection of PCR primers was based on a previous study (Romano, *et al.*, 1991) on primers design, which was based on an alignment of all 16S rRNA sequences from *Halomonas* species available from Ribosomal Database Project and GenBank. (The primers were prepared by Dr Arthur Moir, Molecular Biology and Biotechnology Department, The University of Sheffield, UK).

The reaction was performed in a final volume of 50 µl by the Applied Biosystems Model GeneAmp® PCR System 9700, using the following amplification mixture: 5.0 µl of 10× reaction buffer pH 8.8, 5.0 µl $MgCl_2$ (25 mM), 1.0 µl of dNTP (25 mM), 1.0 µl of forward primer (25 mM), 1.0 µl of reverse primer (25 mM), 1.0 µl of Taq DNA polymerase (HiFi Expand), 1.0 µl of DNA sample (1/50 dilution) and 35.0 µl nuclease-free water. The temperature programme was composed of an initial denaturation at 94°C for 3 min, 30 cycles at 94°C for 1 min, 60°C for 1 min, 72°C for 1 min, a final extension at 72°C for 5 minutes and finally was kept at 10°C overnight. All reactions were repeated at least twice, always including both negative (DNA free) and positive controls. The successful amplification of the expected fragment (approximately 700 bp) was checked by electrophoresis in 1% (w/v) agarose gel at 4V cm^{-1} for 1 h, stained with addition of 2 loading dyes in each PCR tube and observed under UV light. Finally, the PCR product was cleaned using QIAquick® Kit (QIAGEN, Inc., UK) following the procedure stated in the protocol. (Further detailed PCR procedures and results are presented in Appendix B).

5.2.6 Alignment and phylogenetic analyses

The multiple sequence alignment programme Clustal W, version 1.83 (Svenning, *et al.*, 2005) was used to align the 16S rRNA sequence of our isolate with the sequences of representative 16S rRNA gene of organisms belonging to the *Halomonas* cluster. The alignment was corrected using Jalview Multiple Alignment Editor software version 1.8 (Clamp *et al.*, 2004). 16S rRNA sequences of rRNA genes, for comparison, were obtained from the GenBank® genetic sequence database under accession numbers (AY914058, AY914060.1, AY914055.1, AY914057.1, AY914059.1, AY914056.1, AY553076.1, AY553075.1, AY553063.1, AY505523.1, X87218.1, AB189314.1, AJ295146.1, and AY973823.1).

A phylogenetic tree was constructed from the distance matrix data by applying the algorithm of the neighbour-joining (NJ) method (Saitou and Nei, 1987) to *K*nuc values with multiple substitutions corrected and positions with gaps excluded. To evaluate the robustness of branches in the inferred tree, the bootstrap resampling method of Felsenstein (Felsenstein, 1993) with 1000 replicates was used. Maximum likelihood (ML) analysis was also carried out using the OMEGA program, version 3.1 (http://www.megasoftware.net/) based on the same alignment data after positions with gaps were excluded. The ML distance matrix was calculated using NucML, and the initial NJ tree was reconstructed by NJdist in the OMEGA package. The ML tree was finally obtained using NucML with the local rearrangement method from the NJ tree, and local bootstrap probabilities were estimated by a resampling of the estimated log-likelihood method (Felsenstein, 1993).

5.2.7 Substrates Utilisation Experiment

Carbon source utilisation experiment was conducted for the halobacterial species using ecology (ECO) plates (Biolog®, Inc.). The ECO plate contains three replicate wells of 31 carbon substrates; these substrates are predominantly amino acids, carbohydrates, carboxylic acids, polymers, amines, and phenolic compounds as listed in Table 5.1.

Table 5.1: Carbon Substrates in Biolog® ECO Microplates (Choi and Dobbs, 1999).

Category	Carbon Substrate
Polymers	• α-cyclodextrin • glycogen • tween 40 • tween 80
Carbohydrates	• D-cellulobiose • i-erythitol • D-galactonic acid γ-lactone • N-acetyl-D-glucosamine • glucose-1-phosphate • β-methyl-D-glucoside • D,L-α-glycerol phosphate • α- D-lactose • D-mannitol • D-xylose
Carboxylic acids	• γ-hydroxybutyric acid • α-ketobutyric acid • D-galacturonic acid • D-glucosaminic acid • itacconic acid • D-malic acid • pyruvatic acid methyl ester
Amino acids	• L-arginine • L-asparagine • glycyl- L-glutamic acid • L-phenylalanine • L-serine • L-threonine
Amines	• phenyl ethylamine • putrescine
Phenolic compounds	• 2-hydroxybenzoic acid • 4- hydroxybenzoic acid

A control well containing no carbon substrate is also included in this plate, thus any colour development there presumably indicates utilisation of carbon sources inherent in the inoculated sample. Aliquots of 150 µl of the halobacterial culture, grown at optimum conditions, were inoculated into each well of the microplates under sterile conditions. The microplates were then incubated at 30°C and were protected from light by wrapping them with aluminium foil. The optical density, OD, (λ = 590nm)

of each well was determined immediately (0 hr) and after time intervals of 24, 70, 144, 168, 192, 240, 310, 360, 408, and 504 hours.

5.2.8 Extraction of Cellular Solutes

The halobacterial isolate cells were harvested during mid steady-state phase (e.g. OD_{530nm} ~ 1.0 -1.2), by centrifuging 4 × 30 ml aliquots from each culture for 10 minutes at 4000×g and the supernatants were poured away. The pellets were then washed 3 times to remove traces of peptone and yeast extract by suspending them in 30 ml aliquots of NaCl solutions of similar salinities to the original cultures and finally were suspended in 10 ml of similar NaCl salinity and poured into a 25 ml glass beaker. The beaker was surrounded by ice and the sample was sonicated (Soniprep 150, MSE Scientific Instruments, West Sussex, UK) until a thick foam was produced. The sonicated samples were then, transferred to 1.5 ml Eppendorf Tubes and centrifuged at 13000×g in a microcentrifuge for 2 minutes, and the supernatant in these samples were used for amino acid assays, enzyme activity determinations, and NMR analyses of compatible solutes.

5.2.9 Analysis of Amino Acids

0.1 ml of cell-free extract of the halobacterial isolate was added to 1 ml ninhydrin reagent (Sigma Ninhydrin Reagent Solution containing DM50 as a solvent) in 10 ml test tubes, stirred gently, and heated at 80 – 100°C for 4-7 minutes. After cooling the samples to room temperature in a cool water bath, the absorbance at 570 nm was recorded for each sample using Thermo Spectronic spectrophotometer (Model Helios Epsilon).

5.2.10 Enzyme Activity Determinations

In this experiment, determination of malate dehydrogenase activity in the halobacterial isolate was carried out. In order to measure the effect of salinity (e.g. NaCl content) on enzyme activity in this species, malate dehydrogenase activity was measured in cell-extracts of cells grown in various salinities (i.e. 0.5, 1.0, 1.5. and 2M NaCl). Initial experiments were carried out in order to optimise the conditions

for obtaining the maximum activity of malate dehydrogenase in this experiment. The optimised assay contained the following in a 3 ml cuvette:

- 2.0 ml Complex medium
- 0.5 ml cell free extract
- 0.2 ml of 1.5mM NADH
- 0.2 ml of 7.5mM oxaloacetate, pH 7.2
- Total volume = 2.9 ml

The spectrophotometer was set at 340 nm and blanked with distilled water. The above assay was set up in a cuvette, omitting the oxaloacetate and the optical density (OD) at 340 nm was measured at 30 second intervals for 2 minutes. After 2 minutes oxaloacetate was added and the OD absorbance was measured at 30 second intervals for a further 3.5 minutes. A Bradford assay of each cell free-extract was taken in order to calculate the specific activity. (Detailed calculations of the enzyme specific activity at various conditions are presented in Appendix C).

5.2.11 Compatible Solutes Analysis

The cell free extract was prepared by centrifuging 30 ml of mid steady-state phase of each halobacterial culture grown in 0.5, 1.0, 1.5, and 2.0 M NaCl at 4000×g for 15 minutes. The supernatant was poured off and the resulting pellets were washed twice in 30 ml aliquots of NaCl solution of identical salinities to the original cultures. During the washing process the mixtures were vortexed for 1 minute followed by centrifugation for 5 minutes at 4000×g. The washed cells were then suspended in 10 ml aliquots of 80% (v/v) ethanol and were thoroughly vortexed for 8-10 minutes at room temperature. The mixtures were allowed to stand overnight at 65°C until dryness. The dried samples were dissolved in 2 ml Milli-Q water, and the resulting solutions were freeze dried at -80°C. Finally, the dried cells were redissolved in 1-2 ml of Milli-Q water with 10% D_2O, and were sent to NMR laboratory for compatible solute determinations. NMR analyses were carried out as described earlier in Section 3.4.5, Chapter 3.

5.3 Results and Discussion

5.3.1 Characteristic Studies of the Halobacterium Isolate

The isolated halobacterium (BAA003) was the predominant organism and was the only colony forming organism at the highest dilutions. Strain BAA003 cells are aerobic and motile (Figure 5.1). Colonies were milky-cream, circular and opaque. Strain BAA003 is a mesophile, exhibiting optimum growth temperature of 37°C but is able to grow from 10 - 45°C, and at pH 7.0 - 10.5 (optimal is 9.0). The main characteristics of the new isolate are compared to those for various reported *Halomonas* species. These features are listed in Table 5.2. The results of the morphological, physiological and biochemical characterisations of the isolated halobacterial species conducted in this study, together with the previous descriptions of close *Halomonas* species, presented in Table 5.2, shows that BAA003 falls within the *Halomonas* genus.

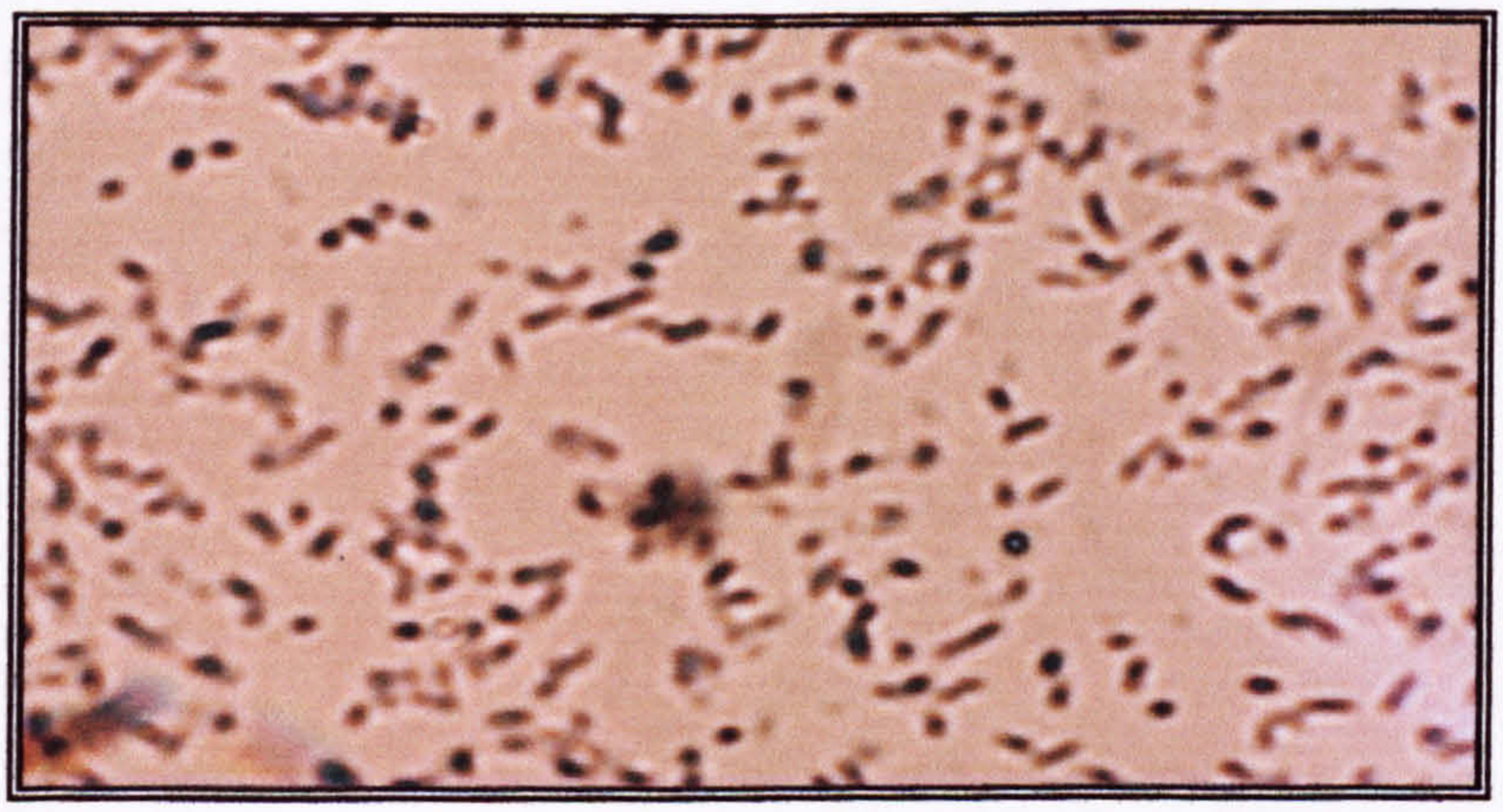

Figure 5.1: A Gram-negative micrograph of isolated halobacterium from Qabar-Onn Lake. (*Picture is taken at 1000× magnification).*

5.3.2 16S rRNA Sequences and Phylogeny

16S rRNA gene sequencing was carried out for the new BAA003 isolate. The gene sequence of BAA003 was deposited in GenBank under accession numbers (EF141076). Table 5.3 presents the similarities between the complete 16S rRNA sequences from strain BAA003 and other selected *Halomonas* strains isolated from various locations.

Table 5.2: Features of the isolated halobacterium and related *Halomonas* species.

***Halomonas* strain**	**Our isolate**	***Halomonas pantelleriensis***	***Halomonas alimentaria***	***Halomonas ventosae***	***Halomonas salina***	***Halomonas desiderata***	***Halomonas campisalis***
Character							
Site sampling	**Qabar-Onn Lake, the Sahara Libya**	**Hard sand, Pantelleria Italy**	**Fermented seafood jeotgal Korea**	**Saline Soil, Jaen Spain**	**Saline Soil, Alicante Spain**	**Municipal sewage works Germany**	**Saline lakes, Washington State USA**
Growth Medium	**Complex**	**DSM 9581^T**	**JCM 10888^T**	**DSM 15911^T**	**ATCC 49509^T**	**DSM 9502^T**	**ATCC 700597^T**
Cell morphology	**Cocci or short rods**	**Rods or pleomorphic**	**Cocci or short rods**	**Short rods**	**Short rods**	**Rods**	**Rods**
Colony colour	**Milky - cream**	**Cream - pink**	**Cream - yellow**	**Cream**	**Yellow - cream**	**White**	**White**
Motility	+	+	-	+	-	+	+
C-source utilisation							
- Glucosamine	+	NR	NR	NR	NR	NR	NR
- Benzoic acid	+	NR	NR	NR	NR	NR	NR
- Tween 40		+	-	-	-	+	-
- Tween 80	+	+	-	-	-	+	-
- Phenylanine	WR	WR	+	+	+	+	-
NaCl requir'ts (%)	**0.5**	**1.25**	**1.0**	**3.0**	**2.0**	**0**	**1.0**
NaCl tolerance (%)	**20**	**15**	**23**	**15**	**20**	**18**	**24**
NaCl optimum (%)	**9**	**10**	**1-13**	**6-9**	**5**	**NR**	**8**
Growth Temp (°C)	**10 - 45**	**10 - 44**	**4 - 45**	**15 - 50**	**4 - 45**	**10 - 45**	**4 - 50**
Optim. Temp (°C)	**37**	**33 - 35**	**30**	**NR**	**NR**	**37.0**	**30**
pH Range	**7 - 10**	**7.5 - 11**	**NG < 5**	**6 - 10**	**5 - 10**	**7 - 11**	**6 - 11**
pH Optimum	**9.0**	**9.0**	**6.5-7.5**	**7.6**	**7.5**	**9.5**	**9.5**
Osmolytes (%)							
- Ectoine	**35%**	**30%**	**NR**	**NR**	**NR**	**NR**	**NR**
- Glycine betaine	**55%**	**56%**	**NR**	**NR**	**NR**	**NR**	**NR**
- Glutamate	**< 1%**	**13%**	**NR**	**NR**	**NR**	**NR**	**NR**
- hydroxyectoine	**10%**	**NR**	**NR**	**NR**	**NR**	**NR**	**NR**
Reference(s)	**This Study**	**Romano, *et al.* (1996) Romano, *et al.* (2001)**	**Yoon, *et al.* (2002)**	**Martinez-Canovas, *et al.* (2004)**	**Baumgarte, *et al* (2001) Arahal, *et al.* (2002)**	**Mata, *et al.* (2002)**	**Mormile, *et al.* (1999) Mata, *et al.* (2002)**

[Legend: WR = weak reaction, NR = not reported, NG = no growth].

Table 5.3: Similarity matrix for 16S rRNA gene fragments comparing the environmental strain (*Halomonas pantelleriensis* sp. BAA003) and some of the most closely related *Halomonas* species.

	(Strain BAA003)	*H. pantelleriense* (Strain AAP)	*Halomonas* (Strain A-7)	*Halomonas* (Strain A-9)	*Halomonas* (Strain A-2)	*Halomonas* (Strain A-4)	*Halomonas* (Strain A-8)	*Halomonas* (Strain A-3)	*Halomonas alimentaria* (GSP26)	*Halomonas alimentaria* (GSP25)	*Halomonas salina* (Strain GSP2)	*Halomonas alimentaria* (GSP1)	*Halomonas eurihalina*	*Halomonas* (Strain SA-Hm1)	*Halomonas elongata*	*Halomonas* (Strain CM4)
Strain BAA003	100															
***Halomonas pantelleriense* Strain AAP**	99	100														
***Halomonas sp.* Strain A-7**	96	95	100													
***Halomonas sp.* Strain A-9**	96	95	99	100												
***Halomonas sp.* Strain A-2**	96	95	99	99	100											
***Halomonas sp.* Strain A-4**	96	95	99	99	99	100										
***Halomonas sp.* Strain A-8**	96	95	99	99	99	99	100									
***Halomonas sp.* Strain A-3**	96	95	99	99	99	99	99	100								
***Halomonas alimentaria* Strain GSP26**	95	95	94	94	94	94	93	93	100							
***Halomonas alimentaria* Strain GSP25**	95	95	94	94	94	94	94	94	99	100						
***Halomonas salina* Strain GSP2**	95	95	94	94	94	94	93	93	99	99	100					
***Halomonas alimentaria* Strain GSP1**	95	95	94	94	94	94	94	94	99	99	99	100				
Halomonas eurihalina	93	93	93	93	93	93	93	93	96	96	96	96	100			
***Halomonas sp.* Strain SA-Hm1**	88	95	95	94	95	95	95	95	94	94	94	94	93	100		
Halomonas elongata	94	93	94	94	94	94	93	93	94	94	94	94	93	94	100	
***Halomonas sp.* Strain CM4**	94	93	92	91	91	91	91	91	94	95	93	92	96	93	90	100

The new isolate was identified based on 16S rRNA gene sequences analyses and chemotaxonomic characterisations. Based on the 16S rRNA sequences and the phylogeny distance tree (Fig 5.2), the Gram-negative isolated species is clearly affiliated with the genus *Halomonas*. However, the phylogenetic differences and the chemotaxonomic characteristics of the new isolate from the validly described *Halomonas* species suggest that the newly isolated strain tentatively represent a new strain within the *Halomonas pantelleriensis* species (i.e..*Halomonas pantelleriensis* strain BAA003), and the species *Halomonas pantelleriensis* sp. strain AAP is a near relative.

The sequence divergence between the newly isolated *H. pantelleriensis* strain BAA003 and *H. pantelleriensis* strain AAP is relatively small (1%, Table 5.3). The sequences of these two species showed the biggest divergence (12% and 5% respectively), with *Halomonas* sp. strain SA-Hm1. Table 5.3 also shows that the *Halomonas* species (strains A-2, A-3, A-4, A-7, A-8 and A-9) are very similar (only 1% divergence), but in fact they are completely different species, and this may be due to a number of factors such as sequence size and stressed conditions of growth for a particular species. A number of studies (Arahal *et al.*, 2002; Burns *et al.*, 2004; Benlloch *et al.*, 2002) have reported the occurrence of closely related sequences in phylogenetic studies of bacterial communities, while others (Garcia-Pichel *et al.*, 1998; Svenning *et al.*, 2005) suggest that the differences may stem from clonal variation within microbial populations, gene families or may represent true subspecies.

In conclusion, our results clearly support that phylogenetically BAA003 is a strain within the species *H. pantelleriensis*. The phenotypic data reported in Table 5.2 tentatively permit the classification of this organism as a new species within the genus *Halomonas*.

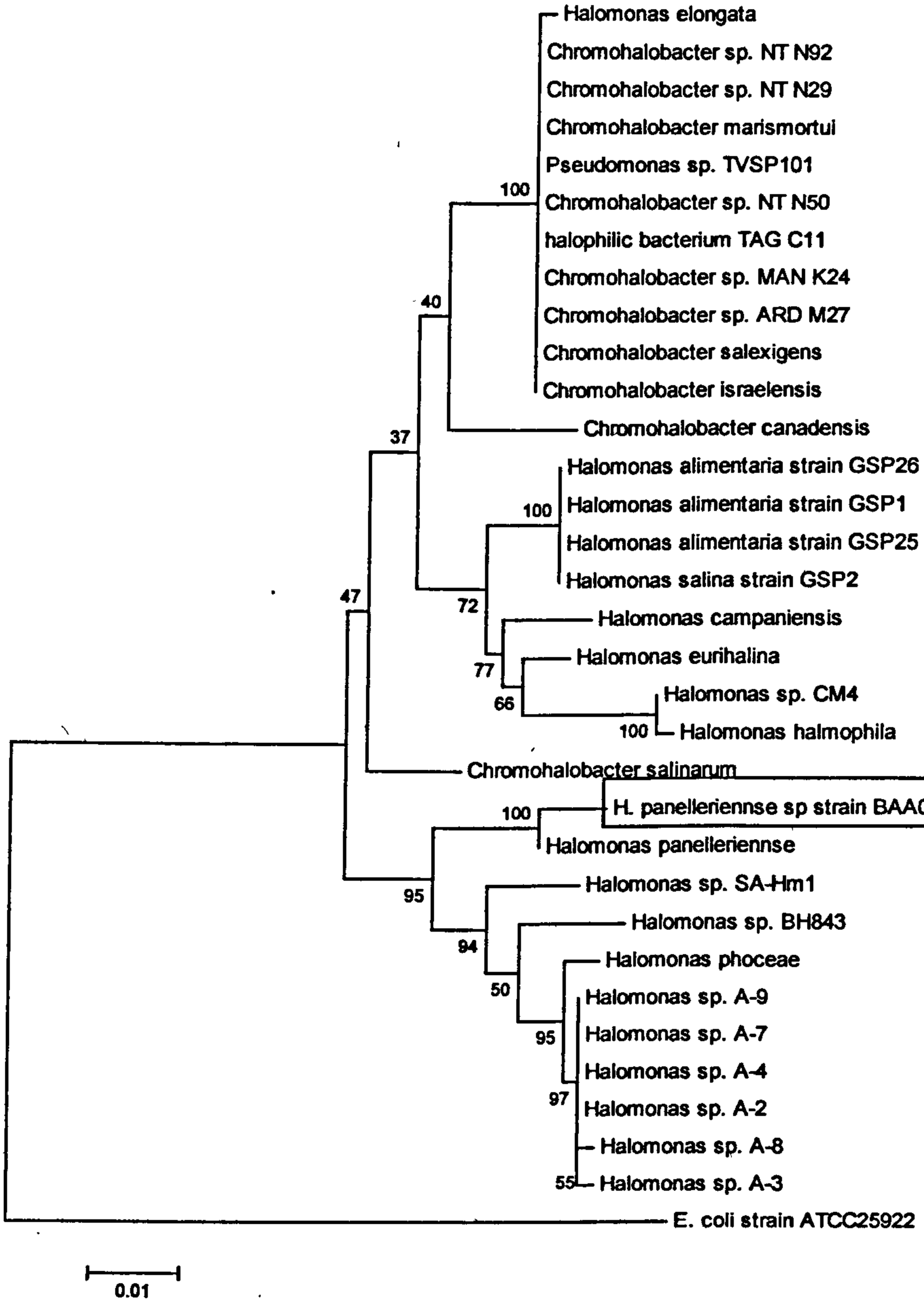

Figure 5.2: 16S rRNA Distance Tree for the proposed new *Halomonas pantelleriensis* sp. (Strain BAA003):[16S rRNA distance tree constructed with the Neighbor-joining method (Saitou and Nei, 1987) using the Tajima-Nei calibration to calculate the evolutionary distances as implemented in the software package MEGA3 Version 1.5. A bootstrap analysis involving 1000 resamplings was performed. Outgroup used in this case is *Escherichia coli* strain ATC25922 and the *H. pantelleriensis* sp. (Strain BAA003) is framed].

5.3.3 Salinity and pH Requirements

Halomonas pantelleriensis BAA003 required aerobic conditions for growth and initial experiments in Complex medium containing 0, 90, 180, and 270 g l^{-1} NaCl, indicated that the optimum NaCl concentration in the medium was 90 g l^{-1}. BAA003 grown in minimal medium had an absolute requirement for sodium ions in the medium. In fact, Complex medium with zero sodium ion concentration has not been used as the minimal percentage (6.6 g l^{-1}) of sodium ion content was from the 26 ml of Qabar-Onn Lake water added as a supplement to the main ingredients of Complex medium.

The effects of salinity on growth of BAA003 were further investigated. Figures 5.3-5.5 show the effect of increasing salinity (from 90 g l^{-1} to 270 g l^{-1}) at three different pH values (pH 7, 9, and 10.5). *H. pantelleriensis* strain BAA003 has only shown sustainable growth in cultures containing 90 g l^{-1} and 180 g l^{-1} NaCl at all pH values, however, no growth was observed in cultures containing 270 g l^{-1} salinity at any pH value. Increase of salinity from 90 g l^{-1} to 180 g l^{-1} caused about a 3-4 fold increase in the lag-phase and to suppress the growth during the exponential phase. However, the increase of salinity by 3 fold (e.g. from 90 – 290 g l^{-1}) resulted in complete dormancy of the bacterial cells at all pH values examined. The maximum growth rate was observed in cultures containing 90 g l^{-1} NaCl at pH 9 (Figure 5.4).

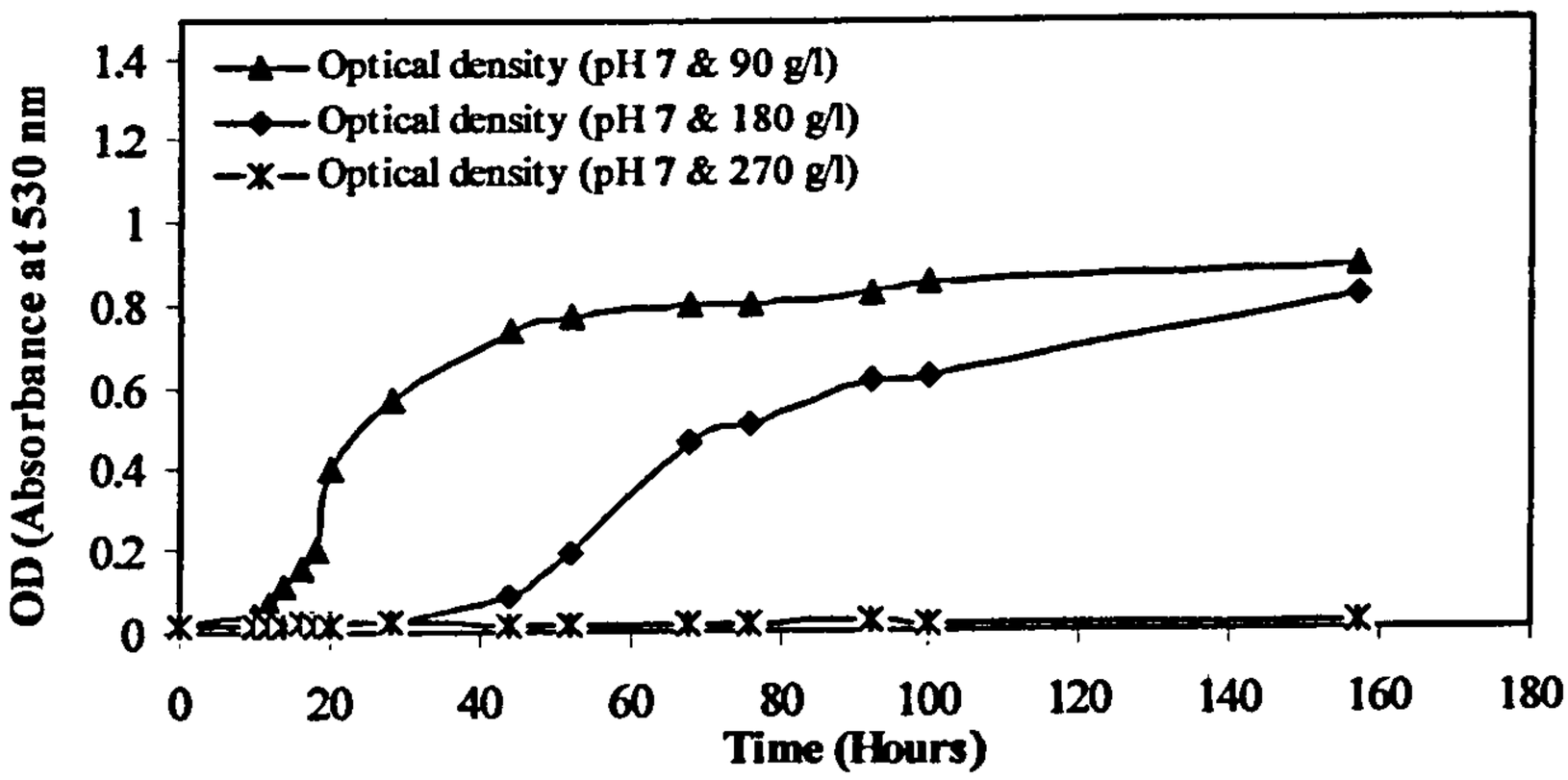

Figure 5.3: Summary of growth profiles of the *Halomonas pantelleriensis* strain BAA003 grown in Complex medium (pH 7 at various salinities)

The slow growth rate at very high salinities (270 g l^{-1} NaCl) of *H. pantelleriensis* strain BAA003 can be attributed at least partially to the tendency to form compact mucilage constraining the dispersability of the cells in the cultures and resulting in the formation of large colonies. Under these conditions, measurement of growth rate (e.g. Abs. $OD_{530\ nm}$) can not be done satisfactorily, and even though growth was very low at 270 g l^{-1} NaCl, it was believed to be steady and non-zero.

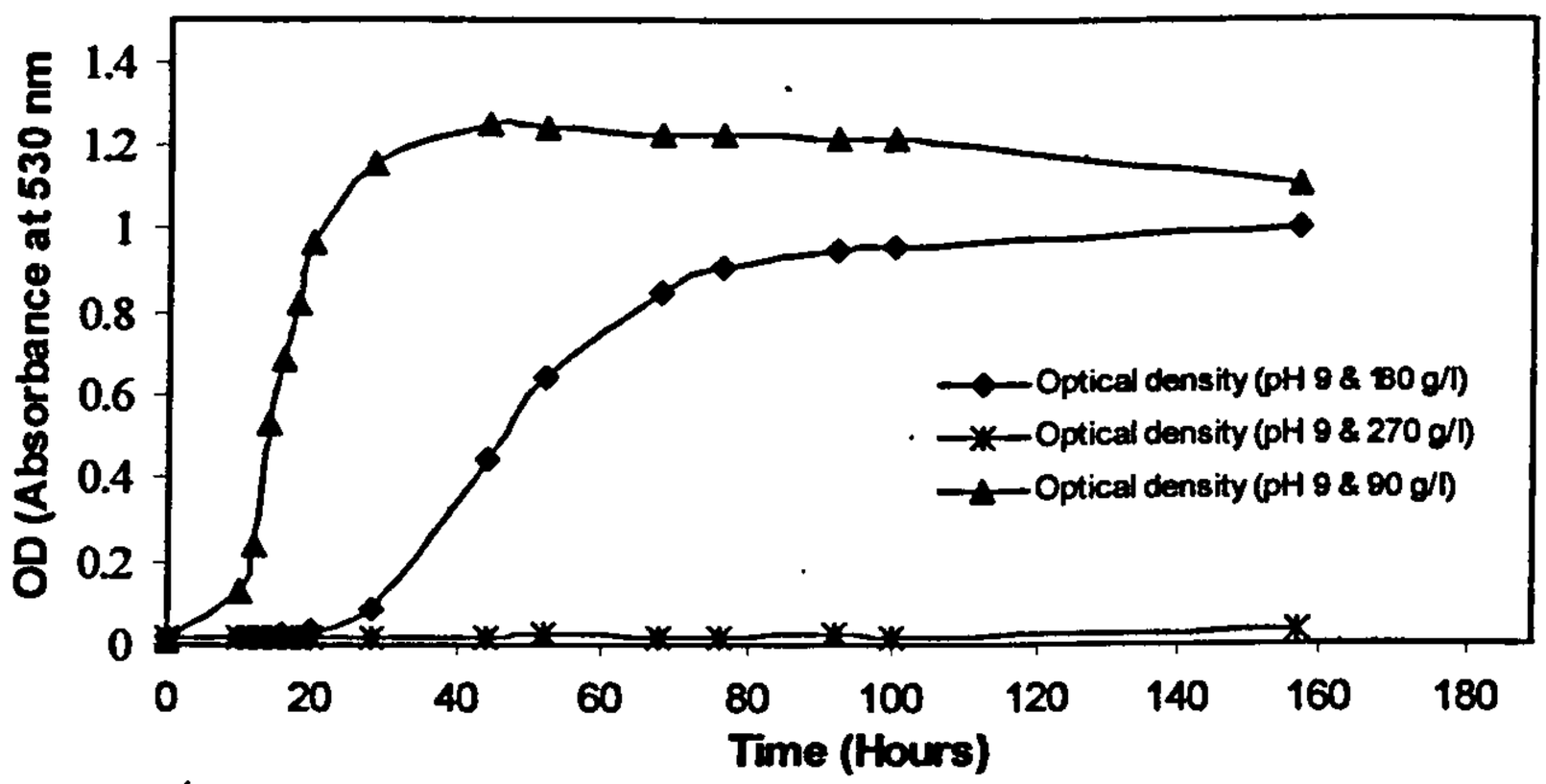

Figure 5.4: Summary of growth profiles of the *Halomonas pantelleriensis* strain BAA003 grown in Complex medium (pH 9 at various salinities)

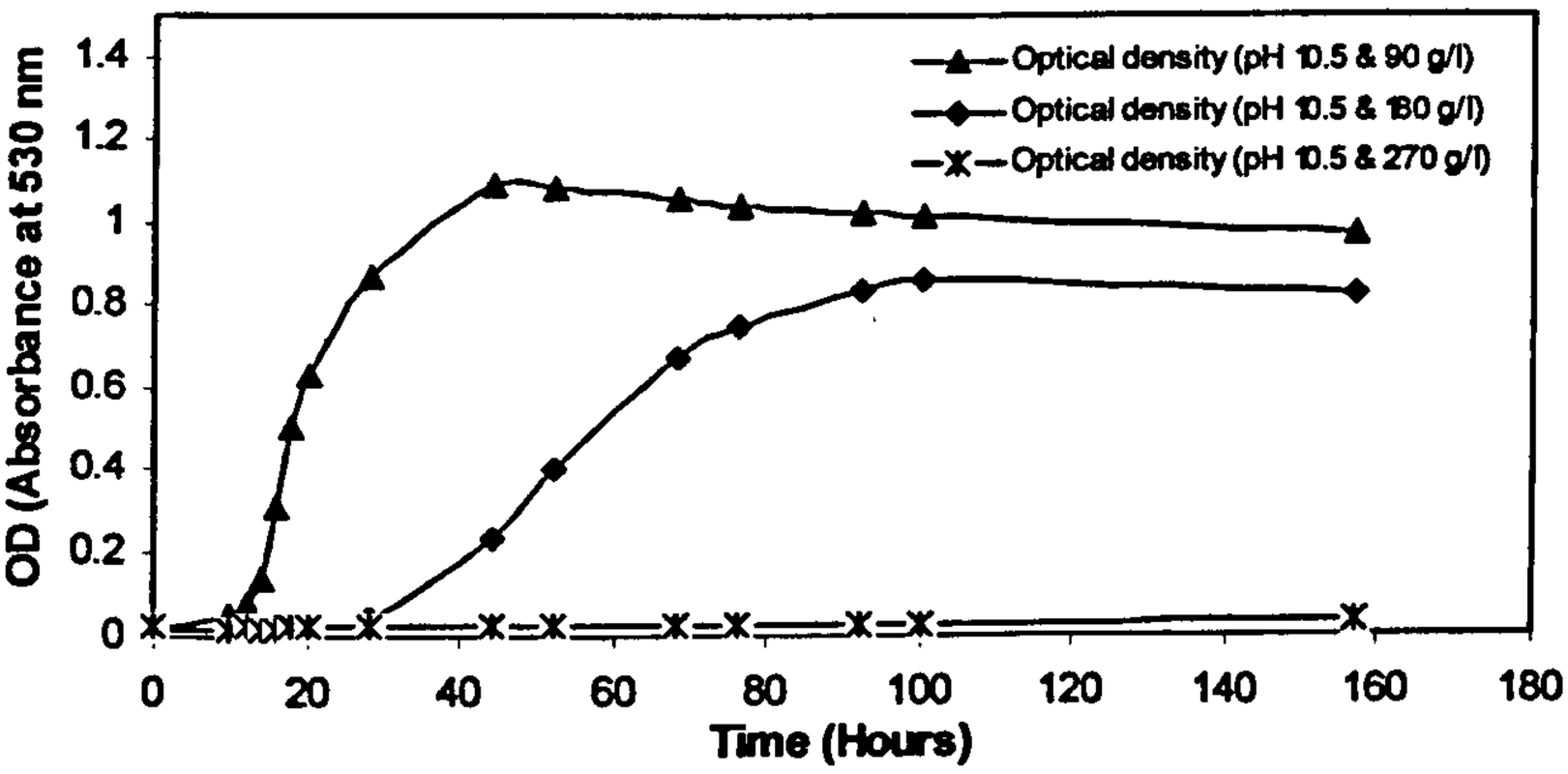

Figure 5.5: Summary of growth profiles of the *Halomonas pantelleriensis* strain BAA003 grown in Complex medium (pH 10.5 at various salinities)

Similarly, the effect of pH (from the same set of experiments) was clearly depicted in Figures 5.6-5.8. Measuring growth at three different pH values (pH 7, 9 and 10.5)

showed that the *H. pantelleriensis* strain BAA003 tends to grow best in alkaline pH with an optimal pH of 9. The optimum pH range of this organism is very close to its original habitat (Qabar-Onn Lake) which has a pH of 10.3. This, therefore gives good evidence that pH is not a limiting factor for growth of this organism in its original habitat (Qabar-Onn Lake). Upon exposure to pH values above and below 9, culture growth was slightly affected at the salinities of 90 g l^{-1} and 180 g l^{-1}, however, cultures at 270 g l^{-1} salinity showed no growth at all due to salt stress. The best growth was observed in cultures with pH values of 9 followed by pH 10.5 while the lowest was observed in cultures with neutral pH (i.e. pH 7). Thus the organism grows better in alkaline medium.

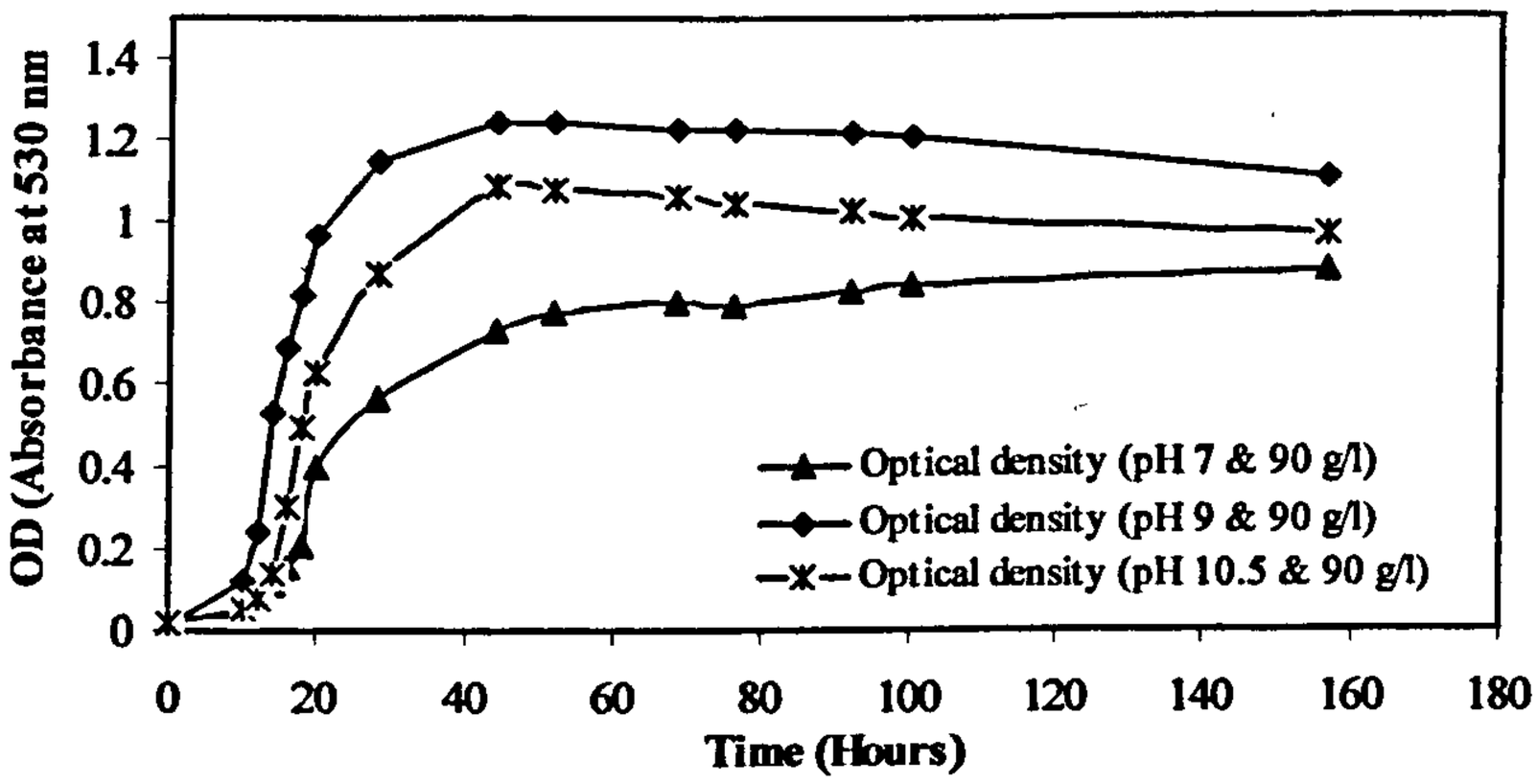

Figure 5.6: Summary of growth profiles of the *Halomonas pantelleriensis* strain BAA003 grown in Complex medium (Salinity 90 g l^{-1} at different pH values)

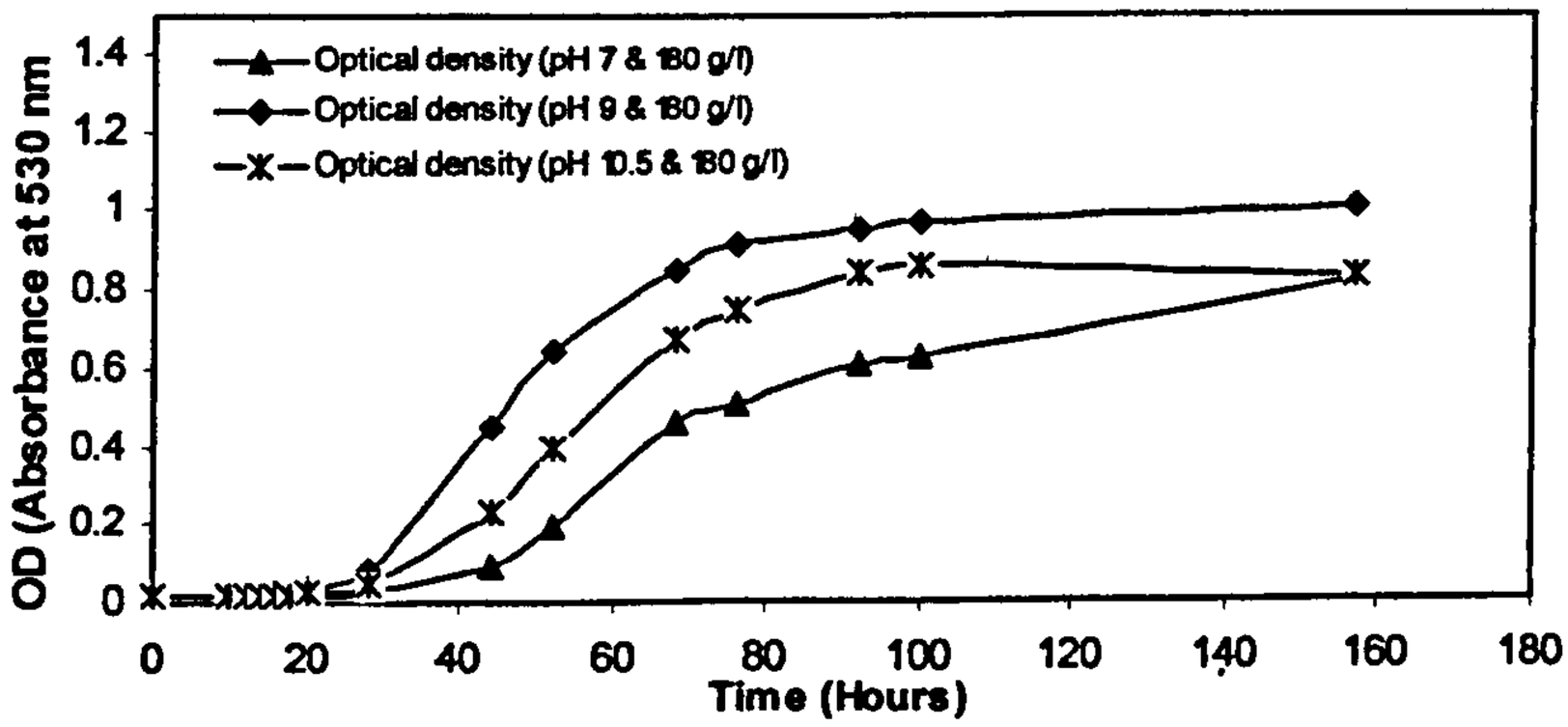

Figure 5.7: Summary of growth profiles of the *Halomonas pantelleriensis* strain BAA003 grown in Complex medium (Salinity 180 g l^{-1} at different pH values)

In order to determine salinity and pH optima more accurately, the maximum biomass yields and specific growth rates were determined. Figure 5.9a shows the maximum biomass yields of the *H. pantelleriensis* strain BAA003, obtained at various salinity and pH conditions, and the specific growth rate (μ) calculated at various conditions is shown in Figure 5.9b. The maximum biomass yield was obtained with 90 g l^{-1} salinity and pH 9, and identically, at double the amount of salinity (180 g l^{-1} NaCl) the maximum biomass yield was also obtained at pH 9. However, with further increase in salinity (270 g l^{-1} NaCl), no growth has been observed.

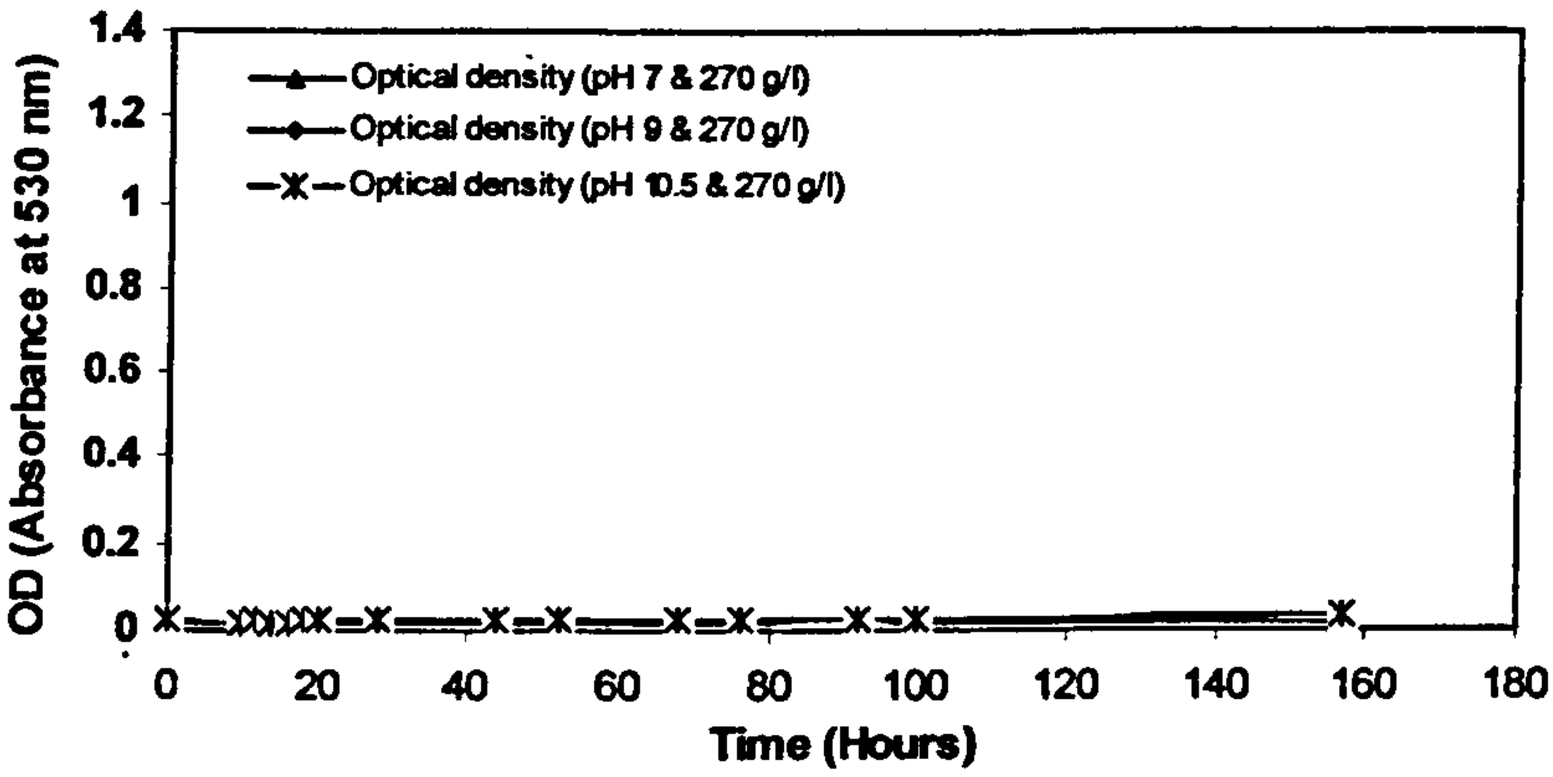

Figure 5.8: Summary of growth profiles of the *Halomonas pantelleriensis* strain BAA003 grown in Complex medium (Salinity 270 g l^{-1} at different pH values)

On the other hand, the maximum calculated specific growth rate (0.128 day^{-1}) of this organism was obtained at the same growth conditions as for the maximum biomass yield. However, at 180 g l^{-1} salinity, the maximum specific growth rate was calculated at neutral pH conditions (pH 7) rather than at the optimal pH value (pH 9). This phenomenon can be attributed to the longer lag-phase (~ 40 hours) compared to ~ 24 hours observed at pH 9 under same growth conditions (Figure 5.7). At high salinity conditions, the longer the lag-phase lasts the bigger the chance for an organism to produce the required osmoprotectants to adapt to high salinity conditions (da Costa, *et al.*, 1998).

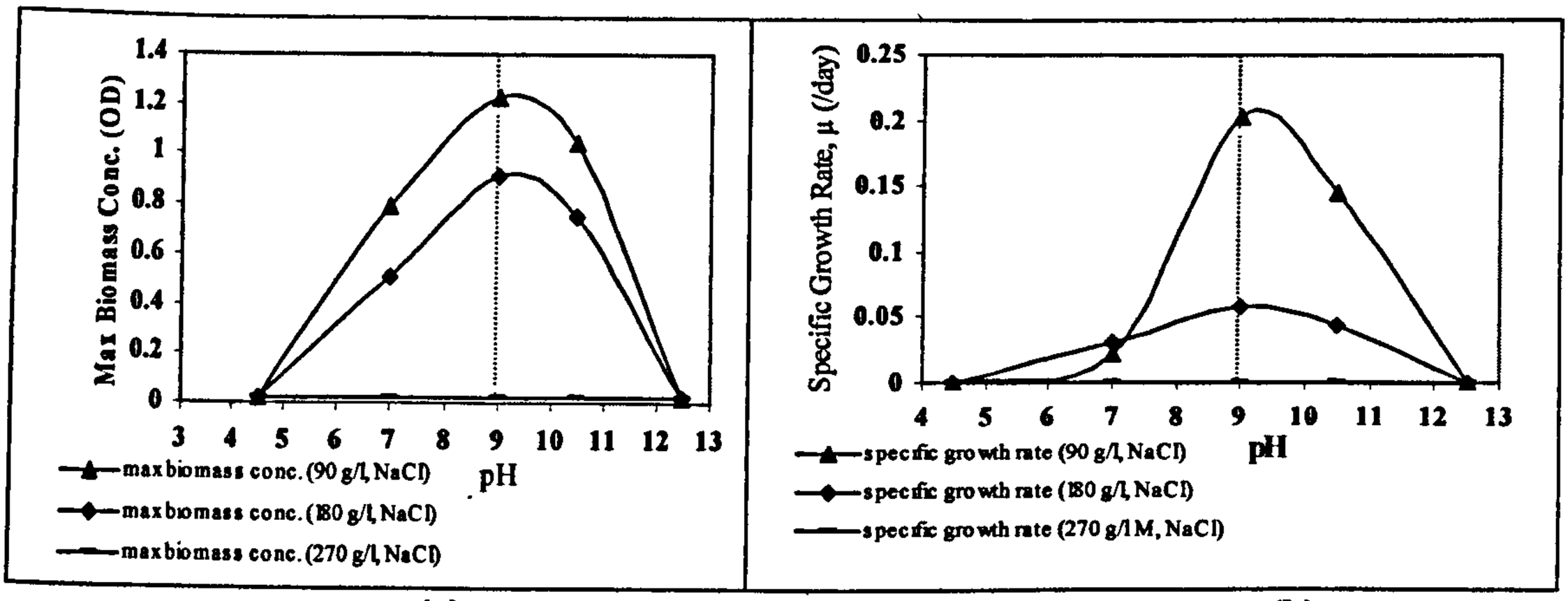

(a) **(b)**

Figure 5.9: Summary of growth profiles for the *Halomonas pantelleriensis* strain BAA003 grown in Complex medium at 37°C: (a) Maximum biomass yield, and (b) Specific growth rate.

5.3.4 Effect of Temperature

Temperature ranges were determined by following growth at optimal salinity and pH values (i.e. 90 g/l NaCl and pH 9, respectively) (Figure 5.10). Temperatures tested were 4, 25, 30, 37, and 45°C, in all cases the cells were pre-adapted to the particular temperature before growth curves were measured. No growth was observed at 4°C, suboptimal growth occurred at 25 and 30°C, and the optimum

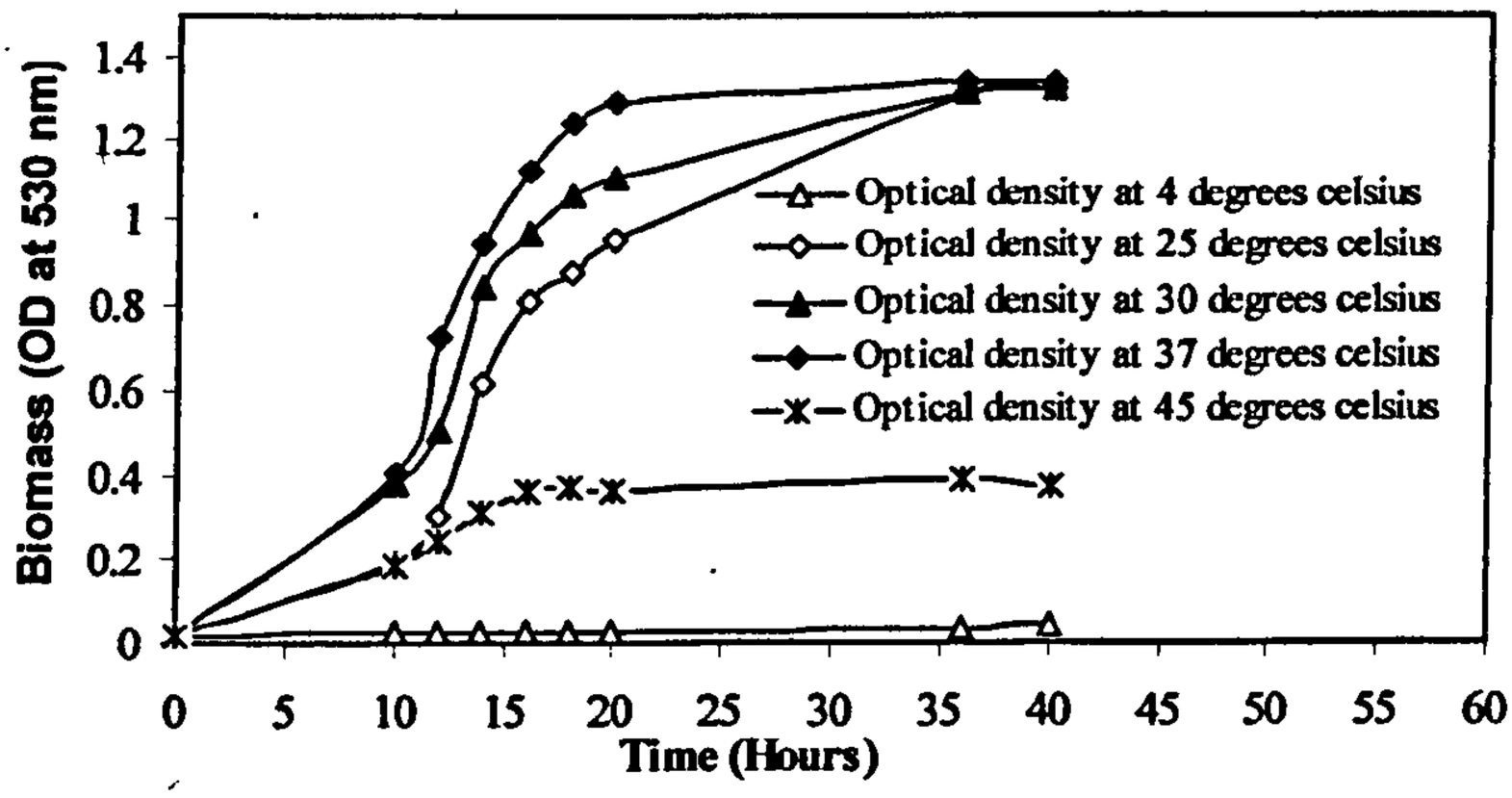

Figure 5.10: Summary of growth profiles for the *Halomonas pantelleriensis* strain BAA003 grown in Complex medium at various temperatures.

growth was observed at 37°C. Except for cultures incubated at 45°C, all grown cultures incubated at different temperatures ultimately ended with similar biomass concentrations during mid stationary-phase growth period. Though very minimal growth occurred at 45°C, the maximal temperature for growth has not been determined, which is expected to be below 50°C for this group of organisms (Ollivier, *et al.,* 1994). Figure 5.11 sows the specific growth rates of this bacterium calculated at the exponential phase of each temperature.

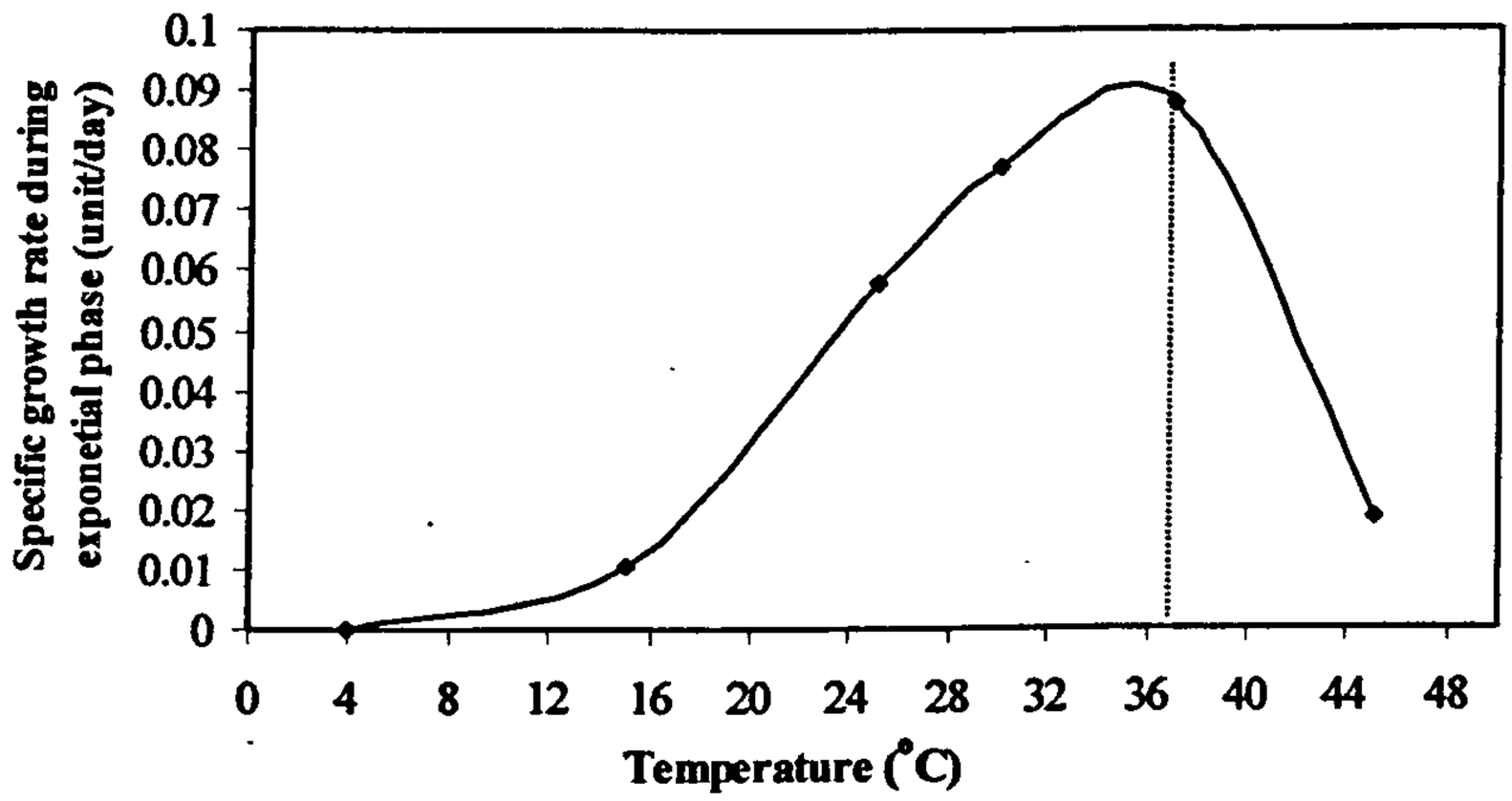

Figure 5.11: Specific growth rates for *Halomonas pantelleriensis* strain BAA003 during exponential phase at various temperatures.

Because of its ability to grow at 45°C, *H. pantelleriensis* strain BAA003 may be regarded as moderately thermophilic. This is a physiological capacity of adaptive value for halophilic organisms since sunlit hypersaline environments (e.g. Qabar-Onn Lake) may easily reach elevated temperatures (Garcia-Pichel, *et al.,* 1998).

5.3.5 Carbon Substrate Utilisation

The ability of the *Halomonas pantelleriensis* strain BAA003 to utilise 31 different carbon substrates was determined by observing growth in Biolog® ECO-Plate cultures where the substrates were supplied as the sole carbon and energy source. The different substrates included: 10 carbohydrates, 6 amino acids, 7 carboxylic acids, 4 polymers, 2 amines and 2 phenolic compounds. Of the 31 carbon

substrates analysed, 7 substrates allowed appreciable growth of the *Halomonas* species throughout the experimental period.

Figure 5.12 summarises the cumulative growth profiles, measured as optical density at 630 nm, of 7 substrates highly utilised by the *Halomonas* species over a period of 21 days. These substrates include: 2 polymers (tween 40 & tween 80), 2 amino acids (L-phenylalanine & L-threonine), a carbohydrate (N-acetyl-D-glucosamine) a carboxylic acid (α-ketobutyric acid), and a phenolic compound (4- hydroxybenzoic acid). Among these substrates, N-acetyl-D-glucosamine (carbohydrate) being the most utilised (100%) followed by 4- hydroxybenzoic acid (74%), tween 40 (58%), tween 80 (50%), L-threonine (36%), α-ketobutyric acid (29%), and finally L-phenylalanine (24%) as indicated in Figure 5.11. Results of the segregated substrate utilisation are presented in Figure 5.13. Based on the daily substrate utilisation, tween 40 was the fastest substrate utilised during the first week followed by 4-hydroxybenzoic acid and tween 80 during the second week. Although N-acetyl-D-glucosamine was utilised moderately during the first week, its utilisation bloomed from day 7 onwards and become one of the substrates most highly utilised during the following two weeks.

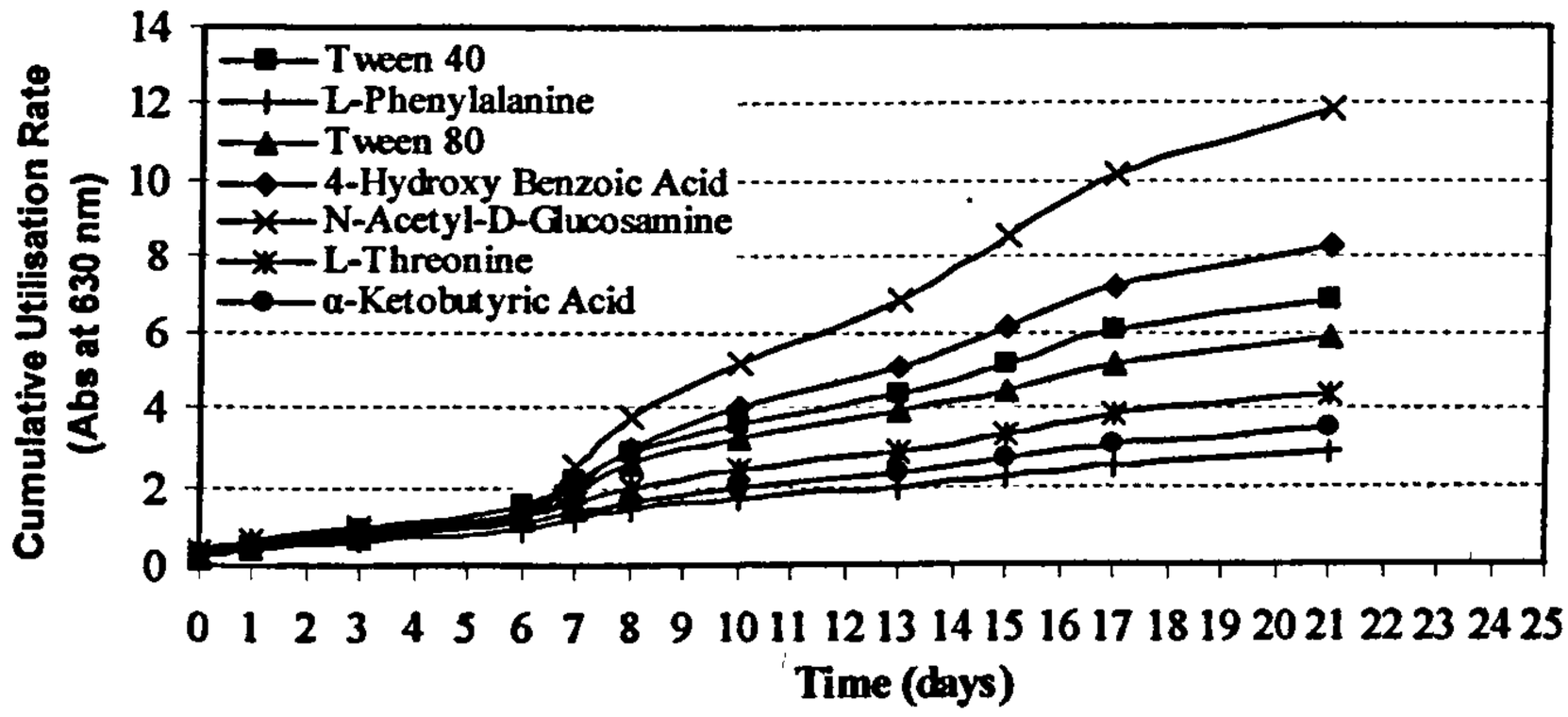

Figure 5.12: Cumulative utilisation rate of various carbon substrates for the *Halomonas pantelleriensis* strain BAA003 grown in Complex medium.

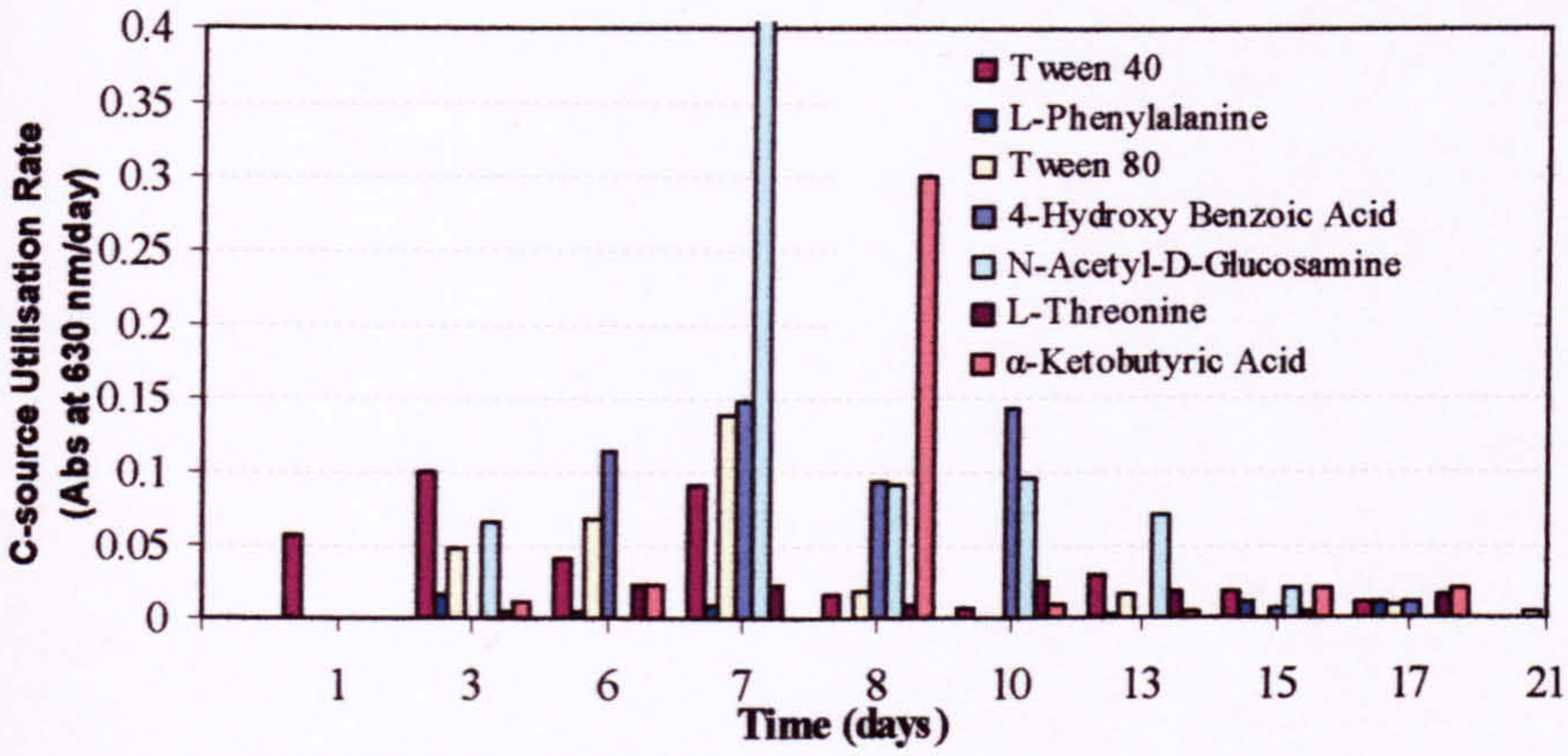

Figure 5.13: Utilisation rate of various carbon substrates for the *Halomonas pantelleriensis* strain BAA003 grown in Complex medium.

Unlike N-acetyl-D-glucosamine, α-ketobutyric acid was utilised very slightly throughout the test period except on the day 8 in which it was utilised very highly, (13 fold higher) compared to its utilisation average during the test period.

In their study, Valderrama, *et al.* (1991) examined 26 strains of *Halomonas salina* using dozens of substrates. Their results showed that patterns of carbon substrate utilisation among the tested strains were similar in extensive utilisation of carboxylic acids and alcohols but there were different in the utilisation of carbohydrates and amino acids. D-Fractose, acetate, citrate, fumarate, D-gluconate, DL-malate, pyruvate, D-mannitol, D-sorbitol, L-aspartic acid, L-glutamic acid, L-leucine, and L-serine were utilised by at least 80% or more of the studied strains as sole sources of carbon and energy. However, the following compounds were not utilised by at least 80% of the studied strains: esculin, D-salicin, benzoate, caprylate, oxalate, L-histidine, and tryptophan.

5.3.6 Amino Acids Assay

Figure 5.14 shows the amino acid concentration measured in cell-free extracts of the *H. pantelleriensis* strain BAA003 grown at various salinity gradients (30, 60, 90, and 120 g l^{-1} NaCl). The results showed that the maximum concentration was obtained in cells grown at 1M salinity; however, further increases in NaCl

concentration (90 g l^{-1} and 120 g l^{-1}) led to sharp drops in amino acid concentration. These results contrast with previous observations by Sossi *et al.* (1998) and Gordon *et al.* (1997) which indicated the accumulation of amino acids was observed as a direct effect of salt increase. These discrepancies may be due to differences between not only species but also because a range of salts were used by Sossi *et al* (1998) and here only NaCl was used (Drevon, *et al.*, 2001).

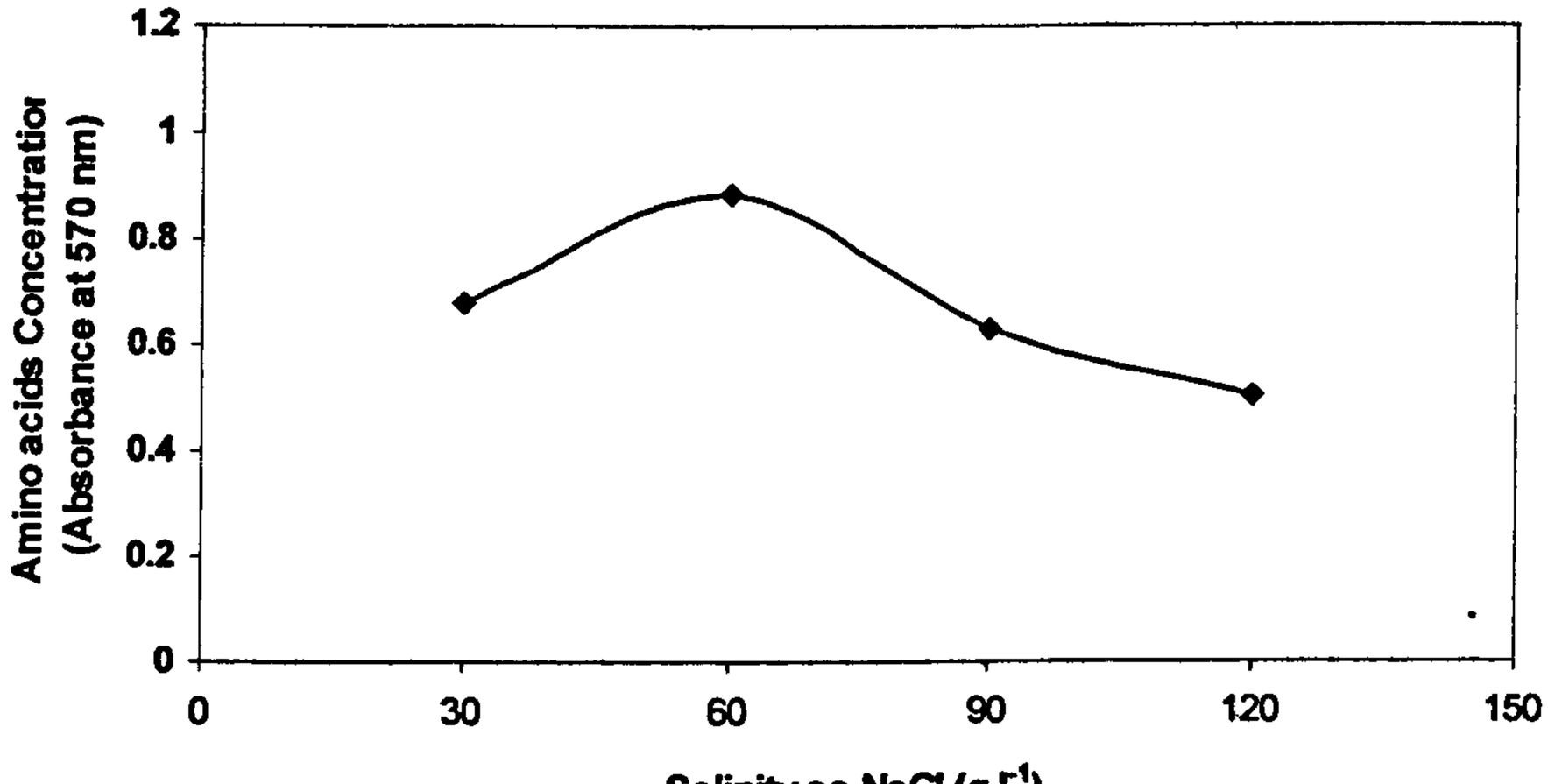

Figure 5.14: Amino acids concentrations of cell-free extract from *H. pantelleriensis* strain BAA003.

5.3.7 Enzyme Activity Determination

The effect of salinity (as NaCl) on malate dehydrogenase activity in the isolated *H. pantelleriensis* strain BAA003 was determined at various NaCl concentrations by monitoring NADH oxidation in cell-free extract (Figure 5.15). The results indicate that malate dehydrogenase extracted from cells grown in optimal NaCl concentration (60 g l^{-1} NaCl) has a higher specific activity than that found in cell-free extracts from cells grown in 30 or 120 g l^{-1} NaCl. However in all cases, increasing NaCl concentration in the assay decreased the specific activity.

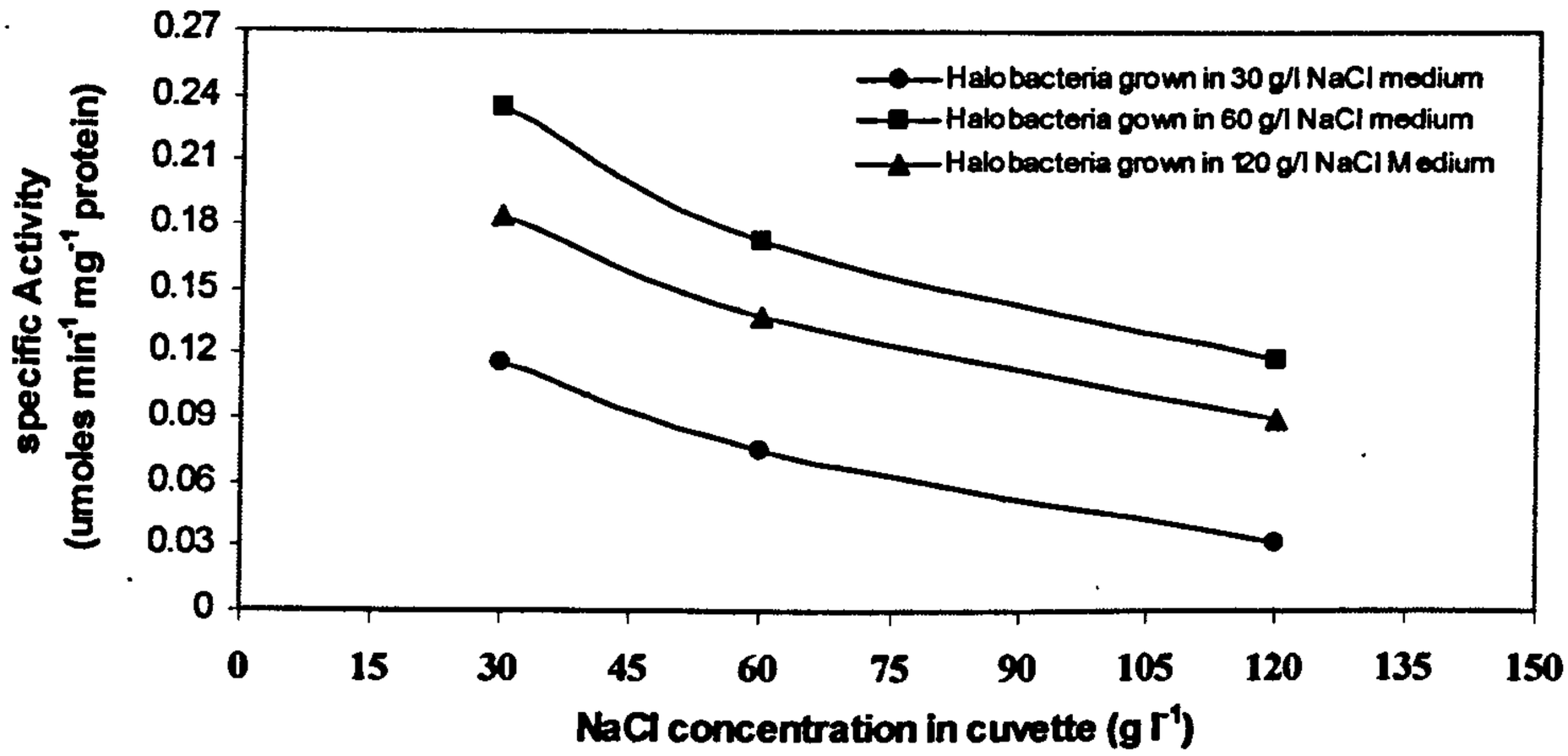

Figure 5.15: Specific activity of malate dehydrogenase in *H. pantelleriensis* strain BAA003 grown in varying NaCl concentrations.

The hMDH activity is highly dependent on the salt concentration and it was observed that the specific activity increased from 0.116 μmole.min^{-1} (mg protein)$^{-1}$ to 0.235 μmole.min^{-1} (mg protein)$^{-1}$ when NaCl concentration was increased from 30 g l^{-1} to 60 g l^{-1} in the medium. However, doubling salt concentration in the medium caused the specific activity to decrease by approximately 20% [e.g. from 0.235 to 0.185 μmole.min^{-1} (mg protein)$^{-1}$].

5.3.8 Compatible Solutes Analyses

Figure 5.16 reports NMR ^{1}H spectra of cell extracts from the *H. pantelleriensis* strain BAA003 cells grown at 30, 60, 90 and 120 g l^{-1} NaCl. Cells were grown in Complex medium in which peptone was used as the carbon source. The H^{1} spectra identified glycine betaine, ectoine, hydroxyectoine and β-glutamate as the most abundant compatible solutes. Confirmation of the identity of these solutes was shown by ^{13}C-H^{1} HSQC spectrum and TOSCY spectrum by identification of the spin systems for cell extracts from cultures grown in Complex media with 30 g l^{-1}, and 120 g l^{-1} NaCl salinities (Figures 5.17 and 5.18). In general, the methyl signals of glycine betaine (GB) were clearly visible at 3.40 and 3.85 ppm at all conditions, as the main compatible solute for the *H. pantelleriensis* strain BAA003. Ectoine (EC) signals appeared at 2.10, and 2.28 ppm which originated

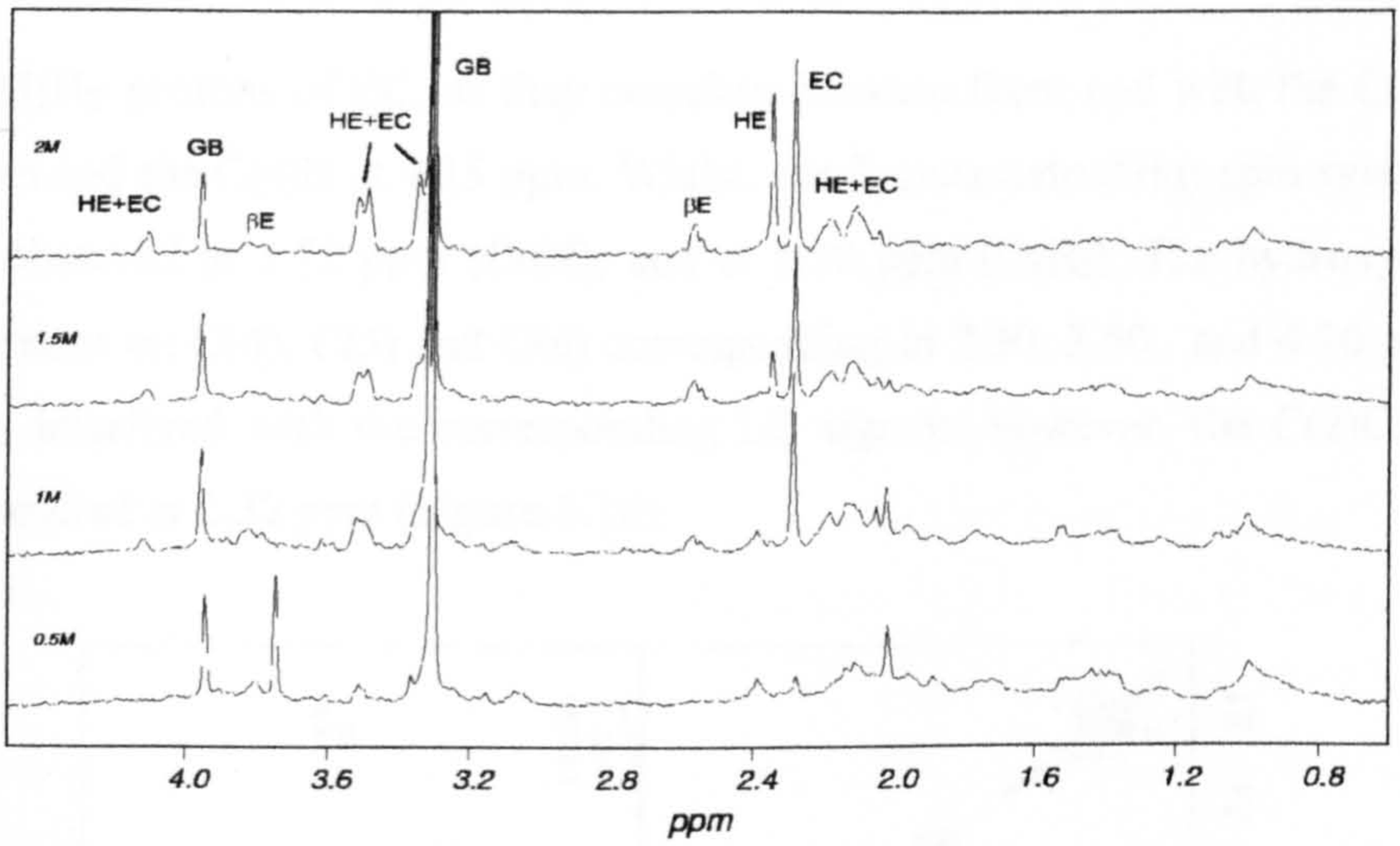

Figure 5.16: One-dimensional 500 MHz ^{1}H spectra of cell extracts from the *H. pantelleriensis* strain BAA003 cells grown at 0.5, 1, 1.5 and 2M salt. [The peaks are labelled with the compounds that give rise to the peaks. Each compound produces more than one peak, because each proton gives rise to a different signal. The peak labels are: GB, glycine betaine; EC, ectoine; HE, hydroxyectoine; βE, β-glutamate. Most of the other unlabelled peaks are presumed to be normal cellular metabolites].

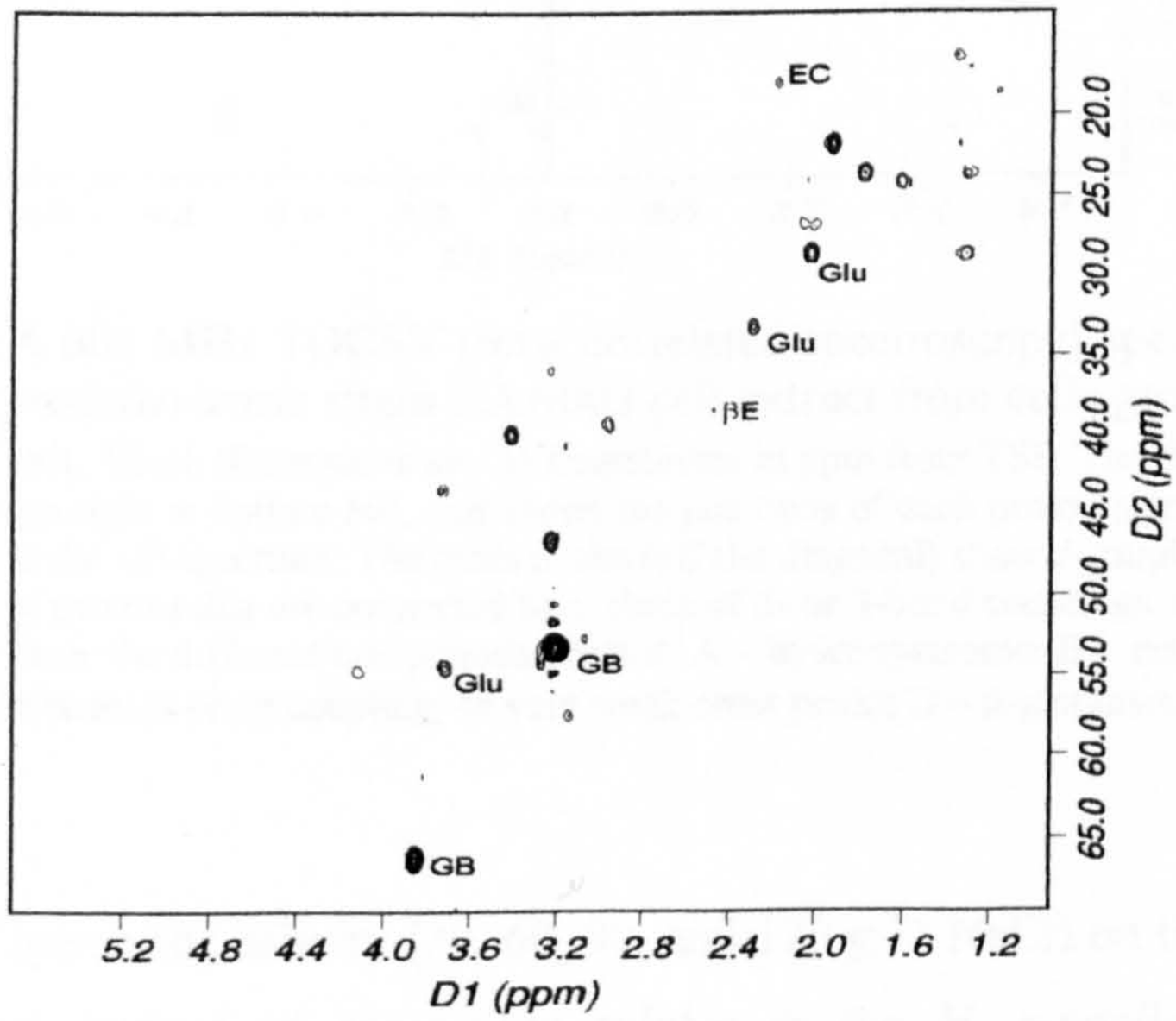

Figure 5.17: A 500 MHz ^{13}C-^{1}H HSQC spectrum of cell extract from the *H. pantelleriensis* strain BAA003 cells grown at 30 g l^{-1} salt. [The two dimensions are labelled with the chemical shift in ppm from TSP. Assignments are marked on the spectrum: GB, glycine betaine; EC, ectoine; βE, β-glutamate; Glu, glutamate. The small peaks above and below the large GB peak are artifacts due to the strong intensity of this peak. Other peaks are presumed to be normal background cellular constituents.]

from C(5)H_2 protons of EC, as they correlate between them and with the C(4)H_2 at 3.32 ppm and the C(6)H at 4.15 ppm. Whilst, the β-glutamate (Glu) spin system was clearly observed at 3.72 ppm (CαH), and at 2.50 ppm (CγH_2). The hydroxyectoine (HE) protons on C(4), C(5) and C(6) corresponding to 2.30, 3.50, and 4.20 ppm are partially interfered with the corresponding EC signals, however, the C(2)CH_3 was well identified at 2.32 ppm (Figure 5.16).

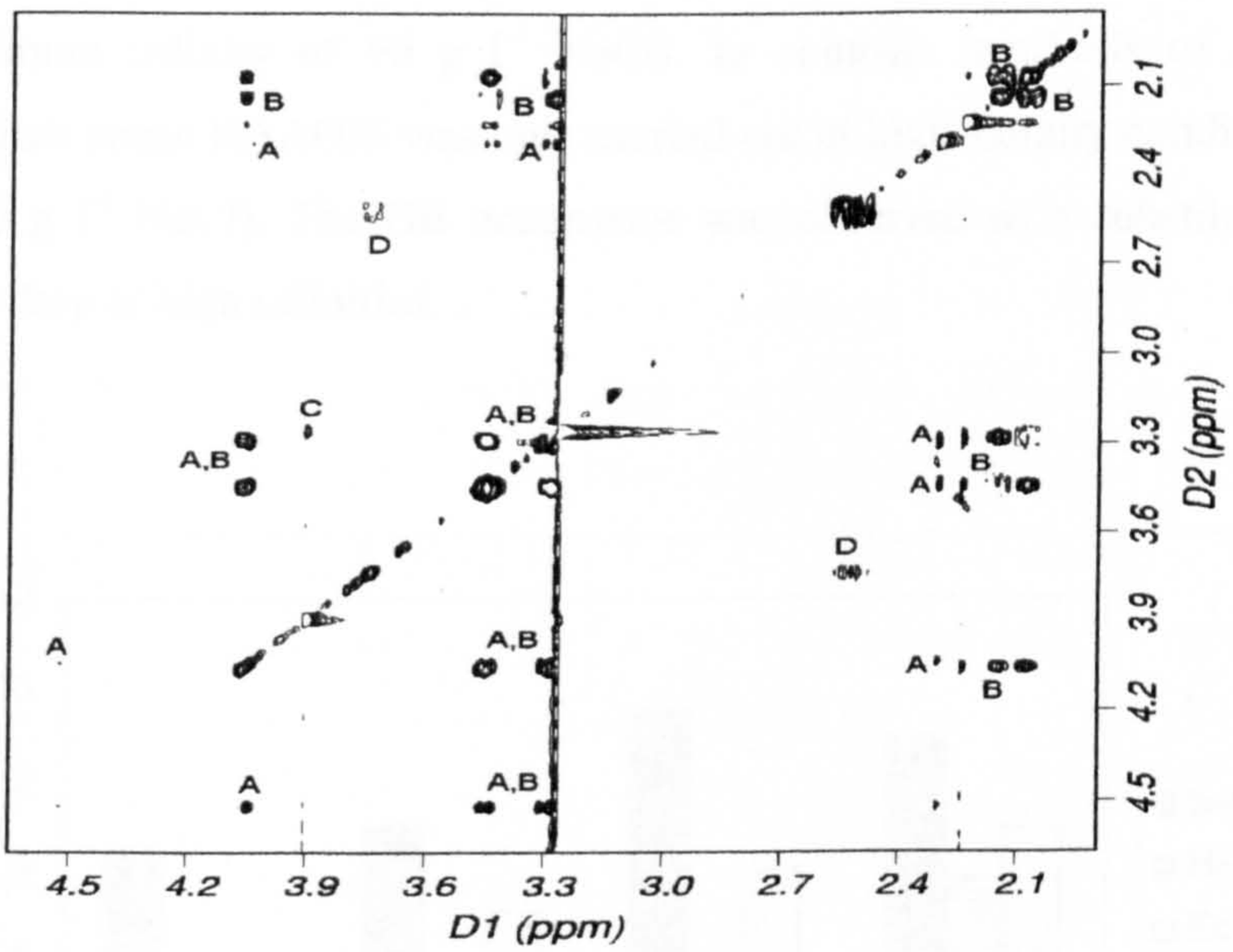

Figure 5.18: A 600 MHz TOCSY (total correlated spectroscopy) spectrum of the *H. pantelleriensis* strain BAA003 cell extract from cells grown at 120 g l^{-1} salt. [Both dimensions are ^{1}H frequencies in ppm from TSP. The diagonal runs from top right to bottom left, and shows the positions of each proton signal, corresponding to the 1D spectrum. The cross peaks (off the diagonal) show *J*-coupling between pairs of protons that are connected by a chain of 2- or 3-bond couplings, and are marked to show the different compounds present: A – hydroxyectoine; B – ectoine; C – glycine betaine (4-bond coupling, so very weak cross peak); D – β-glutamate].

The effect of increasing salinity (30, 60, 90, and 120 g l^{-1} NaCl) on the quantitative and qualitative content of compatible solutes in the *H. pantelleriensis*. strain BAA003 was investigated. Figure 5.19 shows relative concentrations of the analysed compatible solutes determined in BAA003 grown under various salinitie. The obtained results basically showed that three main osmolytes contribute as

osmoprotectants for this organism, namely: glycine-betaine (GB), ectoine (EC), and hydroxyectoine (HE). The highest concentration was obtained for GB under all growth conditions tested, and its relative concentration increased with a salinity increase from 30 g l^{-1} NaCl to 90 g l^{-1} NaCl (the optimum salinity for strain BAA003). However, the concentration of GB slightly dropped with a further salinity increase to 120 g l^{-1} NaCl. The level of EC in strain BAA003 cells increased highly along with salinity increase, from almost undetectable amounts at 30 g l^{-1} NaCl. Interestingly, its concentration steadily increased even at extreme salinities (i.e. above optimum salinity of 90 g l^{-1} NaCl). In contrast, synthesis of HE by *H. pantelleriensis* strain BAA003 was only carried out at high salinity conditions (90 g l^{-1} and 120 g l^{-1} NaCl). The HE occurrence was observed as a substitute for GB production drop at high salinities.

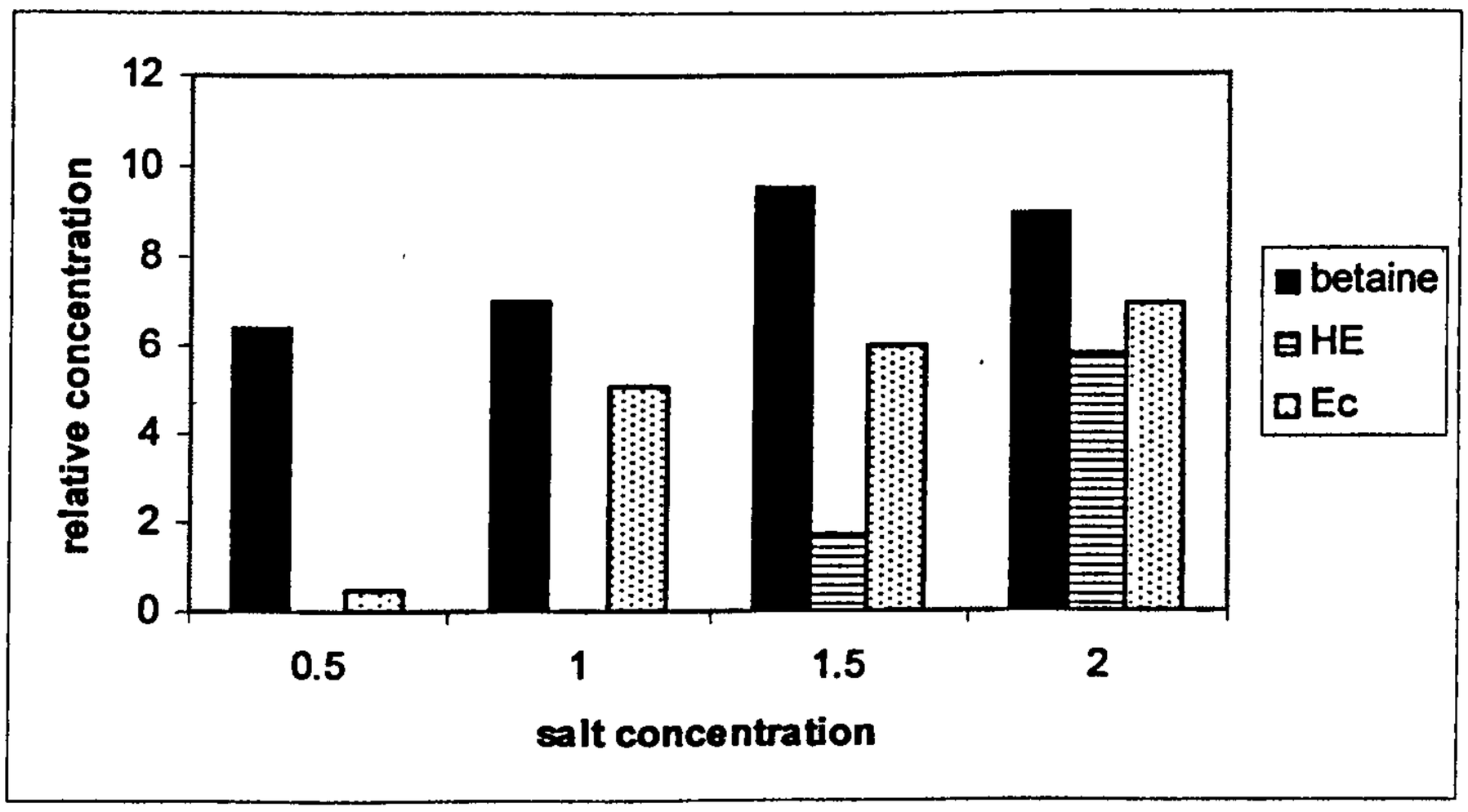

Figure 5.19: Comparative concentrations of the osmoprotectants extracted from cell extracts of the *H. pantelleriensis* strain BAA003 cells grown at various salinities.

The reason behind this scenario might be anticipated to one of two reasons: either that the *H. pantelleriensis* strain BAA003 is only able to synthesise GB at low or optimum conditions and the HE was produced as a substitution of this deficit, or this

organism is only able to produce HE at higher salinities and the GB level drop was as a response of HE accumulation.

The ethanolic extracts of strain BAA003 grown in Complex medium under optimum conditions showed the presence of GB as the major component, with EC and HE, while Glu occurred only in minute amounts. However, Motta, *et al.* (2004) reported the presence of GB as the major component, and EC and Glu, but not HE in *H. pantelleriensis* strain AAP (the closest relative to *H. pantelleriensis* strain BAA003).

NMR analyses of compatible solutes indicated that accumulation of GB and EC is important for osmotic adaptation of *H. pantelleriensis* strain BAA003 isolated from a hypersaline environment (Qabar-Onn Lake) under optimum salinity conditions. However, in higher salinities, this organism equally depends on HE as an osmoprotectant. A clear difference was observed between responses of EC and HE levels increase in *H. pantelleriensis* strain BAA003 cells to salinity increase from optimal level (e.g. 90 g l^{-1} NaCl) to 120 g l^{-1} NaCl, (Figure 5.19). The latter, but not the former solute, showed a good correlation with the growth rate (e.g. EC increased by 15% and HE by 70%). Thus, it can be concluded that HE levels in the cells play a very big role for osmoadaptation of this species at high salinities.

5.4 Summary

This study has specifically addressed halobacterial investigations based on the conventional morphological, physiological, biochemical and chemical examinations plus using 16S rRNA gene sequence analysis approach. The morphological and physiological characteristics of the newly isolated bacterium (BAA003) is similar to those of *Halomonas pantelleriensis*, isolated from a Hard sand, Pantelleria, Italy (Romano *et al.*, 1996). Hence, it is suggested that strain BAA003 is affiliated with the *Halomonas* genus and tentatively represents a novel strain in the species *pantelleriensis*. However, further studies should clarify the phenotypic and genotypic characteristics of the new isolate and may possibly lead to an updated nomenclature.

Halomonas pantelleriensis strain BAA003 does not appear to be ideally suited to life in Qabar-Onn Lake in that their viable count is very low; however, this isolate represents the dominant culturable halotolerant bacterium in this lake. *H. pantelleriensis* strain BAA003 was the predominant organism in the enrichment and was the only colony forming organism at the highest dilutions. Strain BAA003 is a Gram-negative, straight rod, aerobic and motile. The isolate grew in Complex medium containing 5 g l^{-1} to 200 g l^{-1} NaCl with an optimum salinity of 90 g l^{-1} NaCl. The temperature range for the growth of this isolate was from 10-45°C, with an optimum temperature of 37°C. The optimal pH for growth was 9.0; growth was observed at pH 7.0 and 10.5 but not at pH 4.5 or pH 12.5.

Strain BAA003 hydrolysed glucosamine, benzoic acid, 4- hydroxybenzoic acid, N-acetyl-D-glucosamine, tween 40, and tween 80; but not amino acids or putrescine. Moreover, the malate dehydrogenase activity experiments clearly show that the enzyme activity decreases dramatically with increasing salinity i.e. the enzyme is not halophilic and suggests a role for osmolytes in BAA003.

Osmolytes were identified and quantified by NMR. Strain BAA003 mainly utilized glycine betaine (55%), ectoine (35%), and glutamate at very low concentrations (<1%). However, at higher salinities this isolate accumulates hydroxyecotoine (10%).

In conclusion, Qabar-Onn Lake seems to have a rich bacterial diversity. However, the microbiological screening performed in this study was totally based on culture-based methods, which do not allow a reliable measure of microbial diversity due to numerous limitations (Benlloch *et al.*, 1996, 2002). These approaches lead to an underestimation of the actual bacterial diversity of this lake. Molecular techniques have been developed to more rapidly and accurately assess not only the microbial diversity but also the community structure of an ecosystem (Garcia-Pichel *et al.*, 2001; Meyers, 2000). Hence, the halobacterial diversity of this unique and unexplored hypersaline habitat would be better investigated if more molecular techniques are involved and wider samplings of the lake components are taken.

Chapter 6

ASSESSMENT OF BACTERIAL ADHESION TO REVERSE OSMOSIS MEMBRANES

6.1 Introduction

Microbiological fouling (biofouling) of reverse osmosis (RO) membranes is considered to be the main factor for a decline in flux and loss of salt rejection (Schneider *et al.*, 2005; Schneider *et al.*, 1994; Speth *et al.*, 2000). In general, bacterial fouling of a surface can be divided into three phases: transport of the organisms to the surface, attachment to the substratum, and growth at the surface. Attachment of bacteria to membranes initiates the formation of biological fouling layers, the biofilms (Korber *et al.*, 1995). Understanding the mechanisms of bacterial attachment may, therefore, assist in the development of novel antifouling technologies for membrane systems (Ridgway and Safarik, 1991; Knoell *et al.*, 1999).

Numerous factors have been reported to influence initial bacterial attachment to surfaces, including the type of micro-organism (Shams El-Din *et al.*, 2003); the concentration of cells in the suspension (Berrin *et al.*, 2006); the stage in the growth cycle of the bacterium (Mata *et al.*, 2006); the amount and types of nutrients provided to the cells (Shams El-Din *et al.*, 2003; Allison *et al.*, 1998), particularly nutrient starvation (Allison *et al.*, 1998); cell surface charge (Amanatides *et al.*, 2006; Zhao *et al.*, 2004; Busscher *et al.*, 1990) and hydrophobicity (Bejarano *et al.*, 2004); the presence of a glycocalyx (a coating of excreted polymers, the so-called extracellular polymeric substances, or EPS) (Mata *et al.*, 2006; Allison *et al.*, 1998; Bachmann and Edyvean, 2006; Berrin *et al.*, 2006;); pH (Shams El-Din *et al.*, 2003); temperature (Shams El-Din *et al.*, 2003; Bachmann and Edyvean, 2006); electrolyte concentration (Schneider *et al.*, 2005; Chen *et al.*, 2004); and presence of dissolved organic substances (Mata *et al.*, 2006; Bos *et al,* 1999; Sadr-Ghayeni *et al.*, 1998).

The nanoporous morphology of membranes provides suitable characteristics for molecular deposition, which eventually leads to bacterial attachment (Boussu *et al.*, 2006; Bejarano *et al.*, 2004; Johnson *et al.*, 1994). The biofouling process initially starts with the deposition of substrates such as extracellular polymeric substances (EPS), which form a highly hydrated nanogel layer on the membrane surface. EPS are large molecular weight compounds that are excreted by bacteria (Arias, *et al.*, 2003; Korber *et al.*, 1995; Ridgway and Safarik, 1991), and play a significant role in bacterial adhesion onto solid surfaces by altering the physicochemical characteristics such as charge, hydrophobicity, and the polymeric properties (Bowen and Doneva, 2000; Korber *et al.*, 1995; Amanatides *et al.* 2006). The roughness characteristics of the membrane surface can change the surface forces by orders of magnitude (Tansel *et al.*, 2006). The compatibility of the molecular dimensions of EPS and the membrane roughness define the distribution of asperities at points of contact and the adhesion strength. Recent studies (Tansel *et al.*, 2006; Zhao *et al.*, 2004) show that there exists an optimal shape of the contact surface and an object which result in optimal adhesion to a substrate via molecular interaction. However, the contact angle limitation can be overcome by size reduction, and as the size becomes smaller the shape becomes less important for attachment (Hilbert *et al.*, 2003).

The salinity of the bulk solution is one of the prime factors affecting the survival and flourishing of organisms living in it (Shams El-Din *et al.*, 2003). While higher species can, to some extent, tolerate changes in the salt content of the water, microorganisms suffer greatly (Ridgway and Safarik, 1991). Since increasing salinity affects the growth and metabolic activity of a bacterial species, therefore, salinity changes affect the biofilm formation and detachment (Martínez-Cánovas *et al.*, 2004).

In this chapter, a study was carried out to investigate and compare the surface adhesiveness of the ADF membranes (used widely in the RO desalination systems and having a comparatively high surface roughness) with a range of materials of various surface roughness. The impact of salinity on biofilm formation growth and detachment was also included in the study, in order to ascertain possible differences.

Two different bacteria were tested in this study, *Halomonas pantelleriensis* BAA003 and *Euhalothece* sp. BAA001. These were chosen as that were both isolated from the lake water as described in Chapters 4 and 5.

6.2 Materials and Methods

6.2.1 Halobacterial Adhesion Assay

6.2.1.1 Biological Assay Materials

The halobacterial species *H. pantelleriensis* (strain BAA003), which was isolated from Qabar-Onn Lake, was used in this experiment. The halobacterium was grown on Complex medium (as described in Chapter 3, Section 3.3.1.2) at room temperature (22-24°C). The medium was prepared by dissolving the designated amount of sodium chloride in distilled water to which nutrients, trace elements, and vitamins were added (Rosenberg, 1984). The medium contains 1 g l^{-1} peptone, 1 g l^{-1} yeast extract, and 26 ml l^{-1} of the lake water was added as a supplementary source of nutrients and trace elements. Solid medium was prepared by dissolving 15% (w/v) of agar in the Complex medium before autoclaving. pH adjustments (pH 9.0) were also performed before autoclaving using 1M NaOH.

6.2.1.2 Preparation and Conditioning the Specimen's Surfaces

Four different materials: ADF (thin film composite) RO membrane, stainless steel (EN1.4307), Perspex glass, and Teflon, were selected for the investigation of the bacterial adhesion in this study. The selection of these materials was based on their preferences in the filtration and desalination applications, as well as the fact that these materials have different surface roughness compared to the ADF membranes.

Square specimens (15 mm length and approximately 1.5 mm thick) of the four test materials were prepared as shown in Figure 6.1. The coupons were kept standing vertically by fixing them on holders made of Perspex. The ADF membrane slips were kept firm in the solution by using PVC studs to hold both edges of the membrane towards the Teflon holders, and then they were fixed on identical Perspex holders. The square specimens were then washed thoroughly and sterilised in an autoclave at 121°C for 15 minutes before being immersed in the bacterial culture.

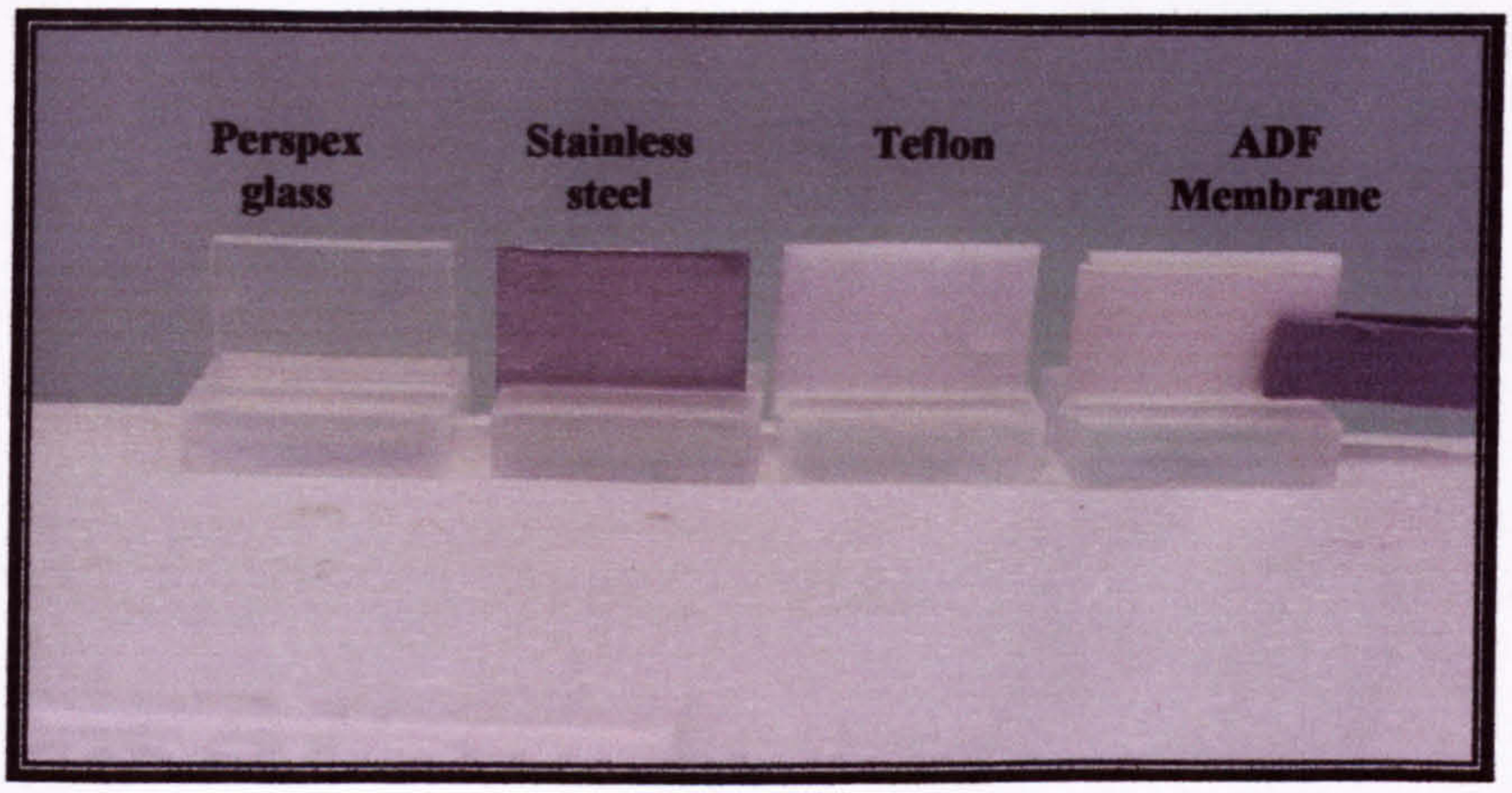

Figure 6.1: A picture of specimens of various substrata examined in the biofilm attachment experiment.

The materials considered ranged across different classes of surface roughness as shown in Figure 6.2. The surface roughness of various substrata, used in this experiment, was obtained from taking the AFM images for each substratum. In inspecting the AFM images, it is noticeable that the scale of the Z axes for the four types of the used materials are quite different (e.g. 200, 600, 1500 and 200 nm/div. for the perspex glass, ADF membrane, Teflon and stainless steel, respectively); a much larger scale Z axes was used for the image of the relatively smooth surfaces because of their marked roughness. The roughness of the tested materials is in the range of a few nanometres to several hundreds of nanometres. The detailed AFM methodology was described earlier in Chapter 3, Section 3.7.

After cleaning the specimens from any finishing dust and/or greases using benzene in an ultrasonic bath (35 kHz, Fisherbrand ultrasonication unit; Fisher, UK) for 30 minutes, they were thoroughly soaked in a 1% (w/v) solution of Virkon powder (VWR International Ltd., UK) overnight. This was followed by sonicating them in the same solution for 30 min and they were rinsed (three times) by vortexing the specimens in 100 ml aliquots of distilled water. The specimens were then autoclaved in the same container used for the experiment. Equally the ADF membrane was washed out from the preservative material as described earlier in Chapter 3, Section 3.1.1.3.1. The membrane sheet was then left overnight to dry at room temperature. Rectangular

membrane slips (32 mm length × 15 mm width) were cut and sterilised with ultra violet (UV) light for 3-5 minutes. Finally, the sterilised membrane slips were fixed onto the Teflon holders and immersed in the bacterial culture.

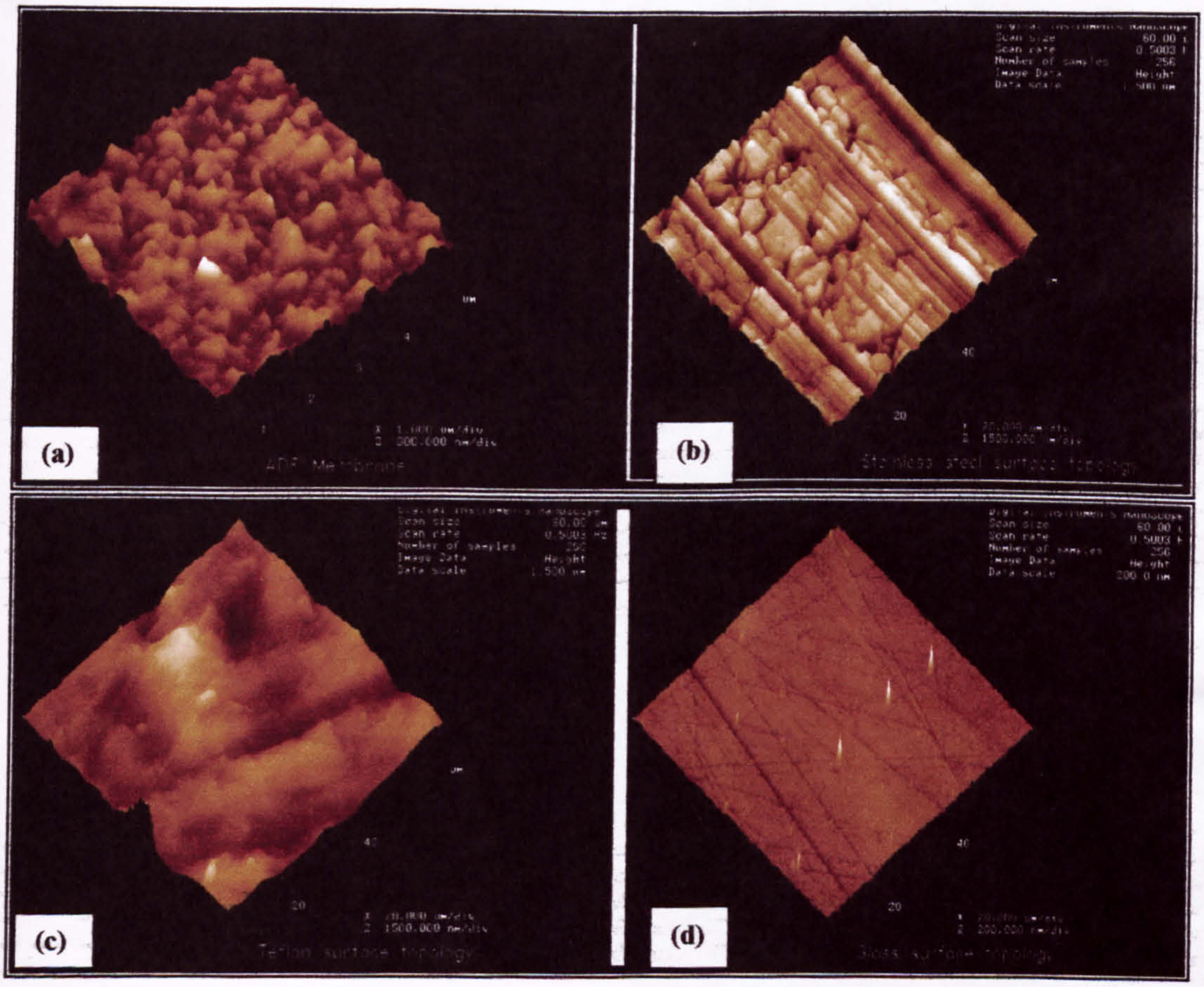

Figure 6.2: Three-dimensional AFM images of various materials topologies: (a) ADF membrane, (b) Stainless steel (EN1.4307), (c) Teflon, and (d) Perspex glass.

6.2.1.3 Halobacterial Adhesion Procedure

A standardised method was used in this experiment (Montanaro, *et.al*, 2004). The prepared specimens of different materials were exposed under sterile and slow shaking conditions (horizontal shaker set at 25 r.p.m) to bacterial suspensions of known concentrations (OD = 1.25). Three 500 ml air-tight and sterile containers were used; which contained media with 30 and 90 g l^{-1} NaCl for low and high salinities, respectively. A set of 6 specimens of each material was placed in each container, and an adequate amount (~ 250 ml) of complex medium was poured under

sterile conditions (inside a laminar-flow cabinet) into each container until the specimens were totally covered with the solution. A third set of specimens were immersed in sterile Complex medium with no added salt (zero salinity), used as a colour control (reference) for visualisation. The experiment was started by introducing 10 ml aliquots of pre-mature bacterial cultures (OD = 1.25) to both experimental sets. The experiment was carried out under sterile conditions at room temperature (23°C - 25°C) with continuous horizontal shaking at slow speed (25 rpm). One set of specimens (one coupon from each material) was removed after specific time intervals (0, 12, 24, 36, 48, 60, and 72 h) and the cells adhered on these specimens were then removed for subsequent quantification. The time of exposure was chosen based on previously determined growth cultures for this bacterium. An extra specimen of each material was reserved for further bacterial visualisation.

6.2.1.4 Quantification of the Adhered Halobacterial Cells

After each designated time of incubation, a set of one specimen of each test material was taken out from each container. The specimens then were washed three times with 5 ml of a sterile 120 g l^{-1} sodium chloride solution, in order to remove non-adherent cells. Each specimen was then placed in a glass tube containing 10 ml of saline solution. The tubes were then placed in an ultrasonic bath cleaner (Fisherbrand® ultrasonication unit; Fisher, United Kingdom) operated at 35 kHz, and sonicated for 10 minutes in order to remove the adhered bacterial cells into suspension. Finally, the specimens were removed and a series of dilutions (100, 1000 and 10000) were made up to 10 ml aliquots. The optical density of the undiluted bacterial suspensions was immediately measured, whilst the bacterial counts (colony forming units, CFU) of the dilution series were performed after 24 h incubation of the tubes at 37°C.

For optical density measurements, the OD was measured at 530nm using a Thermo Spectronic® spectrophotometer (Model Helios Epsilon, UK). The CFU counts were performed by plating triplicate 0.1 ml aliquots of each culture on solid agar Complex media of identical salinities, using a spiral plater (Spiral Biotech. Inc., UK). The

inoculated plates were then sealed with Parafilm tape and incubated at 37°C for 72 h before colony counting.

6.2.1.5 Visualisation of the Halobacterial Biofilm

Coupons of various materials were stained using the (LIVE/DEAD *Bac*Light Bacterial Viability Kit L7007, Molecular Probes Europe BV, The Netherlands) (Biggerstaff *et al.*, 2006). The staining procedure was performed as stated in the staining protocol described in Appendix B. 3 µl of the dye mixture was directly applied to the coupons with attached bacterial cells and incubated in a dark place at room temperature for 15 minutes. The coupons were then covered with cover slips, and observed with an epifluorescence microscope Model Leitz DIALUX 22EB, equipped with UV gun Ernst Leitz Wetzlar GMBH (type 307-143.004 514662, 100 W, Germany) , using an oil immersion lens, giving a total magnification of ×1000. At least 5 fields of view were counted on each coupon. Bacteria with intact cell membranes fluorescing green were counted with the intention of enumerating viable bacteria, whereas cells with damaged membranes stained fluorescent red and were counted as dead cells.

6.2.2 Cyanobacterial Adhesion Assay

6.2.2.1 Biological Assay Materials

The cyanobacterial species *Euhalothece sp.* (strain BAA001), which was isolated from Qabar-Onn Lake, was used in this experiment. The bacterial growth conditions were performed as described in Chapter 4, Sections 4.2.2 – 4.2.4. Initially, starter cultures of cyanobacteria were prepared by inoculating 15% (v/v) of established cyanobacterial cultures (i.e. *Chl-a* = 1.4 µg ml^{-1}) in two 1000 ml aliquots of pre-sterilised BG11 medium. The salinities of the prepared cultures were then adjusted to 30 g l^{-1} and 60 g l^{-1} (as NaCl), and the pH was adjusted to pH 7.0 and buffered by the addition of 50 mM MOPS biological buffer (Sigma, UK). The prepared cultures were left to acclimate to the new medium for one week before being introduced into the rotating annular biofilm reactors (RAB), which was described earlier in Chapter 3, Section 3.1.2.2.

6.2.2.2 Preparation and Conditioning of Specimen's Surfaces

Similar to the halobacterial adhesion experiment, four materials (the ADF membranes, stainless steel (EN1.4307), Perspex glass, and Teflon) were selected for the investigation of cyanobacterial adhesion in this experiment. Slides of 150 mm, 15 mm, 1mm in length, width, and thickness, respectively, of the test materials were prepared and used. After cleaning the slides from any finishing dust and/or grease as described in Section 6.2.1.2, the slides were fixed on the inner drum of the rotating annular biofilm (RAB) reactors and sterilised by autoclaving along with the RAB reactors assemblies. Rectangular slips of the ADF membranes (length 150 mm and width 25 mm) were prepared, washed (as described earlier in Chapter 3, Section 3.1.1.3.1), sterilised with UV light for 3-5 minutes and fixed on the inner drum of the pre-autoclaved RAB reactor in a sterile fashion (inside a laminar-flow cabinet).

6.2.2.3 Cyanobacterial Adhesion Procedure

In order to investigate the effect of salinity on the bacterial adhesion, in this experiment one reactor was operated at low salinity (30 g l^{-1}), whilst the other one was operated at a higher salinity (60 g l^{-1}) under identical operational conditions. After mounting the prepared slides on the inner drum of the RAB reactors, the reactors assemblies were autoclaved and were prepared for the experiment initialisation. The prepared cyanobacterial cultures were then poured into the reactors under sterile conditions (i.e. was performed inside a laminar-flow cabinet). The experimental procedure is described in more detail in Chapter 3, Sections 3.1.2.2 and 3.1.2.3.

6.2.2.4 Quantification of the Cyanobacterial Cells

Due to the slow growth and the culturing difficulty of *Euhalothece sp.* (strain BAA001), the quantification of the viable bacteria embedded in the biofilm was assessed based on the amount of soluble protein in the bacterial cells attached to a substratum surface. At the end of the experiment (16 weeks), the slides were removed for biofilm analysis and cyanobacterial cells quantification. The bacterial cells (biofilm) attached to each substratum surface was detached by sonication of the slides of each material for 30 minutes in sealed 25 ml centrifuge tubes, containing 10

ml sterile NaCl solution of identical salinity to that for cultures. The bacterial suspensions were then centrifuged at 13000×g for 15 minutes, and the pellets were washed (three times) with 1 ml aliquots of a washing solution [(50mM Tris (pH 7.4), 100 mM EDTA (pH 8) and 25% Sucrose)] for exopolysaccharide (EPS) removal, in order to facilitate bacterial cell lysis. Afterwards, the pellets were vortexed for 5 minutes and centrifuged at 15000×g. For protein quantification, the pellets were resuspended in 300 µl B-PER® Reagent, in sulphate buffer (Molecular Probes, UK), disrupted for 10 minutes using a (Disruptor Genec®, Scientific Industries, UK) disruptor, and centrifuged at 21000×g at 4°C for 30 minutes. The resulting supernatant in each tube was then used for a protein assay using RC-DC Protein Assay, Bio-Rad (Chapter 3, Section 3.5.4). The detailed analysis procedure is described in the Protocol stated in Appendix-B. The protein results were then expressed as µg protein/ml of bacterial suspension (slide), whilst the comparative adhered biomass results for various surfaces were expressed based on the relative amount of the extracted protein from biomass adhered to each substratum (suspended in 1 ml aliquots) to the amount of protein extracted from 1 ml of bulk solution as calculated in Equation 6.1.

$$\%\left(\frac{Biomass}{slide}\right)=\left[\frac{\mu g\frac{protein}{ml}\,Bacterial\,suspension}{\mu g\frac{protein}{ml}\,Bulk\,solution}\right]\times 100 \text{ ----------►Equation 6.1}$$

6.2.2.5 Visualisation of the Cyanobacterial Biofilm

The slides were directly viewed under a light microscope (Model *ZEISS Discovery V12 SteREO)*, attached to ZEISS Achromat 1.5× FWD 28 mm objective lens with a maximum magnification of ×150, in order to establish the extent of biofilm coverage, determine the presence of any unusual features of the biofilm, and to ensure the minimum variability among the similar slides. Micrographs were directly taken for fresh slides prior to the biofilm detachment process. Care was taken to avoid biofilm scratching and/or contamination during imaging.

6.3 Results and Discussion

6.3.1 Analysis of Surface Roughness

The surface roughness data for the uncolonised surfaces of various substrata used in this experiment are summarised in Table 6.1. The R_a value is the arithmetic mean surface roughness, while R_{ms} value is the geometric mean of the surface roughness. R_{max} is the maximum height of the profile above the mean line, whereas the Z value denotes the maximum peak-to-valley height profile in the assessment line. For surface roughness analysis, the data presented in Table 6.1 were obtained by executing the total image area ($6.4 \times 10^3 \mu m$) of each material shown in Figures 6.2a-6.2d. Therefore, Teflon is the roughest substratum, followed by stainless steel, ADF membrane and Perspex glass.

Table 6.1: AFM surface roughness data of various substrata used in this experiment.

Substratum	R_a (nm)	R_{ms} (nm)	R_{max} (µm)	Z (µm)
ADF membrane	46.45	56.46	0.474	0.47
Stainless steel	128.60	160.78	1.250	1.250
Teflon	185.47	235.53	2.678	2.635
Perspex glass	20.47	23.95	0.369	0.371

6.3.2 The Halobacterial Adhesion Assay

6.3.2.1 Effect of Material Type on Halobacterial Adhesion

The biofilm monitoring results of *H. pantelleriensis* sp. (strain BAA003) colonising surfaces of various materials over time are shown in Figure 6.3. The results show that the adhesion of halobacterial cells, for all the materials tested in this experiment, presented similar patterns. At low salinity (30 g l^{-1}) and room temperature (22 – 24°C), the biofilm growth on all surfaces except for stainless steel, was exponential between 24th and 36th hour of the experiment, followed by a stationary phase between the 36th and 60th hour of the experiment. Whereas, the exponential phase of the biofilm growth accumulated on the stainless steel substratum was delayed relatively compared to other substrata tested (between the 36th and 48th hour). On the other hand, biofilm sloughing (i.e. cells detachment) from various materials was observed after the 60th hour of the experiment, except for the

ADF membranes, which showed a variant pattern. The extent of the biofilm detachment was wide-ranging among various substrata. It was severe, moderate, and slight corresponding to 93%, 47%, and 33%, for stainless steel, perspex glass, and Teflon, respectively.

Interestingly, for the ADF membranes, the biofilm growth was observed to increase sharply by approximately 40% after the 60th hour of the experiment. This phenomenon indicates that the biofilm has not experienced a detachment phase during this experiment for this material (the ADF membrane). This finding would be referred to the "nanoporous" composition of the membrane material, which allows the penetration of nutrients and oxygen though the membrane to support growth of the bacterial cells composing the "mono-layer" directly attached to membrane surface. This finding was also observed by Boussu *et al.*, (2006).

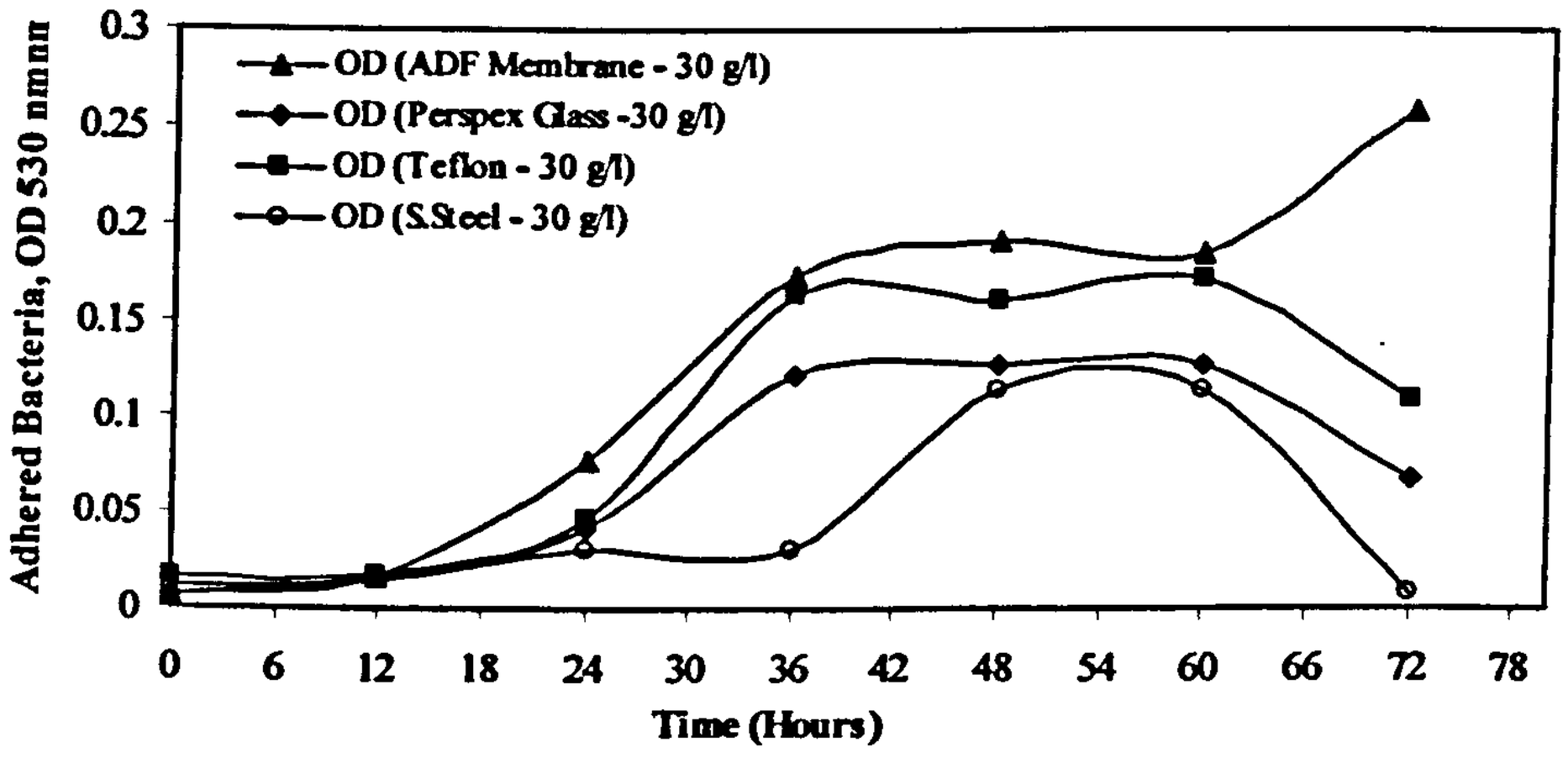

Figure 6.3: Adhered halobacterial concentrations on various substrata at low salinity.

6.3.2.2 Effect of Salinity on Halobacterial Adhesion

The effect of increasing salinity from 30 g l^{-1} to 90 g l^{-1} on the biofilm growth on the surface of various materials surfaces was assessed as a function of time (Figure 6.4). In this experiment, the growth conditions of the halobacterial species (*H. pantelleriensis* sp. strain BAA003) were adjusted to its optimal values

(pH 9.0 and salinity to 90 g l^{-1} NaCl). The effect of salinity on biofilm growth was the same for all substrata.

When the salinity was increased to 90 g l^{-1} the results showed detrimental effects on the biofilm formation and growth, as very small number of cells adhered on the surface of various materials, including the ADF membrane (Figure 6.4).

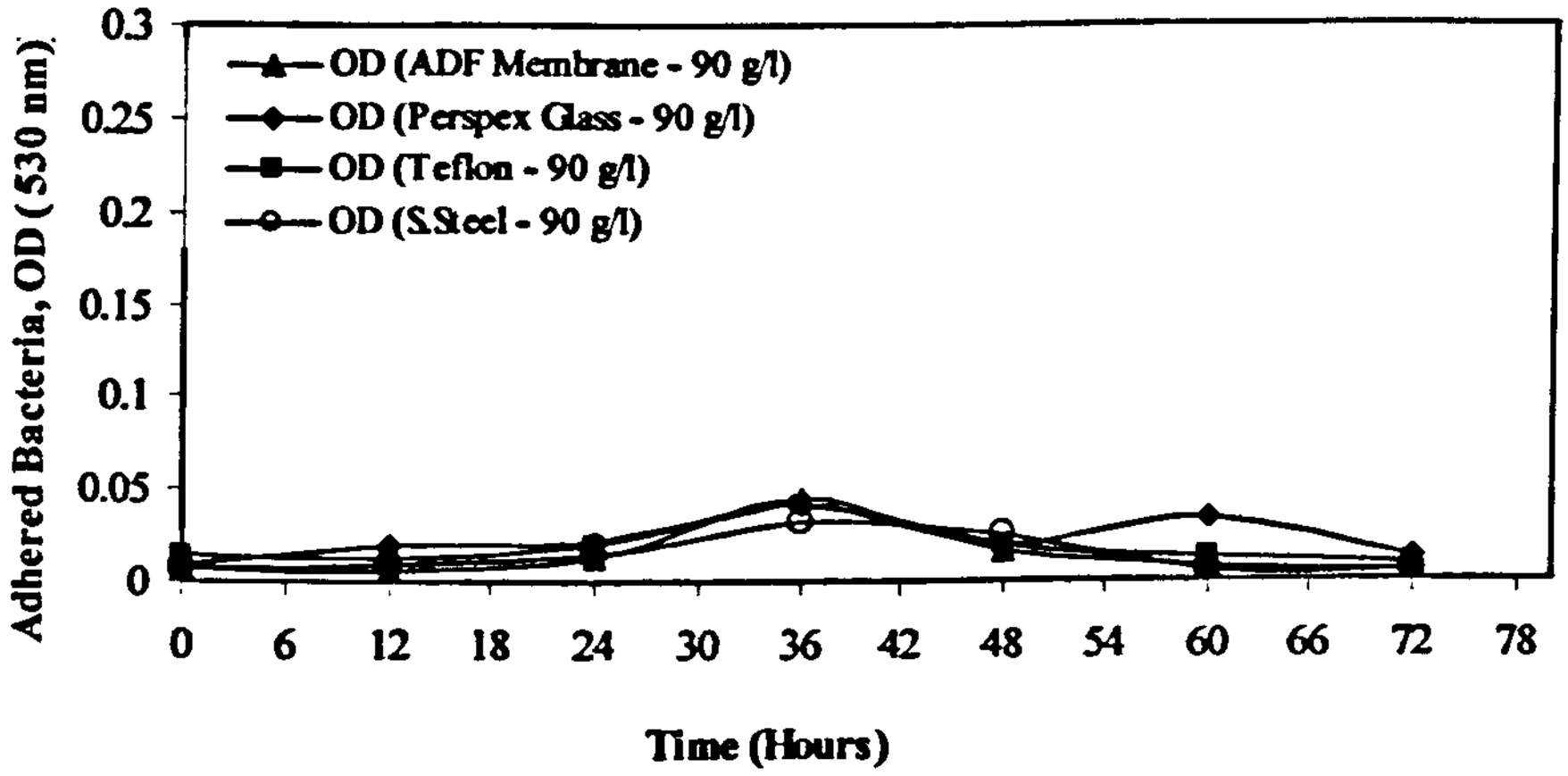

Figure 6.4: Adhered halobacterial concentrations on various substrata at high salinity.

Due to increasing salinity from 30 to 90 g l^{-1} NaCl, counts of *H. pantelleriensis* sp. (strain BAA003) dramatically decreased in the biofilm adhered to various substrata, as seen in Figures 6.5 and 6.6. Overall, the average bacterial count of the adhered bacteria for various substrata was decreased from 2×10^3 cfu to 1.2×10^2 cfu, which represents significant differences due to salinity. Shams El-Din *et al* (2003) also obtained similar results, when they increased the salt concentration of the seawater (feed water) to up to 150%. They concluded that the increase in water salinity retards biofilm formation. Again, the first small salt addition (10%) had the most significant effect when compared to the subsequent salt increments. Also, in parallel with the retardation of biofilm build-up, the final steady-state potential of the filmed metal surface moved towards negative values. As the bacterial count was lower at the high salinity (90 g l^{-1}) compared to the low salinity (30 g l^{-1}), this was reflected on the

microbial activity in this experiment. Hence, the low microbial activity at high salinity could also be another reason for the retardation of the bacterial cells adherence and multiplication (Shams El-Din *et al*, 2003).

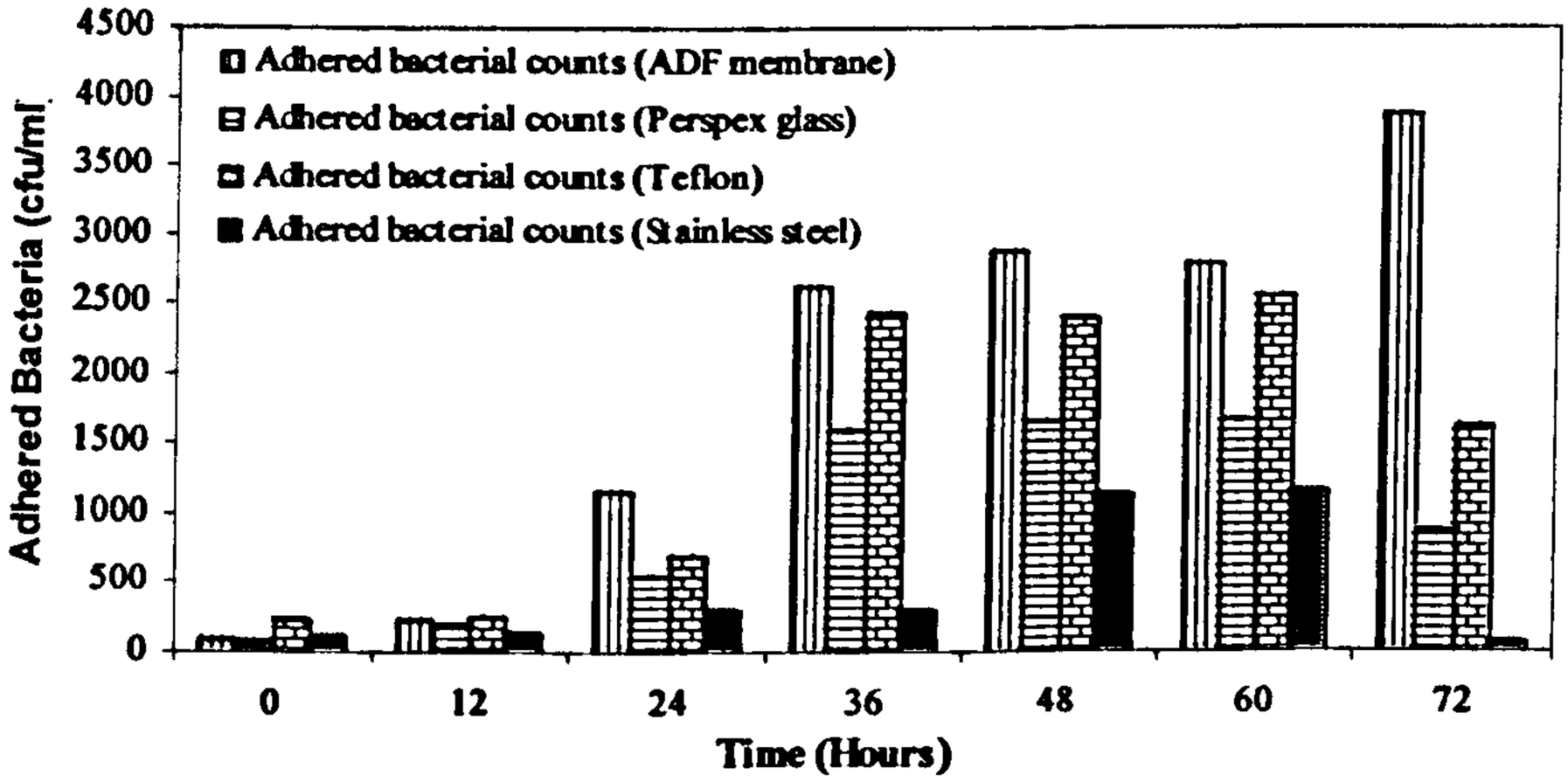

Figure 6.5: Counts of the adhered bacteria on various substrata at low salinity (30 g l^{-1} NaCl).

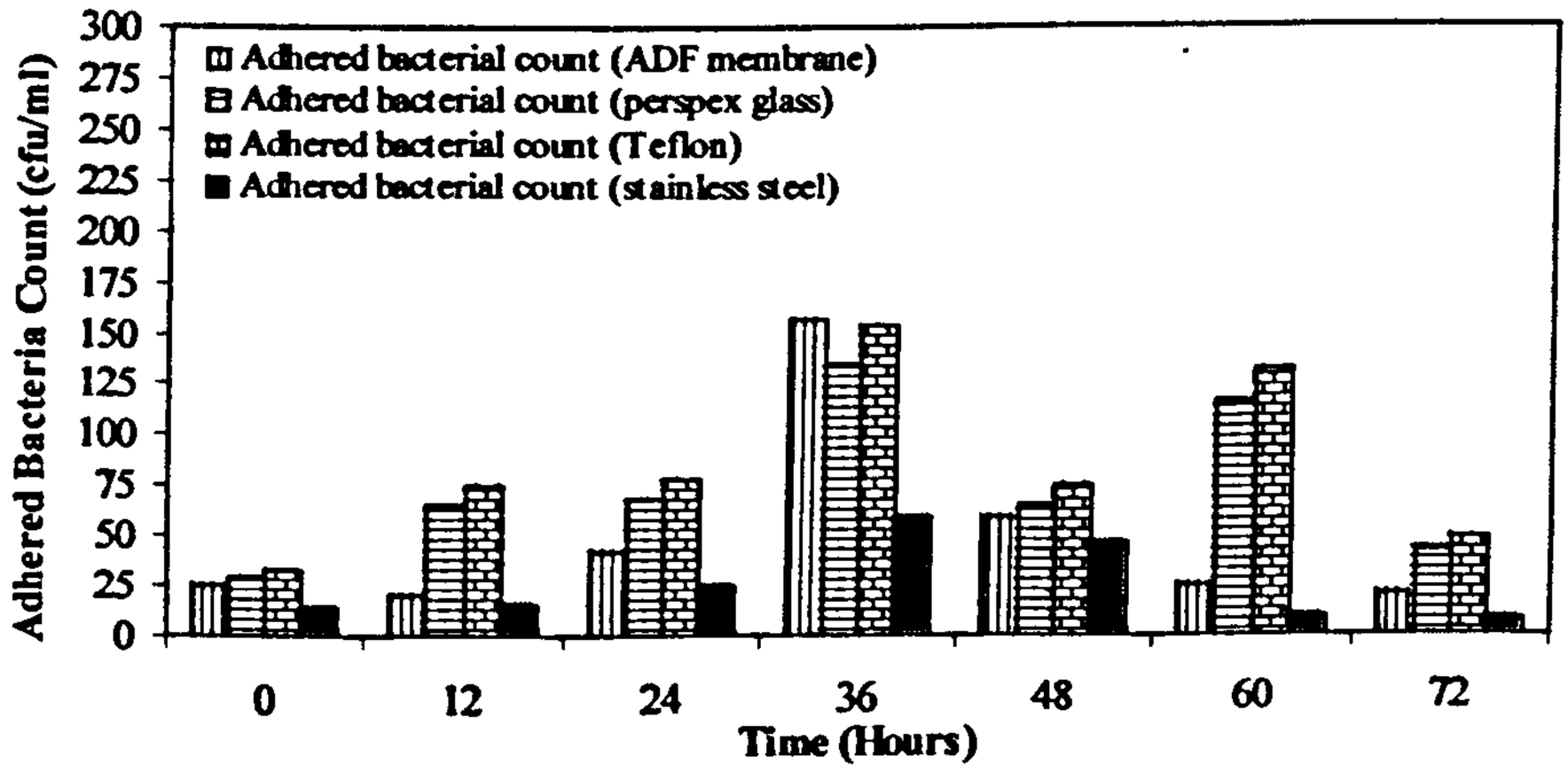

Figure 6.6: Counts of the adhered bacteria on various substrata at high salinity (90 g l^{-1} NaCl).

With low salinity, the maximum bacterial count was 3.9×10^3 cfu observed at steady-state conditions for the ADF membranes, whilst the minimum count was 1.1×10^3 cfu observed at steady-state conditions for the stainless steel specimens. When the

salinity was increased from 30 g l^{-1} to 90 g l^{-1}, the bacterial counts were dramatically decreased to various extents for all substrata tested. At steady-state conditions, the maximum bacterial count was 1.6×10^2 cfu observed at steady-state conditions for the ADF membranes, whilst the minimum count was 0.6×10^2 cfu observed at steady-state conditions for the stainless steel specimens. Minor differences were observed in number of adhered bacteria on the four different substrata.

Figures (6.7a - 6.7d) are epifluorescence microscope images of the biofilms accumulated on the ADF membrane, Teflon, perspex glass, and stainless steel, respectively. The cells stained in green represent "viable" cells while others stained in red are "non-viable". The microphotographs show that the bacterial cells adhered to the ADF membrane were totally viable "green", while the majority of the cells

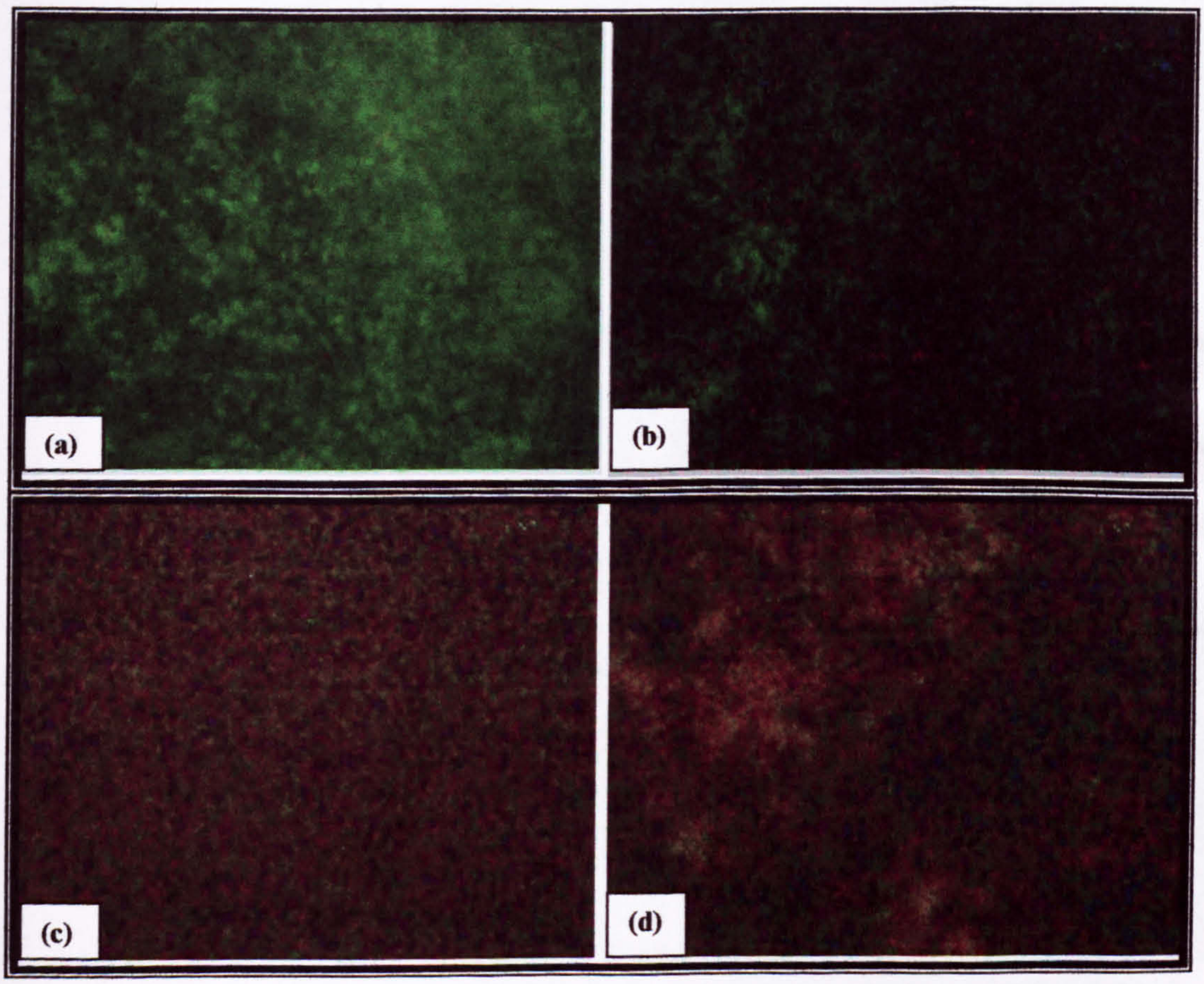

Figure 6.7: Epifluorescence microscope images of various materials topologies: (a) ADF membrane, (b) Teflon, (c) Perspex glass, and (d) Stainless steel (EN1.4307).

adhered to Teflon were viable with a fraction of non-viable cells. The stained cells adhered to Perspex glass showed that almost all the cells were non-viable. This observation applied equally for the stainless steel substratum where only few viable cells were observed. However, several of these "non-viable" cells were actively motile, thus this finding suggests that estimations of cell viability based solely on fluorescent staining patterns should be interpreted with caution. Furthermore, all the substrata showed a slight difference in cell concentration between 30 g l^{-1} and 90 g l^{-1} salinities biofilms. This is because this examination can view only the top "monolayer" of the biofilms adhered to various substrata.

6.3.3 The Cyanobacterial Adhesion Assay

6.3.3.1 Effect of Material Type on Cyanobacterial Adhesion

Exposure of various substrata (ADF membrane, Teflon, perspex glass, and stainless steel, EN1.4307) to the *Euhalothece* sp. (strain BAA001) at various salinities over time induced the formation of biofilms as shown in Figures 6.8a-8d.

The *Euhalothece* sp. (strain BAA001) formed biofilms on all the substrata assayed to various extents, though cells were more abundant on the ADF membranes (Figure 6.8). In all cases, after 6 weeks of exposure to the bacterial culture, the slides of the different materials tested showed copious biofilms derived from this cyanobacterium as observed under the light microscope. This biofilm was easier to observe on the ADF membranes and Teflon surfaces than on Perspex glass and stainless steel, due to the variation in the surfaces roughness (Table 6.1) and chemical composition. At low salinity (30 g l^{-1}), the average biomass percentage was 52%, 39%, 10% and 19% for the ADF membranes, Teflon, perspex glass, and stainless steel substrata, compared to the biomass in the bulk solution, respectively. These results reveal that the ADF membranes and Teflon are most suitable for the colonisation by the *Euhalothece sp.* This observation could be explained by the preferential attraction of the nanoporous texture of the surfaces of these materials compared to the perspex glass and stainless steel substrata. Similar observations were recently reported by Boussu *et al.* (2006) in their study on the filtration performance of nanoporous polyethersulfone membranes.

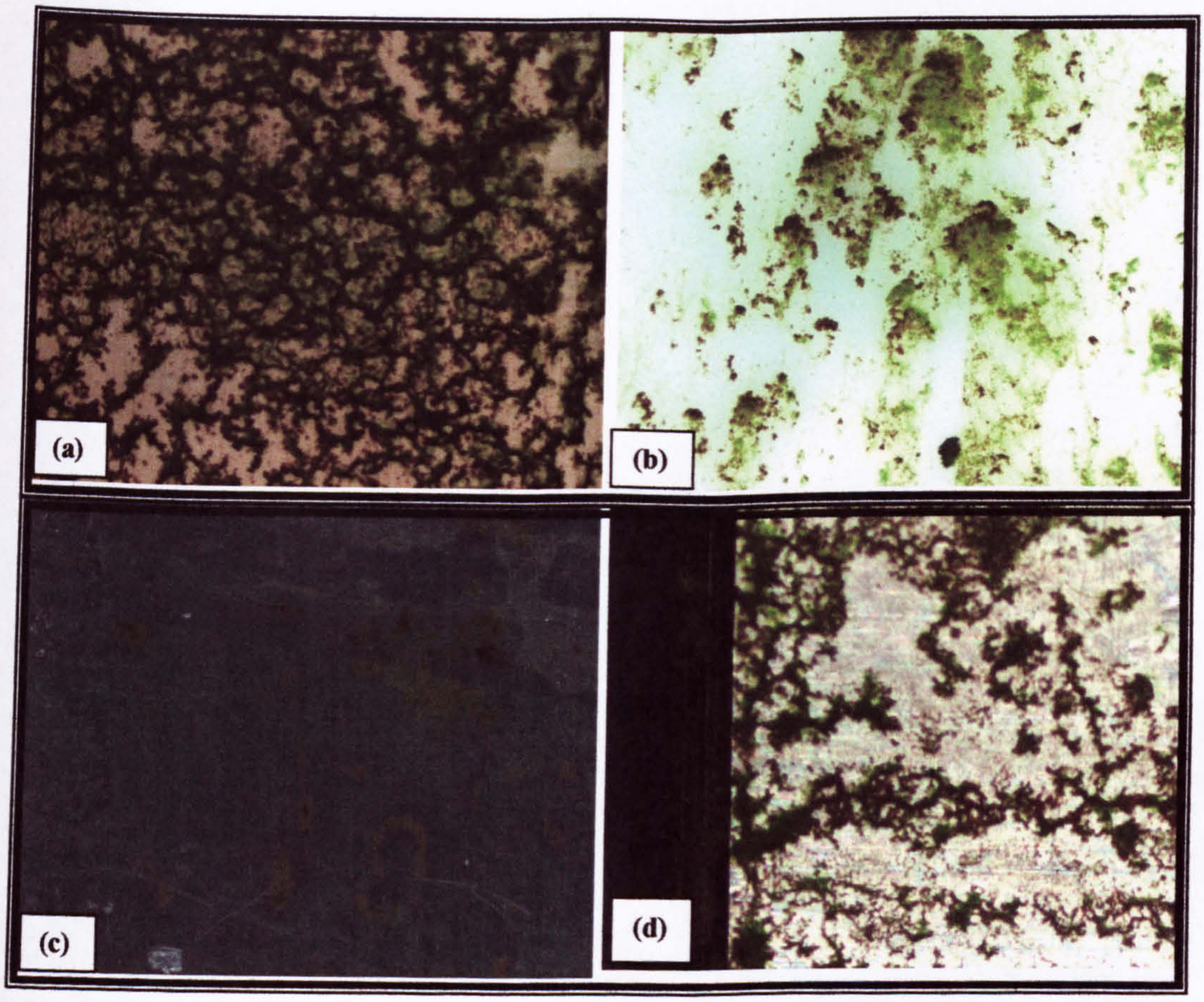

Figure 6.8: Micrographs of biofilms accumulated on various substrata at low salinity (30 g l^{-1}): (a) ADF membrane, (b) Teflon, (c) Perspex glass, and (d) Stainless steel (EN1.4307).

Except for the ADF membranes, the biofilm accumulation was directly proportional to the increase in the surface roughness of the surfaces tested. The high biofilm accumulation on the relatively soft ADF membranes could be due to their high wetability and/or porosity. Figures 6.9a and 6.9b show clear differences in the start of the biofilm invasion of the ADF membranes and the stainless steel surfaces, respectively. The porous structure of the ADF membrane surface might support a relatively even growth of the tissue-like biofilms, denser towards the bulk liquid current. However, the biofilm growth on the stainless steel slides exhibited different patterns with a veins-like distribution, which could have resulted from either the poor wetability or the chemical composition of the steel surface.

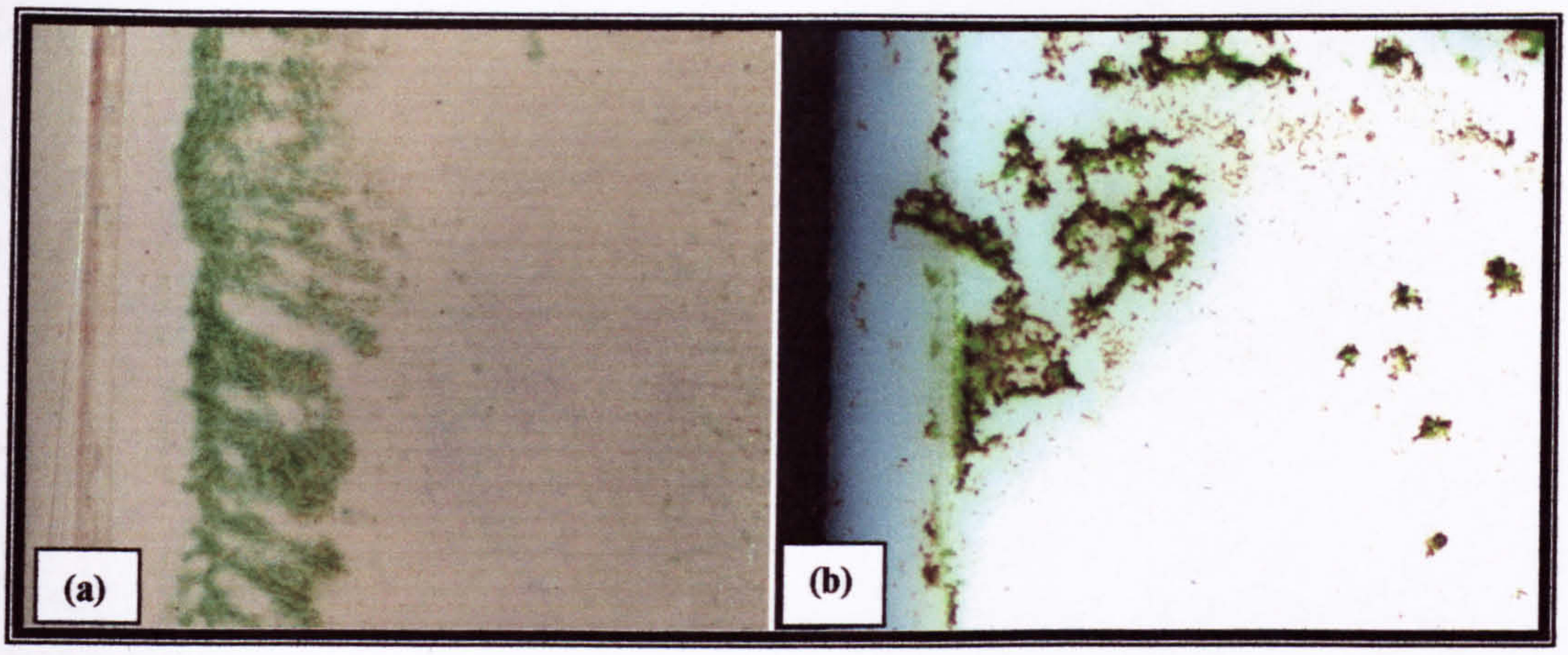

Figure 6.9: Micrographs of biofilms accumulated on edges of various substrata at low salinity (30 g l^{-1}): (a) ADF membrane, (b) Stainless steel (EN1.4307).

Generally, among various parameters affecting biofilm formation on metallic surfaces, the surface composition and roughness are considered the principal parameters influencing the bacteria/surfaces interactions (Korber *et al.*, 1995). The effect of chemical composition is due to the generation of surface charge states, which determine hydrophobicity and electrostatic interactions that may lead to bacterial adhesion (Johnson *et al.*, 1994). The effect of roughness is the mediation of the bacterial establishment due to mechanical retention (Korber *et al.*, 1995). Hence, the sterilisation procedures can produce significant changes in the biofilm properties. Since in this experiment, the ADF membranes and stainless steel slides were sterilised using totally different procedures (i.e. UV radiation and autoclaving, respectively), it is possible that the effect of the different sterilisation processes on surface properties might cause significant impacts. Basically, rough surfaces support more bacterial adhesion (Zhao and Liu, 2006); however, relatively fewer bacterial cells were observed on the relatively rough surfaces of the stainless steel slides, in contrast to what one would expect from a material with high roughness. In their study, Harris *et al.* (2004) reported that bacterial cells respond particularly strongly to features that are smaller than or comparable with the size of the corresponding cells. This means that substrata with extremely rough surfaces sustain less bacterial adhesion; which could be the case observed in this experiment for the stainless steel slides. However, in this study, no further experiments were sought or carried out within this frame in order to support these two findings.

6.3.3.2 Effect of Salinity on Cyanobacterial Adhesion

Besides surface composition and roughness, the impact of the salinity of the bulk solution on biofilm formation and growth was also investigated in this experiment. Since the model cyanobacterium (*Euhalothece* sp.) is a halophilic organism (optimum 60 g l^{-1}, salinity), it grows better and faster in the high salinity medium (60 g l^{-1}) compared to its growth in low salinity (30 g l^{-1}). Due to the variations in the bacterial count at different salinities, the quantification of the adhered bacterial cells to various surfaces was expressed as a percentage of adhered viable bacteria to each slide with respect to the total viable bacteria present in 1 ml of bulk solution. Figure 6.10 summarises the percentages of the adhered viable bacteria adhered to various substrata at low and high salinities. Significant variations were observed in the amount of the adhered bacteria to various substrata at different salinities. When the salinity was increased from 30 to 60 g l^{-1}, the percentages of the adhered bacteria to the ADF membrane, Teflon, Perspex glass, and stainless steel slides markedly decreased by 55%, 63%, 90%, and 84%, respectively.

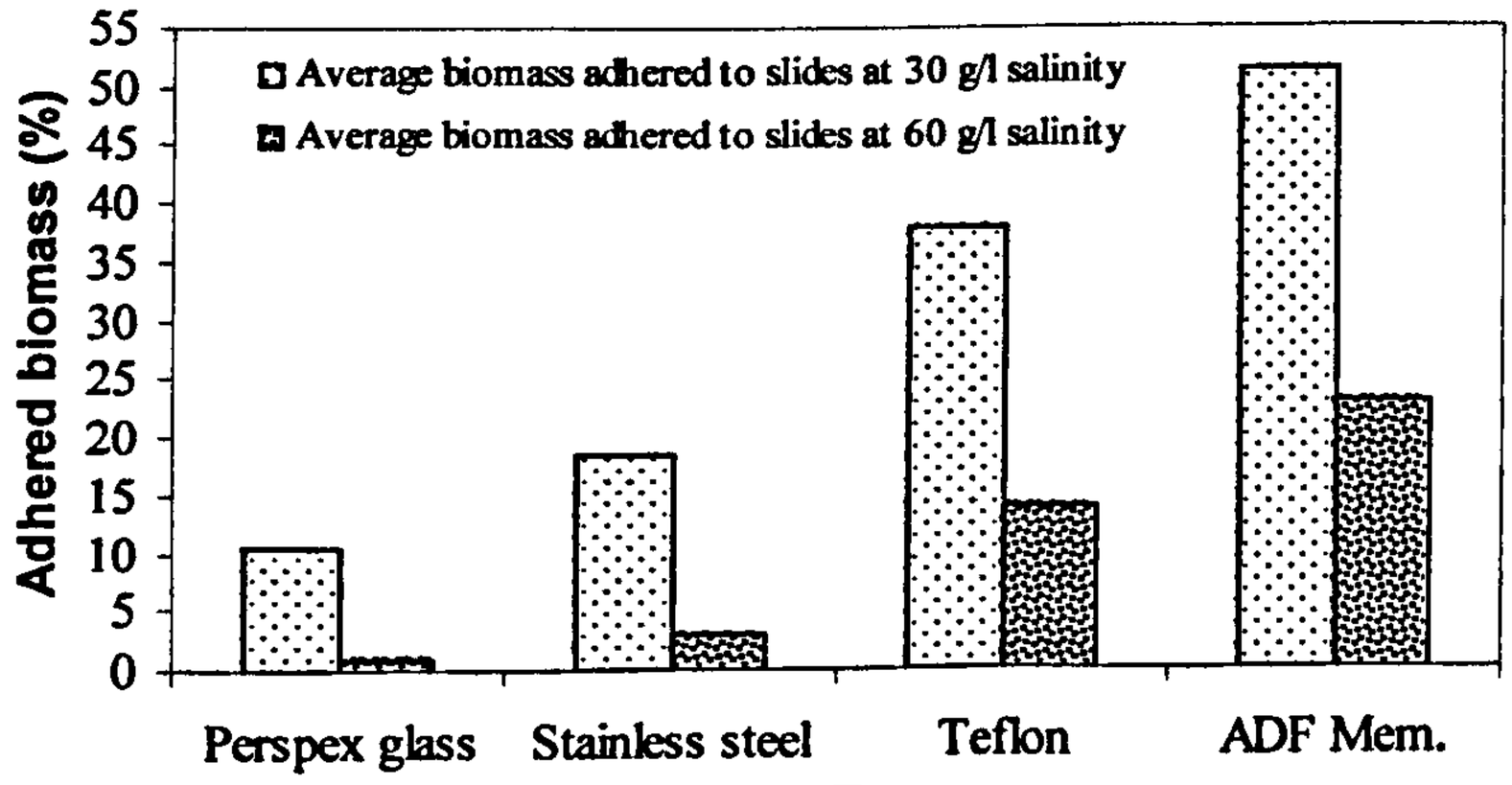

Figure 6.10: Percentage of the adhered cyanobacterial cells to various substrata at different salinities.

The interpretation of the observed variation in the bacterial adhesion in terms of surface roughness now looks somewhat trivial. In spite of nearly similar surface roughness conditions large significant variations in the bacterial adhesion on the ADF membranes and Perspex glass, and on Teflon and stainless steel surfaces are seen. Basically, rough surfaces support more bacterial adhesion. However, the effect of salinity suggests that factors, other than roughness, may be driving biofilm formation. Similar conclusions were drawn by Taylor *et al.* (1998).

Therefore, chemical charge, wetability, coating and surface porosity, and coating concentration and morphology could be other factors responsible for the large variation in the bacterial adhesion of the various surfaces tested. On the other hand, in all cases, increasing salinity of the bulk solution was responsible for a marked decrease in bacterial adhesion on the various materials tested. Bachmann and Edyvean (2006) reported similar observations in their examinations of the *Aquabacterium commune* biofilm formation on stainless steel of similar composition and characteristics. They suggested that the remarkable decline in the biofilm cell density during the plateau phase could be attributed to the plating technique in which the bacteria aggregate instead of producing single cells that formed colonies on the agar, causing a negative bias in the results.

Furthermore, it was observed in this experiment that the topography of the biofilm formed on the various surfaces tested served to increase the specific biofilm surface area providing a larger contact area between the bulk liquid and the bacterial cells, thus improving external mass transfer. Similar observations were also reported by Taylor *et al.* (1998) in their study on the influence of substratum topography on bacterial adhesion to polymethyl methacraylate. This explanation could be correlated to the vine-like morphology of the biofilm accumulated on the stainless steel slides at high salinities (Figure 6.9b).

The effect of the RAB reactor geometry and flow pattern was clearly observed in the preferential colonisation of the edges of the slides by the bacterial cells (Figures 6.9a and 6.9b). This phenomenon was also reported by Bachmann and Edyvean (2006).

6.4 Summary

In this experiment qualitative and quantitative assessments of the bacterial adhesion on RO membranes were carried out. Among the variables affecting the bacterial adhesion and detachment two parameters were investigated namely: surface roughness and salinity. The bacterial adhesion assessment of the ADF membranes, compared to other substrata of various surface roughness (Teflon, Perspex glass, and stainless steel), was performed in two salinities (30 g l^{-1} and 60 g l^{-1}, NaCl for the cyanobacterium *Euhalothece* and at 30 and 90 g l^{-1} for the halobacterium *Halomonas pantelleriensis*). Both strains were isolated from a hypersaline lake (Qabar-Onn Lake).

The effect of surface roughness on the bacterial adhesion showed variable results, which suggests that the biofilm growth was controlled by other parameters such as surface composition and wetability. For the halobacterial species, the biofilm growth exhibited similar patterns for all the materials tested, with an exception for the ADF membranes in which the bacterial counts showed an increment of approximately 40% after reaching its stationary phase (Figure 6.5). The maximum bacterial count was 2.9×10^3 cfu observed for the ADF membranes at low salinity, whilst the minimum was 1.1×10^3 cfu for the stainless steel specimens at similar salinity. Similarly, for cyanobacterial species, *Euhalothece* sp. (strain BAA001) formed biofilms on all the substrata assayed to various extents, with more abundance observed on the ADF membranes. The surface roughness had a direct effect on the biofilm accumulation for all the surfaces tested except for the ADF membranes. The average percentage of the *Euhalothece* biomass that adhered to various surfaces was 52%, 39%, 10% and 19% for the ADF membranes, Teflon, Perspex glass, and stainless steel substrata, compared to the biomass in the bulk solution, respectively.

Salinity had a direct and detrimental effect on the biofilm formation and growth in all cases. Increasing salinity from 30 g l^{-1} to 90 g l^{-1} caused a dramatic decline (> 90%) in the counts of the adhered halobacteria. Equally, for the cyanobacterial species, when the salinity was increased from 30 g l^{-1} to 60 g l^{-1}, the percentage of the adhered bacteria decreased by 55%, 63%, 90%, and 84% for the ADF membranes,

Teflon, perspex glass, and stainless steel substrata, respectively, compared to the biomass in the bulk solution.

In conclusion, ADF membranes are very prone to biofouling at low salinities. However, using the ADF membranes in the desalination of hypersaline waters could be advantageous for improving the biofouling problems, since biofouling was retarded at higher salinity.

There is a great need to determine if one (or several) surface characterising parameters can reflect the degree to which the halobacteria adhere to or are removed from a surface. Several experiments can be suggested to investigate RO membranes surface topology (presence of scratches or porosities) rather than surface roughness, as the latter did not directly correlate with the biofilm formation in RO desalination systems. Surface chemistry and composition is another parameter which is worth investigation in order to assess the biofilm formation. This process involves the initial events of bacterial adhesion, bacterial growth/colonisation, and final biofilm formation.

Chapter 7

FLUX BEHAVIOUR AND BIOFOULING STUDIES OF REVERSE OSMOSIS MEMBRANES

7.1 Introduction

The reverse osmosis (RO) membrane separation process is becoming one important method for separation of solutes from aqueous solutions. The RO process has shown remarkable advantages over many conventional separation processes (Soltanieh and Gill, 1981). For example, in one of its major applications, the RO process converts sea water to drinking water at a price one-third of that for the thermal distillation process (Noble and Stern, 1995; Darwish and Al-Najem, 2000). The continuous improvement in membrane manufacturing for higher water permeability and higher salt rejection at a lower price will lead to wider applications of the process in new fields.

The permeate flux of the RO process is a major concern in both system design and operation optimization. The permeate flux in a RO process is initially controlled by the properties of membrane transport. This means that the initial permeate flux of the RO process is determined by the membrane permeability or resistance to water. As filtration proceeds, solute rejected by the membrane forms a layer of high concentration near the membrane surface. This phenomenon is called concentration polarization. The formation and development of the concentration polarization layer in the RO process reduces the effective driving force for water filtration and, therefore, reduces permeate flux. It has been recognized for a long time that concentration polarization is a major limiting factor to permeate flux in many RO membrane processes (Bhattacharyya *et al.*, 1990; Marinas and Urama, 1996;). The causes of flux decline due to inorganic scaling depend on numerous factors including, but not limited to, membrane properties, module geometry, feed characteristics, type of solute, and various operating conditions (Shaalan, 2002). The

flux decrease can be attributed to concentration polarization, adsorption of solute particles, pore blockage, and gel layer formation (Tansel *et al.*, 2000).

Significant concentration polarization can develop in many RO processes, especially for filtration of high salt concentrations under high pressures (Song and Yu, 1999). The development of the concentration polarization layer in cross-flow filtration is a complex process that is affected by many factors, such as the configuration of the filtration channel, shear rate, solute concentration and diffusivity, operational pressure, and membrane resistance (Damak, *et al.*, 2004). There are two particular features for concentration polarization in a cross-flow RO process. First, as a result of solute rejection and accumulation, the concentration polarization layer grows gradually along the filtration channel. Second, concentration polarization is coupled with permeate flux. On the one hand, the development of concentration polarization is induced by a permeate flux that brings solute to the vicinity of the membrane surface, which creates an additional resistance layer to permeate flux (Bacchin and Aimar, 2005). Neither concentration polarization nor permeate flux can be determined independently. These two features make the investigation of concentration polarization in the cross-flow RO process one of the most challenging tasks in this field.

Biofouling, defined as an accumulation of biomass on a surface by growth and/or deposition to such a level that it causes operational problems, is difficult to quantify. However, the diagnosis of biofouling is only justified when a relationship is found between the encountered operational problems and biomass accumulation as determined with adequate parameters (Vrouwenvelder *et al.*, 2000). Biofouling, which has been described extensively in the literature (Amjad, 1992; Ridgway and Flemming, 1996), may cause permeate flux reduction and/or increased pressure drops. A suite of biomass parameters and analytical tools are available (Flemming, 1997), but the question remains which parameter(s) at which level is conclusive for identifying biofouling as the cause of the operational problems. Biofouling — growth of biomass, i.e. biofilms — may cause flux reduction and/or increased pressure drop in nanofiltration (NF) and reverse osmosis (RO) membranes.

Pretreatment is frequently applied with the goal of eliminating foulants from the feed water to minimize fouling. However, pretreated feed water may still contain dissolved organic compounds, microorganisms and small colloidal particles such as clay, silica, and organic matter which contribute to RO membrane fouling (Winters, 1997). Li and Chen (2004) and Roorda and van der Graaf (2000) have determined that larger particles do not contribute significantly to fouling, and that fouling is controlled by small colloidal particles. Li and Chen (2004) concluded that particles smaller than 0.45μm, including true colloids, microorganisms and dissolved solids, contribute the most to RO membrane fouling.

The work described in this chapter investigates the parameters governing permeate fluxes in RO membranes when treating hypersaline waters. In particular, the study focused on the effect of selected chemical constituents (e.g. anions and cations), combined chemical constituents and biomass (i.e. microorganisms), and pretreatment on permeate flux behaviours and patterns of various RO membranes under controlled conditions. The research is also extended to study the relationship between concentration polarization and bacterial accumulation in an attempt to explain the biofouling phenomenon.

7.2 Methodology

7.2.1 Experimental Strategy and Sample Preparation

The experimental procedures for permeate flux determinations are described in more detail in Chapter 3 Section 3.1.1.3. Initially, the experimental strategy was to address the impact of single chemical constituents on flux decrease by utilising artificial pure chemical water samples that are identical in all characteristics except that they omit the metal ions in question. Two cations (e.g. Na^+ and K^+) and two anions (e.g. Cl^- and SO_4^{2-}) were considered in this experiment, since they were dominant in Qabar-Onn Lake water (Table 4.2, Chapter 4). The artificial samples were prepared by dissolving equal quantities of NaCl and K_2SO_4 salts in lab grade distilled waters, and to substitute NaCl with KCl and K_2SO_4 with Na_2SO_4 when single impacts of Na and K were studied, respectively; and NaCl with Na_2SO_4 and

K_2SO_4 with KCl when Cl^- and SO_4^{2-} single impacts were studied, respectively. A control sample, containing all chemical constituents, was also used as a reference in this experiment.

Two sets of water samples were prepared and used in this experiment. Each set of samples was prepared at two salinities (i.e. 30 g l^{-1} and 60 g l^{-1}), as summarised in Table 7.1. These samples were individually applied to two types of RO membrane (i.e. ADF and Nanomax 95).

Table 7.1: Chemical compositions the osmotic pressure calculations of the prepared chemical water samples.

Sample Type	Chemical composition				Calculated Osmotic Pressure (bar)
	NaCl	KCl	Na_2SO_4	K_2SO_4	
Sample 1 (30 g l^{-1} salinity) (Control)	15 g l^{-1}	–	–	15 g l^{-1}	17.83
Sample 2 (60 g l^{-1} salinity) (Control)	30 g l^{-1}	–	–	30 g l^{-1}	35.57
Sample 3 (30 g l^{-1} salinity) (-Cl)	–	–	15 g l^{-1}	15 g l^{-1}	14.23
Sample 4 (60 g l^{-1} salinity) (-Cl)	–	–	30 g l^{-1}	30 g l^{-1}	28.46
Sample 5 (30 g l^{-1} salinity) (-SO_4)	15 g l^{-1}	15 g l^{-1}	–	–	20.43
Sample 6 (60 g l^{-1} salinity) (-SO_4)	30 g l^{-1}	30 g l^{-1}	–	–	40.85
Sample 7 (30 g l^{-1} salinity) (-Na)	–	15 g l^{-1}	–	15 g l^{-1}	15.36
Sample 8 (60 g l^{-1} salinity) (-Na)	–	30 g l^{-1}	–	30 g l^{-1}	30.71
Sample 9 (30 g l^{-1} salinity) (-K)	15 g l^{-1}	–	15 g l^{-1}	–	19.30
Sample 10 (60 g l^{-1} salinity) (-K)	30 g l^{-1}	–	30 g l^{-1}	–	38.60

The impact of the combined chemical constituents and microorganisms present in the lake water samples (e.g. Qabar-Onn Lake) were also investigated in this study. These samples were named biological samples. The biological samples were prepared by inoculation of two sets of control chemical samples at two salinity concentrations (30 and 60 g l^{-1}) with a 1ml l^{-1} mixture of a halobacterium (*Halomonas pantelleriensis* sp. strain BAA003) and a cyanobacterium (*Euhalothece* sp. strain BAA001) cultures.

These organisms were previously isolated from Qabar-Onn Lake (Chapters 4 and 5). The cultures were grown in media of identical salinities to those chemical samples in which they were inoculated. Designated volumes (1 ml l^{-1}) from mid-stationary phase cultures (i.e. OD = 1.25, and *Chl-a* = 1.4 µg ml^{-1} for halobacteria and cyanobacteria, respectively) were withdrawn and used as microbial ingredients. The inoculation process was carried out just before each run started to ensure that cells did not multiply before these runs were carried out. The assessment of the impact of the pretreatment process of the prepared biological samples has also been performed in this experiment. The detailed pretreatment procedure and equipment was described earlier in Chapter 3, Section 3.1.1.3.2. Table 7.2 presents the ingredients of the biological and pretreated samples used in this experiment.

Table 7.2: Ingredients of the prepared biological and pretreated water samples.

Sample Type	Composition			Pretreatment
	NaCl	K_2SO_4	Biomass	
Sample 11 (Biological sample) (30 g l^{-1})	15 g l^{-1}	15 g l^{-1}	1 ml l^{-1}	–
Sample 12 (Biological sample) (60 g l^{-1})	30 g l^{-1}	30 g l^{-1}	1 ml l^{-1}	–
Sample 13 (Pretreated sample) (30 g l^{-1})	15 g l^{-1}	15 g l^{-1}	1 ml l^{-1}	(0.45 µm + 0.22 µm)
Sample 14 (Pretreated sample) (60 g l^{-1})	30 g l^{-1}l	30 g l^{-1}	1 ml l^{-1}	(0.45 µm + 0.22 µm)

7.2.2 Membrane Autopsy and Visualisation

In-situ membrane surface monitoring was carried during the operation of each experimental run using a *ZEISS Discovery V12 SteREO* microscope attached to a computer (as described in Section 3.1.1.3.3, Chapter 3). The microscope was used to take micrographs of the salt crystals as soon as they formed on the membrane surface during operation. Membrane autopsy was performed after finishing each run by dismantling the membrane module and taking ESEM micrographs of the membrane surface. An environmental scanning electron microscope (model Philips XL30 ESEM FEG, FEI/Philips Electrin Optic equipped with a Schottky Field-emission electron gun (as described in Section 3.6, Chapter 3).

7.3 Results and Discussion

7.3.1 Flux Profiles of RO Membranes

Figure 7.1 shows the initial flux productivity observed using lab grade distilled water for ADF and Nanomax membranes, due to membrane compaction and structure rearrangements. On average, during the membrane setting stage, the Nanomax membranes experienced a higher flux productivity and variability than that for the ADF membranes. The specific flux production rate was 5,565 $kg.m^{-2}.h^{-1}$ for the Nanomax membranes while only 3,400 $kg.m^{-2}.h^{-1}$ was recorded for ADF membranes.

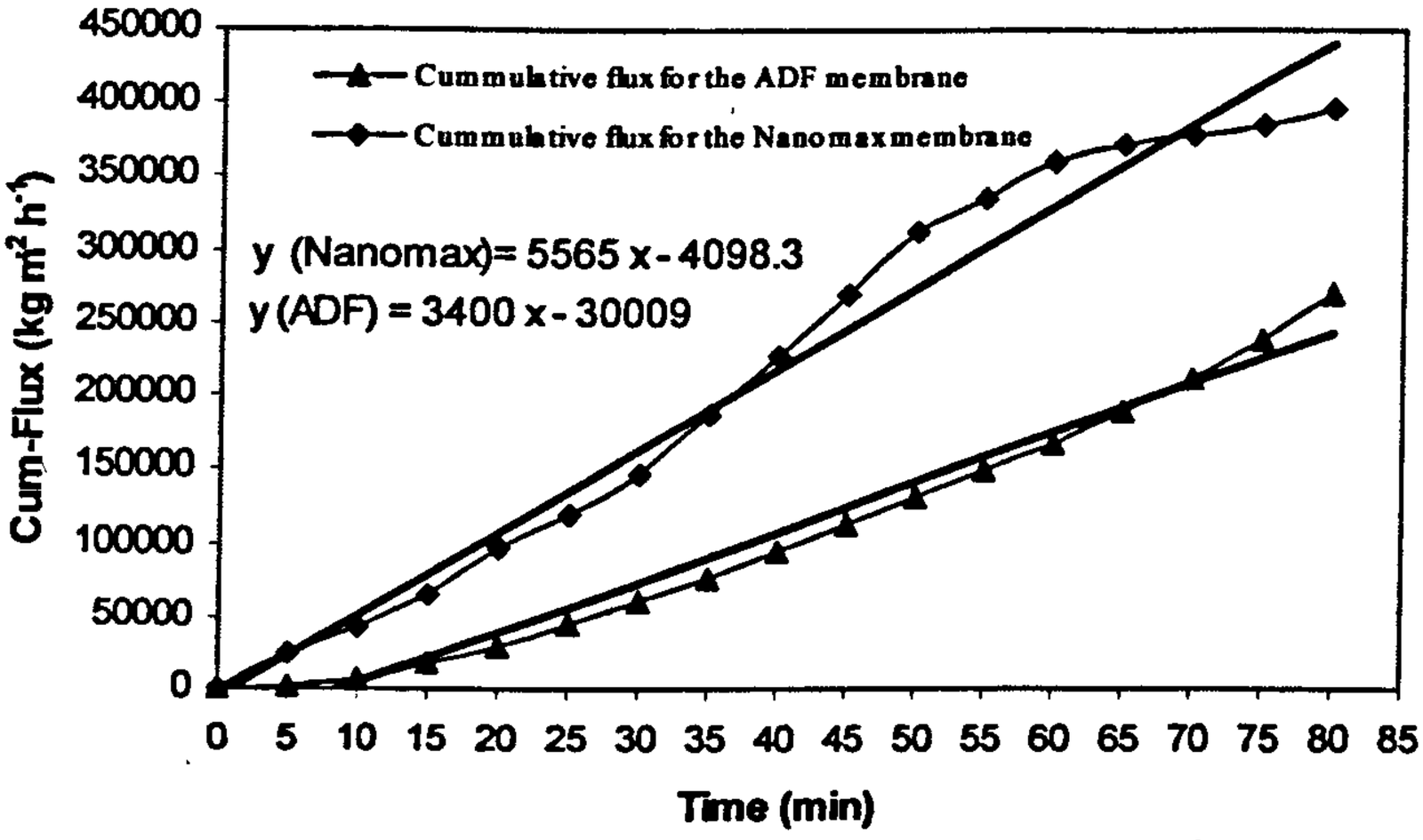

Figure 7.1: Flux decrease observed during membrane setting period for the ADF and Nanomax membranes.

The permeate flux behaviour of the RO membranes (Figures 7.2 and 7.3) for ADF and Nanomax membranes, respectively, revealed generalised patterns at different salinities (30 g l^{-1} and 60 g l^{-1}, NaCl and K_2SO_4). After setting each membrane separately with prefiltered lab grade distilled water, water samples of different salinities were introduced to the system as feed water to each membrane type individually, and the flux behaviour was monitored throughout the run period. The flux exponentially increased with increased pressure until it reached an initial plateau (Figures 7.2 and 7.3), which was most likely due to the effect of concentration

polarisation in chemical samples and due to the combined effect of both concentration polarisation and biomass adsorption (biofouling) in biological samples (more explanations is presented in the next Section 7.3.4) (Kimura, 1995; Mallevialle, 1996 and Ahmad, *et al.*, 2001).

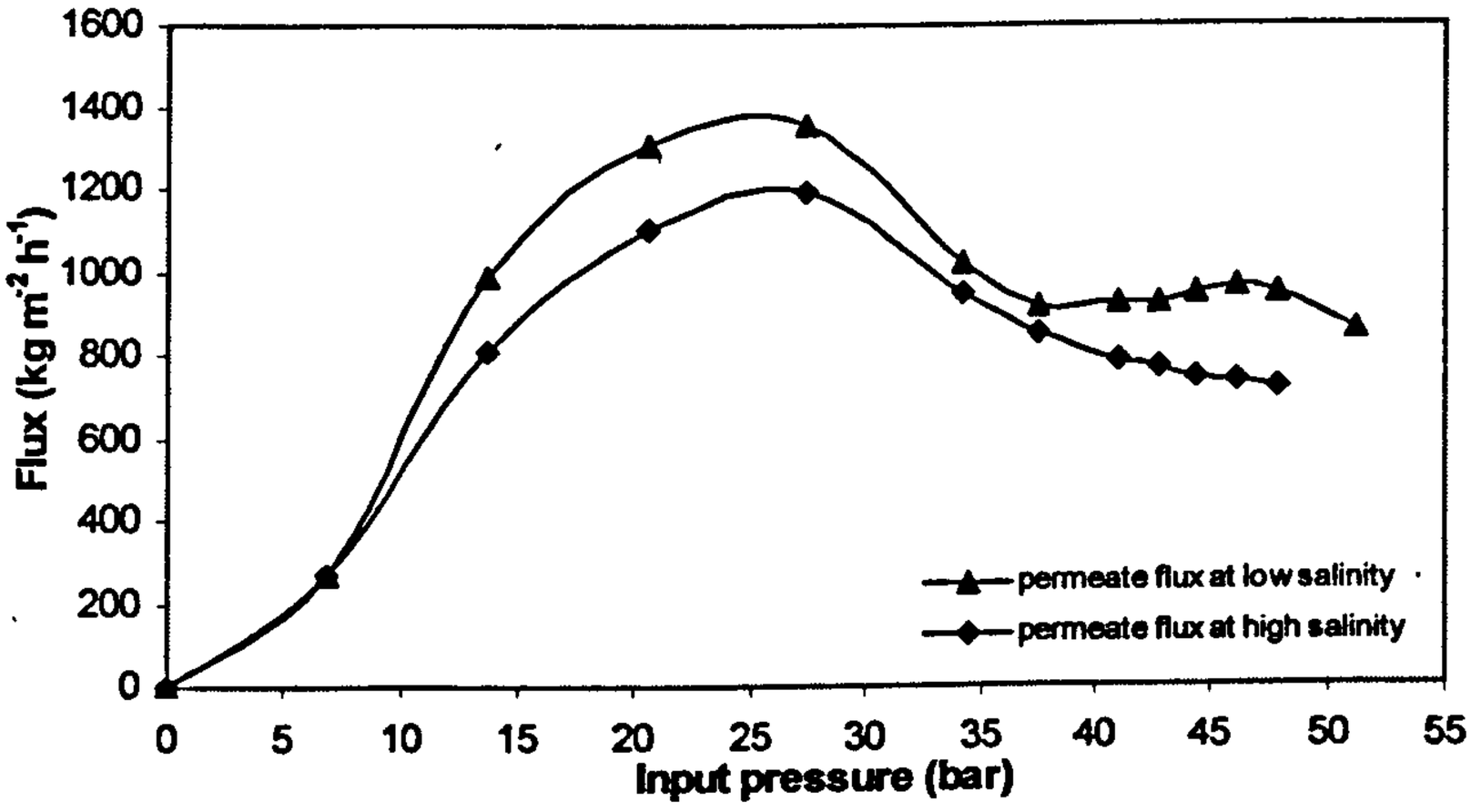

Figure 7.2: Flux profile for the ADF membrane at various salinities.

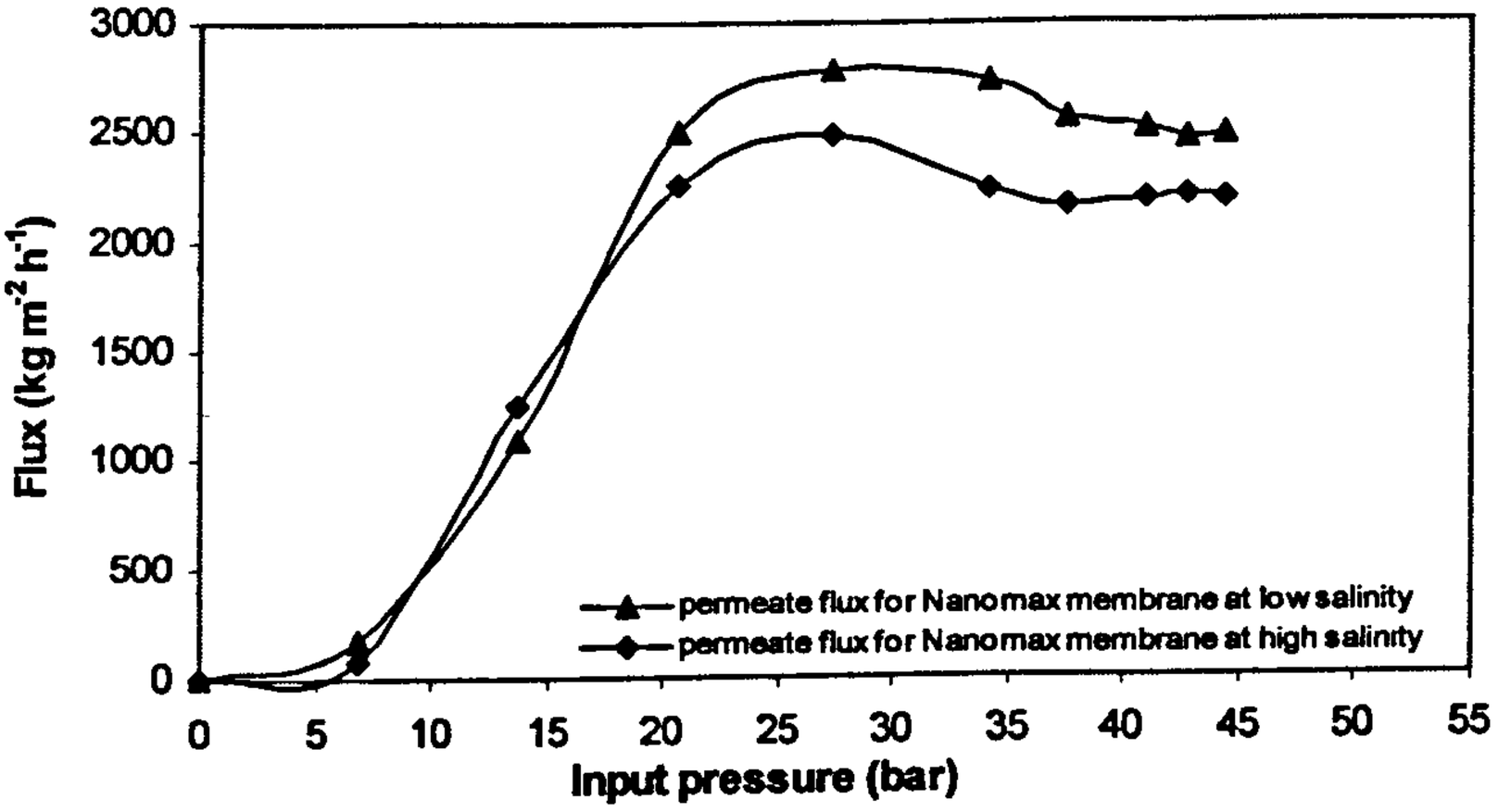

Figure 7.3: Flux profile for the Nanomax membrane at various salinities.

The critical flux is believed to be a measure of where a fouling or cake layer first forms on a membrane surface (Matsuura, 2001; Song and Yu, 1999). However, direct observation methods have shown that even before the critical flux is achieved

in a membrane system, foulants are continuously being deposited on to and removed from the membrane surface. Therefore, the critical flux is most likely the point where the rate of deposition first significantly exceeds the rate of removal and/or a significant increase in resistance is obtained due to deposited materials (Zhang, *et al.*, 2005).

In this experiment, the critical fluxes for the Nanomax membrane were 2,770 and 2,230 $kg.m^{-2}.h^{-1}$ when using samples of salinities 30 and 60 g l^{-1}, respectively. These fluxes occurred at pressures of 27 and 35 bar, respectively. However, when the ADF membrane was used, results showed that lower critical fluxes were observed (i.e. 1,330 and 1,200 $kg.m^{-2}.h^{-1}$ corresponding to 30 and 60 g l^{-1} salinities, respectively). This decrease can be attributed to the membrane specifications and design (e.g. ADF is a high-rejection membrane and Nanomax is a high-productivity membrane).

7.3.2 Effect of Membrane Type on Flux Behaviour

The overall productivity of the ADF membranes was about only 50% of the productivity achieved by the Nanomax membranes under identical conditions. The results indicate that the fouling behaviours of the two types of membranes are considerably different (Figures 7.4 and 7.5).

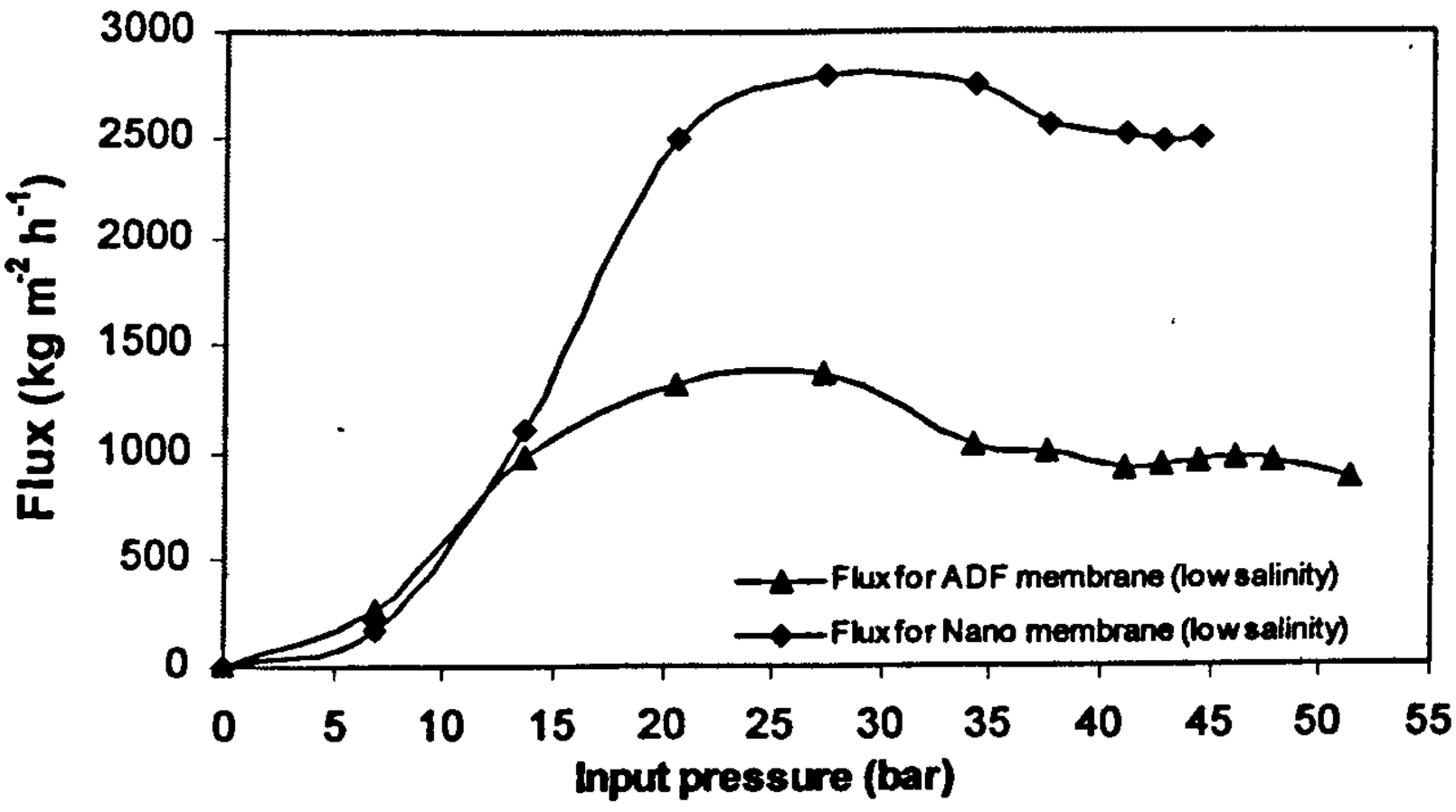

Figure 7.4: Flux response to membrane type-impact at lower salinity (30 g l^{-1}).

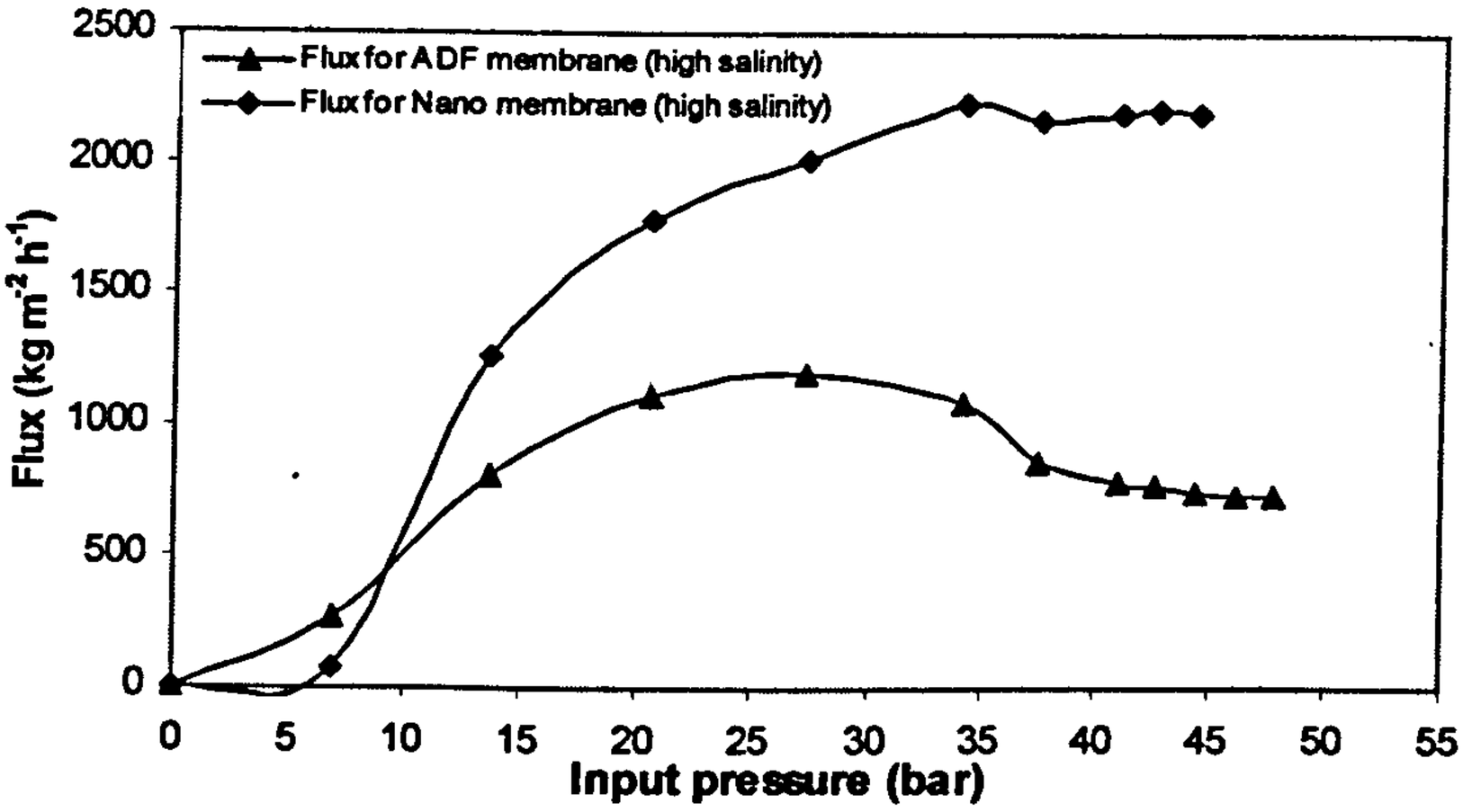

Figure 7.5: Flux response to membrane type-impact at higher salinity (60 g l^{-1}).

When the smooth membranes were used for low salinity filtration, it is believed that the rate of particle deposition was less than the rate of washing out of these particles by the concurrent flow. Increased pressure resulted in stabilising conditions, where the deposition rate was equal to the wash out rate of particles. However, at elevated pressures, it has been shown that the rate of deposition becomes higher than washing out of particles, which represents the irreversible gel or cake layer fouling model (Sheikholesami, 1999; Al-Ahmad, *et al.*, 2000 and Moatty, 2001). The fouling behaviour through the Nanomax (i.e. smooth membrane) exhibited a similar pattern. When pressure was increased from approximately 6 to 20 bar, an exponential flux increase was observed, followed by a steady-state flux at pressures between 20 – 34 bar. Increasing the pressure above 34 bar resulted in a flux decrease, which might be due to the formation of a concentrated salt layer (concentration polarisation) near the membrane surface (Damak, *et al.*, 2004).

Unlike polyamide membranes, composite membranes (e.g. ADF membrane), because of their remarkably high surface roughness, resemble a different fouling behaviour. The flux pattern of the ADF membrane sharply dropped at pressures ≥ 27 bar and declined more gradually at pressures above 37 bar (Figures 7.4 and 7.5).

Results showed that the flow behaviour represents two fouling patterns: the pore narrowing/constriction which occurred at pressures between 20 to 37 bar (as shown in Figure 7.6), and cake layer formation which occurred at pressures above 37 bar (as shown in Figure 7.7).

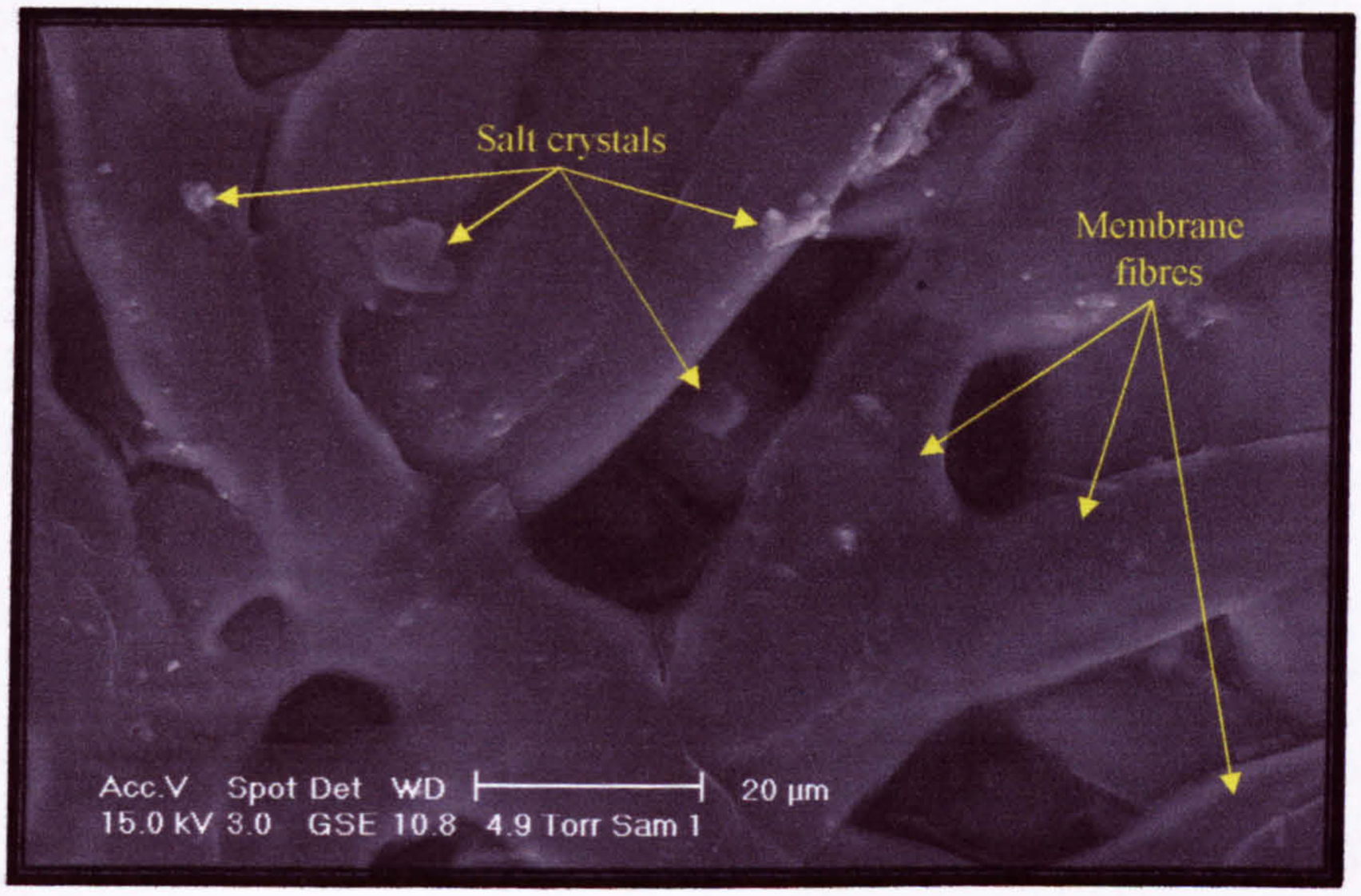

Figure 7.6: ESEM micrograph of ADF membrane showing start of crystal formation near pore mouths on the membrane surface at 60 g/l salinity, bar = 20 µm.

7.3.3 Effect of Chemical Constituents on Flux Behaviour

The type and composition of the cake layer formed on the membrane surface govern the permeate flux, solute rejection efficiency, and/or the pressure drop in an RO system (Song and Yu, 1999). In this experiment, the behaviour of the permeate flux and productivity were extensively governed by the ion type (cations or anions), their valency, and their concentration in the solution, which determines the resulted osmotic pressure in the solution.

The single impacts of four chemical ion types, which constituted the chemical water samples used in this experiment, were investigated individually. Two anions (Cl and SO_4) and two cations (Na and K) were omitted individually as described previously in the methodology, in order to monitor the impact of the absence of each ion type on

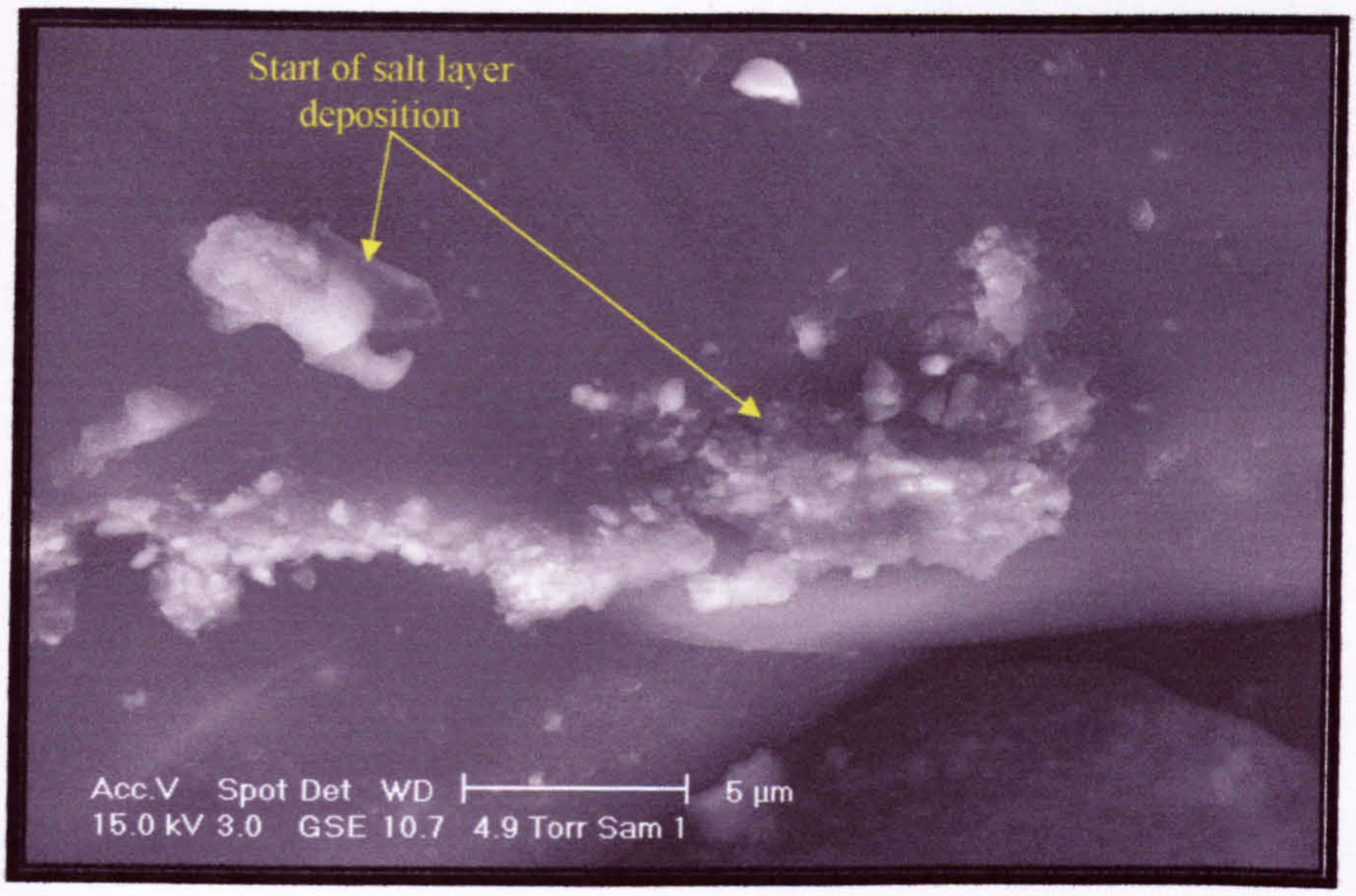

Figure 7.7: ESEM micrograph of ADF membrane showing start of cake layer formation near the membrane surface at 60 g/l salinity, bar = 5 µm.

the flux profile at different salinities. Figures 7.8 and 7.9 show the impact of absence of Cl and SO_4 ions on flux at various salinities using ADF and Nanomax membranes, respectively.

When the ADF membrane was used, the impact of omitting Cl ions resulted in a higher flux at low salinity (i.e. 30 g l^{-1}), however, the flux decreased by an average of 60% at higher salinity (i.e. 60 g l^{-1}). In contrast, when SO_4 ions were omitted from the solution, the results showed similar fluxes at both salinities (i.e. 30 g l^{-1} and 60 g l^{-1}) which indicate the insignificant effect of increasing Cl ions on flux when SO_4 ions were absent. The critical fluxes of samples omitting Cl ions were 2,880 and 1,512 kg.m^{-2}.h^{-1} for 30 and 60 g l^{-1} salinities, respectively. Interestingly, these flux values were obtained at pressures of 13.6 bar, which corresponds to 27 bar when treating control samples containing Cl ions under similar conditions (as presented in Figure 7.3). These results could be due to the relatively lower osmotic pressure values of these samples compared to the control samples which contain Cl ions in the solution (14.23 bar and 28.46 bar corresponding to 17.83 bar and 35.57 bar for the control samples, Table 7.1).

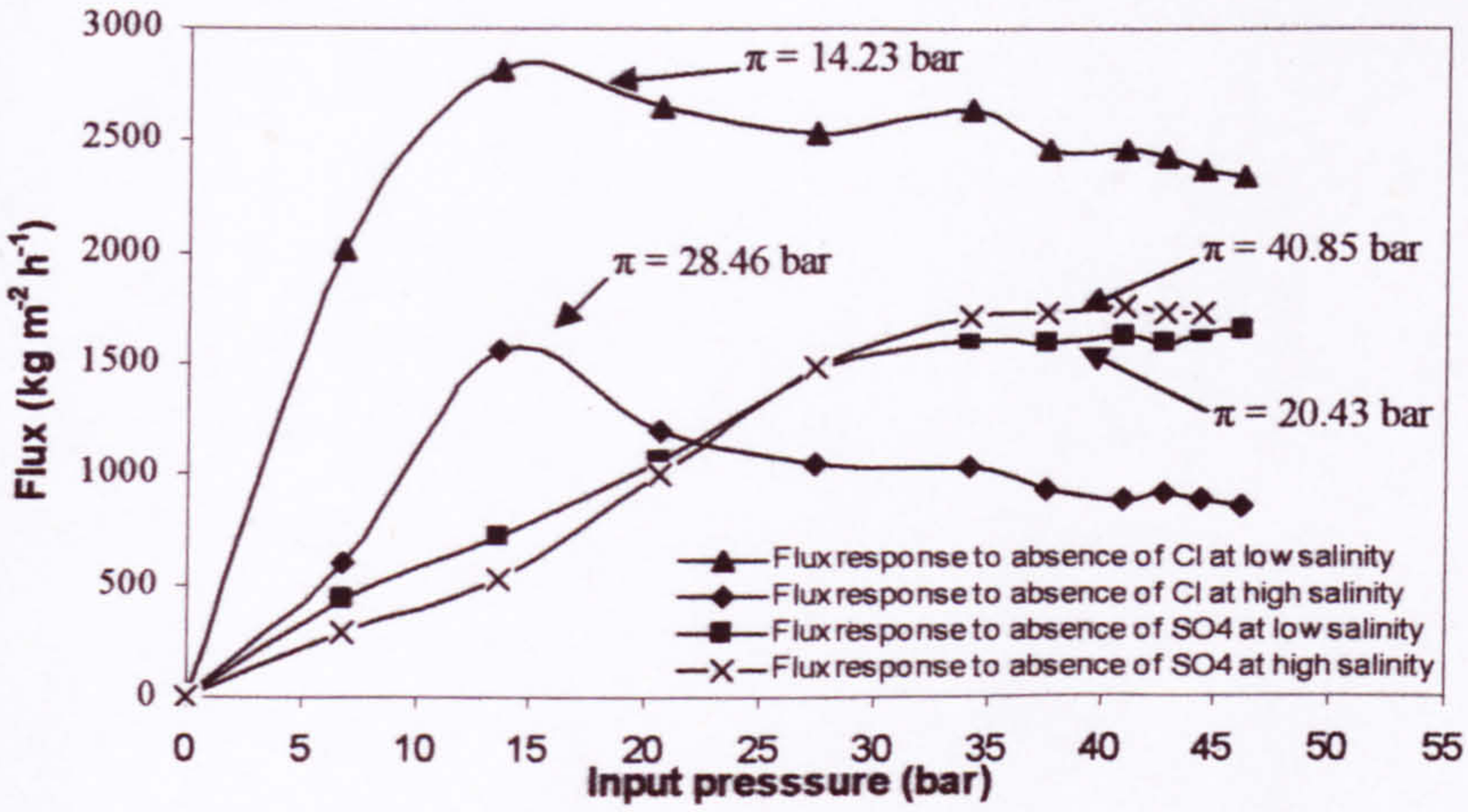

Figure 7.8: Flux responses to various anion absences at two salinities using the ADF membrane.

The explanation of this phenomenon can be referred to the fouling type which most likely occurred in each particular condition. The results indicate that sodium and potassium chloride crystals formed faster, regardless of the salt concentration in the solution. Also these crystals have a rougher texture and larger in size compared to sodium and potassium sulphate crystals (Figures 7.9-a and 7.9-b). Because of the their rough texture, chloride crystals were easily adsorbed by the membrane surface,

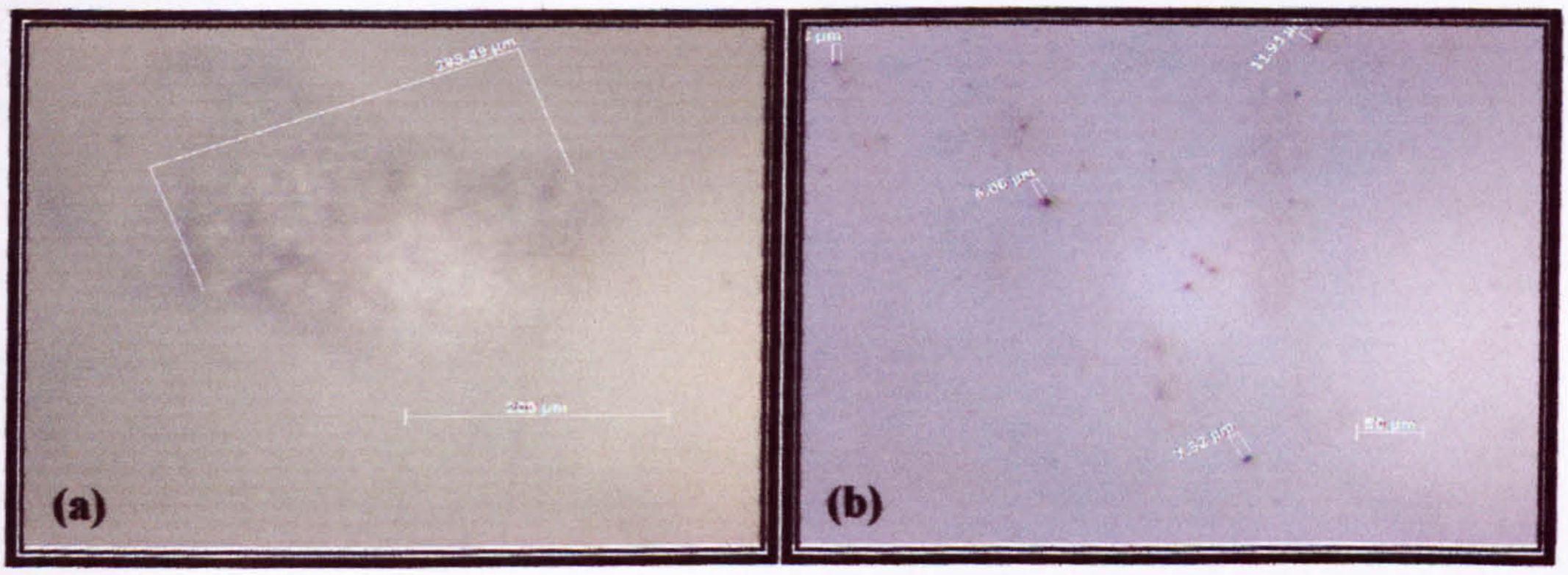

Figure 7.9: *In-situ* micrographs of Cl and SO_4 crystals formed on ADF membrane at 60 g/l salinity: (a) Cl crystal, bar = 200 µm; and (b) SO_4 crystal, bar= 50 µm.

these crystals grew gradually with increased pressure, and finally deposited in the membrane cavities, causing channel narrowing and/or blockage, which causes irreversible fouling, even at elevated concurrent flow rates (Figure 2.17, Chapter 2).

Krieg *et al.* (2004), in their study concluded that the retention of monovalent Cl ions was lower for the salt mixtures than for the single-salt experiments. It was also concluded that the presence of a higher valence anion (e.g. SO_4^{2-}) seems to drive more Cl into the membrane, thus decreasing its retention.

Furthermore, when the Nanomax membrane was used in this experiment, the impact of the absent anions (i.e. Cl^- and SO_4^{2-}) on flux showed similar patterns compared to the ADF membranes, but with higher productivity (Figure 7.10). The fluxes were approximately 1.5 fold higher when compared to the ADF membranes. This increase in flux can be attributed to the smoother Nanomax membrane surface compared to the ADF membranes (Figure 3.6, Chapter 3), as higher membrane surface roughness results in more interaction between colloidal particles and the membrane, thus leading to more fouling in the membrane system (Elimehech *et al.*, 1997).

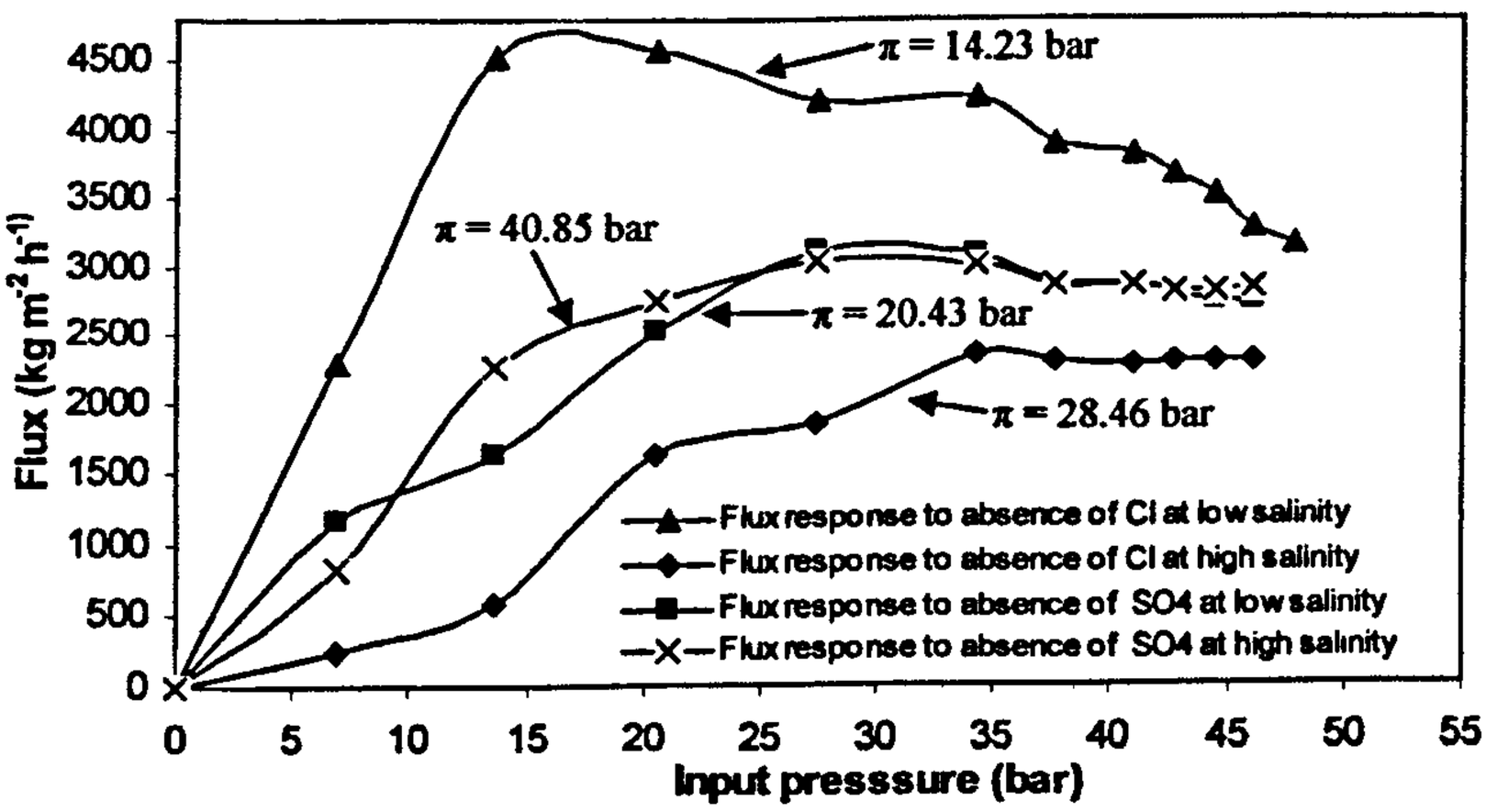

Figure 7.10: Flux response to anions absence at various salinities using Nanomax-95 membrane.

In this experiment, the highest solvent permeability was generally observed for the 1:1 salts (i.e. NaCl and KCl) when SO_4^{2-} ions were absent, and decreasing in the presence of divalent ions (i.e. SO_4^{2-}). This observation fully agrees with Krieg *et al.* (2004) in their study on assessment of salt rejection in NF membranes.

Figures 7.11-a and 7.11-b show *in-situ* micrographs of chloride and sulphate crystals deposited on Nanomax membranes at 60 g l^{-1} salinity, respectively. The long pillar-like shape of the chloride crystals formed in this experiment can be attributed to the decreased mixing rate of feed streams near the membrane surface caused by the smoother Nanomax membrane surface in cross-flow modules (Bessieres *et al.*, 1996). In addition, the unique shape of the chloride ions formed on the membrane surface seems to protect pores mouths on the membrane surface instead of blocking them, and hence no further flux decrease was experienced, even at elevated pressures and higher salinity (i.e. 60 g l^{-1}) (Soffer *et al.*, 2004).

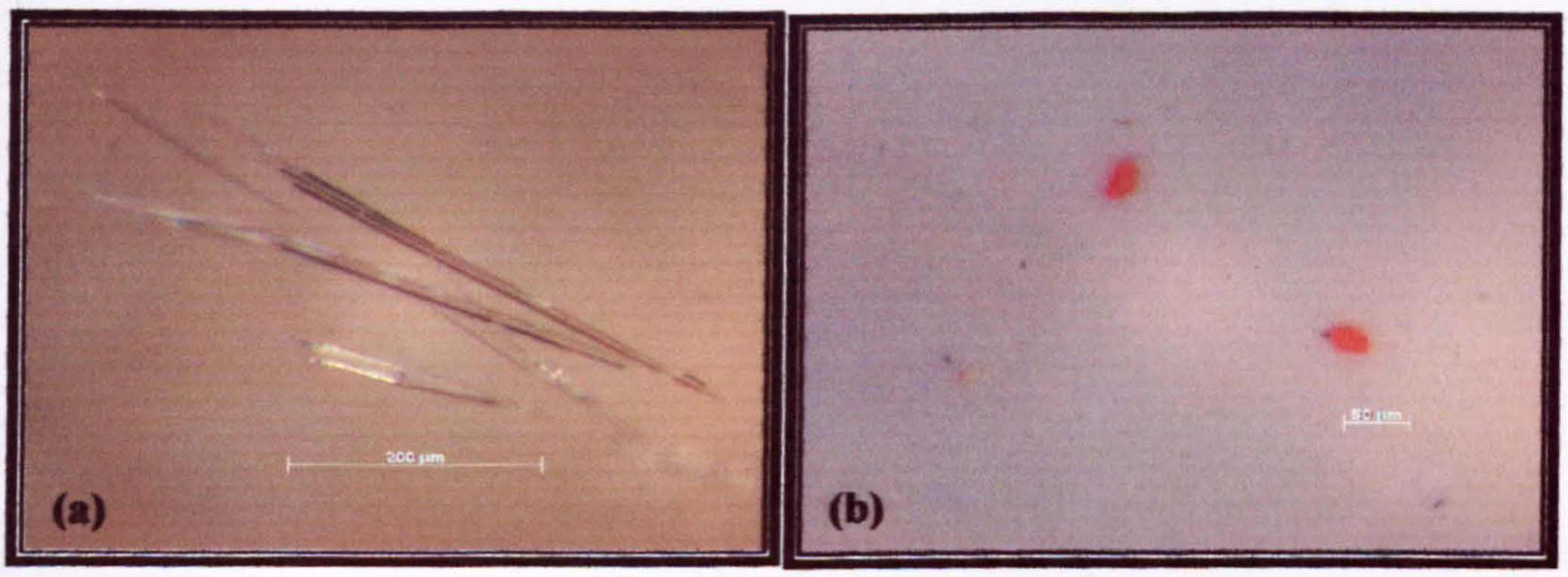

Figure 7.11: *In-situ* micrographs of Cl and SO_4 crystals formed on Nanomax membrane at 60 g l^{-1} salinity: (a) Cl crystals, bar = 200 µm; and (b) SO_4 crystals, bar= 50 µm.

The individual impact of cations was also studied in this experiment. Two cations (i.e. Na^+ and K^+) were assessed for their impacts on permeate flux at 30 g l^{-1} and 60 g l^{-1} salinities. Two different RO membranes (i.e. ADF and Nanomax) were independently examined in this experiment.

For the ADF membrane, the single impacts of the absence of each of Na^+ and K^+ at both salinities on permeate fluxes generally showed irregular patterns, especially at pressures above 27 bar (Figure 7.12). When solutions with Na-free ions were applied, the critical flux was considerably higher at low salinity (i.e. 2,050 and 1,360 $kg.m^{-2}.h^{-1}$ for 30 and 60 g l^{-1} salinities, respectively). However, increasing salinity only caused an increase of 5-8% in the critical fluxes when treating solutions containing no K ions (i.e. 2,050 and 1,900 $kg.m^{-2}.s^{-1}$ for 30 and 60 g l^{-1} salinities, respectively). This is low, especially considering the scatter in the data.

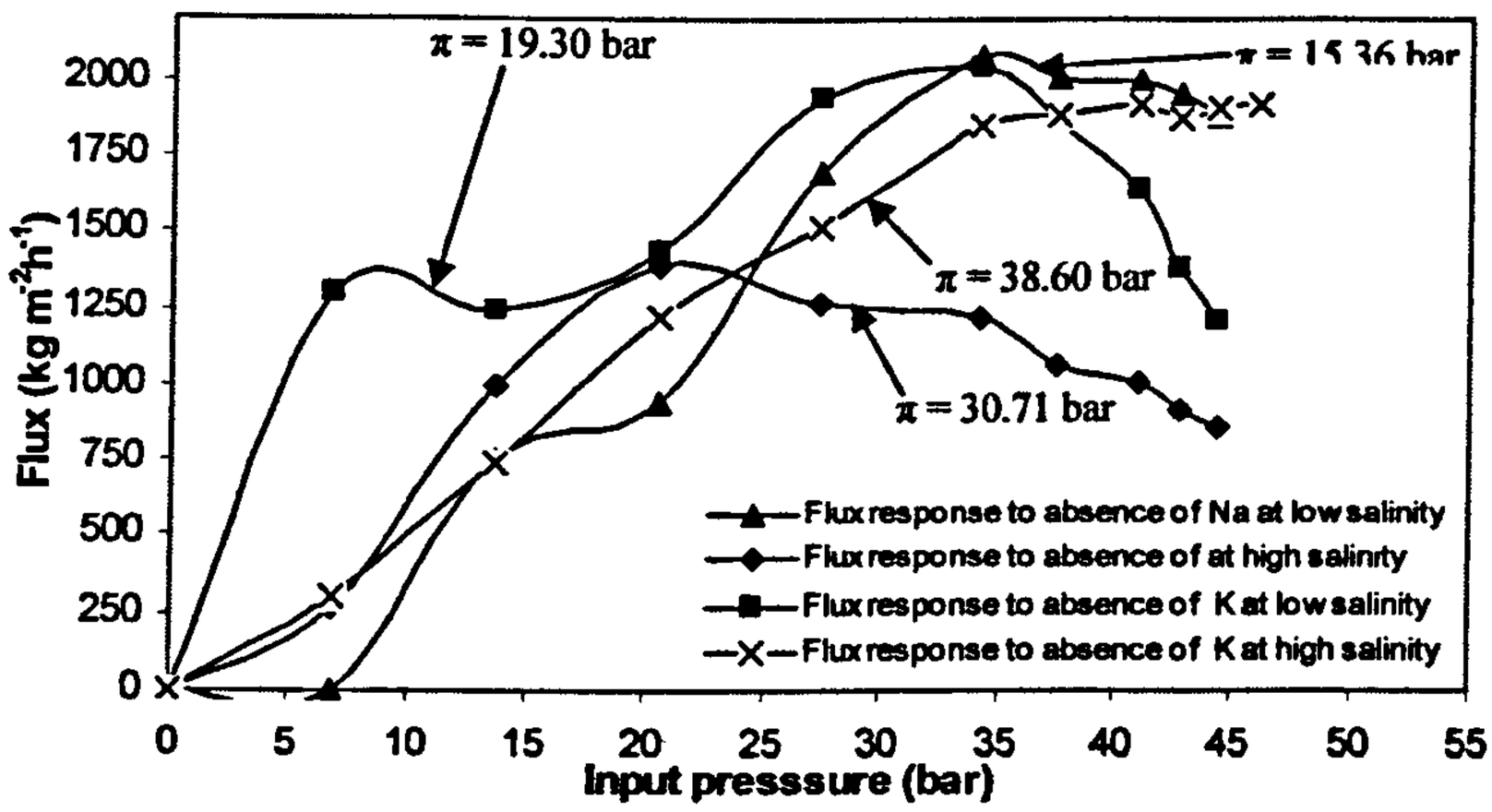

Figure 7.12: Flux response to cations absence at various salinities using ADF membrane.

For the low salinity experiment, the flux patterns exhibited two-stage fouling modules, which were supported by the flux productivity of each case. The first flux decrease occurred at the beginning of the filtration at relatively lower pressures (e.g. 6.8 and 13.6 bar for solutions of K-free and Na-free ions, respectively), indicating the passage of either sodium or potassium crystal nuclei through the membrane channels representing channel-narrowing fouling model (Case A, Figure 2.17, Chapter 2). With increasing pressure, some sodium or potassium crystals deposited into the internal structure of membrane, reducing the overall size of membrane pores, and increasing the rejection. The second flux decline was experienced for both samples when the pressure was increased to 34 bar. This flux decrease indicated that the pores

became too small for internal deposition, and a fouling cake started to build up at the membrane surface, meanwhile the rejection reached a plateau. This flux decrease represented a gel/cake layer formation fouling model (Case C, Figure 2.17, Chapter 2). The *in-situ* micrographs represented in Figures 7.13-a and 7.13-b show the deposited sodium cake layer and potassium crystals on the ADF membrane surface during hypersaline sample filtration (i.e. 60 g/l) at elevated pressures.

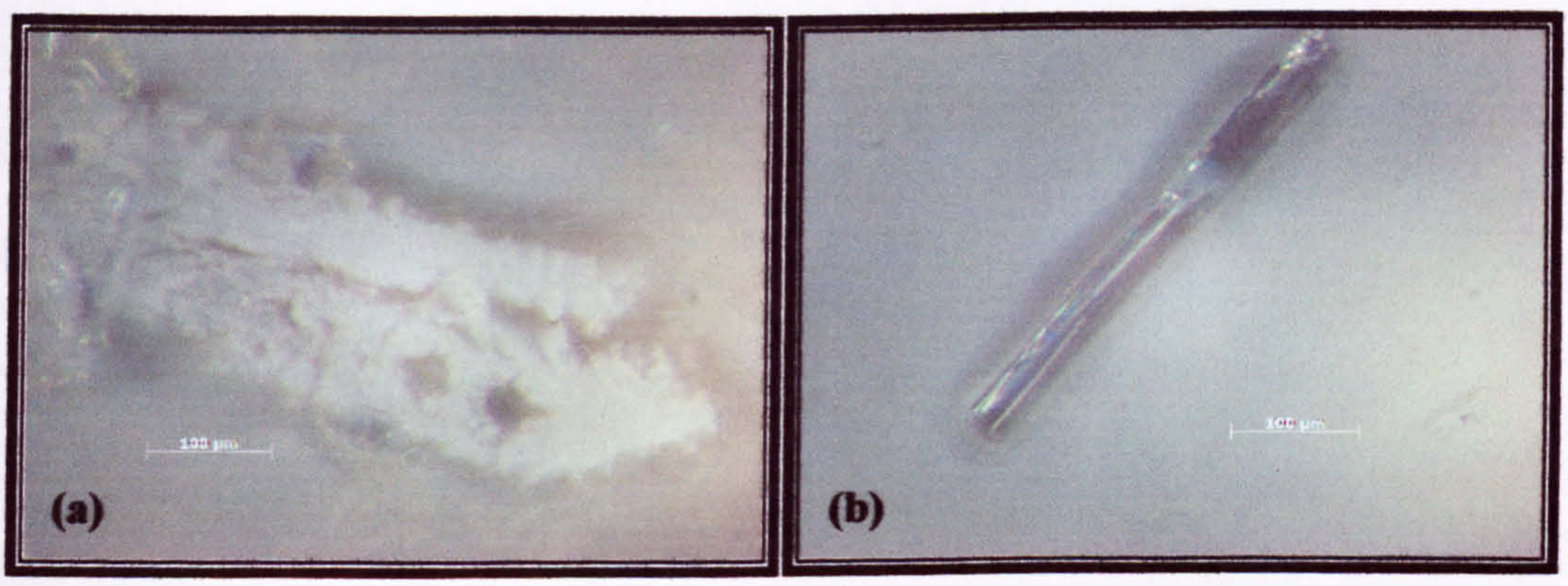

Figure 7.13: *In-situ* micrographs of Na^+ and K^+ crystals formed on ADF membrane at 60 g/l salinity: (a) Na cake layer, bar = 100 µm; and (b) K crystal, bar= 100 µm.

On the other hand, the Nanomax membrane exhibited a higher performance in terms of flux productivity (Figure 7.14). When sodium was absent, the results showed that the critical fluxes were 3,400 and 2,600 $kg.m^{-2}.h^{-1}$, corresponding to 30 and 60 $g\ l^{-1}$ salinities, respectively. These fluxes were produced at similar pressure (i.e. 34 bar), however, a sharp decline in these fluxes was observed beyond this point. This decline may be due to the solid texture of the potassium crystals compared to the comparatively porous sodium crystals (Figures 7.15-a and 7.15-b). This cake layer acts as a double membrane, and allows passage of solution through them at elevated pressures (Song and Yu, 1999).

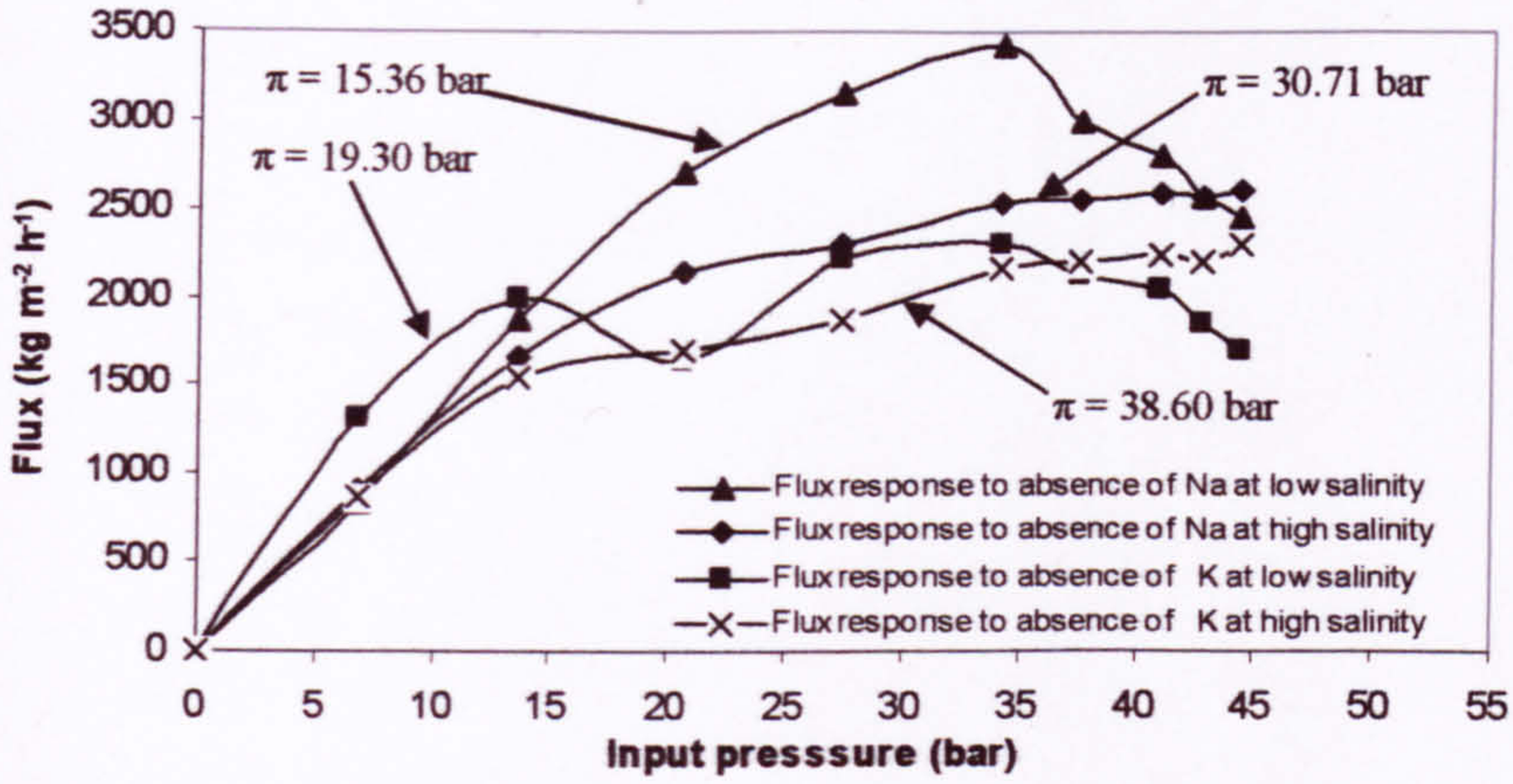

Figure 7.14: Flux response to cation absence at various salinities using the Nanomax membrane.

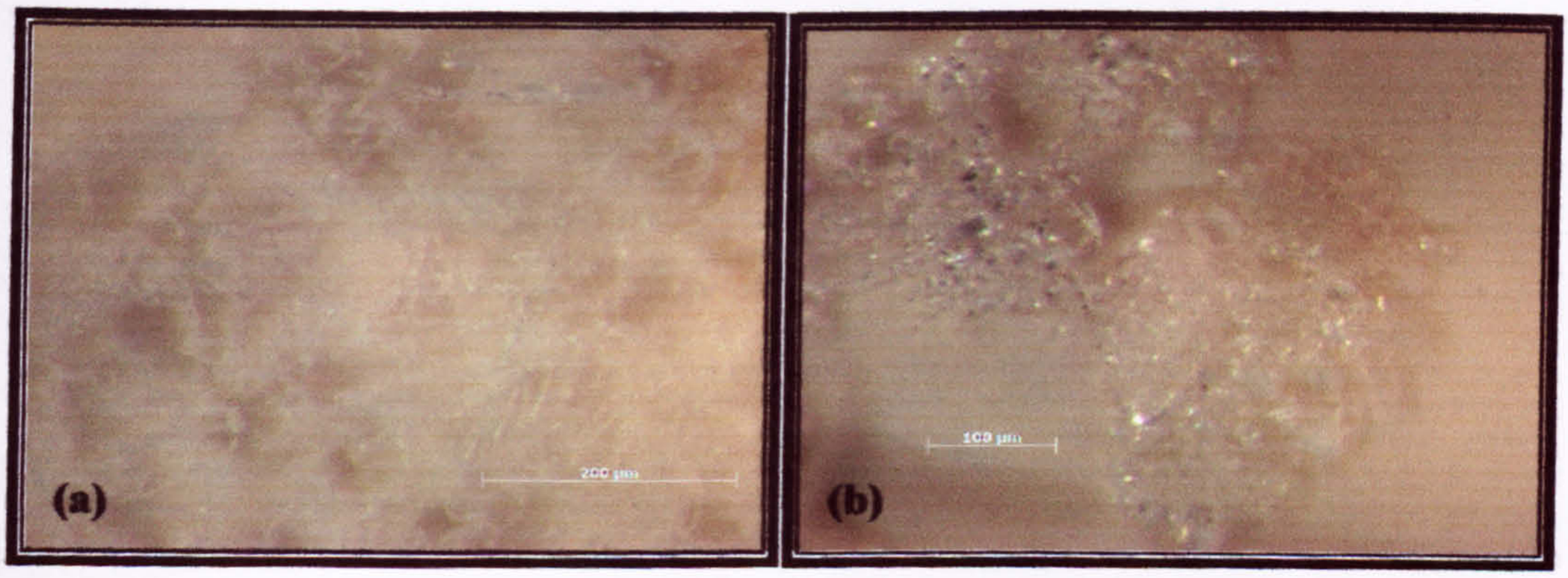

Figure 7.15: *In-situ* micrographs of Na^+ and K^+ crystals formed on Nanomax membrane at 60 g l^{-1} salinity: a) Na crystal, bar = 200 µm; and b) K crystal, bar= 100 µm.

The permeate flux reduction and increased salt rejection can be explained by the reduction of the pore size (or pore volume) of RO membranes. Furthermore, changes in the osmotic pressure at the membrane surface may also explain the decrease in the hydraulic permeability. Increased salt rejection, coupled with concentration polarisation, results in an increase in the osmotic pressure. Because the operating pressure of the system was kept constant, the increased osmotic pressure results in a decreased net driving pressure which in turn leads to a decreased permeate flux.

7.3.4 Effect of Biological Constituents (Biofouling) on Flux Behaviour

Fouling experiments were performed to evaluate the fouling potential of the biomass with two types of RO membranes (ADF and Nanomax membranes) and different salinities (30 and 60 g l^{-1}). All the fouling experiments were performed under identical operational and chemical conditions, and were analysed and visualised as quickly as possible.

As shown in Figure 7.16, when the ADF membrane was used, the results clearly show that an increase of salinity from 30 g l^{-1} to 60 g l^{-1} resulted in a relatively small flux decrease (with an average ≤ 12%). The flux behaviour of chemical samples was very similar, representing pore narrowing in the first instance followed by cake layer formation at elevated pressures, as discussed in the previous section.

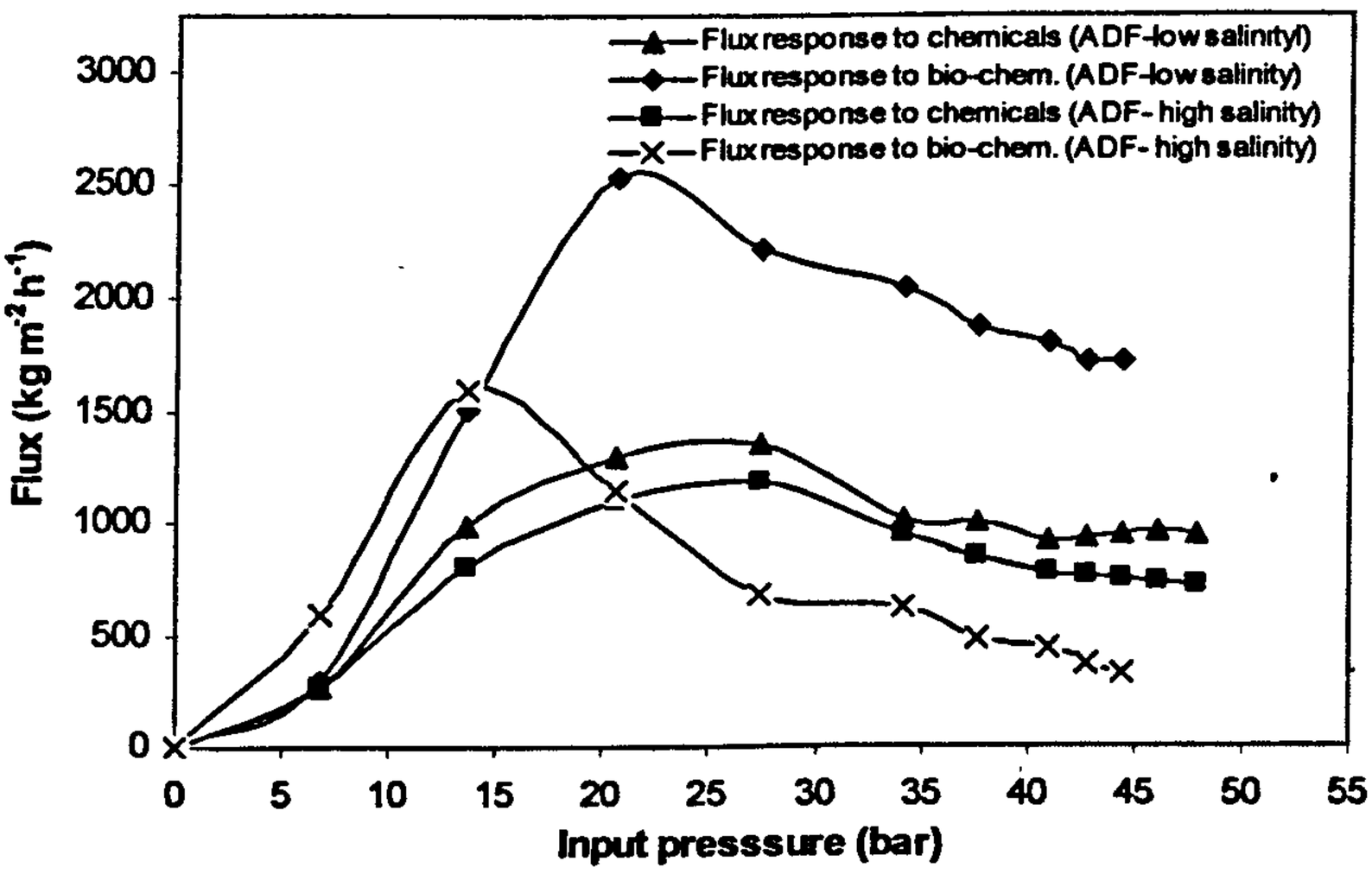

Figure 7.16: Flux response to both chemical and biological species at various salinities using the ADF membrane.

However, the effect of the biomass accumulation on the permeate flux productivity and behaviour showed very different and unexpected patterns. Surprisingly, for the low salinity experiment (30 g l^{-1}), the results showed that the flux productivity improved by approximately 2-fold in the presence of biomass (i.e. the maximum flux

increased from 1,330 to 2,550 $kg.m^{-2}.h^{-1}$). The permeate flux increased from 215 to 2,550 $kg.m^{-2}.h^{-1}$ when the transmembrane pressure was increased from 6.7 to 20 bar, reaching its critical flux at this point, followed by a gradual flux decrease at elevated pressures, ending with a flux productivity of 1,730 $kg.m^{-2}.h^{-1}$ at a pressure of 48.5 bar. Although, the behaviour of the flux pattern did not change when the fouling experiment was performed using a higher salinity (e.g. 60 g l^{-1}). However, the flux decreased by approximately 30-40% during this experimental run compared to the fouling experiment using only chemical-containing samples. In this experiment, when the transmembrane pressure was increased from 0 – 14.7 bar, the flux increased exponentially, reaching its critical flux at a comparatively lower pressure (14.7 bar), then the flux sharply decreased until it stabilised at pressure values $\geq$ 27 bar.

The flux behaviour that occurred during these experiments may be explained based on the *in-situ* micrographs taken during each run, and on the ESEM pictures taken after dismantling the membranes after each run. The *in-situ* micrographs of the ADF membrane surface during biological fouling experiments are illustrated in Figures 7.17-a and 7.17-b for 30 g l^{-1} and 60 g l^{-1} salinities, respectively. Additionally, the ESEM pictures taken after destructive autopsies of the ADF membranes used in this experiment are shown in Figures 7.18 and 7.19.

When the biological fouling experiment was performed at low salinity (i.e. 30 g l^{-1}) using the ADF membrane, the presence of bacterial cells in the solution was advantageous. The flux increase could be attributed to the scavenging role of the bacterial cells to provide bridging sites for the metallic ions in the bulk solution to agglomerate, which, in turn flocculated and became big enough to be washed out with the concurrent feed flow. Hence, the presence of microorganisms in relatively low salinity solutions (i.e. 30 g l^{-1}) is favourable in terms of protecting the membrane pores from blockage and/or becoming narrowed by salt crystals (initiators) formed at low pressures, as illustrated in the in-situ micrograph shown in Figure 7.17-a.

In biofouling systems, deposition rates are likely to be highly affected by the particle or aggregate size. As filtration proceeds with solute concentration and/or pressure increases, solute rejected by the membrane forms a layer of high ionic concentration near the membrane surface (concentration polarisation) during which the high solute ions start to form a thin layer of salt crystals on the membrane surface. In most cases, this layer is fragile and relatively porous with the advantage of protecting the membrane pores from blockage by small salt nuclei suspended in the bulk solution. However, the build-up of microorganisms in this layer makes it relatively hard, which completely fills the membrane's surface valleys forming a totally nonporous cake layer on the membrane surface (Figures 7.17-b and 7.18). This layer, in most cases, results in a sharp decline in the permeate flux, even at elevated pressures.

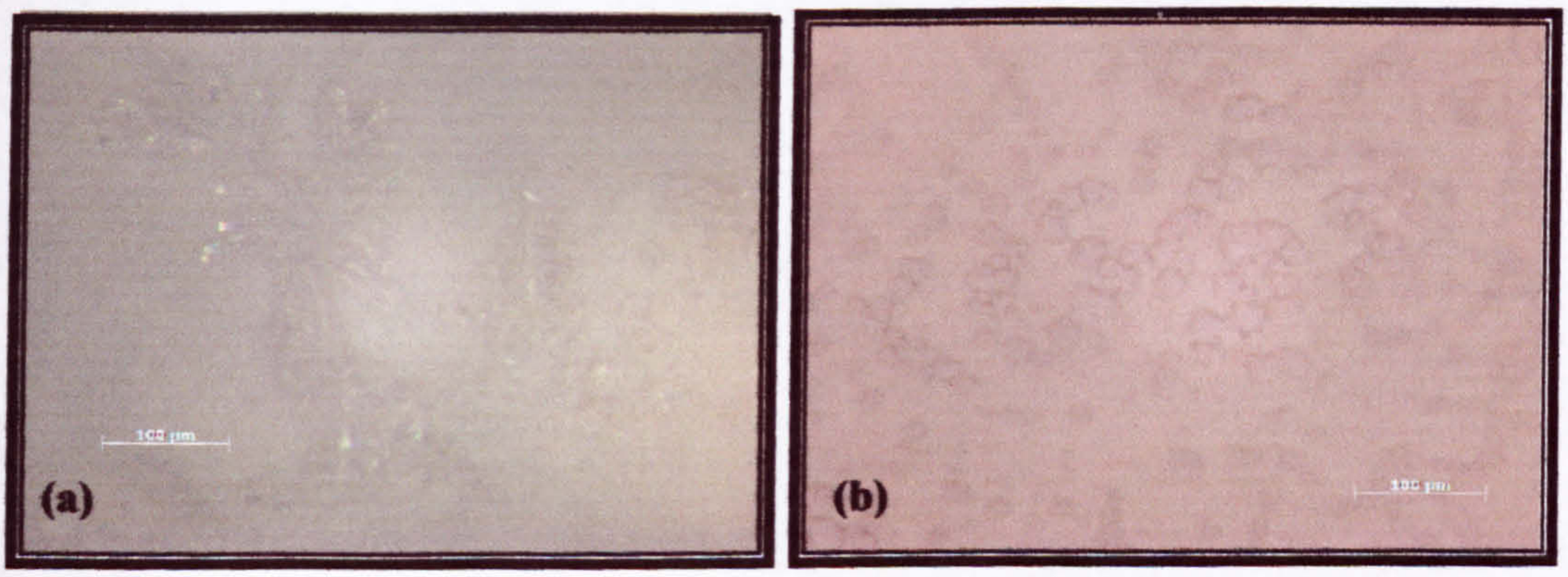

Figure 7.17: *In-situ* micrographs of Na^+ and K^+ crystals formed on ADF membranes at various salinities during biological fouling experiments: (a) 30 g l^{-1}, bar = 100 µm; and (b) 60 g l^{-1}, bar = 100 µm.

Figure 7.19 shows a closer look at the composition of the surface of the cake layer formed on ADF membrane at 60 g l^{-1} salinity. The picture shows a smooth cake layer composed of bacterial cells inter-bridged with salt crystals forming a hard cake shell.

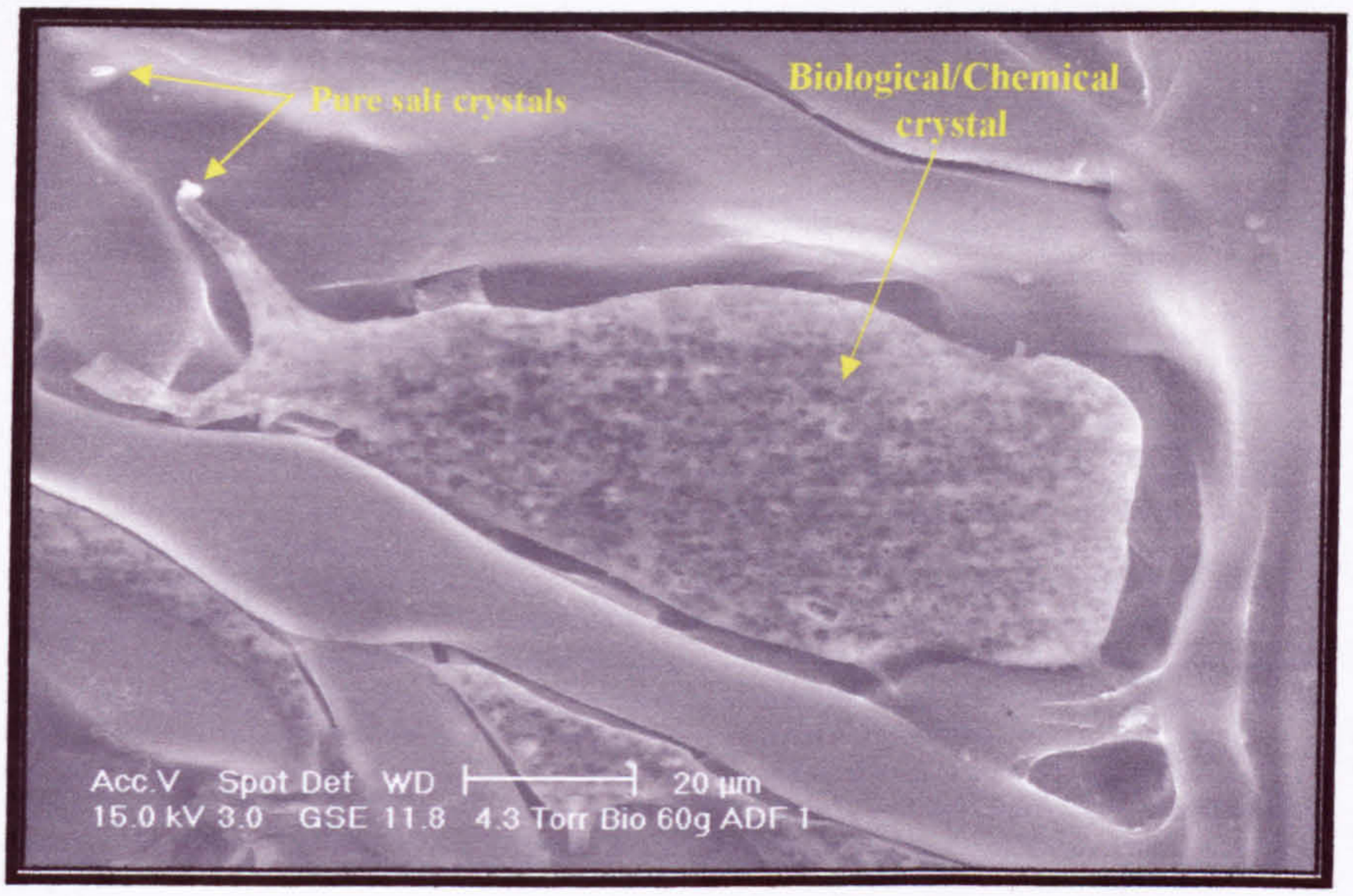

Figure 7.18: ESEM micrograph of ADF membrane showing a biological floc trapping salt crystals filling cavities on the membrane surface, bar = 20 µm.

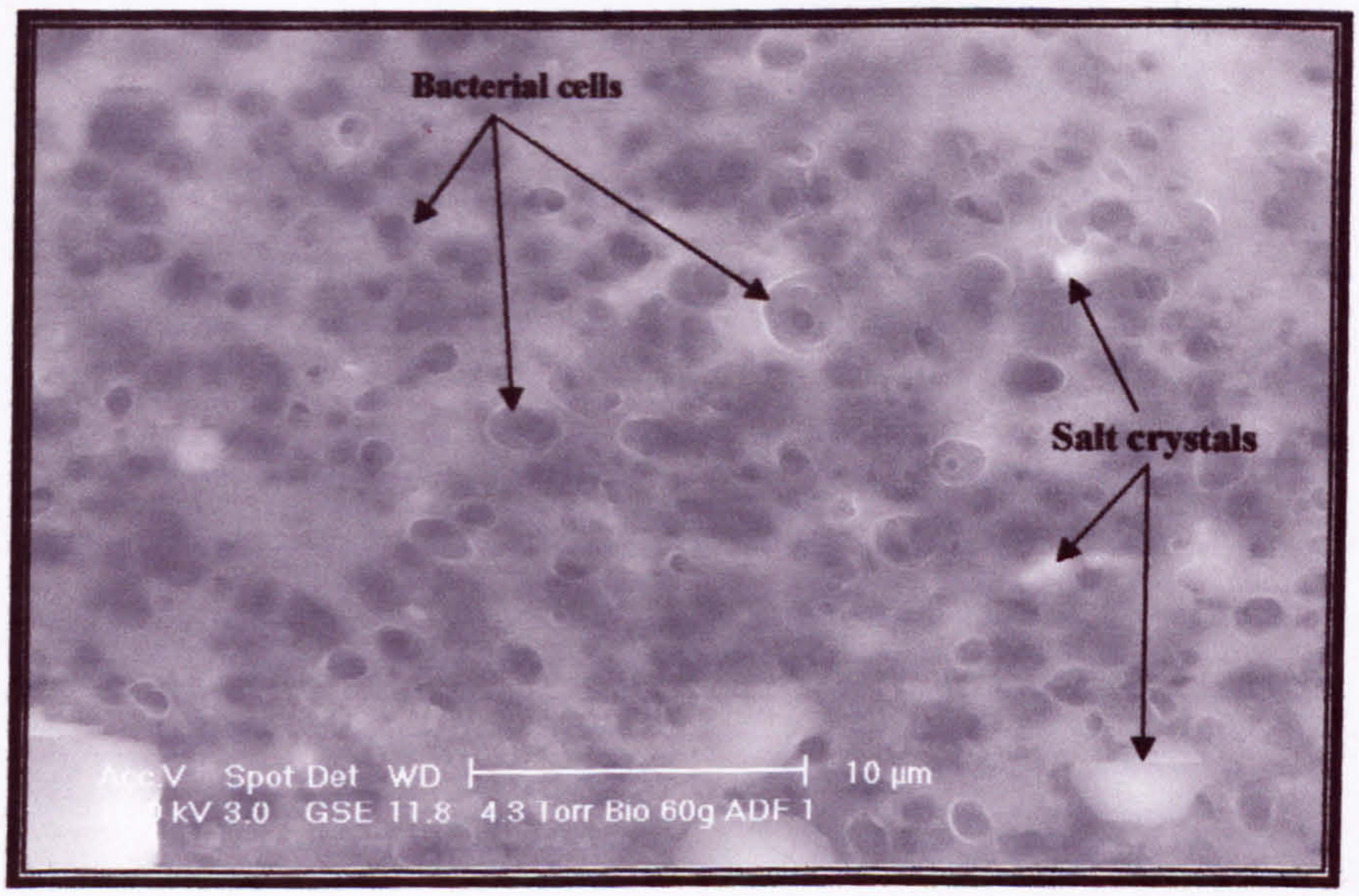

Figure 7.19: ESEM micrograph of ADF membrane showing a closer look at the surface of a biological/chemical floc precipitated on the membrane surface, bar = 10 µm.

When the Nanomax membrane was used, the results clearly show that an increase in salinity from 30 g l^{-1} to 60 g l^{-1} caused an average flux decline of approximately 18% (Figure 7.20). The flux behaviour of the chemical samples revealed similar patterns at different salinities, representing exponential flux productivity when pressures were increased from 6.7 to 20 bar (for 30 g l^{-1} salinity) and 6.7 to 13.7 bar (for 60 g l^{-1} salinity), followed by stabilised fluxes due to cake layer formation at elevated pressures.

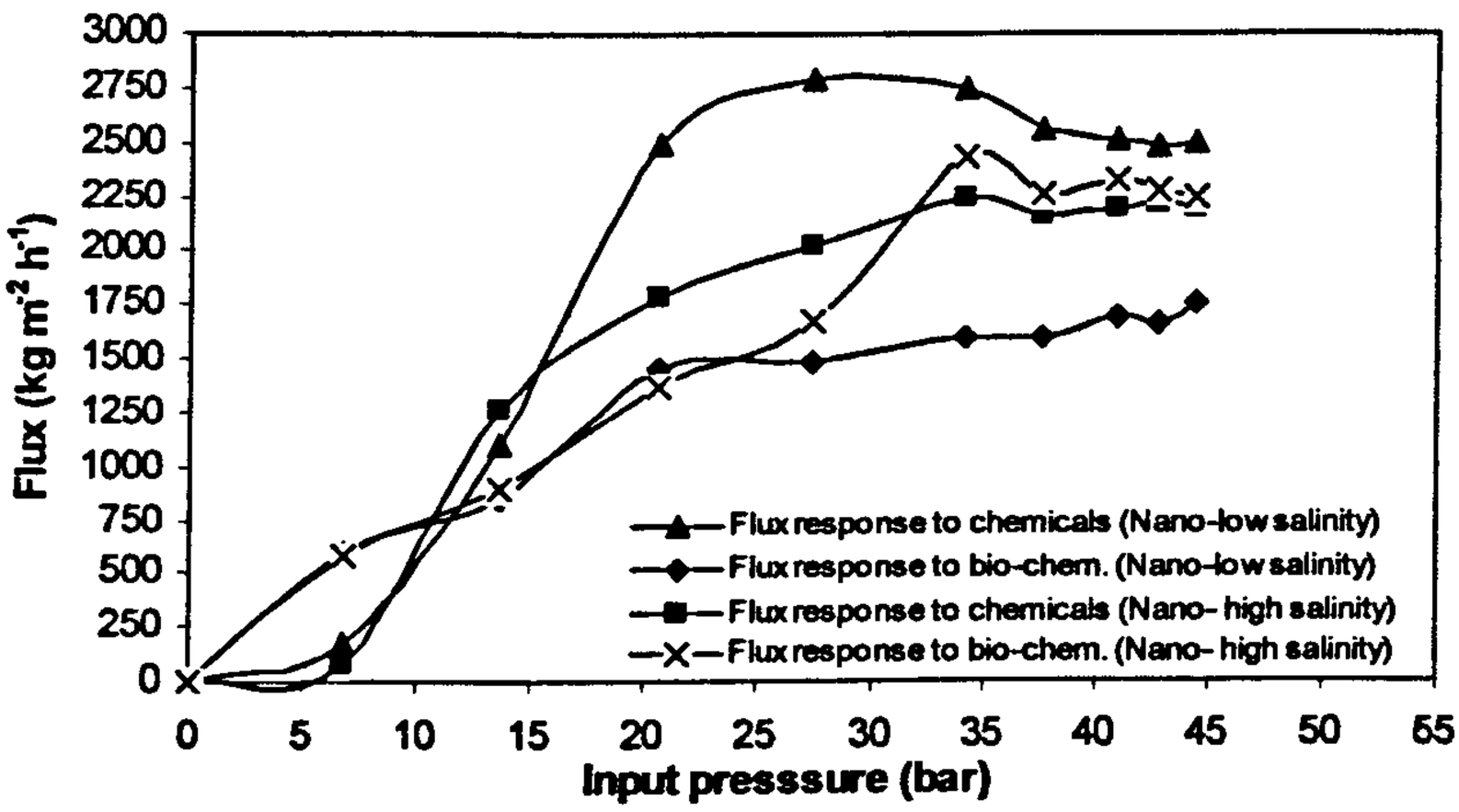

Figure 7.20: Flux response to both chemical and biological impacts at various salinities using the Nanomax membrane.

In the biological fouling experiment using the Nanomax membrane, the flux behaviour exhibited similar patterns at different salinities over a pressure range from 0 to 20 bar. However, at pressure above 20 bar, when this membrane was applied for low salinity operation, the permeate flux decreased remarkably, yielding about 40-50% flux productivity compared to the results of the chemical sample at similar conditions with no biomass added (Figure 7.20). Interestingly, at higher salinity (60 g l^{-1}), the permeate flux increased exponentially, reaching its maximal value (i.e. 2,430 $kg.m^{-2}.h^{-1}$) at a pressure of 34 bar, which was even approximately 8% higher than using a chemical sample without biomass addition under identical conditions.

The *in-situ* micrographs taken during each run, as well as the ESEM pictures taken after membrane autopsies may help in explaining this phenomenon. The *in-situ* micrographs shown in Figures 7.21-a and 7.21-b reveal the Nanomax membrane surface during the biological fouling experiment at 30 g l^{-1} and 60 g l^{-1}, respectively.

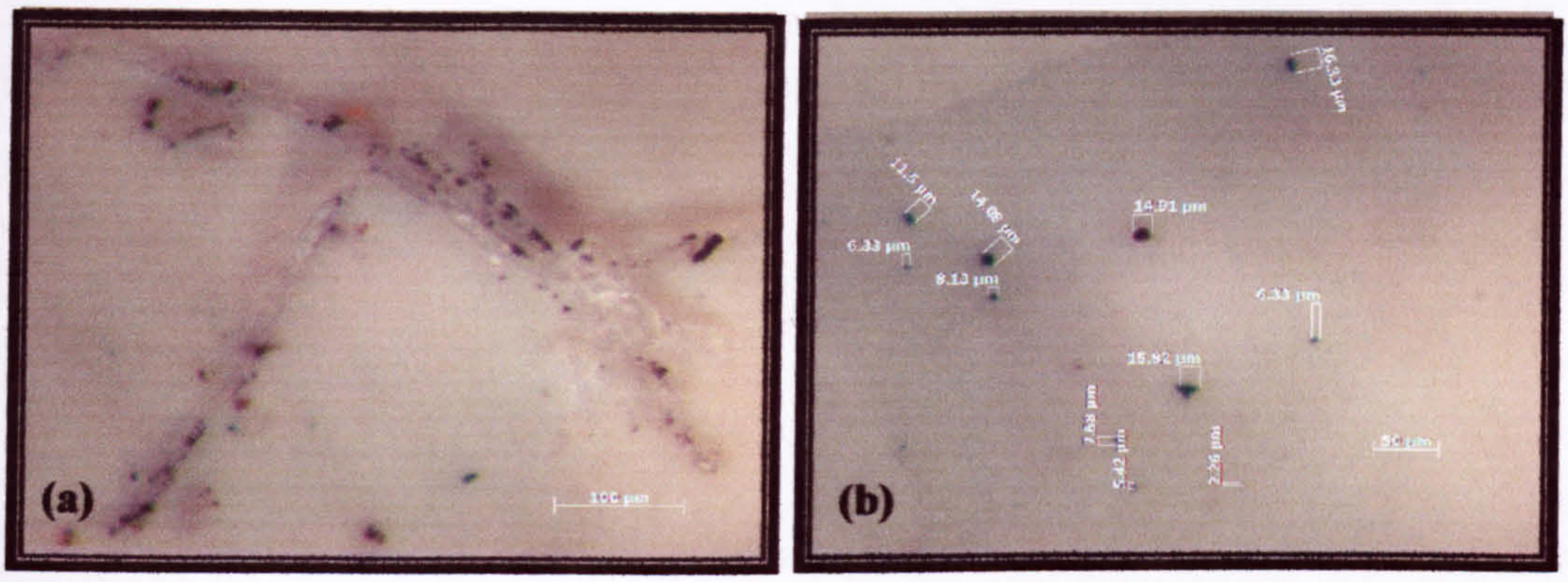

Figure 7.21: Micrographs of metal crystals and biomass flocs formed on Nanomax membrane at various salinities: (a) 30 g l^{-1} salinity, bar = 100 µm; and (b) 60 g l^{-1} salinity, bar = 50 µm.

At low salinity, due to the low solute concentration, the bacterial cells act as bridging sites (nuclei initiators), trapping the salt microcrystals, which could be easily washed out by the concurrent flow with the concentrate. These microcrystals, in conjunction with the bacterial cells, form hard cake layers with various shapes and structures on the membrane surface, which cause a reduction in the flux productivity. On the other hand, at higher salinity (60 g l^{-1}), no salt crystals or cake layers have been spotted on the membrane surface during the experimental run. The *in-situ* micrograph of the membrane surface (Figure 7.21-b) reveals only green accumulations or small flocs of cyanobacteria, ranging in sizes from 2-16 µm, randomly scattered on the membrane surface. The reason that no salt crystals were formed at high solute concentration may be because of the ease of salt microcrystals formation at such solute concentration and elevated pressure. This can also explain the flux reduction at lower pressures (i.e. at 13.7-27 bar) (Figure 7.20). The accumulated cyanobacterial flocs on the membrane surface may continue to grow, until reaching enough mass and volume

to be swept out with the concurrent flow, or to stick on the membrane surface forming a pure bacterial biofilm attached to the membrane surface (Flemming, 1997; Al-Ahmad *et al.*, 2000; Baker Dudley, 1998).

The ESEM micrograph shown in Figure 7.22, taken after dismantling the Nanomax membrane after finishing the experimental run, shows some bacterial flocs and also some salt crystals scattered on the membrane surface. The presence of salt crystals on the membrane surface was only observed after dismantling the membrane, and not during the run. This observation was also noticed when a Nanomax membrane was dismantled after a chemical sample run with no added biomass under similar conditions (Figure 7.23). This phenomenon might be due to the evaporation of some very concentrated water droplets scattered on the membrane surface after dismantling, as the membrane samples were viewed under the ESEM machine a couple of hours later. The other reason of this observation might be the salt scaling build up only starts after prolonged filtration times; however, no further results were obtained in this experiment to support either of these hypotheses.

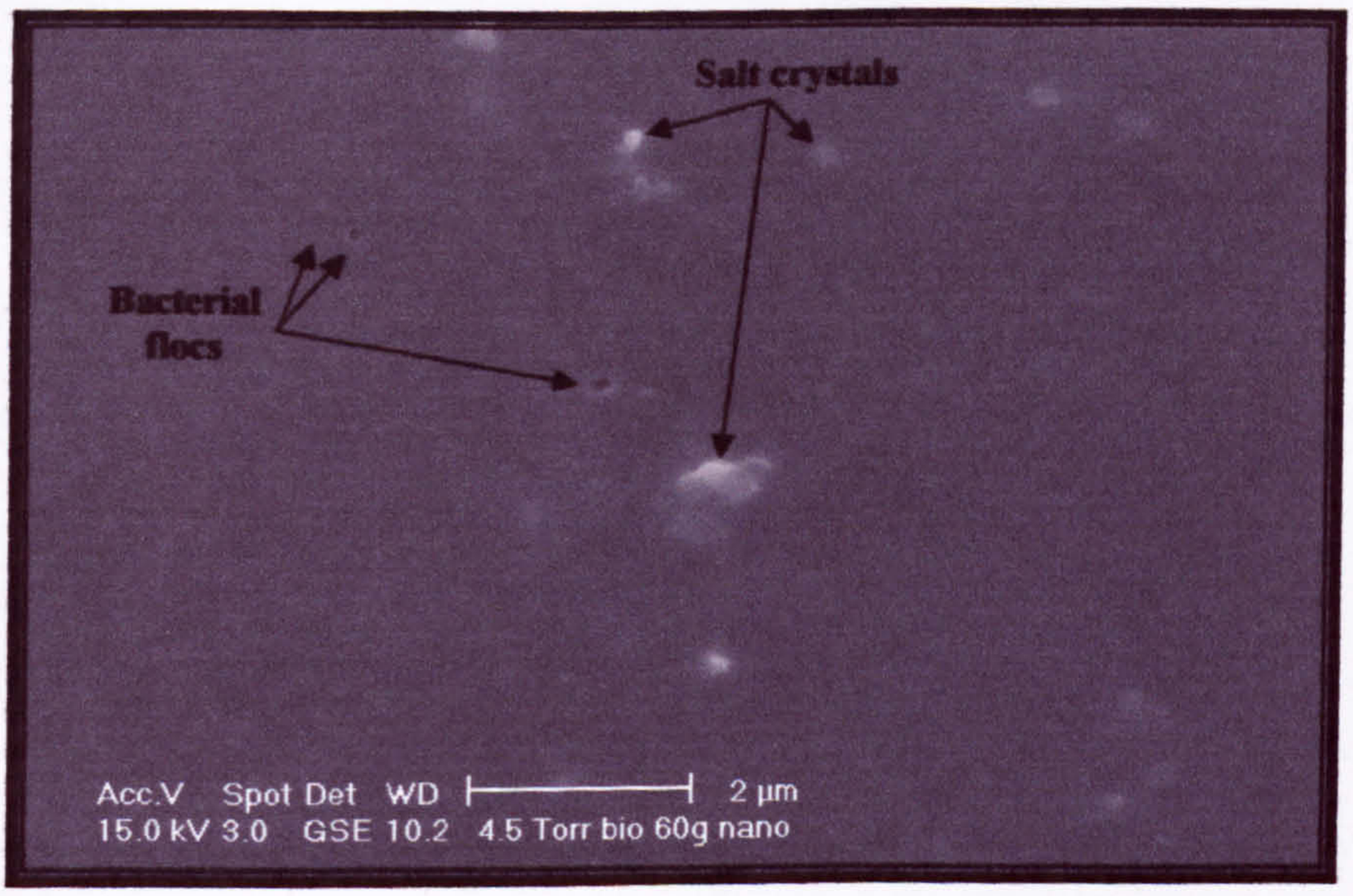

Figure 7.22: ESEM micrograph of Nanomax membrane showing a biological floc and salt crystals scattered on the membrane surface, bar = 2 µm.

Figure 7.23: ESEM micrograph of Nanomax membrane showing salt crystals scattered on the membrane surface deposited during high salinity chemical sample filtration, bar = 2 µm.

7.3.5 Effect of the Biomass Removal on Flux Behaviour

The impact of biomass removal prior to filtration has also been investigated in this experiment. The pretreated samples were applied to two RO membranes: ADF and Nanomax. When the ADF membrane was used, the results in Figure 7.24 show a large recovery in the permeate flux indicating a significant effect of biomass on biological fouling and flux decrease. The flux recovery started with approximately 50% at a pressure of 20 bar, and ended with more than 80% at a pressure of 44 bar, with an average of overall recovery of 62%. The flux behaviour of the pretreated biological sample exhibited a stable pattern, which started with an exponential increase between pressures 6 and 20 bar, followed by stabilisation with a minor flux decrease (8–10%) due to the salt crystal precipitation at elevated pressures. As demonstrated in Figure 7.25, the ESEM picture shows precipitation of salt microcrystals on the membrane surface in or near pore mouths, causing partial pore blockage which ultimately led to pore narrowing and fouling of the module (case A, Figure 2.17, Chapter 2).

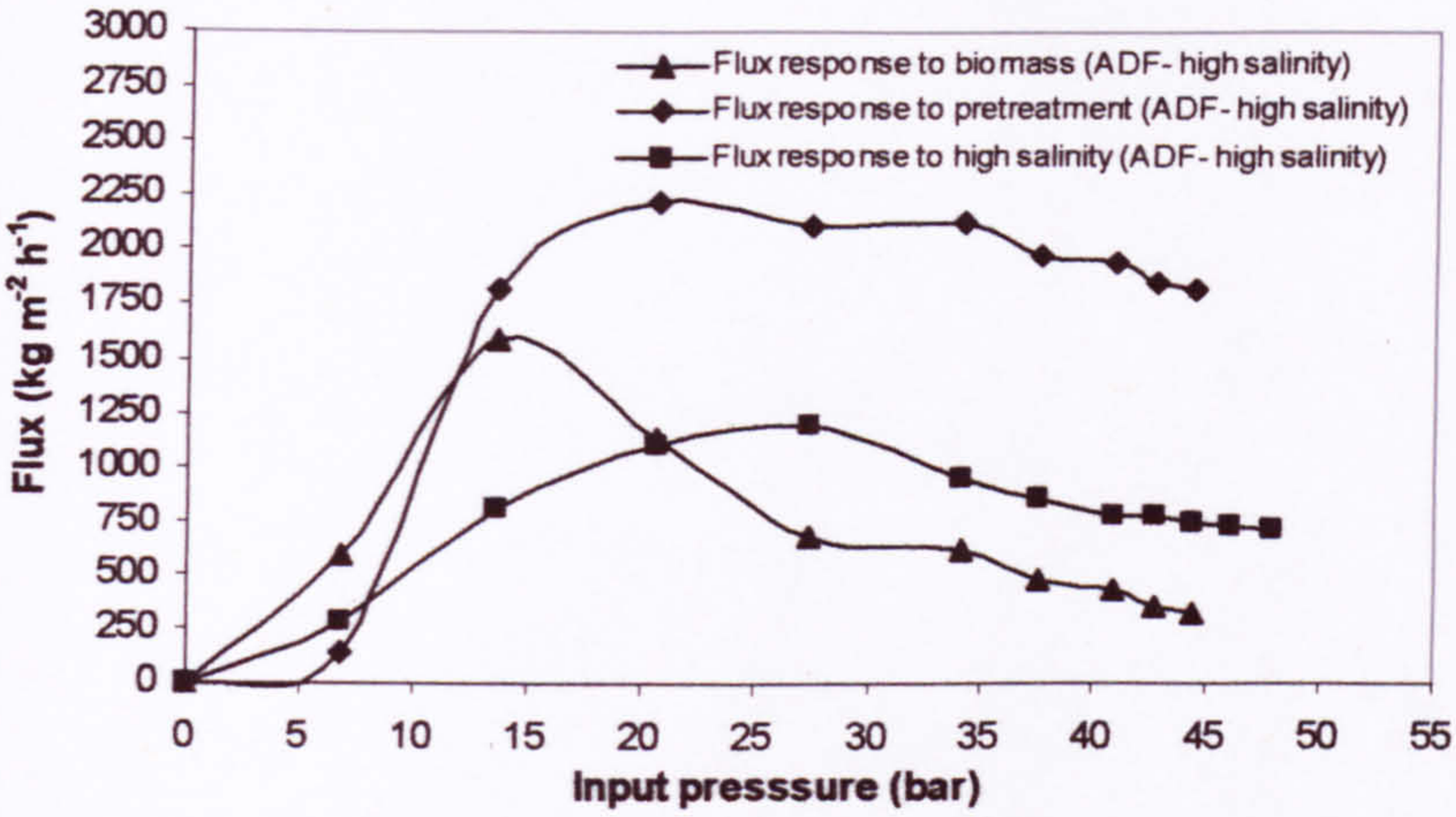

Figure 7.24: Flux response to biomass removal impact using the ADF membrane.

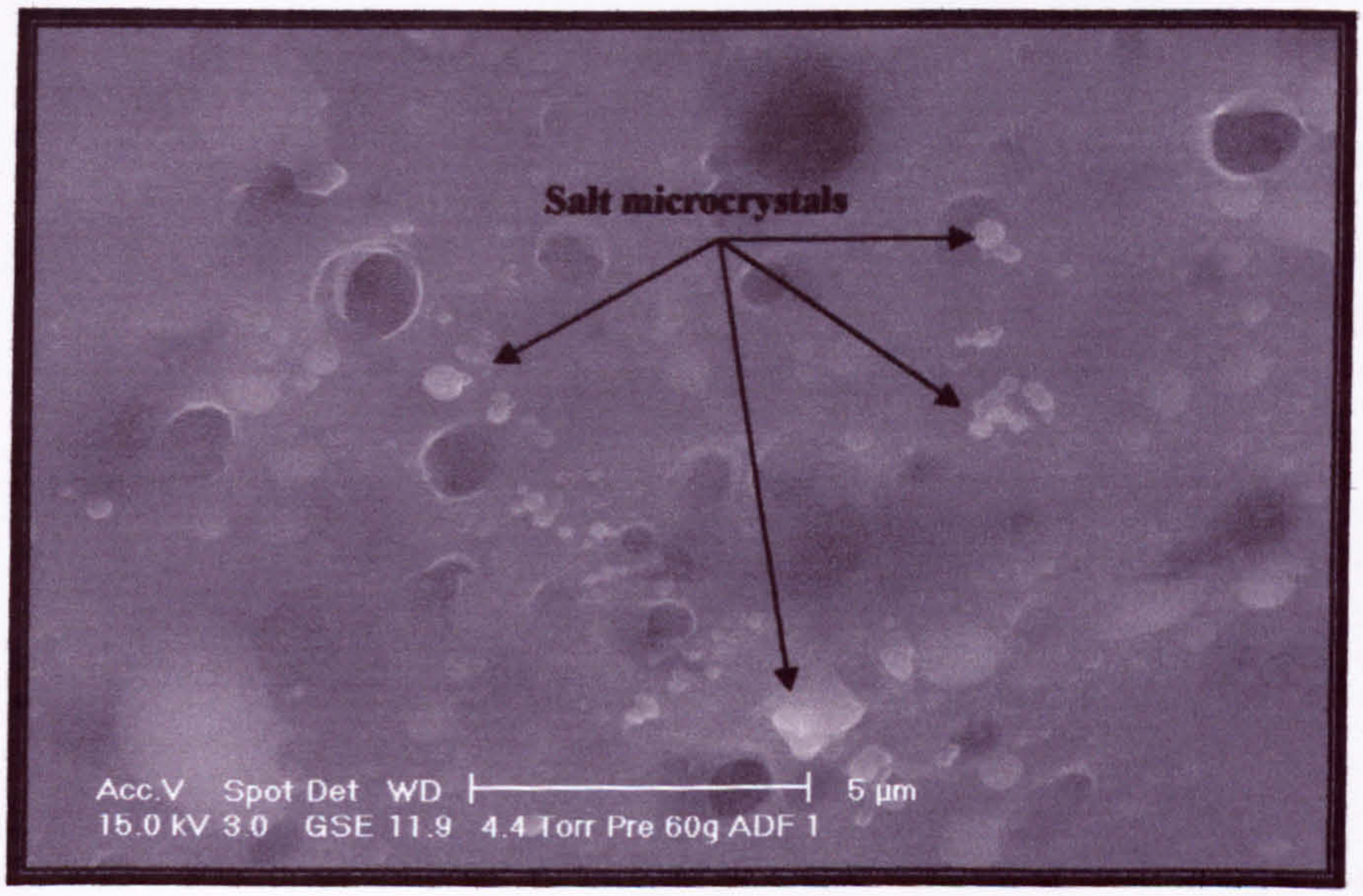

Figure 7.25: ESEM micrograph of ADF membrane surface showing the start of salt crystal deposition in and near membrane pore mouths during pretreated biological sample filtration at 60 g/l salinity, bar = 5 µm.

Since the biological samples were microfiltered (pretreated) through 2-step microfilters (0.45 µm followed by 0.22 µm) prior to filtration, it is assumed that the great majority of the bacterial cells (e.g. all bacterial cells with sizes $\geq$ 0.22 µm), initially added to the biological samples, were removed during the pretreatment

process. Then, only microparticles with sizes of small fractions of a micrometer (i.e. ≤ 0.22 μm) were left in the in the solution. In this experiment, these microparticles may have acted as scavengers, attracting salt microcrystals to agglomerate once they initiated near the membrane surface, hence forming a salt cake layer at low pressures, which in turn protects the membrane channels from being blocked and/or narrowing with these microparticles. This hypothesis might explain the large permeate flux increase in ADF membrane due to pretreatment of the biological samples compared to chemical samples applied under identical conditions.

The flux behaviour of the Nanomax membrane when exposed to pretreated biological samples at high salinity (60 g l^{-1}) showed a similar pattern, compared to the chemical samples applied under similar conditions, as shown in Figure 7.26. The fluctuations in flux measured for the pretreated and chemical samples, performed at 60 g l^{-1} salinity, were in the range of ±7% calculated within the pressure range of 20 - 44 bar. The divergence results from the removal of biomass from biological samples compared to chemical samples and can be considered insignificant in terms of aggravating the biofouling problem. However, it slightly improved the flux productivity by ~5%, and caused more stabilised fluxes at elevated pressures (i.e. ≥ 34 bar).

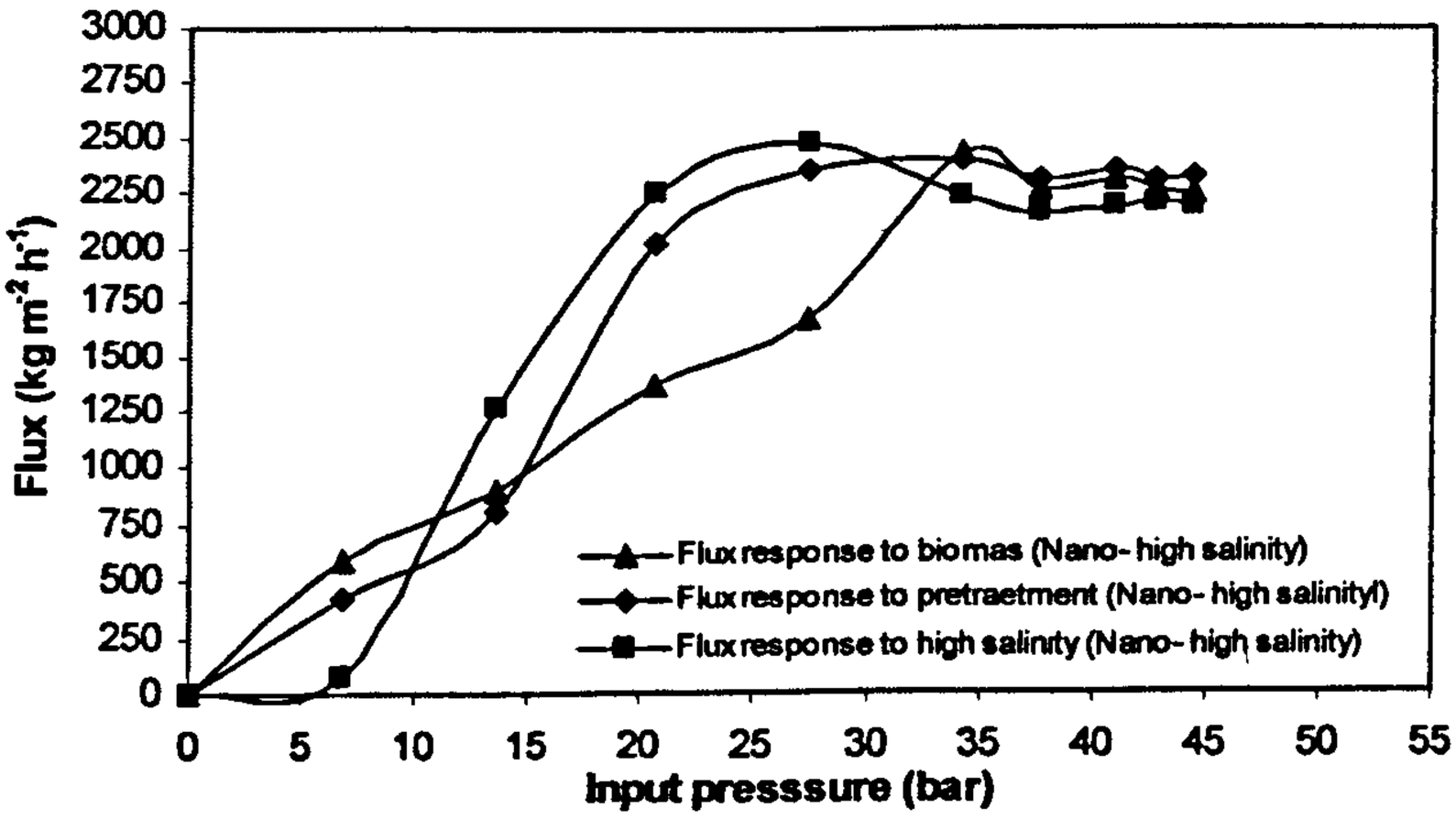

Figure 7.26: Flux response to biomass removal impact using the Nanomax-95 membrane.

Unlike the ADF membranes, due to their relatively smooth surfaces, the Nanomax membranes allow for formation of bigger bar-shape salt crystals (Figure 7.27). This big size and long shape of the salt crystals formed on the membrane surface is believed to help in accumulating other minute salt nuclei until becoming big enough to be washed out with the concurrent flow.

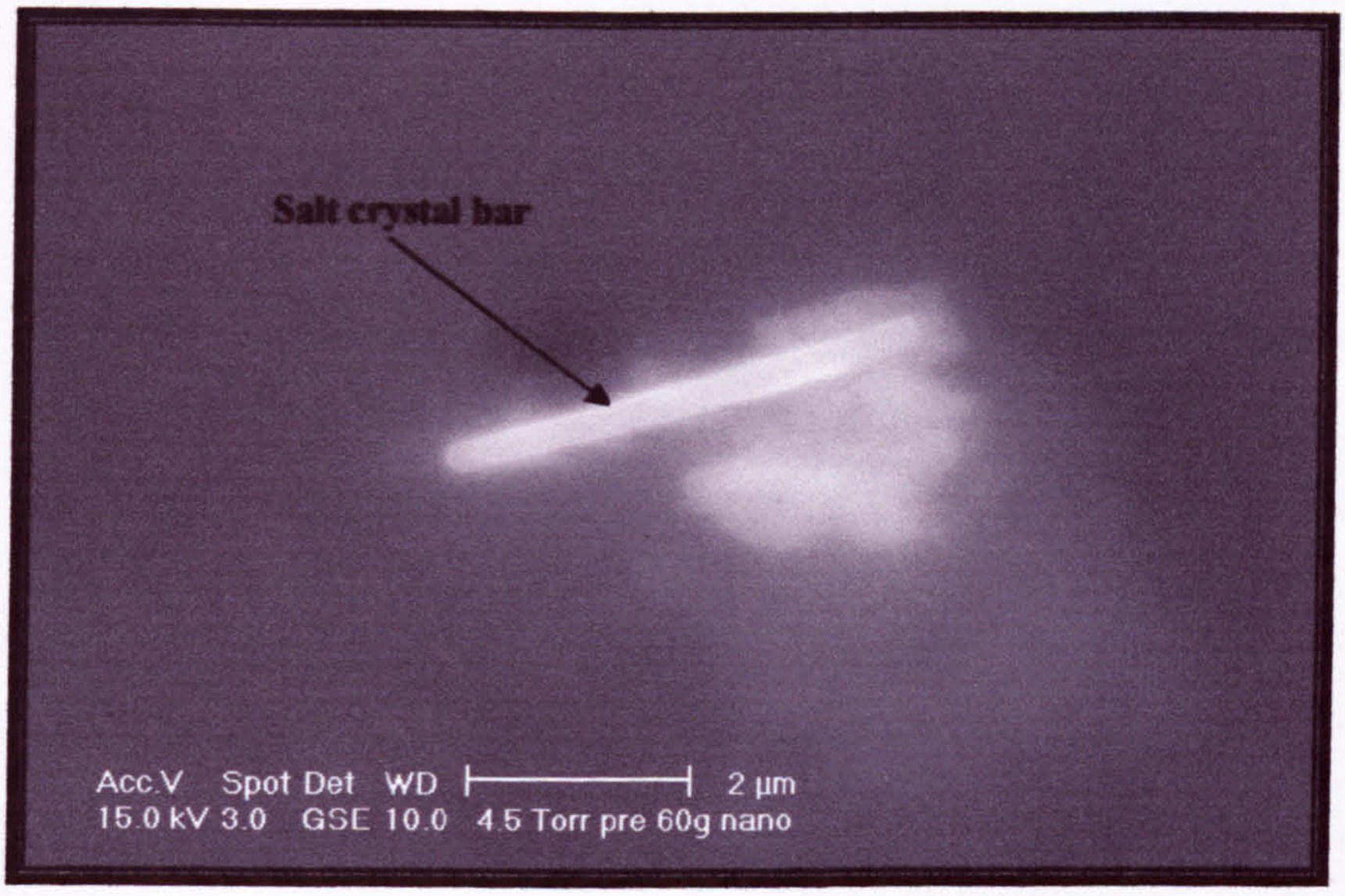

Figure 7.27: ESEM micrograph of the Nanomax membrane surface showing the start of salt cake build-up around the salt crystal bar during filtration of the pretreated biological sample at high salinity, bar = 2 µm.

7.4 Summary

The influence of salinity and biofouling on the permeate flux behaviour of RO membranes was investigated using a laboratory-scale crossflow filtration unit, with artificial water samples containing defined chemical and biological ingredients. In this experiment, two salinities (30 g l^{-1} and 60 g l^{-1}) were used to investigate the permeability of two RO membranes (ADF and Nanomax) of different surface roughness. The permeate flux was measured for each membrane individually at various conditions in order to analyse single and combined impacts of membrane type, specific chemical constituents, biomass, and biomass removal (pretreatment) on the flux behaviour and productivity under controlled conditions.

Membrane surface roughness has significant effects on the flux productivity and fouling potential. The overall productivity of the ADF membranes was about only 50% of the productivity of the Nanomax membranes under identical conditions. Furthermore, the type of membrane used exhibited different flux behaviour patterns at various salinities, based on the type(s) of fouling these membranes encountered. For ADF membranes, the flux behaviour represented two types of fouling, namely: pore blocking/ narrowing, occurring at low pressures, and cake layer formation, occurring at elevated pressures and/or high solute concentration.

Salinity, a measure of solute concentration in a solution, has a considerable impact on permeate flux productivity and membrane permeability. However, in this experiment, the impact of increasing salinity from 30 g l^{-1} to 60 g l^{-1} on permeate flux productivity was relatively insignificant. In this experiment, the permeate flux decreased by averages of 16% and 12% when the salinity was increased by 2-fold (i.e. 60 g l^{-1}) for the ADF and Nanomax membranes, respectively.

The impact of single ions composing the solute concentration in the solution was also evaluated in this study. For both types of membrane, the results showed that the absence of chloride ions improved the permeate flux at low salinity (i.e. 30 g l^{-1}), however, the flux decreased tremendously at high salinity (i.e. 60 g l^{-1}). In contrast, no change was observed on the permeate flux productivity when sulphate ions were absent from the solution for both types of membranes. Unlike anions, when the impact of omitting Na or K (cations) from the solution were evaluated, the permeate flux showed uncertainties in productivity and behaviour patterns, indicating their dependencies on each other for affecting the flux productivity and behaviour.

The severe combined chemical/biological fouling (biofouling) impacts on the permeate flux productivity and behaviour was also investigated. The addition of cultures of a halobacterium (*Halomonas pantelleriensis* sp. strain BAA003) and a cyanobacterium (*Euhalothece* sp. strain BAA001) to the chemical samples resulted in unexpected findings. When ADF membranes were used, the permeate flux

productivity was surprisingly extremely enhanced (by 41%) when biomass was added to low salinity samples. However, at higher salinity, the productivity of the permeate flux increased sharply (by 35%) only at low pressures and severely deteriorated (by an average of 86%) at pressures higher than 13.7 bar. On the other hand, the impact of biomass addition to the chemical samples on the permeate flux productivity and behaviour showed completely different results when the Nanomax membranes were used. The permeate flux showed a remarkable decrease (by an average of 35%) at low salinity. In contrast, at high salinity, the permeate flux decreased moderately (by an average of 22%) only at pressures below 27 bar, however, it increased gradually (by an average of 4%) with a pressure increase above 27 bar.

To minimise the biofouling impact on the permeate flux; pretreatment was carried out to eliminate the biomass from the biological samples used as feed water. The results of these experiments revealed that adequate pretreatment was performed, as the pretreated biological samples fully recovered their permeate flux productivity. Surprisingly, when the ADF membrane was used at high salinity, the permeate flux recovered by an average of 154% using pretreated samples compared to biological samples, however, the Nanomax membranes showed a smaller recovery of an average of 82% at pressures below 27 bar, and of an average of 106% at pressures above 27 bar.

Chapter 8

CONCLUSIONS AND RECOMMENDATIONS

8.1 Conclusions

Selected parameters were monitored in regard to the biological fouling "biofouling" impact of selected halotolerant bacteria on the permeate flux of RO membranes in hypersaline conditions. Two model microorganisms (a cyanobacterium *Euhalothece sp.*, strain BAA001; and a halobacterium *Halomonas pantelleriensis,* strain BAA003), which were recently isolated from Qabar-Onn Lake (located in the middle of the Sahara), were used in this research, due to their ability to grow in hypersaline waters and their capacity to extensively produce biofilms. Two RO membranes, made of different materials (a thin-film composite, ADF membranes; and a polyamide, Nanomax-95), were used in this research, due to their different surface roughness and their capacity to withstand higher pressure (up to 60 bar).

The bacterial isolation from Qabar-Onn Lake was performed based on conventional culturing methods; however, identifications were based on 16S rRNA gene sequencing. Although the cyanobacterial adhesion experiments were performed using rotating annular biofilm (RAB) reactors, the halobacterial adhesion assays were carried out using square coupons immersed in the bacterial cultures. All membrane tests were performed with a bench-scale high pressure reverse osmosis membrane test system (HPROMTS), using artificial saline samples, and operated in a continuous recirculation mode.

Based on the results of this research, the following conclusions can be drawn:

- Despite the high salinity of Qabar-Onn Lake (an average of 125 g l^{-1}), the preliminary studies showed a large biodiversity in the lake, which includes planktonic organisms such as brine shrimps (i.e. *Artemia salina*), diatoms

(Ajaili *et al.*, 1984), cyanobacteria, and halobacteria. In this research, two species of cyanobacteria (*Euhalothece* species, strains BAA001 and BAA002) and a halobacterium (*Halomonas pantelleriensis,* strain BAA003) were isolated and identified based on 16S rRNA techniques, which revealed that the new isolates were tentatively new species.

- The rapidly changing environment of Qabar-Onn Lake maintains microbial populations with versatile capabilities. Increases in salinity over time, caused by high evaporation, have led to a microbial community that exhibits a wide range of compatible solutes synthesis and accumulation. Whilst, the halobacterial species (i.e.*Halomonas pantelleriensis*), inhabiting this lake, accumulates glycine betaine, ectoine, and glutamate; the *Euhalothece* species accumulates glycine betaine as the sole compatible solute for their osmoadaptation.

- In addition to salinity, pH seems to be an important limiting factor in Qabar-Onn Lake biodiversity, especially for the cyanobacterial species (i.e. *Euhalothece*) inhabiting the lake. Furthermore, light transparency contributes, to some extent, to limit growth of numerous phototrophic microorganisms at the lake bottom (Ajaili *et al.*, 1984).

- Direct comparison between biofilms developed on various substrata of different materials of a wide range of surface roughness, and the RO membranes, was difficult due to the interference of other uncontrollable characteristics such as surface charge, wetability, and porosity. Biofilms were developed on all the substrata tested in various patterns and concentrations. The results showed that the increase of surface roughness had a direct impact (except for the ADF membranes) on the biofilm development and growth of all the substrata tested. A rougher surface can offer more shelter to fluid shear, hence reducing bacterial detachment. However, the ADF membranes, which have ridged topology, exhibited a higher tendency for bacterial adherence compared to the various substrata tested.

- Salinity had a significant and detrimental impact on the bacteria adherence to various substrata. At hypersalinities, the bacterial cells' adhesion to various material surfaces were minimal, which could be correlated to the impact of the high ionic concentrations on enhancing the surface charge values of various substrata, and/or effecting the production of the extracellular polymeric substances (EPS), which play a key role in the attachment mechanism.

- The quantitative determinations of permeate flux and direct qualitative autopsies of various RO membranes (e.g. the thin-film composite and the polyamide membranes) treating hypersaline waters provides a useful database concerning biofouling and scaling. Membrane surface roughness and salinity were found to hinder the membrane permeability. However, the latter had only minimal effects.

- Increased concentration polarization led to a higher concentration of retained salt crystals at the membrane surface. Regardless of the membrane type used, the impact of divalent (sulphate) ions improved the permeate flux at low salinity (i.e. 30 g l^{-1}), however, the flux decreased tremendously at high salinity (i.e. 60 g l^{-1}).

- In general, the effects of precipitation of divalent and monovalent crystals showed the former enhance fouling, while the latter hinder fouling at hyper salinities. Crystals from pure chemical crystallization are usually hard and tenacious, while the deposits in particulate fouling can be porous and susceptible to removal. Composite fouling is likely to be less significant in the polyamide (smoother) RO membranes than in the thin-film composite (rougher) RO membranes, because of lower shear stress in the former.

- Bacterial cells in supersaturated salts would foul the surface by either adhering to the surface, or acting as nucleation sites for further crystallization,

or simply by pure particulate fouling. However, the structure of the fouled layer depends on the type and size of bacteria; bacterial cells might either both reduce the tenacity and increase the porosity of the fouled layer, or only increase the tenacity of the fouled layer, depending on the ion concentrations in the solution.

- The influence of the pretreatment (microfiltration + ultrafiltration) on RO membrane filtration was significant. It was found that the presence of smaller particles (dia $\leq$ 0.22 μm), mainly halobacterial cells, played a major role in initialization of crystallization of the micronuclei near the membrane surface trapping the salt microcrystals, preventing them moving towards the membrane channels causing channel blockage/narrowing. This markedly enhanced the permeate flux, especially at hypersalinities.

8.2 Recommendations and Future Work

Although the halobacterial investigations of Qabar-Onn Lake has provided a good foundation for exploring this unique hypersaline ecosystem, the culture-based methods, used in this study, were not enough on their own to fully explore the halotolerant bacterial diversity in this lake due to limitations associated with culturing. Since, in their studies, Martinez-Canovas, *et al.* (2004) found that the EPS-producing halophilic bacteria are generally present in hypersaline habitats, but not in great abundance, and can be isolated mainly from samples of the surrounding soils, urgent investigations on the bacterial diversity of the soils surrounding the lake, as well as benthic samples are very highly recommended.

Future predictions of the community metabolism from molecular systematic determinations will be complemented by future studies focusing on design of more appropriate media to isolate uncultured organisms, targeting of specific functional genes and conducting rational *in-situ* experiments to detect specific enzyme activities. Additionally, a molecular genetic examination of unculturable organisms should be undertaken to assess the full biodiversity of the lake. Tools such as

denaturing gradient gel electrophoresis (DGGE) can be applied to this situation (Abed *et al.*, 2002b; Nubel *et al.*, 1999).

Due to the nutritionally poor habitat of Qabar-Onn Lake, the isolated species from this lake were versatile in their nutritional abilities as might be expected; however, many of the microorganisms not isolated may well be more fastidious. It will be interesting to examine these different strategies and their role in maintaining the microbial community observed in the lake ecosystem.

Adhesion is a very important part in the process of biofilm formation. This process is controlled by several parameters, which include production of extracellular polymeric substances (EPS), which play a major role in the surface conditioning and biofilm initiation. However, correlations between this parameter and high ion concentrations in the bulk medium have not yet been studied, and highly warrant investigation.

Further work is required concerning method development for *in-situ* biofilm monitoring, under more realistic conditions and parameters. This work would include continuous visualization of various stages of bacterial cell adhesion on membrane surface with correlation to salt crystals, using a cross-flow transparent cell operated under conditions resembling membrane filtration processes.

REFERENCES

1. Abbas, A and Al-Bastaki, N. M (2000). Flux enhancement of RO desalination processes, *Desalination*. **132** : 21–27.

2. Abed, R. M. M. and F. Garcia-Pichel (2002a). Polyphasic characterisation of benthic, moderately halophilic, moderately thermophilic cyanobacteria with very thin richomes and the proposal of *Halomicronema excentricum* gen. nov., sp. nov., *Arch. Microbiol.*. **177** : 361–370.

3. Abed, R. M. M., N. M. D. Safi, J. Koster, D. de Beer, Y. El-Nahhal, J. Rullkotter, and F. Garcia-Pichel (2002b). Microbial diversity of a heavily polluted microbial mat and its community changes following degradation of petroleum compounds, *Appl.Environ. Microbiol*, **68** (4) : 1674–1683.

4. Abufayed, A. A. (2001). Performance characteristics of a cyclically operated seawater desalination plant in Tajoura, Libya, *Desalination*. **139** : 131–132.

5. Ahmad, A.L. and K.K. Lau (2006). Impact of different spacer filaments geometries on 2D unsteady hydrodynamics and concentration polarization in spiral wound membrane channel, *J. Membr. Sci.*, **286**: 77–92.

6. Ahmed, M., W. H. Shayya, D. Hoey, and J. Al-Handaly (2001). Brine disposal from reverse osmosis desalination plants in Oman and the United Arab Emirates, *Desalination*. **135** : 135–147.

7. Ajaili, A.; J. E. Furet and J. Tanti (1984). Diatoms of a hypersaline lake in the Libyan Sahara, *8th Diatom-Symposium, Paris, France, 12–14 Mar. 1984.*

8. Al-Ahmad, M., F. A. Abdul Aleem, A. Mutiri and A. Ubaisy (2000). Biofouling in RO membrane systems Part1: fundamentals and control, *Desalination*. **132**: 173–179.

9. Al-Bastaki, N. M. and A. Abbas (1999a). Improving the permeate flux by unsteady operation of a reverse osmosis desalination unit, *Desalination*. **123** : 173–176.

10. Al-Bastaki, N. M. and A. Abbas (1999b). Modelling an industrial reverse osmosis unit, *Desalination*. **126** : 33–39.

11. Allison, D.G.; B. Ruiz; C. SanJose; A. Jaspe and P. Gilbert (1998). Extracellular products as mediators of the formation and detachment of *Pseudomonas fluorescens* biofilms, *FEMS Microbiol. Lett.*, **167** : 179–184.

12. Al-Rammah, A. (2000). The application of acid free antiscalant to mitigate scaling in reverse osmosis membranes, *Desalination*. **132**: 83–87.

13. Al-Shammiri, M., M. Safar and M. Al-Dawas (2000). Evaluation of two different antiscalants in real operation at the Doha research plant, *Desalination*. **128** : 1–16.

14. Al-Suleimani, Z., and V. Rajendran Nair (2000). Desalination by solar-powered reverse osmosis in a remote area of the sultanate of Oman, *Appl. Energy*, **65**: 367–380.

15. Alvarez, V.; S. Alvarez; F. A. Riere and R. Alvarez (1997). Permeate flux prediction in apple juice concentration by reverse osmosis, *J. Membr. Sci.*, **127** (1): 25–34.

16. Al-Wazzan, Y.; M. Safar; S. Ebrahim; N. Burney and A. Mesri (2002). Desalting of subsurface water using spiral-wound reverse osmosis (RO) system: technical and economic assessment, *Desalination*, **143**: 21–28.

17. Amanatides, E.; D. Mataras; M. Katdikogianni and Y.F. Missirlis (2006). Plasma surface treatment of polyethylene terephalate films for bacterial repellence, *Surface & Coating Tech.* **200** : 6331–6335.

18. Amjad, Z. (Ed.) (1992). Reverse Osmosis, Membrane Technology, Water Chemistry and Industrial Applications, by Van Nostrand Reinhold, New York.

19. APHA, AWWA and WPCF, Standard methods for the examination of water and wastewater. (1998) *18th edition*, American Public Health Association, Washington D. C.

20. Arahal, D. R.; W. Ludwig; K.H. Scheleifer; and A. Ventosa (2002). Phylogeny of the family Halomonadaceeae based on 23S and 16S rDNA sequence analyses, *Int. Syst. Evol. Microbiol.*, **52**: 241–249.

21. Arias, S.; A. del Moral; M.R. Ferrer; R. Tallon, E. Quesada; V. Béjar (2003). Mauran an exopolysaccharide produced by the halophilic bacterium *Halomonas maura*, with a novel composition and interesting properties for biotechnology, *Extremophiles*, **7** : 319–326.

22. Avolonitis, S.; W. T. Hanbury and M. Ben Boudinar (1993). Spiral wound models performance an analytical solution: Part II, *Desalination*. **89** (3): 227–246.

23. AWWA (1992). Membrane Technology Research Committee report: membrane processes in portable water treatment, *J. AWWA*, **84**: 59-67.

24. AWWARF (1999). Reverse Osmosis and Nanofiltration Manual. American Water Works Association. Denver, CO.

25. Bacchin, P. and P. Aimar (2005). Critical fouling conditions induced by colloidal surface interaction: from causes to concequenes, *Desalination*, **175** : 21–27.

26. Bachmann, R.T. and R. J. Edyvean (2006). AFM study of the colonization of stainless steel by *Aquabacterium commune, Int. Biodeter. Biodeg., in press, corrected proof.*

27. Baker, J. S. and L. Y. Dudley, (1998). Biofouling in membrane systems-A review, *Desalination.* **118** : 81–90.

28. Balows, A.; H. G. Truper; M. Dowrkin; W. Harder and K. H. Schleifer (Eds) (1992a). The Prokaryotes, A Handbook on the Biology of Bacteria: Ecophysiology, Isolation, Identification, Application, *2nd edition, Vol I, Springer-Verlag press.*

29. Balows, A.; H. G. Truper; M. Dowrkin; W. Harder and K. H. Schleifer (Eds) (1992b). The Prokaryotes, A Handbook on the Biology of Bacteria: Ecophysiology, Isolation, Identification, Application, *2nd edition, Vol II, Springer-Verlag press.*

30. Balows, A.; H. G. Truper; M. Dowrkin; W. Harder and K. H. Schleifer (Eds) (1992c). The Prokaryotes, A Handbook on the Biology of Bacteria: Ecophysiology, Isolation, Identification, Application, *2nd edition, Vol IV, Springer-Verlag press.*

31. Baumgarte, S. Moore and B. J. Tyndall (2001). Re-examining the 16S rDNA sequence of *Halomonas salina, Int. Syst. Evol. Microbiol.*, **51**: 51–53.

32. Bejarano, E.M. and R.P. Schneider (2004). Use of fluorescent lectin probes for analysis of footprints from *Pseudomonas aeruginosa* MDC on hydrophilic and hydrophobic glass substrata, *Appl. Environ. Microbiol.* **70** : 4356–4365.

33. Benlloch, S.; A. Lopez; E. O. Casamayor; L. Ovraes; V. Goddard; F. L. Daae; G. Smerdon; R. Massana; I. Joint; F. Thingstad; C. Pedros-Allio and F. Rodriguez-Valera (2002). Prokaryotic genetic diversity throughout the salinity gradient of a coastal solar saltern, *Environ. Microbiol.*, 4(6) : 349–360.

34. Berrin, T.; J. Sager; J. Garland; S. Xud; L. Levine; P. Bisbee (2006). Deposition of extracellular polymeric substances (EPS) and microtopographical changes on membrane surfaces during intermittent filtration conditions, *J. Memb. Sci.*, **285** : 225–231.

35. Bessieres, A., M. Meireles, R. Coratger, J. Beauvillain and V. Sanches (1996). Investigations of surface properties of polymeric membranes by near field microscopy, *J. Membr. Sci.* **109** : 271–284.

36. Bhattacharyya, D.; S. L. Back; and R. I. Kermode (1990). Prediction of Concentration Polarization and Flux Behavior in Reverse Osmosis by Numerical Analysis, *J. Memb. Sci.*, **48** : 231–238.

37. Bhattacharyya, D. and S.T. Hwang (1997). Concentration polarization separation factor and Peclet number in membrane processes, *J. Memb. Sci.*, **132** : 73–90.

38. Biggerstaff, J.P.; M. Le Puil; B.L. Weidow; J. Prater; K. Glass; M. Radosevich; D.C. White (2006). New methodology for viability testing in environmental samples, *Molecular and Cellular Probes*, **20** : 141–146.

39. Bilstad, T. (1997). Membrane operations, *Water Sci. Tech.* **36** (2): 17–24.

40. Boland, T.; R.A. Latour and F.J. Stutzenberger (2000). Molecular basis of bacterial adhesion. Handbook of Bacterial Adhesion-Principles, Methods and Applications, pp 29-41. Y.H. An and R.J. Friedman (Eds). Humana Press, Totowa, NJ.

41. Bos, R.; H.C. van der Mei and H.J. Busscher (1999). Physicochemistry of initial microbial adhesive interactions–its mechanisms and methods of study, *FEMS Microbiol. Rev.* **23** : 179–191.

42. Bouhidel, K. E. and K. Oulmi (2000). Concentration polarisation in electrodialysis: Buffer solutions experimental method, *Desalination.* **132** : 199–204.

43. Boussu, K.; C. Vandecasteele; B. Van der Bruggen; (2006). Study of the characteristics and the performance of self-made nanoporous polyethersulfone membranes, *Polymer*, **47** : 3464 – 3476.

44. Bowen, W. R. and T.A. Doneva (2000). Atomic force microscopy studies of membranes: effect of surface roughness on double-layer interactions and particle adhesion, *J. Colloid Interface Sci.* **229** : 544–556.

45. Bremere, I., M. Kennedy, S. Mhyio, A. Jaljuli, G. Witkamp, and J. Schippers (2000). Prevention of silica scale in membrane systems: removal of monomer and polymer silica, *Desalination.* **132** : 89–100.

46. Burns, B. P.; F. Goh; M. Allen and B. A. Neilan (2004). Microbial diversity of extant stromatolites in the hypersaline marine environment of Shark Bay, Australia. *Environ. Microbiol.*, **6**: 1096–1101.

47. Busscher, H. J.; J. Sjollema and H. C. van der Mei (1990). Relative importance of surface free energy as a measure of hydrophobicity in bacterial adhesion to solid surfaces, in: R.J. Doyle and M. Rosenberg (Eds.), Microbial Cell Surface Hydrophobicity, American Society for Microbiology, Washington D.C., pp. 335–359.

48. Chen, C.-L.; W.-T. Liu; M.-L. Chong; M.-T. Wong; S.L. Ong; H. Seah and W.J. Ng (2004). Community structure of microbial biofilms associated with membrane-based water purification processes as revealed using a polyphasic approach, *Appl. Microbiol. Biotechnol.* **63 : 466–478.**

49. Christensen, B.E. (1999). Physical and chemical properties of extracellular polysaccharides associated with biofilms and related systems, Bacterial Extracellular Polymeric Substances. pp 143-154, J. Wingender; T. Neu and H.-C. Flemming (Eds). Springer-Verlag, Berlin.

50. Clamp, M.; J. Cuffl; S. M. Searle and G. J. Barton (2004). The Jalview Java alignment editor, *Bioformatics*, **20** (3) : 426–427.

51. Coker, S and P. Sehn (2000). Four years field experience with fouling resistant reverse osmosis membranes, *Desalination.* **132 : 211–215.**

52. Cummings, S. P.; M. P. Williamson and D. J. Gilmour (1993). Turgor regulation in a novel *Halomonas* species. *Arch. Microbiol.* **160 : 319–323.**

53. da Costa, M.S.; H. Santos; and E. A. Gailinski (1998). An overview of the role and diversity of compatible solutes in bacteria and Archaea, *Advances in Biochemical Engineering/Biotechnology*, **61: 118–141.**

54. Damak, K.; A.Ayadi; B. Zeghmati; P. Schmitz (2004). Concentration polarisation in tubular membranes -a numerical approach, *Desalination*, **171 : 139–153.**

55. Darwish, M. A., and N. Al-Najem (2000). Cogeneration power desalting plants in Kuwait: a new trend with reverse osmosis desalters, *Desalination.* **128 : 17–33.**

56. Diaz, M.R. and B.F. Taylor (1996). Metabolism of methylated osmolytes by aerobic bacteria from Mono Lake, a moderately hypersaline, alkaline environment, *FEMS Micrbiol. Ecol.*, **19 : 239–247.**

57. Drevon, J. J., C. Abdelly; N. Amarger; E.A. Aouani; J. Aurag; H. Gherbi; M. Jebara; C. Lluch; H. Payre; O. Schump; M. Soussi; B. Sifi f and M. Trabelsi (2001). An interdisciplinary research strategy to improve symbiotic nitrogen fixation and yield of common bean (*Phaseolus ulgaris*) in salinised areas of the Mediterranean basin, *J. Biotechnol.*, **91: 257–268.**

58. Elimehech, M., X. Zhu, A. E. Childress and S. Hong (1997). Role of membrane surface morphology in colloidal fouling of cellulose acetate and composite aromatic polyamide reverse osmosis membranes, *J. Membr. Sci.* **127 : 101–109.**

59. El-Saedi, M. (2002). A survey study on Qabar-Onn Lake. *BSc. Thesis, Faculty of Engineering, Department of Environmental Studies, University of Sebha, Libya.*

60. Felsenstein, J. (1993). PHYLIP (Phylogeny Interface Package) version 3.5c. D*epartment of Genetics, University of Washington, Seattle, USA.*

61. Flemming, H. -C. (1997). Reverse osmosis membrane biofouling, *Thermal and Fluid Science,* **14**: 382–391.

62. Flemming, H. -C.; G. Schaule and T. Griebe (1997). Biofouling: the achilles heel of membrane processes, *Desalination*, **113** : 215–225.

63. Flemming, H. C.; G. Schauls, R. McDonogh and F. Ridgway (Eds) (1994). Effect and extent of biofilm accumulation in membrane systems. Biofouling and biocorrosion in industrial water systems, pp. 63-89. G. G. Geesey; Z. Lewandowsky and H. C. Flemming, CRC Press, Lewis Publishers.

64. Garcia-Pichel, F.; A. Lopez and U. Nubel, (2001). Phylogenetic and morphological diversity of cyanobacteria in soil desert crusts from Colorado plateau, *Appl. Environ. Microbiol.* **67** : 1902–1910.

65. Garcia-Pichel, F.; U. Nubel, and G. Muyzer (1998). The Phylogeny of unicellular, extremely halotolerant cyanobacteria, *Arch Microbiol*, **169** : 469–482.

66. Geesey, G. G. (1987). Survival of microorganisms in low nutrient waters. Biofouling of industrial water systems: a problem solving approach, pp. 1–23. (Eds): Mark W. Mittelman and Gill G. Geesey. *Water Micro Associates, San Diago, CA.*

67. Gilron, J., D. Chaihin and N. Daltrophe (2000). Demonstration of CAPS pretreatment of surface water for RO, *Desalination.* **127** : 271–282.

68. Glucina, K.; A. Alvarez and J. M. Laine (2000). Assessment of an integrated membrane system for surface water treatment, *Desalination.* **132** : 73–82.

69. Gordon, A. J.; F. R. Minchin; L. Skot and C. L. James (1997). Stress induced declines in soybean N2 fixation are related to nodule sucrose synthase activity, *Plant Physiol.* **114**: 937–946.

70. Griebi, T. and H. C. Flemming (1998). Biocide-free antifouling strategy to protect RO membranes from biofouling, *Desalination.* **118** : 153–156.

71. Hamrouni, B. and M. Dhahbi (2001). Analytical Aspects of silica in saline waters-application to desalination of brackish waters, *Desalination.* **136** : 225–232.

72. Harris, L.G.; S. Tosatti; M. Wieland; M. Textor and R.J. Richards (2004). *Staphylococcus aureus* adhesion to titanium oxide surfaces coated with non-functionalised and peptide-functionalised poly (L-lysine)-*grafted*-poly (ethylene glycol) copolymers, *Biomater.*, **25** : 4135–4148.

73. Heitmann, Hans-Gunter, (ed) (1990). Saline water processing: desalination and treatment of seawater, brackish water, and industrial waste water, *VCH Verlagsellschaft, Weinheim, Germany.*

74. Hentzer, M.; K. Riedel; T.B. Rasmudsen; A. Heydorn; J.B. Andersen; M.R. Parsek; S. Rice; L. Eberl; *et al.* (2000). Detection and inhibition of quorum sensing in *Pseudomonas aeruginosa* biofilms, ASM Conference-Biofilms 2000, Big Ski, MT.

75. Hilbert, L.R.; D. Bagge-Ravn; J. Kold and L. Gram (2003). Influence of surface roughness of stainless steel on microbial adhesion and corrosion resistance, *Int. Biodeter. And Biodeg.* **52** : 175 –185.

76. Hochstein, L., I. and G. A. Tomlinson. (1985). Denitrification by extremely halophilic bacteria, *FEMS Microbiol. Lett.* **27** : 329–331.

77. Imhoff, J. F. (1986). Osmoregulation and compatible solutes in eubacteria, *FEMS Mirobiol. Rev.*, **39**: 57-66.

78. Incharoensakdi, A. and A. Kamchanatat (2003). Salt stress enhances choline uptake in the halotolerant cyanobacterium *Aphanothece halophytica*, *Biochimica et Biophysica Acta*, **1621** : 102–109.

79. Jaber, I. S. and M. R. Ahmed (2004). Technical and economic evaluation of brackish groundwater desalination by reverse osmosis process, *Desalination*, **165** : 209–213.

80. Jackangelo, J.G.; S. Adham and J.-. Laine (1997). Membrane Filtration for Microbial Removal. American Water Works Association Research Foundation. Denver, CO.

81. Jing, X.; D.J. Tagliente and D.G. Davies (2000). Biofilm development: The *Pseudomonas aeruginosa* paradigm. ASM Conference-Biofilms 2000, Big Ski, MT.

82. Johnson, B. D.; K. Kranck and D. K. Muschenheim (1994). Physicochemical factors in particle aggregation, in: R.S. Wotton (Ed.), The Biology of Particles in Aquatic Systems, CRC Press, Boca Raton, Ann Arbor, London, Tokyo, pp 75–96.

83. Karode, S. K. and A. Kumar (2001). Flow visualization through spacer filled channels by computational fluid dynamics I. Pressure drop and shear rate calculations for flat sheet geometry, *J. Memb. Sci.*, **193** : 69–84.

84. Kershman, S.A. (2001). 25 years of experience in operating thermal desalination plants, *Desalination.* **136** : 141–145.

85. Kievit, T.R.; R. Gillis; S. Marx ; S. Brown and B.H. Iglewski (2001). Quorum-sensing in *Pseudomonas aeruginosa* biofilms: Their role and expression patterns, *Appl. Environ. Microbiol.*, **67** (4) : 1865–1873.

86. Kimura, S. (1995). Analysis of Reverse Osmosis Membrane Behaviors in a Long-Term Verification Test, *Desalination*, **100** : 77–87.

87. Klein-BenDavid, O.; E. Sass and A. Katz (2004). The evaluation of marine evaporatitic brines in inland basins: The Jordan-Dead Sea Rift valley, *Geochemica Acta*, **68** (8): 1763–1775.

88. Knoell, T.; J. Safarik; T. Cormack; R. Riley; S.W. Lin and H.F. Ridgway (1999). Biofouling potentials of microporous polysulfone membranes containing a sulfonated polyether-ethersulfone/polyethersulfone block copolymer: correlation of membrane surface properties with bacterial attachment, *J. Membr. Sci.* **157** : 117–129.

89. Korber, D. R.; J. R. Lawrence; H. M. Lappin-Scott and J. W. Costerton (1995). Growth of microorganisms on surfaces, in: H. M. Lappin-Scott, J. W. Costerton (Eds.), Microbial Biofilms, Cambridge University Press, Cambridge, pp. 15–45.

90. Krieg, H. M.; S. J. Modise; K. Keizei and H. A. J. P. Neomagus (2004). Salt rejection in nanofiltration for single and binary salt mixtures in view of sulphate removal, *Desalination*, **171** : 205–215.

91. Kruithof, J.C.; P.C. Kamp; and H.C. Folmer (2001). Membrane integrity monitoring at the UF/RO Heemskerk Plant, Membrane Practices for Water Treatment, pp 191–204. S.J. Duranceau (Ed), American Water Works Association, Denver, CO.

92. Kumar, S.; K. Tamura and M. Nei (2004). MEGA3: Integrated software for molecular evolutionary genetics analysis and sequence alignment, *Briefings In Bioinformatics*, **5** (2): 150–163.

93. Kushner, D. J. and M. Kamekula (1988). Halophilic bacteria (Rodriguez-Valera, F., Ed.), pp. 109–140. *CRC Press, Boca Raton*, Finland.

94. Lane, D.J. (1991). In Nucleic Acid Techniques in Bacterial Systematics (E. Stackebrandt and M. Goodfellow, Eds). John Wiley & Sons, Chichester, UK, pp 115–175.

95. LeChevallier, M.W.; C.D. Cawthon; R.G. Lee (1988). Inactivation of biofilm bacteria, *Appl. Environ. Microbiol.*, **54** (10): 2492–2499.

96. Li, C. W. and Y. S. Chen (2004). Fouling of UF membrane by humic substance: Effects of molecular weight and powder-activated carbon (PAC) pretreatment, *Desalination,* **170 : 59–57.**

97. Llamas, I.; a. del Moral; V. Bejar; M. D. Giron; R. Salto and E. Quesada (1997). Plasmids from *Halomonas eurihalina,* a microorganism which produces an exopolysaccharides of biotechnological interest, *FEMS Microbiol. Lett.,* **156: 251–257.**

98. Luo, M and Z. Wang (2001). Complex fouling and cleaning-in-place of a reverse osmosis desalination system, *Desalination.* **141 : 15–22.**

99. Ma, H., L. F. Hakeem, C. N. Bowman and R. H. Daves (2001). Factors affecting membrane fouling reduction by surface modification and back-pulsing, *J. Membr. Sci.* **189 : 255–270.**

100. Maartens, A., P. Swart and E. P. Jacobs (1999). Feed-water pretreatment: methods to reduce membrane fouling by natural organic matter, *J. Membr. Sci.* **163 : 51–62.**

101. Madaeni, S. S.; T. Mohamamdi and M. K. Moghadam (2001). Chemical cleaning of reverse osmosis membranes, *Desalination.* **134 : 77–82.**

102. Madireddi, K.; R. B. Babcock; B. Levine; J. T. Kim and K. Stenstorm (1999). An unsteady-state model to predict concentration polarisation in commercial spiral wound membranes, *J. Membr. Sci.,* **157** (1): 13–34.

103. Mairal, A. P., A. R. Greenberg and W. B. Krantz (2000). Investigation on membrane fouling and cleaning using ultrasonic time-domain refrectometry, *Desalination.* **130 : 45–60.**

104. Mallevialle, J.; P. E. Odendaal and M. R. Wiesner, (Eds.) (1996). Membrane fouling, Water Treatment Membrane Processes, Ch. 6 by H. F. Ridgway, and H.-C. Flemming, McGraw-Hill, New York.

105. Marshall, K.C.; K.N. Angles; R.P. Schneider and A.E. Goodman (1994). Analysis of bacterial behaviour during biofouling of surfaces, *Biofouling and Biocorrosion in Industrial Water Systems,* CRC Press, Lewes Publishers.

106. Marinas, B. J., and R. I. Urama (1996). Modeling Concentration-Polarization in Reverse Osmosis Spiral-Wound Elements," *J. En˜. Eng. ASCE,* **4 : 292–298 .**

107. Martinez-Canovas, M. J.; E. Quesada ; I. Llamas and V. Bejar (2004). *Halamonas ventosae* sp. Nov., a moderately halophilic denitrifying exopolysaccharides-producing bacterium, *Int. Syst. Evol. Microbiol.,* **54: 733–737.**

108. Martínez-Cánovas, M.J.; E. Quesada; F. Martínez-Checa and V. Béjar (2004). A taxonomic study to establish the relationship between exopolysaccharide producing bacterial strains living in diverse hypersaline habitats, *Curr. Microbiol,* **48 :** 348–353.

109. Maskow, T. and W. Babel (2001). Calorimetrically obtained information about the efficiency of ectoine synthesis from glucose in *Halomonas elongate, Biochimica et Biophysica Acta,* **1527**: 4–10.

110. Mata, J. A.; J. M. Canovas; E. Quesada and A. Ventosa (2002). A detailed phenotypic characterization of the type strains of *Halomonas* species, *Syst. Appl. Microbiol.* **25**:360–375.

111. Mata, J.A.; V. Béjar; I. Llamas; S. Arias; P. Bressollier ; R. Tallon ; M. C. Urdaci ; E. Quesada (2006). Exopolysaccharides produced by the recently described halophilic bacteria *Halomonas ventosae* and *Halomonas anticariensis, Res. Microbiol.*, **157 :** 827–835.

112. Matsuura, T. (2001). Progress in membrane science and technology for seawater desalination-A review, *Desalination.* **134 :** 47–54.

113. Melo, L. F. and T. R. Bott (1997). Biofouling in water systems, *Exper. Therm. Fluid Sci.,* **14**: 375–381.

114. Meyers, S. (2000). Developments in aquatic microbiology, *Int. Microbiol*, **3 :** 203–211.

115. Moatty, N. (2001). Water management and desalination in Israel, *Desalination.* **136 :** 101–104.

116. Mohsen, M. S. and O. R. Al-Jayyousi (1999). Brackish water desalination: an alternative for water supply enhancement in Jordan, *Desalination.* **124 :** 163–174.

117. Moore, G.F.; B.C. Dunsmore; S.M. Jones; C.W. Smejkal; J. Jass; P. Stoodley and H.M. Lappin-Scott (2000). Icrobial detachment from biofilms. SGM symposium 59: Community structure and co-operation in biofilms. Allison, D.; P. Gilbert; H. Lappin-Scott; and M. Wilson (Eds). Cambridge University Press, Cambridge, MA.

118. Moran, R. (1982). Formulae for determination of chlorophyllous pigments extended with N, N-dimethylformamide, *Plant Physiol.*, **69 :** 1367–1381.

119. Moremile, M.R.; M.F. Romine; M.T. Garcia; A. Ventosa ; T.J. Bailey and B.M. Peyton (1999). *Halomonas campisalis* sp. nov., a denitrifying, moderately haloalkaliphilic bacterium, *Syst. Appl. Microbiol.*, **22**: 551–558.

120. Motta, A.; I. Romano and A. Gambacota (2004). Rapid and sensitive NMR method for osmolyte determination, *J. Microbiol. Methods*, **58**: 289–294.

121. Mulder, M. (Ed.) (1996). Basic principles of membrane technology, *Dordrecht, Netherlands, Kluwer Academic Publishers.*

122. Nagata, S.; K. Adachi and H. Sano (1996). NMR analyses of compatible solutes in a halotolerant *Brevibacterium* sp., *Microbiol.*, **142**: 3355–3362.

123. Noble, R. D. and S. A. Stern (Ed) (1995). Membrane separations technology: Principles and applications, *Elsevier Science B.V. Amsterdam, The Netherlands.*

124. Nubel, U.; F. Garcia-Pichel and G. Muyzer (1997). PCR primers to amplify 16S rRNA genes from cyanobacteria, *Appl. Env. Microbiol.* **63** (8) : 3327–3332.

125. Nubel, U.; F. Garcia-Pichel; M. Kuhl and G. Muyzer (1999). Quantifying microbial diversity: Morphotypes, 16S rRNA genes, and carotenoids of oxygenic phototrophs in microbial mats, *Appl. Env. Microbiol.* **65** (2) : 422–430.

126. Nys, R.D.; P.D. Steinberg; P. Willemsen; S.A. Dworjanyn and R.J. King (1995). Broad spectrum effects of secondary metabolites from the red algae *Delisea pulchra* in antifouling assay, *Biofouling*, **8** : 259–271.

127. Ollivier, B.; P. Caumette; J. L. Garcia and R. Mah (1994). Anaerobic bacteria from hypersaline environments, *Microbiol. Rev.*. **58** (1) : 27–38.

128. Paerl, H. W.; J. L. Pinckney and T. F. Steppe (2000). Cyanobacterial-bacterial mat consortia: examining the functional unit of microbial survival and growth in extreme environments, *Env. Microbiol.* **2** (1) : 11–26.

129. Page-Sharp, M.; C. A. Behm; G. D. Smeth (1999). Involvement of the compatible solutes trehalose and sucrose in the response to salt stress of a cyanobacterial *Scytonema* species isolated from desert soils, *Biochimica et Biophysica Acta*, **1472**: 519–528.

130. Percival, S.L.; T.W. James and P.R. Hunter (2000). Microbial aspects of biofilms and drinking water. Boca Raton, FL, CRC Press LLC.

131. Pfluger, K. and V. Muller (2004). Transport of compatible solutes in extremophiles, *J. Bioenergitic and Biomembranes*, **36** (1) : 17–24.

132. Redondo, J. A. (1999). Improve RO system performance and reduce operating cost with FILMTEC fouling-resistant (FR) elements, *Desalination.* **126** : 249–259.

133. Ridgway, H. F. and H.-C. Flemming (1996). Membrane biofouling: Water Treatment Membrane Processes, pp 6.1–6.62. Mallevialle, J.; P. E. Odendaal and M. R. Wiesner, (Eds). McGraw-Hill.

134. Ridgway, H. F. and J. Safarik (1991). Biofouling of reverse osmosis membranes, in: H-C. Flemming, G. G. Geesey (Eds.), Biofouling and Biocorrosion in Industrial Water Systems, Springer, Berlin, Heidelberg, pp. 81–111.

135. Romano, I; B. Nicolaus; L. Lama; D. Trabasso; G. Caracciolo and A. Gambacorta (2001). Accumulation of osmoprotectants and lipid pattern modulation in response to growth conditions by *Halomonas pantelleriensis*, *Sys. Appl. Microbiol.* **24**:342–352.

136. Romano, I; B. Nicolaus; L. Lama; D. Trabasso; M. C. Manca and A. Gambacorta (1996). Characterisation of a haloalkaliphilic strictly aerobic bacterium, isolated from pantelleria, *Sys. Appl. Microbiol.* **19**:326–333.

137. Rothrock Jr, M. J. and F. Garcia-Pichel (2005). Microbial diversity of benthic mats along a tidal desiccation gradient, *Environ. Microbiol.*, **7** (4) : 593–601.

138. Sadhwani, J. J. and J.M. Veza (2001). Cleaning tests for seawater reverse osmosis membranes, *Desalination.* **139** : 177–182.

139. Sadr-Ghayeni, S.B.; P.J. Beatson; R.P. Schneider and A.G. Fane (1998). Adhesion of wastewater bacteria to reverse osmosis membranes, *J. Membr. Sci,* **138** : 29–38.

140. Saitou, N. and M. Nei (1987). The neighbour-joining method: a new method for reconstructing phylogenetic trees, *Mol. Biol. Evol.* **4**: 406–425.

141. Schafer, A. (2001). Natural organic removal using membranes. *Technomic Publishing Co., Inc. Lencaster, PA.*

142. Schneider, R. P.; B. R. Chadwick; R. Pembrey; J. Jankowski and I. Acworth (1994). Retention of the Gram-negative bacterium SW8 on surfaces under conditions relevant to the subsurface environment: effects of conditioning films and substratum nature, *FEMS Microbiol. Ecol.,* **14** : 243–254.

143. Schneider, R. P.; L. M. Ferreira; P. Binder; E. M. Bejarano; K. P. G'oes; E. Slongo; C. R. Machadob; G. M. Z. Rosa (2005). Dynamics of organic carbon and of bacterial populations in a conventional pretreatment train of a reverse osmosis unit experiencing severe Biofouling, *J. Memb Sci,* **266** : 18–29.

144. Scott, K. and R. Hughes (Ed) (1996). Industrial membrane separation technology, *Blackie academic & Professional, Glasgow, UK.*

145. Shaalan, H.F. (2002). Development of fouling control strategies pertinent to nanofllltration membranes, *Desalination*, **153** : 125–131.

146. Shams El-Din, A.M.; M. E. El-Dahshan; and A. M. Tag El-Din (2003). Biofilm formation on stainless steels Part 2. The role of seasonal changes, seawater composition and surface roughness, *Desalination*, **154** : 267– 278.

147. Shaposhnik, V. A., N. N. Zubets, B. E. Mill and I. P. Strigina (2001). Demineralization of water by electrodialysis with ion-exchange membranes, grains and nets, *Desalination*. **133** : 211–214.

148. Sheikholeslami, R. (1999). Fouling mitigation in membrane processes, *Report on a Workshop held Jannuary 26-29, 1999, Technion-Israel Institute of Technology, Haifa, Israel, Desalination.* **123** : 45–53.

149. Soffer, Y. A. Adin, and J. Gilron. (2004). Threshold flux in the foulng of UF membranes by colloidal iron, *Desalination*. **161** : 207–221.

150. Soltanieh, M. and W. N. Gill (1981). Review of Reverse Osmosis Membranes and Transport Models, *Chem. Eng. Commun.*, **12** : 279–288.

151. Song, L. and S. Yu (1999). Concentration polarisation in cross-flow reverse osmosis, *AICHE Journal*, **45** (5): 921–928.

152. Sossi, M.; A. Ocana and C. Lluch (1998). Effects of salt stress on growth, photosynthesis and nitrogen fixation in chick-pea (*Cicer arietimum* L.), *J. Exp. Bot*, **49**: 1329–1337.

153. Speth, T.F.; A.M. Gusses' R.S. Summers (2000). Evaluation of nanofiltration pretreatments for flux loss control, *Desalination*, **130** : 31–40.

154. Squire, D. (2000). Reverse osmosis concentrate disposal in the UK, *Desalination*. **132**: 47–54.

155. Stein, J. R. (1979). Handbook of phycological methods: culture methods and growth measurements, *Cambrige University Press.*

156. Stoodley, P.; S. Wilsen; L. Hall-Stoodley; J.D. Boyle; H.M. Lappin-Scott and J.W. Costerton (2001). Growth and detachment of cell clusters from mature mixed-species biofilms, *Appl. Environ. Microbiol.*, **67** (12): 5608–5613.

157. Stradhmann, H. (2000). Introduction to membrane science and technology, University of Colorado at Boulder, Class Notes.

158. Svenning, M. M., T. Eriksson, and U. Rasmussen (2005) Phylogeny of symbiotic cyanobacteria within the genus *Nostoc* based on 16S rDNA sequence analyses, *Arch Microbiol*, **183** : 19–26.

159. Tamura, K; M. Nei and S. Kumar (2004). Prospects for inferring very large phylogenies by using the neighbour-joining method, *PNAS*, **101** (3): 11030–11035.

160. Tanaka, T.; J. G. Burgress and P. C. Wright (2001). High-pressure adaptation by salt stress in a moderately halophilic bacterium obtained from open seawater. *Appl. Microbiol. Biotechnol.* **57** : 200–204.

161. Tansel, B.; J. Sager; J. Garland; S. Xu; L. Levine and P. Bisbee (2006). Deposition of extracellular polymeric substances (EPS) and microtopographical changes on membrane surfaces during intermittent filtration conditions, *J. Memb Sci,* **285** (1–2) : 225–231.

162. Tansel, B.; W. Y. Bao and I. N. Tansel (2000), Characterization of fouling kinetcs in ultra filtration systems by resistances in series model, *Desalination*, **129** : 7–14.

163. Taylor, R. L.; J. Verran; G. C. Lees; A. J. Ward; (1998). The influence of substratum topography on bacterial adhesion to polymethyl methacrylate, *J. Mater. Sci. Mater. Med.*, **9** : 17–25.

164. Toole, E.T.O.; T.H. Giddings; J.R. McIntosh and S.K. Dutcher (2003). Three-dimensional organization of Basel bodies from wide-type and δ-tubulin deletion strains of Chlamydomonas reinhardtii, *Molecular Biology of the Cell*, **14** : 2999–3012.

165. Valderrama, M. J.; E. Quesada; V. Bejar ; A. Ventosa ; M. C. Gutierrez ; F. Ruiz-Berraquero and A. Ramos-Cormenzana (1991). *Deleya salina* sp. Nov., a moderately halophilic Gram-negative bacterium, *Int. J. Sys. Bacteriol.* **41**: 377–384.

166. Van der Bruggen, B.; J.Scheap; D. Wilms and C. Vandecasteele (1999). Influence of molecular size polarity and charge on the retention of organic molecules by nanofiltration, *J. Memb. Sci.*, **156** : 29–41.

167. Van der Hoek, J.P.; P.A.C. Bonne; E.A.M. Van Soest; and A. Graveland (1997). *Proc. 21st IWSA Congress, Madrid,* **ss1**, pp. 11–16.

168. Van der Hoek, J.P.; J.A.M.H. Hofman; P.A.C. Bonne; M.M. Nederlof and H.S. Vrouwenvelder (2000). RO tearment: selection of a pretreatment scheme based on fouling characteristics and operating conditions based on environmental impact, *Desalination*, **127**: 89–101.

169. Van der Meer, W. G. J.; M. Riemersma and J. C. van Dijk (1998). Only two membrane modules per pressure vessel? Hydraulic optimisation of spiral wound membrane filtration plants, *Desalination*. **119** (1–3): 57–64.

170. Ventosa, A.; J. J. Nieto ; and A. Oren (1998). Biology of moderately halophilic bacteria, *Microbiol. Mol. Biol. Rev.* **62**: 504–544.

171. Voros, N. G.; Z. B. Maroulis and M. Kouris (1996). Salt and water permeability in reverse osmosis membranes, *Desalination*. **104** (3): 141–154.

172. Vrouwenvelder, J. S.; S. A. Manolarakis; H. R. Veenendaal; D. van der Kooij (2000). Biofouling potential of chemicals used for scale control in RO and NF membranes, *Desalination* **132** : 1–10.

173. Winters, H. (1997). Twenty years experience in seawater reverse osmosis and how chemicals in pretreatment affect fouling of membranes, *Desalination,* **110** : 93–96.

174. Yoon, J. -H.; K. –C. Lee; Y. –H. Kho, K. H. Kang; C. –J. Kim and Y. –Ha. Park (2002). *Halomonas alimentaria* sp. Nov., isolated from jeogal, a traditional Korean fermented seafood, *Int. J. Sys. Evol. Microbiol.* **52**: 123–130.

175. Zhang, R.; D. E. Wiley and A. G. Fane (2005). The effect of hetero-aggregated feeds on critical flux, *Desalination,* **175** (2005) I–5.

176. Zhao, Q. and Y. Liu (2006). Modification of stainless steel surfaces by electroless Ni-P and small amount of PTFE to minimise bacterial adhesion, *J. Food Eng.*, **72** : 266–272.

177. Zhao, Q.; S. Wang; and H. Muller-Steinhagen (2004). Tailored surface free energy of membrane diffusers to minimise microbial adhesion, *Appl. Surface Science*, **230** : 371–378.

APPENDICES

APPENDIX A

FLUX EXPEIMENTAL DATA AND QABAR-ONN LAKE REPORTED DATA

Run (1)

Dist-H_2O-ADF

Time (min)	P-in (psig)	P-in (bar)	P-out (bar)	Vol (ml)	Cum Vol (ml)	Flux ($kg/m^2.sec$)	Cum Flux ($kg/m^2.sec$)
0	0	0	0	0	0	0	0
5	0	0.00	0.012	170	170	0.2137	0.2137
10	50	3.42	0.015	794	964	0.9979	1.2115
15	100	6.83	0.017	1403	2367	1.7633	2.9748
20	150	10.25	0.018	1660.43	4027.43	2.0868	5.0617
25	200	13.67	0.017	1998.26	6025.69	2.5114	7.5731
30	250	17.08	0.019	2037.77	8063.46	2.5611	10.1341
35	300	20.50	0.02	2221.75	10285.21	2.7923	12.9264
40	350	23.92	0.023	2259.92	12545.13	2.8403	15.7667
45	400	27.33	0.026	2355.38	14900.51	2.9602	18.7269
50	450	30.75	0.028	2356.58	17257.09	2.9617	21.6886
55	500	34.17	0.029	2351.85	19608.94	2.9558	24.6444
60	550	37.58	0.03	2461	22069.94	3.0930	27.7374
65	600	41.00	0.033	2925.4	24995.34	3.6766	31.4140
70	650	44.41	0.033	3114.5	28109.84	3.9143	35.3283
75	700	47.83	0.035	3643.84	31753.68	4.5796	39.9079
80	740	50.56	0.037	4118.89	35872.57	5.1766	45.0845

Run (2)

Dist-H_2O-Nano

Time (min)	P-in (psig)	P-in (bar)	P-out (bar)	Vol (ml)	Cum. Vol (ml)	Flux ($kg/m^2.sec$)	Cum. Flux ($kg/m^2.sec$)
0	0	0	0	0	0	4.958	18.333
5	0	0.00	0.012	170	170	8.436	26.667
10	50	3.42	0.015	794	964	12.622	33.333
15	100	6.83	0.017	1403	2367	16.890	40.536
20	150	10.25	0.018	1660.43	4027.43	21.544	51.706
25	200	13.67	0.017	1998.26	6025.69	26.278	63.067
30	250	17.08	0.019	2037.77	8063.46	31.211	74.908
35	300	20.50	0.02	2221.75	10285.21	36.148	86.754
40	350	23.92	0.023	2259.92	12545.13	41.074	93.333
45	400	27.33	0.026	2355.38	14900.51	46.229	100.000
50	450	30.75	0.028	2356.58	17257.09	52.357	103.333
55	500	34.17	0.029	2351.85	19608.94	58.880	105.000
60	550	37.58	0.03	2461	22069.94	66.513	106.667
65	600	41.00	0.033	2925.4	24995.34	75.141	110.000
70	650	44.41	0.033	3114.5	28109.84	4.958	18.333
75	700	47.83	0.035	3643.84	31753.68	8.436	26.667
80	740	50.56	0.037	4118.89	35872.57	12.622	33.333

Run (3) Chem-30g-ADF

Time (min)	P-in (psig)	P-in (bar)	P-out (bar)	Vol (ml)	Cum Vol (ml)	Flux (kg/m^2.sec)	Cum Flux (kg/m^2.sec)
0	0	0	0	0	0	0	0
5	100	6.83	0.007	59.54	59.54	0.0748	0.0748
10	200	13.67	0.008	217.67	277.21	0.2736	0.3484
15	300	20.5	0.006	288.07	565.28	0.3620	0.7104
20	400	27.33	0.008	300.17	865.45	0.3773	1.0877
25	500	34.16	0.005	225.37	1090.82	0.2832	1.3709
30	550	37.58	0.005	220.21	1311.03	0.2768	1.6477
35	600	41	0.004	203.45	1514.48	0.2557	1.9034
40	625	42.71	0.004	204.74	1719.22	0.2573	2.1607
45	650	44.42	0.003	209.85	1929.07	0.2637	2.4244
50	675	46.13	0.003	212.55	2141.62	0.2671	2.6916
55	700	47.83	0.002	209.18	2350.8	0.2629	2.9545
60	750	51.25	0.004	190.3	2541.1	0.2392	3.1936

Run (4) Chem-60g-ADF

Time (min)	P-in (psig)	P-in (bar)	P-out (bar)	Vol (ml)	Cum Vol (ml)	Flux (kg/m^2.sec)	Cum Flux (kg/m^2.sec)
0	0	0	0	0	0	0	0
5	100	6.83	0.004	60.23	60.23	0.0757	0.0757
10	200	13.67	0.005	179	239.23	0.2250	0.3007
15	300	20.5	0.004	243.91	483.14	0.3065	0.6072
20	400	27.33	0.004	237.56	720.7	0.2986	0.9058
25	500	34,16	0.004	238.62	959.32	0.2999	1.2057
30	550	37.58	0.004	188.54	1147.86	0.2370	1.4426
35	600	41	0.004	173.09	1320.95	0.2175	1.6602
40	625	42.71	0.005	170.2	1491.15	0.2139	1.8741
45	650	44.42	0.005	164.35	1655.5	0.2066	2.0806
50	675	46.13	0.005	161.98	1817.48	0.2036	2.2842
55	700	47.83	0.005	159.62	1977.1	0.2006	2.4848
60	750	51.25					

Run (5) Chem-30g-Nano

Time (min)	P-in (psig)	P-in (bar)	P-out (bar)	Vol (ml)	Cum. Vol (ml)	Flux (kg/m^2.sec)	Cum. Flux (kg/m^2.sec)
0	0	0	0	0	0	0	0
5	100	6.83	0.005	37.21	37.21	0.0468	0.0468
10	200	13.67	0.005	244.23	281.44	0.3069	0.3537
15	300	20.5	0.006	553.04	834.48	0.6951	1.0488
20	400	27.33	0.006	930.82	1765.3	1.1698	2.2186
25	500	34.16	0.007	1338.06	3103.36	1.6817	3.9003
30	550	37.58	0.007	1560.22	4663.58	1.9609	5.8612
35	600	41	0.008	1744.25	6407.83	2.1922	8.0533
40	625	42.71	0.007	1882.75	8290.58	2.3662	10.4196
45	650	44.42	0.006	2062.43	10353.01	2.5921	13.0116
50	675	46.13					
55	700	47.83					
60	750	51.25					

Run (6) Chem-60g-Nano

Time (min)	P-in (psig)	P-in (bar)	P-out (bar)	Vol (ml)	Cum Vol (ml)	Flux ($kg/m^2.sec$)	Cum Flux ($kg/m^2.sec$)
0	0	0	0	0	0	0	0
5	100	6.83	0.022	17.73	17.73	0.0223	0.0223
10	200	13.67	0.023	278.06	295.79	0.3495	0.3717
15	300	20.5	0.021	394.6	690.39	0.4959	0.8677
20	400	27.33	0.021	445.94	1136.33	0.5605	1.4281
25	500	34.16	0.02	494.58	1630.91	0.6216	2.0497
30	550	37.58	0.019	478.95	2109.86	0.6019	2.6517
35	600	41	0.022	484.12	2593.98	0.6084	3.2601
40	625	42.71	0.023	488.54	3082.52	0.6140	3.8741
45	650	44.42	0.022	485.3	3567.82	0.6099	4.4840
50	675	46.13					
55	700	47.83					
60	750	51.25					

Run (7) Chem-Cl-30g-ADF

Time (min)	P-in (psig)	P-in (bar)	P-out (bar)	Vol (ml)	Cum Vol (ml)	Flux ($kg/m^2.sec$)	Cum Flux ($kg/m^2.sec$)
0	0	0	0	0	0	0	0
5	100	6.83	0.011	444.94	444.94	0.5592	0.5592
10	200	13.67	0.013	623.94	1068.88	0.7842	1.3434
15	300	20.5	0.013	586.8	1655.68	0.7375	2.0808
20	400	27.33	0.01	560.82	2216.5	0.7048	2.7857
25	500	34.16	0.012	584.01	2800.51	0.7340	3.5197
30	550	37.58	0.011	543.05	3343.56	0.6825	4.2022
35	600	41	0.011	544.5	3888.06	0.6843	4.8865
40	625	42.71	0.01	538.55	4426.61	0.6768	5.5633
45	650	44.42	0.01	523.13	4949.74	0.6575	6.2208
50	675	46.13	0.009	518.36	5468.1	0.6515	6.8723
55	700	47.83					
60	750	51.25					

Run (8) Chem-Cl-60g-ADF

Time (min)	P-in (psig)	P-in (bar)	P-out (bar)	Vol (ml)	Cum Vol (ml)	Flux ($kg/m^2.sec$)	Cum Flux ($kg/m^2.sec$)
0	0	0	0	0	0	0	0
5	100	6.83	0.004	133.24	133.24	0.1675	0.1675
10	200	13.67	0.004	344.86	478.1	0.4334	0.6009
15	300	20.5	0.003	263.69	741.79	0.3314	0.9323
20	400	27.33	0.002	230.64	972.43	0.2899	1.2221
25	500	34.16	0.002	228.36	1200.79	0.2870	1.5091
30	550	37.58	0.002	206.49	1407.28	0.2595	1.7687
35	600	41	0.003	197.05	1604.33	0.2477	2.0163
40	625	42.71	0.003	201.12	1805.45	0.2528	2.2691
45	650	44.42	0.003	197.22	2002.67	0.2479	2.5169
50	675	46.13	0.002	190.45	2193.12	0.2394	2.7563
55	700	47.83					
60	750	51.25					

Run (9) Chem-Cl-30g-Nano

Time (min)	P-in (psig)	P-in (bar)	P-out (bar)	Vol (ml)	Cum Vol (ml)	Flux ($kg/m^2.sec$)	Cum Flux ($kg/m^2.sec$)
0	0	0	0	0	0	0	0
5	100	6.83	0.009	505.05	505.05	0.6347	0.6347
10	200	13.67	0.005	999.23	1504.28	1.2558	1.8906
15	300	20.5	0.005	1012.73	2517.01	1.2728	3.1634
20	400	27.33	0.004	930.18	3447.19	1.1690	4.3324
25	500	34.16	0.004	935.15	4382.34	1.1753	5.5077
30	550	37.58	0.003	864.01	5246.35	1.0859	6.5936
35	600	41	0.002	844.07	6090.42	1.0608	7.6544
40	625	42.71	0.002	815.64	6906.06	1.0251	8.6795
45	650	44.42	0.002	779.24	7685.3	0.9793	9.6588
50	675	46.13	0.002	728.55	8413.85	0.9156	10.5745
55	700	47.83	0.001	700.9	9114.75	0.8809	11.4554
60	750	51.25					

Run (10) Chem-Cl-60g-Nano

Time (min)	P-in (psig)	P-in (bar)	P-out (bar)	Vol (ml)	Cum Vol (ml)	Flux ($kg/m^2.sec$)	Cum Flux ($kg/m^2.sec$)
0	0	0	0	0	0	0	0
5	150	10.25	0.006	52.9	52.9	0.0665	0.0665
10	200	13.67	0.007	126.72	179.62	0.1593	0.2257
15	300	20.5	0.008	358.56	538.18	0.4506	0.6764
20	400	27.33	0.008	406.96	945.14	0.5115	1.1878
25	500	34.16	0.009	522.05	1467.19	0.6561	1.8440
30	550	37.58	0.009	511.33	1978.52	0.6426	2.4866
35	600	41	0.015	506.38	2484.9	0.6364	3.1230
40	625	42.71	0.014	510.68	2995.58	0.6418	3.7648
45	650	44.42	0.013	509.61	3505.19	0.6405	4.4053
50	675	46.13	0.013	510.83	4016.02	0.6420	5.0473
55	700	47.83					
60	750	51.25					

Run (11) Chem-SO_4-30g-ADF

Time (min)	P-in (psig)	P-in (bar)	P-out (bar)	Vol (ml)	Cum Vol (ml)	Flux ($kg/m^2.sec$)	Cum Flux ($kg/m^2.sec$)
0	0	0	0	0	0	0	0
5	150	10.25	0.004	95.61	95.61	0.1202	0.1202
10	200	13.67	0.001	160.05	255.66	0.2011	0.3213
15	300	20.5	0.003	234.06	489.72	0.2942	0.6155
20	400	27.33	0.004	324.04	813.76	0.4073	1.0227
25	500	34.16	0.005	355.15	1168.91	0.4464	1.4691
30	550	37.58	0.005	352.91	1521.82	0.4435	1.9126
35	600	41	0.007	356.52	1878.34	0.4481	2.3607
40	625	42.71	0.001	352.4	2230.74	0.4429	2.8036
45	650	44.42	0.005	361.45	2592.19	0.4543	3.2579
50	675	46.13	0.001	365.27	2957.46	0.4591	3.7169
55	700	47.83					
60	750	51.25					

Run (12) Chem-SO_4-60g-ADF

Time (min)	P-in (psig)	P-in (bar)	P-out (bar)	Vol (ml)	Cum Vol (ml)	Flux (kg/m^2.sec)	Cum Flux (kg/m^2.sec)
0	0	0	0	0	0	0	0
5	150	10.25	0.006	62.87	62.87	0.0790	0.0790
10	200	13.67	0.007	116.2	179.07	0.1460	0.2251
15	300	20.5	0.009	220.97	400.04	0.2777	0.5028
20	400	27.33	0.011	327.74	727.78	0.4119	0.9147
25	500	34.16	0.011	378.52	1106.3	0.4757	1.3904
30	550	37.58	0.011	380.58	1486.88	0.4783	1.8687
35	600	41	0.011	387.93	1874.81	0.4875	2.3563
40	625	42.71	0.011	380.23	2255.04	0.4779	2.8341
45	650	44.42	0.009	380.71	2635.75	0.4785	3.3126
50	675	46.13					
55	700	47.83					
60	750	51.25					

Run (13) Chem-SO_4-30g-Nano

Time (min)	P-in (psig)	P-in (bar)	P-out (bar)	Vol (ml)	Cum Vol (ml)	Flux (kg/m^2.sec)	Cum Flux (kg/m^2.sec)
0	0	0	0	0	0	0	0
5	150	10.25	0.001	257.6	257.6	0.3238	0.3238
10	200	13.67	0.001	358.71	616.31	0.4508	0.7746
15	300	20.5	0.004	558.28	1174.59	0.7016	1.4762
20	400	27.33	0.005	690.87	1865.46	0.8683	2.3445
25	500	34.16	0.005	684.97	2550.43	0.8609	3.2054
30	550	37.58	0.005	635.97	3186.4	0.7993	4.0047
35	600	41	0.005	636.36	3822.76	0.7998	4.8044
40	625	42.71	0.005	617.9	4440.66	0.7766	5.5810
45	650	44.42	0.005	607.15	5047.81	0.7631	6.3441
50	675	46.13	0.004	610.64	5658.45	0.7674	7.1115
55	700	47.83					
60	750	51.25					

Run (14) Chem-SO_4-60g-Nano

Time (min)	P-in (psig)	P-in (bar)	P-out (bar)	Vol (ml)	Cum Vol (ml)	Flux (kg/m^2.sec)	Cum Flux (kg/m^2.sec)
0	0	0	0	0	0	0	0
5	100	6.83	0.002	182.3	182.3	0.2291	0.2291
10	200	13.67	0.002	501.98	684.28	0.6309	0.8600
15	300	20.5	0.004	609.66	1293.94	0.7662	1.6262
20	400	27.33	0.005	675.23	1969.17	0.8486	2.4748
25	500	34.16	0.005	668.5	2637.67	0.8402	3.3150
30	550	37.58	0.005	633.57	3271.24	0.7963	4.1113
35	600	41	0.005	635.94	3907.18	0.7992	4.9105
40	625	42.71	0.005	627.2	4534.38	0.7883	5.6988
45	650	44.42	0.005	626.88	5161.26	0.7879	6.4866
50	675	46.13	0.005	628.32	5789.58	0.7897	7.2763
55	700	47.83					
60	750	51.25					

Run (15) Chem-Na-30g-ADF

Time (min)	P-in (psig)	P-in (bar)	P-out (bar)	Vol (ml)	Cum Vol (ml)	Flux (kg/m^2.sec)	Cum Flux (kg/m^2.sec)
0	0	0	0	0	0	0	0
5	100	10.25	0	0	0	0	0
10	250	17.08	0.007	166.81	166.81	0.2096	0.2096
15	300	20.5	0.008	208.63	375.44	0.2622	0.4719
20	400	27.33	0.009	374.51	749.95	0.4707	0.9425
25	500	34.16	0.01	459.2	1209.15	0.5771	1.5197
30	550	37.58	0.01	445.3	1654.45	0.5597	2.0793
35	600	41	0.004	441.28	2095.73	0.5546	2.6339
40	625	42.71	0.004	431.5	2527.23	0.5423	3.1762
45	650	44.42	0.003	416.7	2943.93	0.5237	3.6999
50	675	46.13					
55	700	47.83					
60	750	51.25					

Run (16) Chem-Na-60g-ADF

Time (min)	P-in (psig)	P-in (bar)	P-out (bar)	Vol (ml)	Cum Vol (ml)	Flux (kg/m^2.sec)	Cum Flux (kg/m^2.sec)
0	0	0	0	0	0	0	0
5	100	6.83	0.009	59.51	59.51	0.0748	0.0748
10	200	13.67	0.008	220.91	280.42	0.2776	0.3524
15	300	20.5	0.008	306.68	587.1	0.3854	0.7379
20	400	27.33	0.008	280.22	867.32	0.3522	1.0900
25	500	34.16	0.008	270.61	1137.93	0.3401	1.4301
30	550	37.58	0.006	236.84	1374.77	0.2977	1.7278
35	600	41	0.005	223.02	1597.79	0.2803	2.0081
40	625	42.71	0.005	202.99	1800.78	0.2551	2.2632
45	650	44.42	0.004	191.92	1992.7	0.2412	2.5044
50	675	46.13					
55	700	47.83					
60	750	51.25					

Run (17) Chem-Na-30g-Nano

Time (min)	P-in (psig)	P-in (bar)	P-out (bar)	Vol (ml)	Cum Vol (ml)	Flux (kg/m^2.sec)	Cum Flux (kg/m^2.sec)
0	0	0	0	0	0	0	0
5	100	6.83	0.003	182.87	182.87	0.2298	0.2298
10	200	13.67	0.001	414.96	597.83	0.5215	0.7513
15	300	20.5	0.004	599.87	1197.7	0.7539	1.5053
20	400	27.33	0.005	695.73	1893.43	0.8744	2.3797
25	500	34.16	0.006	754.68	2648.11	0.9485	3.3281
30	550	37.58	0.005	662.99	3311.1	0.8332	4.1614
35	600	41	0.004	620.6	3931.7	0.7800	4.9413
40	625	42.71	0.004	567.94	4499.64	0.7138	5.6551
45	650	44.42	0.003	543.6	5043.24	0.6832	6.3383
50	675	46.13					
55	700	47.83					
60	750	51.25					

Run (18) Chem-Na-60g-Nano

Time (min)	P-in (psig)	P-in (bar)	P-out (bar)	Vol (ml)	Cum Vol (ml)	Flux ($kg/m^2.sec$)	Cum Flux ($kg/m^2.sec$)
0	0	0	0	0	0	0	0
5	100	6.83	0.008	199.67	199.67	0.2509	0.2509
10	200	13.67	0.01	365.66	565.33	0.4596	0.7105
15	300	20.5	0.006	472.83	1038.16	0.5943	1.3048
20	400	27.33	0.003	507.72	1545.88	0.6381	1.9429
25	500	34.16	0.003	559.46	2105.34	0.7031	2.6460
30	550	37.58	0.003	563.7	2669.04	0.7085	3.3544
35	600	41	0.003	572.88	3241.92	0.7200	4.0744
40	625	42.71	0.003	568.33	3810.25	0.7143	4.7887
45	650	44.42	0.003	575.23	4385.48	0.7229	5.5116
50	675	46.13					
55	700	47.83					
60	750	51.25					

Run (19) Chem-K-30g-ADF

Time (min)	P-in (psig)	P-in (bar)	P-out (bar)	Vol (ml)	Cum Vol (ml)	Flux ($kg/m^2.sec$)	Cum Flux ($kg/m^2.sec$)
0	0	0	0	0	0	0	0
5	100	6.83	0.026	288.46	288.46	0.3625	0.3625
10	200	13.67	0.015	275.14	563.6	0.3458	0.7083
15	300	20.5	0.015	318.45	882.05	0.4002	1.1086
20	400	27.33	0.018	428.98	1311.03	0.5391	1.6477
25	500	34.16	0.01	452.71	1763.74	0.5690	2.2167
30	550	37.58	0.009	411.72	2175.46	0.5174	2.7341
35	600	41	0.008	362.75	2538.21	0.4559	3.1900
40	625	42.71	0.007	305.73	2843.94	0.3842	3.5742
45	650	44.42	0.007	268.55	3112.49	0.3375	3.9118
50	675	46.13					
55	700	47.83					
60	750	51.25					

Run (20) Chem-K-60g-ADF

Time (min)	P-in (psig)	P-in (bar)	P-out (bar)	Vol (ml)	Cum Vol (ml)	Flux ($kg/m^2.sec$)	Cum Flux ($kg/m^2.sec$)
0	0	0	0	0	0	0	0
5	150	10.25	0.001	66.75	66.75	0.0839	0.0839
10	200	13.67	0.001	162.71	229.46	0.2045	0.2884
15	300	20.5	0.001	271.65	501.11	0.3414	0.6298
20	400	27.33	0.002	334.55	835.66	0.4205	1.0503
25	500	34.16	0.002	409.72	1245.38	0.5149	1.5652
30	550	37.58	0.002	417.55	1662.93	0.5248	2.0900
35	600	41	0.002	423.75	2086.68	0.5326	2.6225
40	625	42.71	0.002	414.79	2501.47	0.5213	3.1438
45	650	44.42	0.002	421.56	2923.03	0.5298	3.6736
50	675	46.13	0.002	423.92	3346.95	0.5328	4.2064
55	700	47.83					
60	750	51.25					

Run (21) Chem-K-30g-Nano

Time (min)	P-in (psig)	P-in (bar)	P-out (bar)	Vol (ml)	Cum Vol (ml)	Flux (kg/m^2.sec)	Cum Flux (kg/m^2.sec)
0	0	0	0	0	0	0	0
5	100	6.83	0.001	292.58	292.58	0.3677	0.3677
10	200	13.67	0.001	440.71	733.29	0.5539	0.9216
15	300	20.5	0.002	363.14	1096.43	0.4564	1.3780
20	400	27.33	0.002	490.84	1587.27	0.6169	1.9949
25	500	34.16	0.002	508.44	2095.71	0.6390	2.6339
30	550	37.58	0.002	471.3	2567.01	0.5923	3.2262
35	600	41	0.002	451.38	3018.39	0.5673	3.7935
40	625	42.71	0.001	409.46	3427.85	0.5146	4.3081
45	650	44.42	0.001	377.39	3805.24	0.4743	4.7824
50	675	46.13					
55	700	47.83					
60	750	51.25					

Run (22) Chem-K-60g-Nano

Time (min)	P-in (psig)	P-in (bar)	P-out (bar)	Vol (ml)	Cum Vol (ml)	Flux (kg/m^2.sec)	Cum Flux (kg/m^2.sec)
0	0	0	0	0	0	0	0
5	100	6.83	0.01	191.34	191.34	0.2405	0.2405
10	200	13.67	0.008	340.82	532.16	0.4283	0.6688
15	300	20.5	0.008	376.95	909.11	0.4737	1.1426
20	400	27.33	0.004	414.35	1323.46	0.5208	1.6633
25	500	34.16	0.005	479.38	1802.84	0.6025	2.2658
30	550	37.58	0.005	487.18	2290.02	0.6123	2.8781
35	600	41	0.005	497.49	2787.51	0.6252	3.5033
40	625	42.71	0.005	485.28	3272.79	0.6099	4.1132
45	650	44.42	0.005	507.66	3780.45	0.6380	4.7512
50	675	46.13					
55	700	47.83					
60	750	51.25					

Run (23) Biol-30g-ADF

Time (min)	P-in (psig)	P-in (bar)	P-out (bar)	Vol (ml)	Cum Vol (ml)	Flux (kg/m^2.sec)	Cum Flux (kg/m^2.sec)
0	0	0	0	0	0	0	0
5	100	6.83	0.039	65.52	65.52	0.0823	0.0823
10	200	13.67	0.017	332.78	398.3	0.4182	0.5006
15	300	20.5	0.006	559.67	957.97	0.7034	1.2040
20	400	27.33	0.004	490.76	1448.73	0.6168	1.8208
25	500	34.16	0.003	453.86	1902.59	0.5704	2.3912
30	550	37.58	0.002	414.94	2317.53	0.5215	2.9127
35	600	41	0.002	400.58	2718.11	0.5034	3.4161
40	625	42.71	0.002	382.48	3100.59	0.4807	3.8968
45	650	44.42	0.002	381.62	3482.21	0.4796	4.3764
50	675	46.13					
55	700	47.83					
60	750	51.25					

Run (24) Biol-60g-ADF

Time (min)	P-in (psig)	P-in (bar)	P-out (bar)	Vol (ml)	Cum Vol (ml)	Flux (kg/m^2.sec)	Cum Flux (kg/m2.sec)
0	0	0	0	0	0	0	0
5	100	6.83	0.001	130.81	130.81	0.1644	0.1644
10	200	13.67	0.007	351.66	482.47	0.4420	0.6064
15	300	20.5	0.006	252.12	734.59	0.3169	0.9232
20	400	27.33	0.003	151.11	885.7	0.1899	1.1131
25	500	34.16	0.003	136.34	1022.04	0.1714	1.2845
30	550	37.58	0.002	105.34	1127.38	0.1324	1.4169
35	600	41	0.002	97.57	1224.95	0.1226	1.5395
40	625	42.71	0.001	79.99	1304.94	0.1005	1.6400
45	650	44.42	0.001	71.8	1376.74	0.0902	1.7303
50	675	46.13					
55	700	47.83					
60	750	51.25					

Run (25) Biol-30g-Nano

Time (min)	P-in (psig)	P-in (bar)	P-out (bar)	Vol (ml)	Cum Vol (ml)	Flux (kg/m^2.sec)	Cum Flux (kg/m^2.sec)
0	0	0	0	0	0	0	0
5	150	10.25	0.02	131.04	131.04	0.1647	0.1647
10	200	13.67	0.024	190.05	321.09	0.2389	0.4035
15	300	20.5	0.018	322.39	643.48	0.4052	0.8087
20	400	27.33	0.018	328.79	972.27	0.4132	1.2219
25	500	34.16	0.018	352.65	1324.92	0.4432	1.6652
30	550	37.58	0.013	351.21	1676.13	0.4414	2.1066
35	600	41	0.014	372.4	2048.53	0.4680	2.5746
40	625	42.71	0.011	368.15	2416.68	0.4627	3.0373
45	650	44.42	0.008	387.26	2803.94	0.4867	3.5240
50	675	46.13					
55	700	47.83					
60	750	51.25					

Run (26) Biol-60g-Nano

Time (min)	P-in (psig)	P-in (bar)	P-out (bar)	Vol (ml)	Cum Vol (ml)	Flux (kg/m^2.sec)	Cum Flux (kg/m^2.sec)
0	0	0	0	0	0	0	0
5	150	10.25	0.021	130.19	130.19	0.1636	0.1636
10	200	13.67	0.025	199.28	329.47	0.2505	0.4141
15	300	20.5	0.028	303.68	633.15	0.3817	0.7957
20	400	27.33	0.027	369.32	1002.47	0.4642	1.2599
25	500	34.16	0.03	538.03	1540.5	0.6762	1.9361
30	550	37.58	0.029	499.88	2040.38	0.6282	2.5643
35	600	41	0.03	512.46	2552.84	0.6441	3.2084
40	625	42.71	0.029	502.84	3055.68	0.6320	3.8404
45	650	44.42	0.029	497.14	3552.82	0.6248	4.4652
50	675	46.13					
55	700	47.83					
60	750	51.25					

Run (27) Pre-Biol-30g-ADF

Time (min)	P-in (psig)	P-in (bar)	P-out (bar)	Vol (ml)	Cum Vol (ml)	Flux ($kg/m^2.sec$)	Cum Flux ($kg/m^2.sec$)
0	0	0	0	0	0	0	0
5	150	10.25	0.004	92.76	92.76	0.1166	0.1166
10	200	13.67	0.003	178.14	270.9	0.2239	0.3405
15	300	20.5	0.001	446.49	717.39	0.5611	0.9016
20	400	27.33	0.001	520.44	1237.83	0.6541	1.5557
25	500	34.16	0.002	531.24	1769.07	0.6677	2.2234
30	550	37.58	0.001	513.03	2282.1	0.6448	2.8681
35	600	41	0.001	520.5	2802.6	0.6542	3.5223
40	625	42.71	0.001	512.42	3315.02	0.6440	4.1663
45	650	44.42	0.001	514.57	3829.59	0.6467	4.8130
50	675	46.13					
55	700	47.83					
60	750	51.25					

Run (28) Pre-Biol-60g-ADF

Time (min)	P-in (psig)	P-in (bar)	P-out (bar)	Vol (ml)	Cum Vol (ml)	Flux ($kg/m^2.sec$)	Cum Flux ($kg/m^2.sec$)
0	0	0	0	0	0	0	0
5	100	6.83	0.006	32.05	32.05	0.0403	0.0403
10	200	13.67	0.001	402.07	434.12	0.5053	0.5456
15	300	20.5	0.001	489.57	923.69	0.6153	1.1609
20	400	27.33	0.001	467.66	1391.35	0.5878	1.7486
25	500	34.16	0.001	469.64	1860.99	0.5902	2.3389
30	550	37.58	0.001	435.23	2296.22	0.5470	2.8859
35	600	41	0.001	428.68	2724.9	0.5388	3.4246
40	625	42.71	0.001	409.08	3133.98	0.5141	3.9388
45	650	44.42	0.001	402.22	3536.2	0.5055	4.4443
50	675	46.13					
55	700	47.83					
60	750	51.25					

Run (29) Pre-Biol-30g-Nano

Time (min)	P-in (psig)	P-in (bar)	P-out (bar)	Vol (ml)	Cum Vol (ml)	Flux ($kg/m^2.sec$)	Cum Flux ($kg/m^2.sec$)
0	0	0	0	0	0	0	0
5	150	10.25	0.004	92.76	92.76	0.1166	0.1166
10	200	13.67	0.003	178.14	270.9	0.2239	0.3405
15	300	20.5	0.001	446.49	717.39	0.5611	0.9016
20	400	27.33	0.001	520.44	1237.83	0.6541	1.5557
25	500	34.16	0.002	531.24	1769.07	0.6677	2.2234
30	550	37.58	0.001	513.03	2282.1	0.6448	2.8681
35	600	41	0.001	520.5	2802.6	0.6542	3.5223
40	625	42.71	0.001	512.42	3315.02	0.6440	4.1663
45	650	44.42	0.001	514.57	3829.59	0.6467	4.8130
50	675	46.13					
55	700	47.83					
60	750	51.25					

Run (30) Pre-Biol-60g-Nano

Time (min)	P-in (psig)	P-in (bar)	P-out (bar)	Vol (ml)	Cum Vol (ml)	Flux ($kg/m^2.sec$)	Cum Flux ($kg/m^2.sec$)
0	0	0	0	0	0	0	0
5	150	10.25	0.004	92.76	92.76	0.1166	0.1166
10	200	13.67	0.003	178.14	270.9	0.2239	0.3405
15	300	20.5	0.001	446.49	717.39	0.5611	0.9016
20	400	27.33	0.001	520.44	1237.83	0.6541	1.5557
25	500	34.16	0.002	531.24	1769.07	0.6677	2.2234
30	550	37.58	0.001	513.03	2282.1	0.6448	2.8681
35	600	41	0.001	520.5	2802.6	0.6542	3.5223
40	625	42.71	0.001	512.42	3315.02	0.6440	4.1663
45	650	44.42	0.001	514.57	3829.59	0.6467	4.8130
50	675	46.13					
55	700	47.83					
60	750	51.25					

Qabar-Onn Lake Data

A1: Published work on Qabar-Onn Lake

The following results were reported from the published paper which was presented by J. Furet in the *8th Diatom-Symposium, Paris, France, 12-14 Mar. 1984*, (Ajaili, *et al*, 1984).

Depth / Constituent		0.1 m	1 m	2 m	3 m	4 m	5 m	6 m	7.8 m
Cl^-	($mg\ l^{-1}$)	60,000	69,500	67,500	70,000	71,500	71,500	85,000	70,000
Na^+	($mg\ l^{-1}$)	39,100	55,200	55,200	55,200	55,200	57,500	55,200	57,500
K^+	($mg\ l^{-1}$)	12,512	16,422	16,813	16,422	17,986	17,204	16,422	17,595
Ca^{++}	($mg\ l^{-1}$)	175	175	175	175	175	175	175	175
Mg^{++}	($mg\ l^{-1}$)	21	40	40	40	40	40	40	40
$SO_4^=$	($mg\ l^{-1}$)	12,916	12,697	11,672	11,748	12,814	13,138	12,326	12,969
HCO_3^-	($mg\ l^{-1}$)	105	125	124	127	128	124	· 119	123
$CO_3^=$	($mg\ l^{-1}$)	131	158	159	161	165	161	158	168
Conductivity (μmhos/cm)		1.0×10^5	1.0×10^5	1.0×10^5	1.0×10^5	1.0×10^5	1.0×10^5	1.0×10^5	1.0×10^5

Table A-1: Major chemical constituents at eight depths in Qabar-Onn Lake during cold season (8th December 1983).

A-2 Reported Data and information

The following results and information were collected from undergraduate students' project reports, which were carried out in the year 2001 at *Faculty of Engineering and Technology, The University of sebha* (El-Saedi, 2002).

Parameter		Surface water	Half depth	Bottom
pH		10.33	9.72	9.52
TDS	($mg\ l^{-1}$)	173,000	185,000	189,000
DO	($mg\ l^{-1}$)	8.7	7.5	4.3
Salinity	($mg\ l^{-1}$)	149,000	159,000	160,000
Hardness	($mg\ l^{-1}$)	310	323	325
Chloride	($mg\ l^{-1}$)	45,920	57,900	69,879
SO_4	($mg\ l^{-1}$)	14,150	10,288	9,315
Total Alkaline	($mg\ l^{-1}$)	311	320	335
OH Alkalinity	($mg\ l^{-1}$)	907	901	1,044
CO_3 Alkalinity	(mg/l)	866	932	846

Table A-2: Reported chemical analyses of Qabar-Onn Lake in 2001.

APPENDIX B

EXPERIMENTAL PROCEDURES AND PROTOCOLS

DNA Extraction For the Cyanobacterial Isolate (Euhalothece sp. BAA001) From Qabar-Onn Lake

(based on Mo Bio Instruction Manual for UltraClean™ Microbial DNA Isolation Kit)

A: DNA extraction

Date of Analysis: 26/09/2003

Requriments:

- Product No. of DNA Kit: 12225-250
- Autoclaved blue 1mL pipette tips
- 50-200uL and 100-1000uL pipettors
- Molecular Biology Reagent Water (e.g. Promega, P119C)
- Micro centrifuge (10'000g)
- Vortex and cell disrupter

Protocol:

1. Transfer 1.8 mL from culture to 1.9mL microcentrifuge tube;
2. Centrifuge at 10'000xg for 0.5min;
3. Decant supernatant, add 'washing buffer' in 1:2 volumes (sample:buffer), vortex for a few seconds and centrifuge again;
4. Repeat step 3 for 3 times,
5. Add **50uL** of solution **MD1** and Microbeads from Microbead tube;
6. Resuspend cell pellets in 300uL MicroBead solution and gently vortex to mix;
7. To increase yields: heat at 70°C for 10min, then 10min cell disruptor;
8. Centrifuge at 10'000g for 30s;
9. Transfer supernatant to clean microcentrifuge tube (provided);
10. Note: expect 300-350uL of supernatant;
11. Add **100uL** of solution **MD2** to supernatant, vortex (5s) and incubate in refrigerator for 20min;
12. Centrifuge the tubes for 2min at 10'000g;
13. Avoiding the pellet, transfer supernatant to a clean 1.9mL tube (provided) (expect 400- 450uL);
14. Add **900uL** of solution **MD3** to supernatant and vortex (5s);
15. Load about 700uL into spin filter and centrifuge at 10'000g for 30s;
16. Discard filtrate (flow-through) and add the rest from 14. and centrifuge at 10'000g for 30s;
17. Discard filtrate;
18. Add **300uL** of solution **MD4** and centrifuge for 30s at 10'000g;
19. Discard filtrate and centrifuge again for 1min;
20. Being careful not to splash liquid on the filter basket, place spin filter in a new 1.9mL tube (provided);
21. Add **50uL** of solution **MD5** to the center of the white filter membrane;
22. Centrifuge for 30s;
23. Discard spin filter. DNA tube is now ready for any application.
24. Eluted DNA sample recommended to be stored at -20°C

B: Determination of genomic DNA concentration by spectrophotometric analysis

Procedure:

1. Add 70µL of DNA-free DDW to clean UV quartz cuvette (control);
2. Add 65µ of DNA-free DDW and 5µL of the eluted DNA sample to another clean UV quartz cuvette;
3. Use spectrophotometer program number 3. (Nucleic Acid) and press OK;
4. Select '1. DNA';
5. Select 10nm path length and press OK;
6. Select 'ng/µL' as unit and press OK;
7. Select 320nm correction;
8. Select 'Yes' for scan options;
9. Select dilution factor, DF, of 30;
10. Press green button to start reference measurement;
11. Add 2µL DNA sample and mix by pipetting in and out repeatedly;
12. Press green button to measure DNA content

Results (Date of Analysis: 26/09/2003):

λ	Au
230	*2.775*
260	***0.482***
280	***0.426***
320	*0.388*

Sample	260/230	260/280	DNA content [ng/uL]	Comments
Control				
Run 1	0.000	1.07	0	
Sample (1)				
Run 1	0.04	2.25	**93**	High concentration

C: Size and quality check for genomic DNA

Equipment required:

Electrophoresis Apparatus (EA)
Horizon® 58, Life Technologies, Gibeo BRL Horizontal Gel EA
PowerPac, Bio-Rad, Basic 300V, 400mA, 75W
Imaging system
Syngene, Synoptics Ltd., UK.

Procedure:

1. Assemble EA and put in freezer;
2. Prepare 50mL 1x TAE buffer (or 0.5x TBE; Sigma, T-4323) and add to 100mL Erlenmeyer flask;
3. Add 1%-wt (0.5g) agarose (for Routine Use; Sigma, A9539) and mix;
4. Microwave for 3min at medium heat, take out when boiling, mix and put back (wait one round and repeat until all colloidal matter has dissolved)
5. Add 1.25uL intercalating dye (Ethidium bromide stored in cupboard, NB: wear gloves!!) and mix;
6. Tilt EA and pour little bit of agar onto bottom of black wall to seal it off (wait until agar has solidified and repeat for other side);
7. Pour in remaining agar avoiding bubbles, wait ca. 20min for agar to set
8. Remove white cone and black walls;
9. Fill EA with 1x TAE buffer (agar must be covered completely by buffer);
10. Add drop(s) of 2uL Blue/Orange 6x loading dye (stored in centrifuge tube at -20°C; Promena, G190A) onto parafilm (Kev's 'new school' technique);
11. Mix drop with 5uL of sample and add immediately (this is to avoid pipette tip wastage) to agarose well avoiding piercing the bottom of the well with the pipette tip;
12. Connect EA to Power Pac and set time to 120min and voltage to 55V (higher voltage reduces run time but heats and melts the agar; Problem can be avoided if crushed ice is placed beneath gel bed);

The genomic DNA should migrate as a single, high molecular weight band with little evidence of shearing.

DNA Extraction For the Cyanobacterial Isolate (Euhalothece sp. BAA002) From Qabar-Onn Lake

(based on Mo Bio Instruction Manual for UltraClean™ Microbial DNA Isolation Kit)

A: DNA extraction **Date of Analysis: 19/04/2004**

Requriments:

- Product No. of DNA Kit: 12225-250
- Autoclaved blue 1mL pipette tips
- 50-200uL and 100-1000uL pipettors
- Molecular Biology Reagent Water (e.g. Promega, P119C)
- Micro centrifuge (10'000g)
- Vortex and cell disrupter

Protocol:

25. Transfer 1.8 mL from culture to 1.9mL microcentrifuge tube;
26. Centrifuge at 10'000xg for 0.5min;
27. Decant supernatant, add ' washing buffer' in 1:2 volumes (sample:buffer), vortex for a few seconds and centrifuge again;
28. Repeat step 3 for 3 times,
29. Add **50uL** of solution **MD1** and Microbeads from Microbead tube;
30. Resuspend cell pellets in 300uL MicroBead solution and gently vortex to mix;
31. To increase yields: heat at 70°C for 10min, then 10min cell disruptor;
32. Centrifuge at 10'000g for 30s;
33. Transfer supernatant to clean microcentrifuge tube (provided);
34. Note: expect 300-350uL of supernatant;
35. Add **100uL** of solution **MD2** to supernatant, vortex (5s) and incubate in refrigerator for 20min;
36. Centrifuge the tubes for 2min at 10'000g;
37. Avoiding the pellet, transfer supernatant to a clean 1.9mL tube (provided) (expect 400- 450uL);
38. Add **900uL** of solution **MD3** to supernatant and vortex (5s);
39. Load about 700uL into spin filter and centrifuge at 10'000g for 30s;
40. Discard filtrate (flow-through) and add the rest from 14. and centrifuge at 10'000g for 30s;
41. Discard filtrate;
42. Add **300uL** of solution **MD4** and centrifuge for 30s at 10'000g;
43. Discard filtrate and centrifuge again for 1min;
44. Being careful not to splash liquid on the filter basket, place spin filter in a new 1.9mL tube (provided);
45. Add **50uL** of solution **MD5** to the center of the white filter membrane;
46. Centrifuge for 30s;
47. Discard spin filter. DNA tube is now ready for any application.
48. Eluted DNA sample recommended to be stored at -20°C

B: Determination of genomic DNA concentration by spectrophotometric analysis

Procedure:

13. Add 70µL of DNA-free DDW to clean UV quartz cuvette (control);
14. Add 65µ of DNA-free DDW and 5µL of the eluted DNA sample to another clean UV quartz cuvette;
15. Use spectrophotometer program number 3. (Nucleic Acid) and press OK;
16. Select '1. DNA';
17. Select 10nm path length and press OK;
18. Select 'ng/µL' as unit and press OK;
19. Select 320nm correction;
20. Select 'Yes' for scan options;
21. Select dilution factor, DF, of 30;
22. Press green button to start reference measurement;
23. Add 2µL DNA sample and mix by pipetting in and out repeatedly;
24. Press green button to measure DNA content

Results (Date of Analysis: 19/04/2004):

λ	Au
260	*0.022*
280	*0.014*

λ	Au
260	*0.035*
280	*0.022*

Sample	260/280	DNA content [ng/uL]	Comments
Control			
Run 1	0.000	0	
Sample (3A) 3M			
Run 1	1.57	**15.4**	low concentration
Sample (2A) 2M			
Run 1	1.59	**24.5**	fair concentration

C: Size and quality check for genomic DNA

Equipment required:

Electrophoresis Apparatus (EA)
Horizon® 58, Life Technologies, Gibeo BRL Horizontal Gel EA
PowerPac, Bio-Rad, Basic 300V, 400mA, 75W
Imaging system
Syngene, Synoptics Ltd., UK.

Procedure:

13. Assemble EA and put in freezer;
14. Prepare 50mL 1x TAE buffer (or 0.5x TBE; Sigma, T-4323) and add to 100mL Erlenmeyer flask;
15. Add 1%-wt (0.5g) agarose (for Routine Use; Sigma, A9539) and mix;
16. Microwave for 3min at medium heat, take out when boiling, mix and put back (wait one round and repeat until all colloidal matter has dissolved)
17. Add 1.25uL intercalating dye (Ethidium bromide stored in cupboard, NB: wear gloves!!) and mix;
18. Tilt EA and pour little bit of agar onto bottom of black wall to seal it off (wait until agar has solidified and repeat for other side);
19. Pour in remaining agar avoiding bubbles, wait ca. 20min for agar to set
20. Remove white cone and black walls;
21. Fill EA with 1x TAE buffer (agar must be covered completely by buffer);
22. Add drop(s) of 2uL Blue/Orange 6x loading dye (stored in centrifuge tube at -20°C; Promena, G190A) onto parafilm (Kev's 'new school' technique);
23. Mix drop with 5uL of sample and add immediately (this is to avoid pipette tip wastage) to agarose well avoiding piercing the bottom of the well with the pipette tip;
24. Connect EA to Power Pac and set time to 120min and voltage to 55V (higher voltage reduces run time but heats and melts the agar; Problem can be avoided if crushed ice is placed beneath gel bed);

The genomic DNA should migrate as a single, high molecular weight band with little evidence of shearing.

Results:

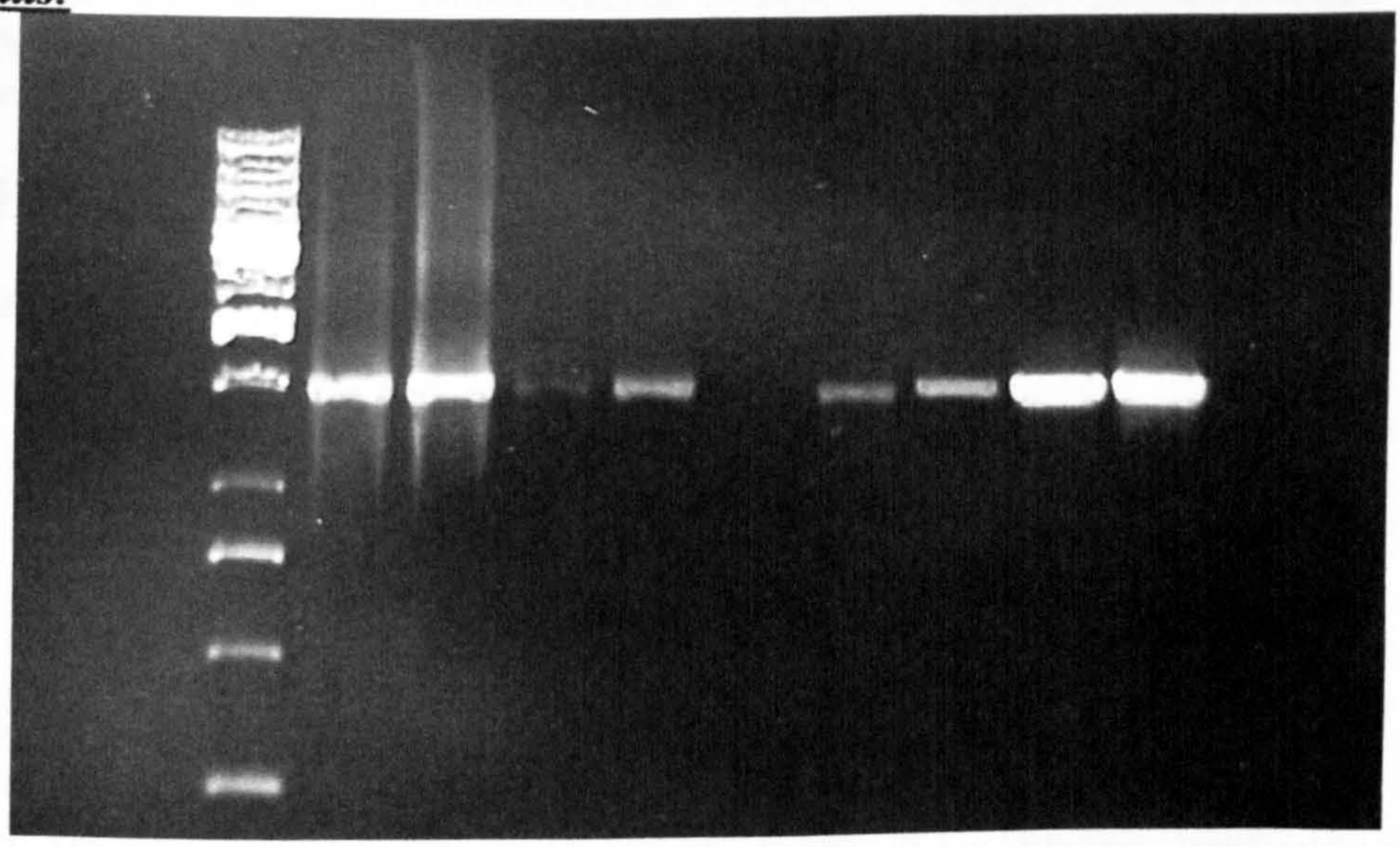

Lane 1= 100 base pair (bp) marker (very weak, but can make out 500 bp band)
Lane 2= Species BAA002 (sample 1)
Lane 3= Species BAA002 (sample 2)
Lane 6=negative control (water).
Lane 10=Positive control (*Prochlorococcus*)

The bands for species BAA002 (both samples) around the expected 800bp mark and to back this up the positive control *Prochlorococcus* has the same size band. The negative control is blank as expected.

DNA Extraction for the Halobacterial Isolate (*Halomonas pantelleriensis* BAA003) From Qabar-Onn Lake
(based on Mo Bio Instruction Manual for UltraClean™ Microbial DNA Isolation Kit)

A: DNA extraction **Date of Analysis: 26/07/2004**

Requriments:

- Product No. of DNA Kit: 12225-250
- Autoclaved blue 1mL pipette tips
- 50-200uL and 100-1000uL pipettors
- Molecular Biology Reagent Water (e.g. Promega, P119C)
- Micro centrifuge (10'000g)
- Vortex and cell disrupter

Protocol:

49. Transfer 1.8 mL from culture to 1.9mL microcentrifuge tube;
50. Centrifuge at 10'000xg for 0.5min;
51. Decant supernatant, add 'secret washing buffer' in 1:2 volumes (sample:buffer), vortex for a few seconds and centrifuge again;
52. Repeat step 3 for 3 times,
53. Add **50uL** of solution **MD1** and Microbeads from Microbead tube;
54. Resuspend cell pellets in 300uL MicroBead solution and gently vortex to mix;
55. To increase yields: heat at 70°C for 10min, then 10min cell disruptor;
56. Centrifuge at 10'000g for 30s;
57. Transfer supernatant to clean microcentrifuge tube (provided);
58. Note: expect 300-350uL of supernatant;
59. Add **100uL** of solution **MD2** to supernatant, vortex (5s) and incubate in refrigerator for 20min;
60. Centrifuge the tubes for 2min at 10'000g;
61. Avoiding the pellet, transfer supernatant to a clean 1.9mL tube (provided) (expect 400- 450uL);
62. Add **900uL** of solution **MD3** to supernatant and vortex (5s);
63. Load about 700uL into spin filter and centrifuge at 10'000g for 30s;
64. Discard filtrate (flow-through) and add the rest from 14. and centrifuge at 10'000g for 30s;
65. Discard filtrate;
66. Add **300uL** of solution **MD4** and centrifuge for 30s at 10'000g;
67. Discard filtrate and centrifuge again for 1min;
68. Being careful not to splash liquid on the filter basket, place spin filter in a new 1.9mL tube (provided);
69. Add **50uL** of solution **MD5** to the center of the white filter membrane;
70. Centrifuge for 30s;
71. Discard spin filter. DNA tube is now ready for any application.
72. Eluted DNA sample recommended to be stored at -20°C

B: Determination of genomic DNA concentration by spectrophotometric analysis

Procedure:

25. Add 70µL of DNA-free DDW to clean UV quartz cuvette (control);
26. Add 65µ of DNA-free DDW and 5µL of the eluted DNA sample to another clean UV quartz cuvette;
27. Use spectrophotometer program number 3. (Nucleic Acid) and press OK;
28. Select '1. DNA';
29. Select 10nm path length and press OK;
30. Select 'ng/µL' as unit and press OK;
31. Select 320nm correction;
32. Select 'Yes' for scan options;
33. Select dilution factor, DF, of 30;
34. Press green button to start reference measurement;
35. Add 2µL DNA sample and mix by pipetting in and out repeatedly;
36. Press green button to measure DNA content

Results (Date of Analysis: 26/07/2004):

Sample 1

λ	Au
230	*0.093*
260	*0.054*
280	*0.021*
320	*-0.016*

Sample2

λ	Au
230	*0.315*
260	*0.049*
280	*0.039*
320	*0.031*

Sample	260/230	260/280	DNA content [ng/uL]	Comments
Control				
Run 1	0.000			
Sample (1)				
Run 1	0.064			low concentration
Run 2	1.86			low concentration
Sample (2)				
Run 1	0.06			low concentration
Run 2	2.29			fair concentration

C: Size and quality check for genomic DNA

Equipment required:

Electrophoresis Apparatus (EA)
Horizon® 58, Life Technologies, Gibeo BRL Horizontal Gel EA
PowerPac, Bio-Rad, Basic 300V, 400mA, 75W
Imaging system
Syngene, Synoptics Ltd., UK.

Procedure:

25. Assemble EA and put in freezer;
26. Prepare 50mL 1x TAE buffer (or 0.5x TBE; Sigma, T-4323) and add to 100mL Erlenmeyer flask;
27. Add 1%-wt (0.5g) agarose (for Routine Use; Sigma, A9539) and mix;
28. Microwave for 3min at medium heat, take out when boiling, mix and put back (wait one round and repeat until all colloidal matter has dissolved)
29. Add 1.25uL intercalating dye (Ethidium bromide stored in cupboard, NB: wear gloves!!) and mix;
30. Tilt EA and pour little bit of agar onto bottom of black wall to seal it off (wait until agar has solidified and repeat for other side);
31. Pour in remaining agar avoiding bubbles, wait ca. 20min for agar to set
32. Remove white cone and black walls;
33. Fill EA with 1x TAE buffer (agar must be covered completely by buffer);
34. Add drop(s) of 2uL Blue/Orange 6x loading dye (stored in centrifuge tube at -20°C; Promena, G190A) onto parafilm (Kev's 'new school' technique);
35. Mix drop with 5uL of sample and add immediately (this is to avoid pipette tip wastage) to agarose well avoiding piercing the bottom of the well with the pipette tip;
36. Connect EA to Power Pac and set time to 120min and voltage to 55V (higher voltage reduces run time but heats and melts the agar; Problem can be avoided if crushed ice is placed beneath gel bed);

The genomic DNA should migrate as a single, high molecular weight band with little evidence of shearing.

Results:

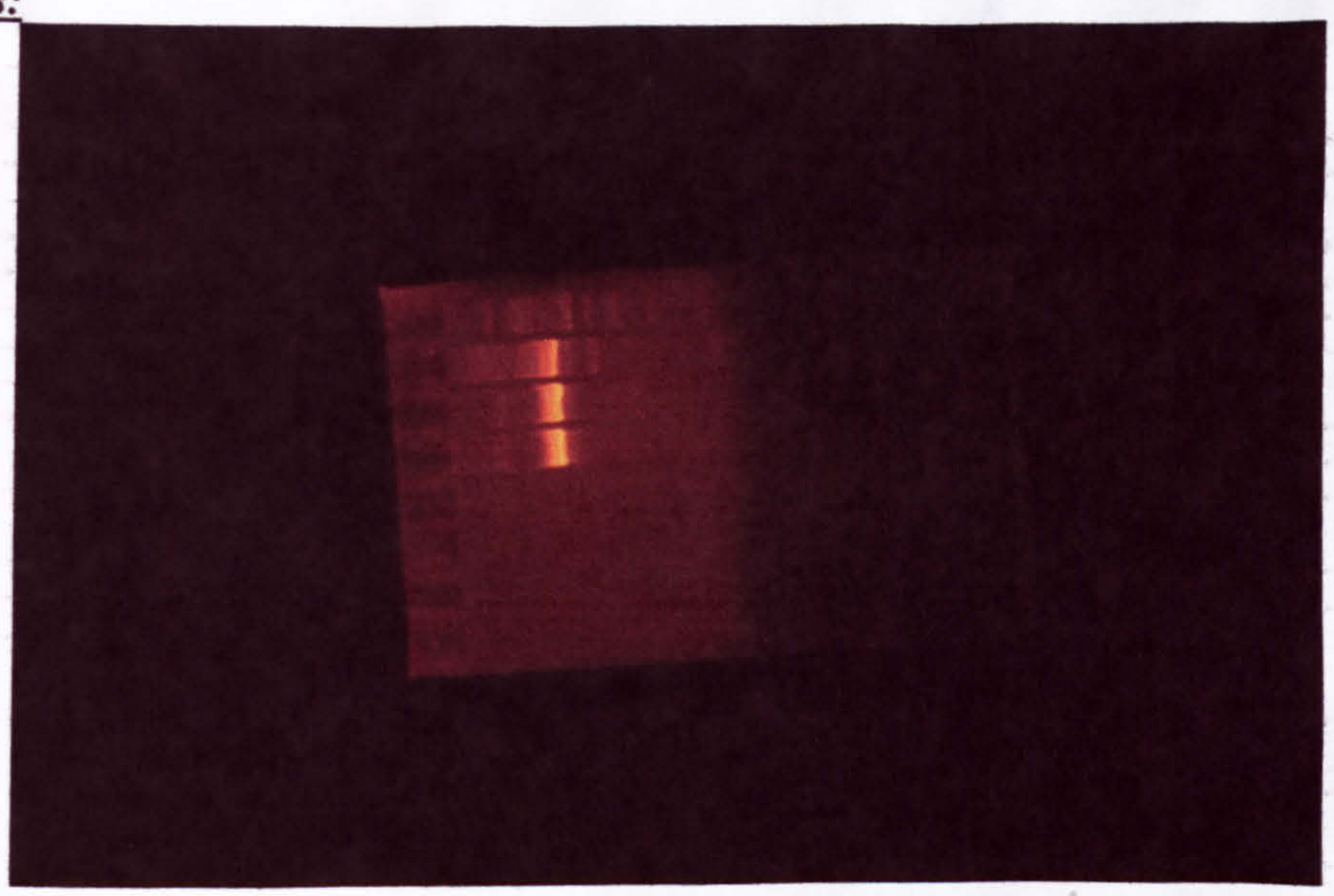

Lane 1= 100 base pair (bp) marker (very weak, but can make out 500 bp band)
Lane 2= Species *x*
Lane 3= Species *y*
Lane 4=Positive control (*Prochlorococcus*)
Lane 5=negative control (water).

The bands for species *x* and *y* are around the expected 800bp mark and to back this up the positive control *Prochlorococcus* has the same size band. The negative control is blank as expected.

Gram's Staining Protocol

Gram's staining experiment was carried out on the halotolerant bacterial species, isolated fro Qabar-Onn Lake, in order to characterise them for the purpose of identification. A Gram's Staining Kit (Catalogue No. PL8055/25, which contains 250 ml Crystal Violet, 250 ml PL7000/25; 250 ml Gram's Iodine, PL7003/25; 250 ml Gram's Differentiator, PL7006/25; 250 ml Safranin, PL7012/25) was used for both Gram-positive and Gram-negative staining of the isolated halobacteria in this experiment.

The staining procedure was carried out as described in the protocol of this product (a detailed staining procedure is presented in Appendix B). 100 µl of the thick centrifuged halobacterial culture was used to prepare a smear on a microscope slide. Having the staining process was done, the stained slides were observed under a light microscope (OLYMPUS, reflected light/fluorescence attachment, Model BH2-RFCA, Japan) using oil immersion objective ×100 magnification.

Procedure:

1. Prepare smear of material to be examined, dry and heat fix using gentle heat. Alternatively, smear may be fixed in methanol.
2. Apply Crystal Violet and stain for 1 minute.
3. Remove excess stain by rinsing slide in water. Shake off excess water.
4. Apply Gram's Iodine for 1 minute.
5. Remove excess stain by rinsing slide in water. Shake off excess water.
6. Apply Gram's Differentiator until no more colour washes out (do not over decolourise). Rinse quickly and shake off excess water.
7. Apply Safranin for 1 minute.
8. Remove excess stain by rinsing slide in water. Shake off excess water.
9. Blot slide gently on clean blotting paper and dry using gentle heat.
10. Examine stained slide under light microscope using oil immersion objective ×100 under oil.

When the Gram's stain procedure is performed correctly, organisms or cells that retain the primary stain/mordant complex will appear as blue to purple in colour and are termed Gram-positive. Organisms and cells that are decolourised by the Differentiator and take up the counter-stain will appear as pink to red in colour and are termed as Gram-negative.

RC-DC Protein Assay (Bio-Rad) Procedure

1. Prepare five standards for the calibration curve as follows:

Dilution Factor	Concentration (mg/ml)	Amount of standard (µg)	Amount of H2O (µl)
0	1.450	25.00	0
1	0.725	12.5	12.50
2	0.483	8.33	16.67
3	0.363	6.25	18.75
4	0.290	5.00	20.00
5	0.58	1.00	24.00

2. Pipette 25 ml of sample(s) into a clean Eppendorf tubes,
3. Add 125 ml RC Reagent I in to each sample and standards tubes, incubate at room temperature for 1 minute,
4. Add 125 ml RC Reagent II to each tube, vortex. Centrifuge tubes at 13,000x for 5 minutes,
5. Discard supernatant using a pipette, drain as much as possible,
6. Add 127 ml Reagent A to each tube, vortex. Incubate at room temperature for 5 minutes (as ppt dissolves).
7. Vortex and then add 1 ml of DC Reagent B to each tube, vortex immediately, incubate at room temperature for 15 minutes,
8. Read absorbance at 750 nm (absorbance is stable for 1 hour),
9. Plot graph (standard curve) of protein concentration (x-axis) against absorbance (y-axis). Calculate protein concentration from linear equation obtained from standard curve.

Protein Analysis of Cyanobacterial Biofilm on Various Substrata

	Dil. factor	Absor @ 750nm	protein conc. (µg/ml)	Stand (µl)	water (µl)
Std 1	5	0.077	0.058	1	24
Std 2	4	0.115	0.29	5	20
Std 3	3	0.134	0.363	6.25	18.75
Std 4	2	0.149	0.483	8.33	16.67
Std 5	1	0.188	0.725	12.5	12.5
Std 6	0	0.318	1.45	25	0

At zero salinity

	Absorbance @ 750nm	protein conc. (µg/ml)	% [µg/ml (substratum)/µg/ml (culture)]
S. steel	0.064	0.305	35
Teflon	0.069	0.334	39
ADF-membrane	0.073	0.357	41
Perspex glass	0.063	0.299	35
Bulk solution	0.16	0.861	100

At 60 g/l salinity

	Absorbance @ 750nm	protein conc. (µg/ml)	% [µg/ml (substratum)/µg/ml (culture)]
S. steel	0.064	0.305	35
Teflon	0.069	0.334	39
ADF-membrane	0.073	0.357	41
Perspex glass	0.063	0.299	35
Bulk solution	0.16	0.861	100

APPENDIX C

CALCULATIONS OF REQUIRED CHEMICAL INGREDIENTS AND THE OSMOTIC PRESSURE

Calculations of
Chemical Ingredients and osmotic pressure For Chemical Samples

Sample 1 (30 g l^{-1} salinity):

15 g l^{-1} (NaCl) + 15 g l^{-1} (K_2SO_4)
(15/58.442 moles NaCl) + (15/174.252 moles K_2SO_4)
(0.2567 moles NaCl) + (0.0861 moles K_2SO_4)
Total: (0.2567 moles Na + 0.2567 moles Cl + 0.172 moles K + 0.0861 moles SO_4)

Sample 2 (60 g l^{-1} salinity):

30 g l^{-1} (NaCl) + 30 g l^{-1} (K_2SO_4)
(30/58.442 moles Na Cl) + (30/174.252 moles K_2SO_4)
(0.513 moles NaCl) + (0.172 moles K_2SO_4)
Total: (0.513 moles Na + 0.513 moles Cl + 0.344 moles K + 172 moles SO_4)

Sample 3 (30 g l^{-1} salinity) (-Cl):

15 g l^{-1} (Na_2SO_4) + 15 g l^{-1} (K_2SO_4)
(15/141.998 moles Na_2SO_4) + (15/174.252 moles K_2SO_4)
(0.1056 moles Na_2SO_4) + (0.0861 moles K_2SO_4)
(0.2567 moles Na + 0.1056 moles SO_4) + (0.172 moles K + 0.0861 moles SO_4)
Total: (0.2567 moles Na + 0.172 moles K + 0.1917 moles SO_4)

Sample 4 (60 g l^{-1} salinity) (-Cl):

30 g l^{-1} (Na_2SO_4) + 30 g l^{-1} (K_2SO_4)
(30/141.998 moles Na_2SO_4) + (30/174.252 moles K_2SO_4)
(0.211 moles Na_2SO_4) + (0.172 moles K_2SO_4)
(0.422 moles Na + 0.2113 moles SO_4) + (0.344 moles K + 0.172 moles SO_4)
Total: (0.422 moles Na + 0.344 moles K + 0.3833 moles SO_4)

Sample 5 (30 g l^{-1} salinity) (-SO_4):

15 g l^{-1} (NaCl) + 15 g l^{-1} (KCl)
(15/58.442 moles NaCl) + (15/74.551 moles KCl)
(0.2567 moles NaCl) + (0.2012 moles KCl)
(0.2567 moles Na + 0.2567 moles Cl) + (0.2012 moles K + 0.2012 moles Cl)
Total: (0.2567 moles Na + 0.2012 moles K + 0.458 moles Cl)

Sample 6 (60 g l^{-1} salinity) (-SO_4):

30 g l^{-1} (NaCl) + 30 g l^{-1} (KCl)
(30/58.442 moles NaCl) + (30/74.551 moles KCl)
(0.513 moles NaCl) + (0.4024 moles KCl)
(0.513 moles Na + 0.513 moles Cl) + (0.4024 moles K + 0.4024 moles Cl)
Total: (0.513 moles Na + 0.4024 moles K + 0.915 moles Cl)

Sample 7 (30 g l^{-1} salinity) (-Na):

15 g l^{-1} (KCl) + 15 g l^{-1} (K_2SO_4)
(15/74.551 moles KCl) + (15/174.252 moles K_2SO_4)
(0.2012 moles KCl) + (0.0861 moles K_2SO_4)
(0.2012 moles K + 0.2012 moles Cl) + (0.172 moles K + 0.0861 moles SO_4)
Total: (0.3752 moles K + 0.2012 moles Cl + 0.0861 moles SO_4)

Sample 8 (60 g l^{-1} salinity) (-Na):

30 g l^{-1} (KCl) + 30 g l^{-1} (K_2SO_4)
(30/74.551 moles KCl) + (30/174.252 moles K_2SO_4)
(0.4024 moles KCl) + (0.1722 moles K_2SO_4)
(0.4024 moles K + 0.4024 moles Cl) + (0.3443 moles K + 0.1722 moles SO_4)
Total: (0.3752 moles K + 0.7467moles Cl + 0.1722 moles SO_4)

Sample 9 (30 g l^{-1} salinity) (-K):

15 g l^{-1} (NaCl) + 15 g l^{-1} (Na_2SO_4)
(15/58.442 moles NaCl) + (15/141.998 moles Na_2SO_4)
(0.2567 moles NaCl) + (0.1056 moles Na_2SO_4)
(0.2567 moles Na + 0.2567 moles Cl) + (0.2113 moles Na + 0.1056 moles SO_4)
Total: (0.468 moles Na + 0.2567 moles Cl + 0.1056 moles SO_4)

Sample 10 (60 g l^{-1}salinity) (-K):

30 g l^{-1} (NaCl) + 30 g l^{-1} (Na_2SO_4)
(30/58.442 moles NaCl) + (30/141.998 moles Na_2SO_4)
(0.5133 moles NaCl) + (0.2113 moles Na_2SO_4)
(0.5133 moles Na + 0.5133 moles Cl) + (0.4225 moles Na + 0.2113 moles SO_4)
Total: (0.9358 moles Na + 0.5133 moles Cl + 0.2113 moles SO_4)

Osmotic Pressure Calculations Of The Prepared Saline Water Samples

Water Sample 1:

The osmotic pressure (at 25°C) of 30 g l^{-1} saline water sample (15 g l^{-1} NaCl and 15 g l^{-1} K_2SO_4) can be calculated using the following equation:

$$\pi = viciRT \qquad \text{Equation C-1}$$

where

π	= osmotic pressure	(atm)
c_i	= molar concentration of the solute	(mole)
v_i	= number of ions formed when a solute dissociates	(Dimensionless)
R	= gas constant	(L.atm. K^{-1}.mole^{-1})
T	= absolute temperature	(Kelvin)

For NaCl:

Convert grams to moles: 15.0 g ÷ 58.4428 g/mol = 0.2567 mol

Now, plug into the equation: $\pi = vi\ (0.2567)\ (0.08206)\ (298)$

Theoretically, the value of *vi* (van 't Hoff factor) for NaCl equals to 2, however, we use 1.8 and this has to do with a concept called ion pairing. In solution, a certain number of Na^+ ions and Cl^- ions will randomly come together and form NaCl ion pairs. This reduces the total number of particles in solution, hereby reducing the van 't Hoff factor.

So, plug again and then solve: $\pi = (1.8)\ (0.2567)\ (0.08206)\ (298)$

= 11.3 atm. That's about **11.45** bar

For K_2SO_4:

Convert grams to moles: 15.0 g ÷ 174.252 g/mol = 0.0861 mol

So, plug again and then solve: $\pi = (3)\ (0.0861)\ (0.08206)\ (298)$

= 6.3 atm. That's about **6.38** bar

The total pressure of the prepared water sample = 11.45 + 6.38 = **17.83 bar**

Water Sample 2:

The osmotic pressure (at 25°C) of 60 g l^{-1} saline water sample (30 g l^{-1} NaCl and 30 g l^{-1} K_2SO_4) can be calculated using the above equation:

For NaCl:

Convert grams to moles: 30.0 g ÷ 58.4428 g/mol = 0.513 moles

Now, plug into the equation: $\pi = (1.8)(0.513)(0.08206)(298)$

= 22.6 atm. That's about **22.90** bar

For K_2SO_4:

Convert grams to moles: 30.0 g ÷ 174.252 g/mol = 0.172 mol

So, plug again and then solve: $\pi = (3)(0.172)(0.08206)(298)$

= 12.6 atm. That's about **12.67** bar

The total pressure of the prepared water sample = 22.90 + 12.67 = **35.57 bar**

Water Sample 3:

The osmotic pressure (at 25°C) of 30 g l^{-1} saline water sample (15 g l^{-1} Na SO_4 and 15 g l^{-1} K_2SO_4) can be calculated using the above equation:

For Na_2SO_4:

Convert grams to moles: 15.0 g ÷ 141.998 g/mol = 0.1056 moles

Now, plug into the equation: $\pi = (3)(0.1056)(0.08206)(298)$

= 7.75 atm. That's about **7.85** bar

For K_2SO_4:

Convert grams to moles: 15.0 g ÷ 174.252 g/mol = 0.0861 mol

So, plug again and then solve: $\pi = (3)(0.0861)(0.08206)(298)$

= 6.3 atm. That's about **6.38** bar

The total pressure of the prepared water sample = 7.85 + 6.38 = **14.23 bar**

Water Sample 4:

The osmotic pressure (at 25°C) of 60 g l^{-1} saline water sample (30 g l^{-1} Na SO_4 and 30 g l^{-1} K_2SO_4) can be calculated using the above equation:

For Na_2SO_4:

Convert grams to moles: 30.0 g ÷ 141.998 g/mol = 0.211 moles

Now, plug into the equation: $\pi = (3)(0.211)(0.08206)(298)$

= 15.5 atm. That's about **15.70** bar

For K_2SO_4:

Convert grams to moles: 30.0 g ÷ 174.252 g/mol = 0.172 mol

So, plug again and then solve: $\pi = (3)(0.172)(0.08206)(298)$

= 12.6 atm. That's about **12.76** bar

The total pressure of the prepared water sample = 15.70 + 12.76 = **28.46 bar**

Water Sample 5:

The osmotic pressure (at 25°C) of 30 g l^{-1} saline water sample (15 g l^{-1} NaCl and 15 g l^{-1} KCl) can be calculated using the above equation:

For NaCl:

Convert grams to moles: 15.0 g ÷ 58.4428 g/mol = 0.2567 moles

Now, plug into the equation: $\pi = (1.8)(0.2567)(0.08206)(298)$

= 11.3 atm. That's about **11.45** bar

For KCl:

Convert grams to moles: 15.0 g ÷ 74.551 g/mol = 0.2012 mol

So, plug again and then solve: $\pi = (1.8)(0.2012)(0.08206)(298)$

= 8.86 atm. That's about **8.98** bar

The total pressure of the prepared water sample = 11.45 + 8.98 = **20.43 bar**

Water Sample 6:

The osmotic pressure (at 25°C) of 60 g l^{-1} saline water sample (30 g l^{-1} NaCl and 30 g l^{-1} KCl) can be calculated using the above equation:

For NaCl:

Convert grams to moles: 30.0 g ÷ 58.4428 g/mol = 0.513 moles

Now, plug into the equation: $\pi = (1.8)(0.513)(0.08206)(298)$

= 22.6 atm. That's about **22.90** bar

For KCl:

Convert grams to moles: 30.0 g ÷ 74.551 g/mol = 0.4024 mol

So, plug again and then solve: $\pi = (1.8)(0.40.24)(0.08206)(298)$

= 17.72 atm. That's about **17.95** bar

The total pressure of the prepared water sample = 22.90 + 17.95 = **40.85 bar**

Water Sample 7:

The osmotic pressure (at 25°C) of 30 g l^{-1} saline water sample (15 g l^{-1} KCl and 15 g l^{-1} K_2SO_4) can be calculated using the above equation:

For KCl:

Convert grams to moles: 15.0 g ÷ 74.551 g/mol = 0.2012 mol

So, plug again and then solve: $\pi = (1.8)(0.2012)(0.08206)(298)$

= 8.86 atm. That's about **8.98** bar

For K_2SO_4:

Convert grams to moles: 15.0 g ÷ 174.252 g/mol = 0.0861 mol

So, plug again and then solve: $\pi = (3)(0.0861)(0.08206)(298)$

= 6.3 atm. That's about **6.38** bar

The total pressure of the prepared water sample = 8.98 + 6.38 = **15.36 bar**

Water Sample 8:

The osmotic pressure (at 25°C) of 60 g l^{-1} saline water sample (30 g l^{-1} KCl and 30 g l^{-1} K_2SO_4) can be calculated using the above equation:

For KCl:

Convert grams to moles: 30.0 g ÷ 74.551 g/mol = 0.4024 mol

So, plug again and then solve: π = (1.8) (0.40.24) (0.08206) (298)

= 17.72 atm. That's about **17.95** bar

For K_2SO_4:

Convert grams to moles: 30.0 g ÷ 174.252 g/mol = 0.172 mol

So, plug again and then solve: π = (3) (0,172) (0.08206) (298)

= 12.6 atm. That's about **12.76** bar

The total pressure of the prepared water sample = 17.95 + 12.76 = **30.71 bar**

Water Sample 9:

The osmotic pressure (at 25°C) of 30 g l^{-1} saline water sample (15 g l^{-1} NaCl and 15 g l^{-1} $NaSO_4$) can be calculated using the above equation:

For NaCl:

Convert grams to moles: 15.0 g ÷ 58.4428 g/mol = 0.2567 mol

So, plug again and then solve: π = (1.8) (0.2567) (0.08206) (298)

= 11.3 atm. That's about **11.45** bar

For Na_2SO_4:

Convert grams to moles: 15.0 g ÷ 141.998 g/mol = 0.1056 moles

Now, plug into the equation: π = (3) (0.1056) (0.08206) (298)

= 7.75 atm. That's about **7.85** bar

The total pressure of the prepared water sample = 11.45 + 7.85 = **19.30 bar**

Water Sample 10:

The osmotic pressure (at 25°C) of 60 g l^{-1} saline water sample (30 g l^{-1} NaCl and 30 g l^{-1} $NaSO_4$) can be calculated using the above equation:

For NaCl:

Convert grams to moles: 30.0 g ÷ 58.4428 g/mol = 0.5133 mol

So, plug again and then solve: $\pi = (1.8)\ (0.5133)\ (0.08206)\ (298)$

= 22.6 atm. That's about **22.90** bar

For Na_2SO_4:

Convert grams to moles: 30.0 g ÷ 141.998 g/mol = 0.2113 moles

Now, plug into the equation: $\pi = (3)\ (0.2113)\ (0.08206)\ (298)$

= 15.50 atm. That's about **15.70** bar

The total pressure of the prepared water sample = 22.90 + 15.70 = **38.60 bar**

Table C-1: Chemical Ingredients and Calculated Osmotic Pressure for Various Sample Preparations

Chemical Samples	NaCl g l^{-1}	KCl g l^{-1}	Na_2SO_4 g l^{-1}	K_2SO_4 g l^{-1}	Calculated Osmotic pressure (bar)
Sample 1 (30 g l^{-1} salinity)	15	-	-	15	17.83
Sample 2 (60 g l^{-1} salinity)	30	-	-	30	35.57
Sample 3 (30 g l^{-1} salinity) (-Cl)	-	-	15	15	14.23
Sample 4 (60 g l^{-1} salinity) (-Cl)	-	-	30	30	28.46
Sample 5 (30 g l^{-1} salinity) (-SO_4)	15	15	-	-	20.43
Sample 6 (60 g l^{-1} salinity) (-SO_4)	30	30	-	-	40.85
Sample 7 (30 g l^{-1} salinity) (-Na)	-	15	-	15	15.36
Sample 8 (60 g l^{-1} salinity) (-Na)	-	30	-	30	30.71
Sample 9 (30 g l^{-1} salinity) (-K)	15	-	15	-	19.30
Sample 10 (60 g l^{-1} salinity) (-K)	30	-	30	-	38.60

Biological Samples	NaCl g l^{-1}	KCl g l^{-1}	Na_2SO_4 g l^{-1}	K_2SO_4 g l^{-1}	Calculated Osmotic pressure (bar)
Sample 11 (30 g l^{-1} salinity)	15	-	-	15	17.83
Sample 12 (60 g l^{-1} salinity)	30	-	-	30	35.57

Pre-treated Biological Samples	NaCl g l^{-1}	KCl g l^{-1}	Na_2SO_4 g l^{-1}	K_2SO_4 g l^{-1}	Calculated Osmotic pressure (bar)
Sample 13 (30 g l^{-1} salinity)	15 g	-	-	15 g	17.83
Sample 14 (60 g l^{-1}salinity)	30 g	-	-	30 g	35.57

Reynolds Number Calculations

a) The value of the Reynolds number (Re) of the membrane test cell (module) can be calculated using the following equation:

$$Re = \frac{\rho \nu L}{\eta}$$

where:

ρ = density (kg m^{-3})

ν = cross flow velocity (m s^{-1})

L = Characteristic distance (or pipe diameter) (m)

η = fluid viscosity (dynamic) (N s m^{-2})

The cross flow velocity (ν) is a function of the feed flow rate (Q = 4.161 l min^{-1}) and the area of the membrane surface (A) (diameter = 12.5 cm):

$$Q\ (m^3\ s^{-1}) = \nu (m\ s^{-1}) * A\ (m^2)$$
$$6.935 \times 10^{-5}\ (m^3\ s^{-1}) = \nu (m\ s^{-1}) \times 0.01228\ (m^2)$$
$$\nu (m\ s^{-1}) = 5.647 \times 10^{-3}\ (m\ s^{-1})$$

$$Re = [1000\ (kg\ m^{-3}) \times 5.647 \times 10^{-3}\ (m\ s^{-1}) \times 0.01\ (m)] / [8.9 \times 10^{-4}\ (N\ s\ m^{-2})]$$

$$Re = \boxed{63}$$

b) The value of the Reynolds number (Re) of the Annular Rotating Bioreactor (RAB) can be calculated using the following equation:

$$Re = \frac{\rho \nu L}{\eta}$$

where:

ρ = density (kg m^{-3})

ν = cross flow velocity (m s^{-1})

L = Characteristic distance (or pipe diameter) (m)

η = fluid viscosity (dynamic) (N s m^{-2})

The circulation velocity (ν) is a function of the circulation frequency (C_f) (rpm = 28 rpm) and the preference of the inner drum (c) (diameter = 14 cm):

$$\nu (m\ s^{-1}) = C_f\ (rps) * c\ (m)$$
$$\nu (m\ s^{-1}) = 1680\ (m\ s^{-1}) \times 0.44\ (m)$$
$$\nu (m\ s^{-1}) = 0.2053\ (m\ s^{-1})$$

$$Re = [1000\ (kg\ m^{-3}) \times 0.2053\ (m\ s^{-1}) \times 0.07\ (m)] / [8.9 \times 10^{-4}\ (N\ s\ m^{-2})]$$

$$Re = \boxed{16{,}147}$$

Strain	Time	Ln(OD)
H. pantelleriensis (90 g/l, pH 7)	18	-1.584745
	20	-0.903868
	28	-0.562119
	44	-0.309246
	52	-0.254892
	68	-0.220647
H. pantelleriensis (90 g/l, pH 9)	10	-2.079442
	12	-1.422958
	14	-0.634878
	16	-0.373966
	18	-0.194799
	20	-0.035627
	28	0.1441
	44	0.222343
H. pantelleriensis (90 g/l, pH 10.5)	12	-2.538307
	14	-1.980502
	16	-1.187444
	18	-0.691149
	20	-0.465215
	28	-0.141564
H. pantelleriensis (180 g/l, pH 7)	14	-3.963316
	16	-4.017384
	18	-3.816713
	20	-3.912023
	28	-3.863233

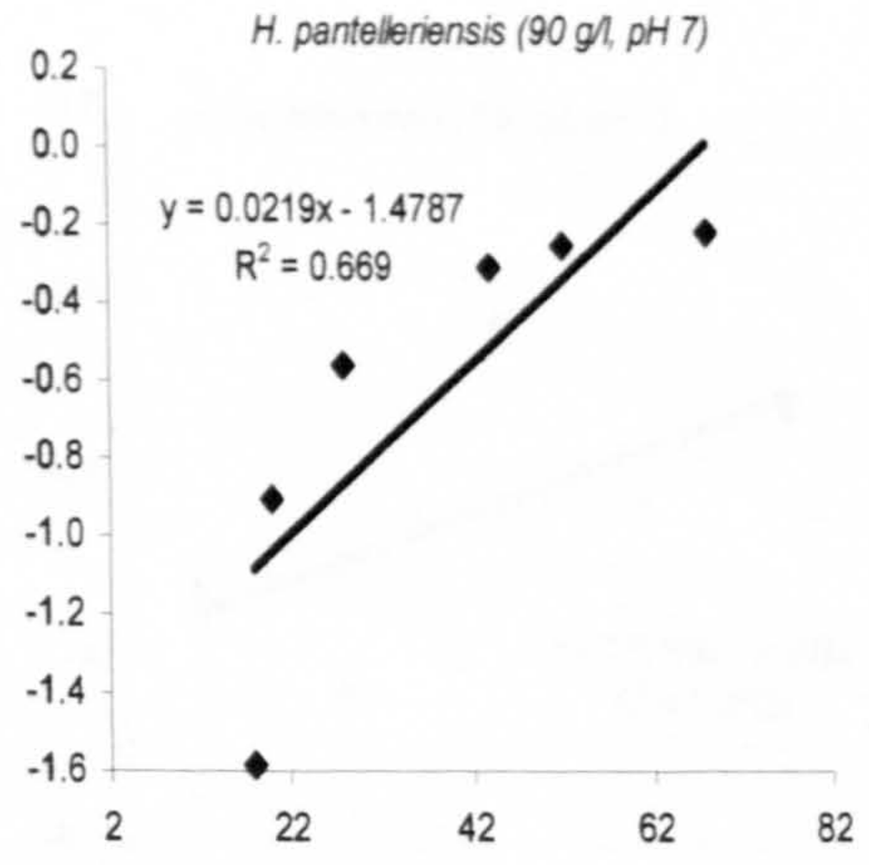

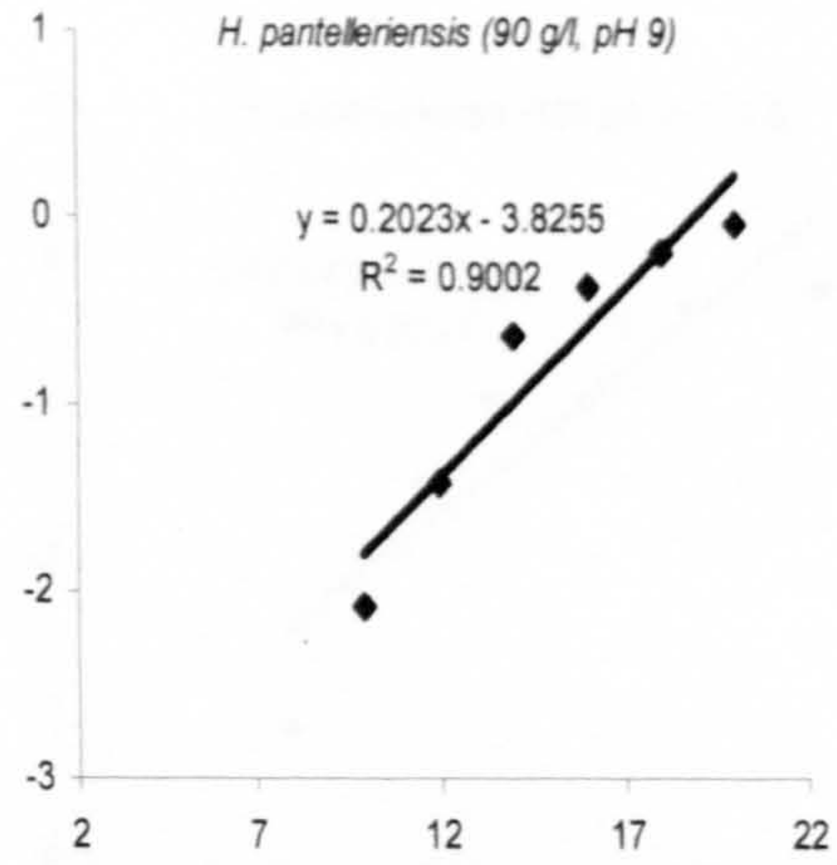

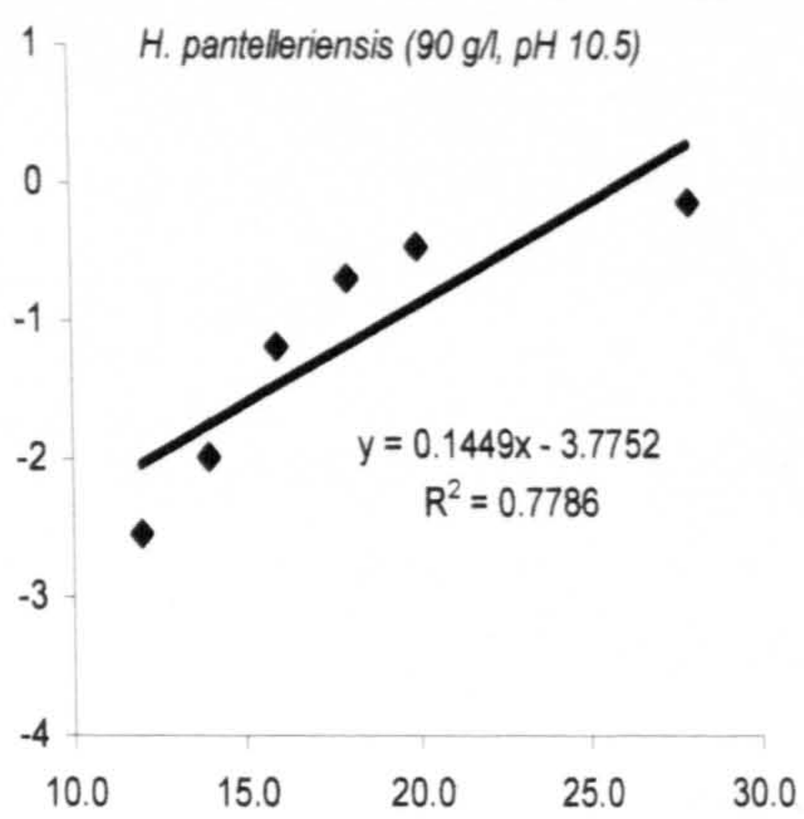

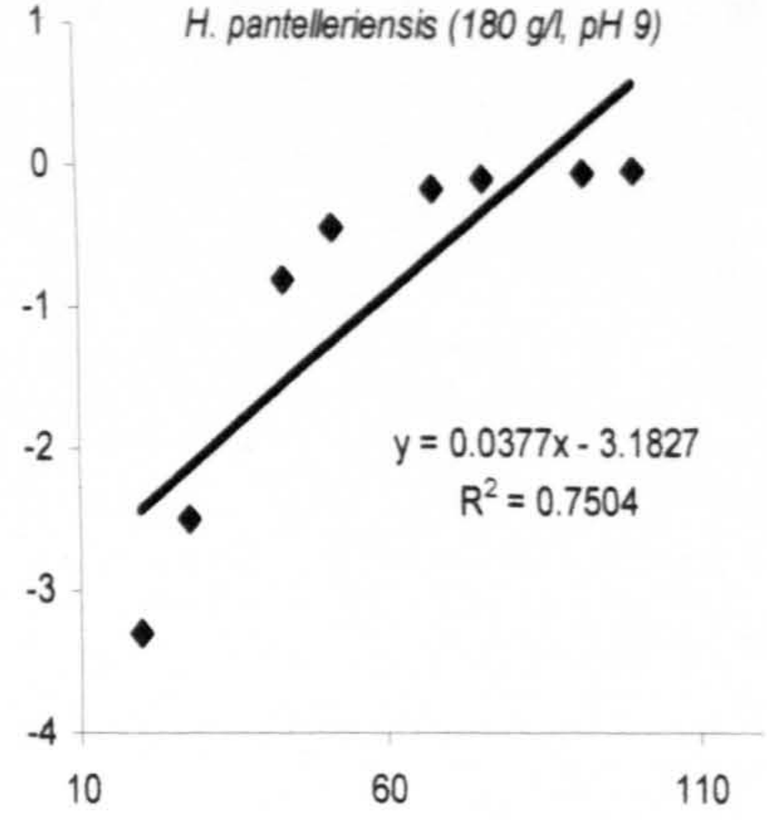

H. pantelleriensis (180 g/l, pH 9)	20	-3.296837
	28	-2.488915
	44	-0.802962
	52	-0.438505
	68	-0.166055
	76	-0.094311
	92	-0.053401
	100	-0.037702
H. pantelleriensis (180 g/l, pH 10.5)	28	-3.101093
	44	-1.482805
	52	-0.918794
	68	-0.398986
	76	-0.29303
	92	-0.175545

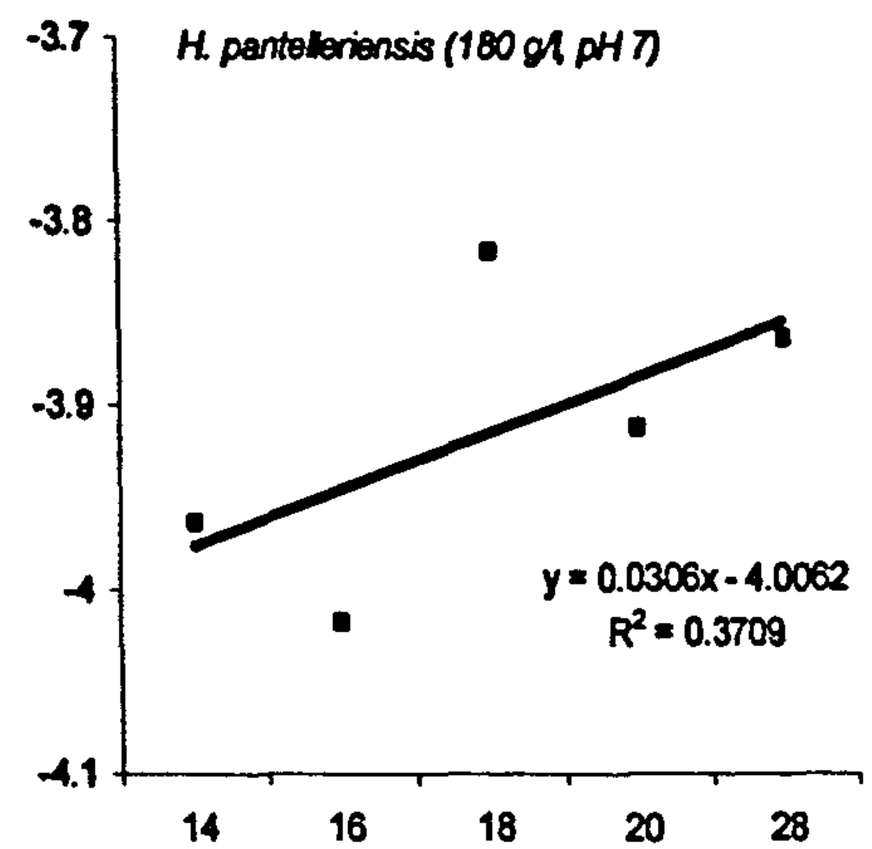

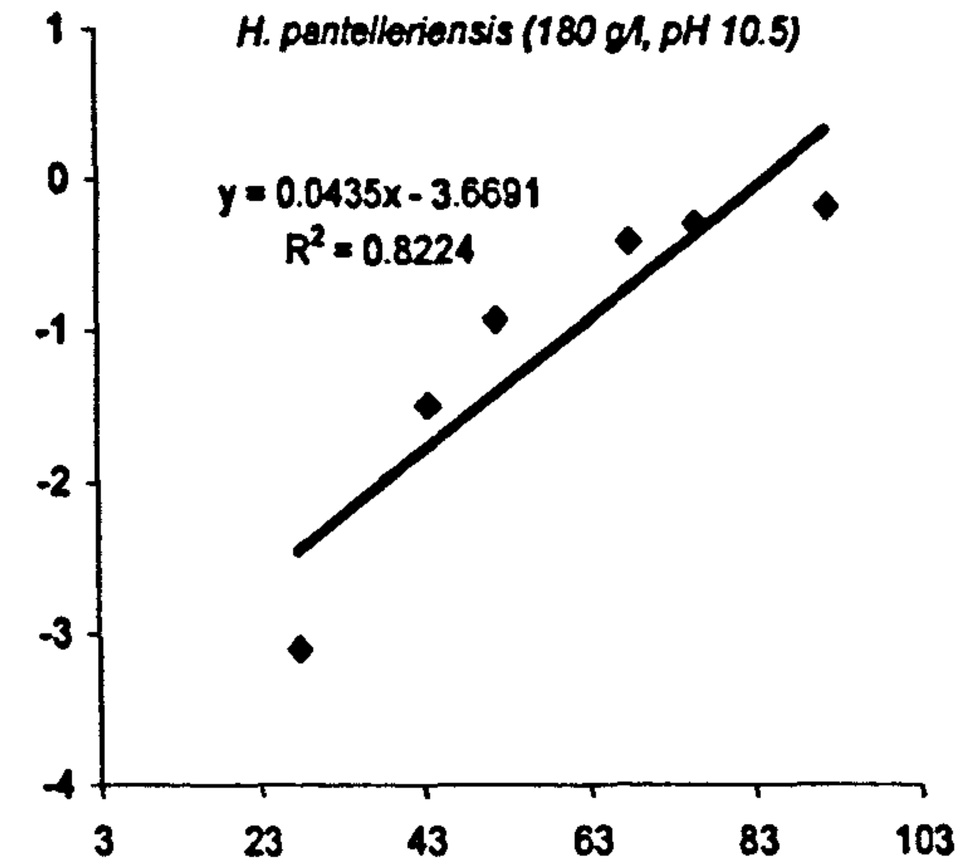

DESAL™
MEMBRANE PRODUCTS

General Information

High Pressure Cell Test Unit

OSMONICS
DESAL

760 Shadowridge Dr., Vista, CA 92083-7986 USA. Phone (619) 598-3334. Fax (619) 598-3335

DESAL™
MEMBRANE PRODUCTS

High Pressure Cell Test Unit
Unit Specifications

Crated Dimensions	**18" x 18" x 18" (l x h x w) 46 x 46 x 46 cm**
Shipping Weight	**175 lbs. (79.45 kg.)**
Power Requirements	**0.75 hp, 115/120 VAC, 10 AMPS, 50/60 Hz**
Maximum Operating Pressure	**1000 psig (70 bar)**
Maximum Operating Temperature	**90°**
Operating pH Limits	**1 – 13 pH**
Pump	**P.D. type, 1.1 GPM (250 liters/hr)**
Unit Capacity	**Feed tank 15 gallons (60 liters)**
Pressure Test Cells	**2 stainless test cells, each cell with an area of 12.56 square inches (81 cm^2)**

OSMONICS
DESAL

760 Shadowridge Dr., Vista, CA 92083-7986 USA, Phone (619) 598-3334, Fax (619) 598-3335

DESAL™
MEMBRANE PRODUCTS

High Pressure Cell Test Unit
Piping and Instrumentation Diagram

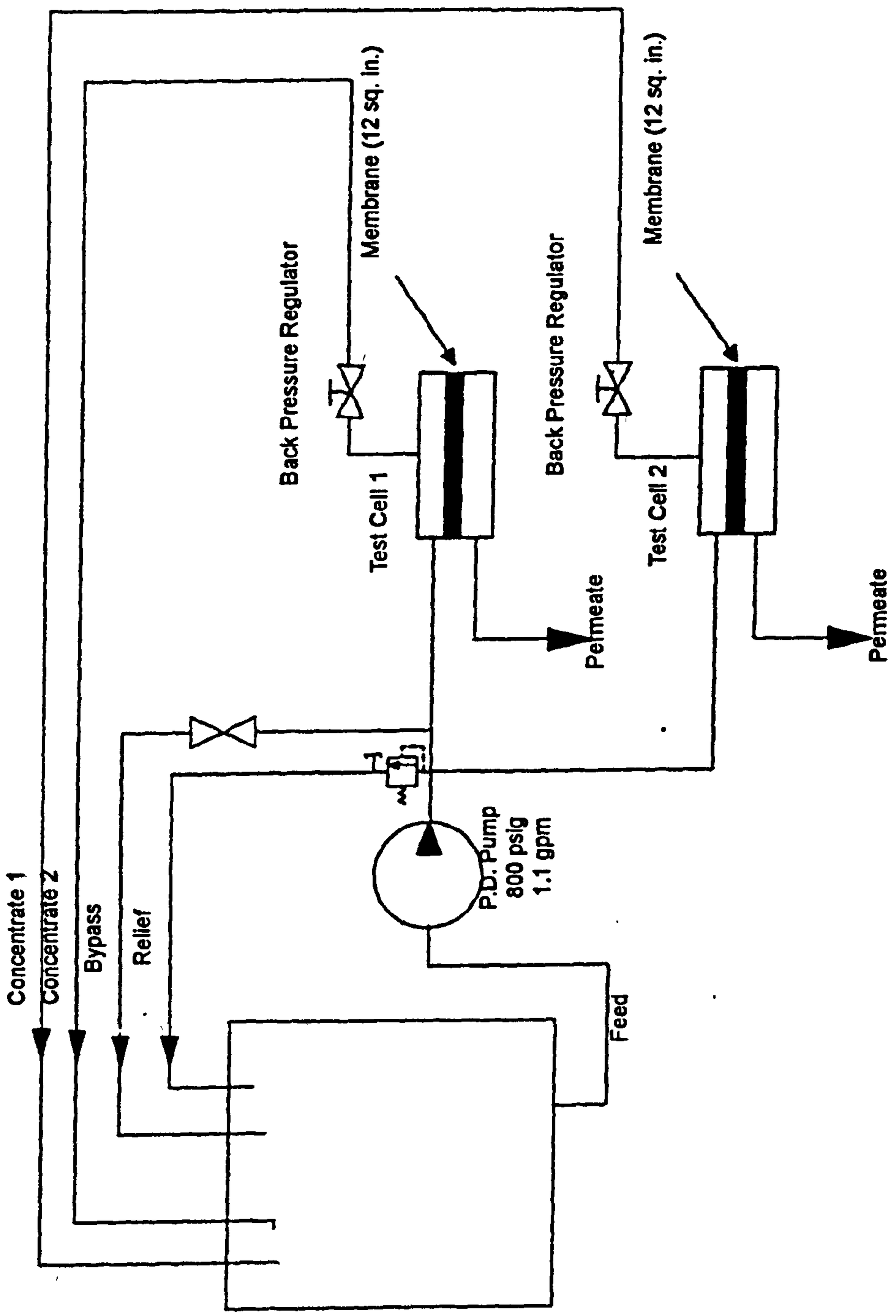

OSMONICS
DESAL

760 Shadowridge Dr . Vista. CA 92083-7986 USA. Phone (619) 598-3334. Fax (619) 598-3335